TU Delft

Delft University of Technology

Document Version
Final published version

Citation (APA)
Tan, J. (2022). *Improving the Techno-Economic Performance of Wave Energy Converters: From the Perspective of Systematic Sizing*. [Dissertation (TU Delft), Delft University of Technology]. https://doi.org/10.4233/uuid:de50235b-1d2a-43f3-bcfa-1dd5f570ab5a

Important note
To cite this publication, please use the final published version (if applicable).
Please check the document version above.

Copyright
In case the licence states “Dutch Copyright Act (Article 25fa)”, this publication was made available Green Open Access via the TU Delft Institutional Repository pursuant to Dutch Copyright Act (Article 25fa, the Taverne amendment). This provision does not affect copyright ownership.
Unless copyright is transferred by contract or statute, it remains with the copyright holder.

Sharing and reuse
Other than for strictly personal use, it is not permitted to download, forward or distribute the text or part of it, without the consent of the author(s) and/or copyright holder(s), unless the work is under an open content license such as Creative Commons.

Takedown policy
Please contact us and provide details if you believe this document breaches copyrights.
We will remove access to the work immediately and investigate your claim.

This work is downloaded from Delft University of Technology.

Improving the Techno-Economic Performance of Wave Energy Converters

from the Perspective of Systematic Sizing

IMPROVING THE TECHNO-ECONOMIC PERFORMANCE OF WAVE ENERGY CONVERTERS

FROM THE PERSPECTIVE OF SYSTEMATIC SIZING

Dissertation

ter verkrijging van de graad van doctor
aan de Technische Universiteit Delft,
op gezag van de Rector Magnificus prof.dr.ir. T.H.J.J. van der Hagen,
voorzitter van het College voor Promoties,
in het openbaar te verdedigen op maandag 5 december 2022 om 12:30 uur

by

Jian TAN

Master of Science in Turbine Engineering,
Wuhan University of Technology, China.
born in Suizhou, Hubei, China.

Dit proefschrift is goedgekeurd door de

Dr.ir. S.A. Miedema
Dr.ir. H. Polinder
Dr.ir. A.J. Laguna

Samenstelling promotiecommissie:

Rector Magnificus	voorzitter
Dr.ir. S.A. Miedema	Technische Universiteit Delft, promotor
Dr.ir. H. Polinder	Technische Universiteit Delft, promotor
Dr.ir. A.J. Laguna	Technische Universiteit Delft, copromotor

Onafhankelijke leden:

Prof. dr. S.J. Watson	Technische Universiteit Delft
Prof. dr. G.D. Weymouth	Technische Universiteit Delft
Prof. dr. H. Shi	Ocean University of China, China
Prof. dr. A. Vakis	University of Groningen, The Netherlands
Prof. dr. ir. C. van Rhee	Technische Universiteit Delft, reservelid

The research was financially supported by Delft University of Technology (TU Delft) and China Scholarship Council (CSC) under grant 201806950003.





Printed by: Ridderprint, Alblasserdam

Copyright © 2022 by J. Tan

ISBN 978-94-6458-745-6

An electronic version of this dissertation is available at
http://repository.tudelft.nl/.

To my wife Xu,

who makes my Joy complete.

CONTENTS

Summary xi

Samenvatting xv

Nomenclature xix

1 Introduction 1
- 1.1 Background: The role of ocean wave energy towards energy transition 2
- 1.2 Research motivation: Sizing matters to the techno-economics of WECs? 3
- 1.3 Research objectives 4
- 1.4 Principal contributions 6
- 1.5 Research scope 6
- 1.6 Outline and approach 6

2 Wave Energy Technology and Sizing of WECs 11
- 2.1 Introduction 12
- 2.2 Review of wave energy technologies 13
  - 2.2.1 Overview of wave energy converters 13
  - 2.2.2 Overview of power take-off systems 18
  - 2.2.3 Literature review of linear generators in wave energy conversion 20
- 2.3 Review of sizing methods of WECs 22
  - 2.3.1 Froude similarity 23
  - 2.3.2 Budal diagram 25
  - 2.3.3 Numerical simulation 28
- 2.4 Summary and conclusions 30

3 A Collective Sizing Method for WECs 31
- 3.1 Introduction 32
- 3.2 WEC Concept and concerned sea sites 32
- 3.3 Methodology 34
  - 3.3.1 Collective sizing method 34
  - 3.3.2 Frequency domain Modeling 36
- 3.4 Results 45
  - 3.4.1 The Effects of Sizing on the Performance of the WEC 45
  - 3.4.2 Size Optimization for Typical Realistic Sea Sites 47
  - 3.4.3 The Proposed Method Versus Other Size Optimization Methods 52
- 3.5 Discussion 54
- 3.6 Summary and conclusions 56

4 A Spectral Domain Model for PTO Sizing 59
4.1 Introduction . . . 60
4.2 Numerical modeling . . . 61
4.2.1 Frequency domain modeling . . . 61
4.2.2 Time domain modeling . . . 61
4.2.3 Spectral domain modeling . . . 63
4.2.4 Implementation of simulation . . . 65
4.3 Verification of spectral domain modeling . . . 65
4.4 Comparison of three models on the prediction of the power absorption . . . 67
4.5 Case study: Determining the optimal PTO size for Yeu island . . . 70
4.5.1 Incorporation of viscous drag force . . . 70
4.5.2 The tuning of PTO parameters . . . 72
4.5.3 The techno-economic analysis . . . 76
4.6 Discussion . . . 79
4.7 Summary and conclusions . . . 80

5 The Influence of PTO Sizing on the Power Conversion Efficiency 83
5.1 Introduction . . . 84
5.2 Concept description . . . 84
5.3 Generator modeling . . . 86
5.3.1 Generator sizing . . . 88
5.3.2 Cost estimation of the linear generator . . . 90
5.4 Generator performance . . . 91
5.5 Comparison of sizing methods . . . 91
5.5.1 On the generator performance . . . 91
5.5.2 On the Techno-Economics and the PTO size determination . . . 93
5.6 Dependence of the generator sizing on wave resources . . . 95
5.7 Conclusion . . . 98

6 Improving the Power Performance with a Downsized PTO Capacity: Adjustable Draft System 99
6.1 Introduction . . . 101
6.2 Concept description . . . 102
6.3 Nonlinear time domain model . . . 105
6.4 Results . . . 108
6.4.1 Frequency domain analysis . . . 108
6.4.2 Nonlinear time domain analysis . . . 115
6.5 Discussion . . . 124
6.6 Summary and conclusions . . . 125

7 The Performance of the Adjustable Draft Point Absorber Integrated with a Linear PM Generator 127
7.1 Introduction . . . 128
7.2 System specification . . . 129
7.2.1 The specification of the buoy size and positioning . . . 129
7.2.2 Specification of the electric generator . . . 130

7.3 Wave-to-wire modeling 132
7.4 Results 132
7.4.1 Wave-to-wire response of the WEC 133
7.4.2 Negative effects of the draft adjustment 134
7.4.3 Performance identification 138
7.5 Summary and conclusions 143

8 Conclusions and Recommendations **145**
8.1 Conclusions 146
8.1.1 To the first research objective 146
8.1.2 To the second research objective 147
8.2 Recommendations 147
8.2.1 To the systematic sizing method 147
8.2.2 To the adjustable draft system 149

A Appendix **151**
A.1 Convergence verification of hydrodynamic calculation 152
A.2 The hydrodynamic coefficients for different buoy drafts 153
A.3 The verification of the selected number of starting points in the Multistart optimization 154
A.4 The verification of the reproduced nonlinear time domain model 155

Bibliography **156**

Acknowledgements **171**

Curriculum Vitæ **173**

List of Publications **175**

SUMMARY

Ocean wave energy has a huge potential to make a contribution to global energy transition. However, the high Levelized Cost of Energy (LCOE) is currently a big hurdle to the development of wave energy converters (WECs). This thesis is motivated to improve the techno-economic competitiveness of WECs. It focuses on the effects of systematic sizing of WECs. "Systematic sizing" is reflected in this thesis by considering the effects of sizing on the two main components of WECs, namely the buoy and PTO system.

The main body of this thesis starts with a literature review. First, it is intended to provide an overview of current wave energy technologies and the application of power take-off (PTO) systems. Secondly, the studies relevant to sizing of WECs are reviewed, and sizing methods used in the context are discussed and compared. It indicates that the existing studies mainly focus on the effects of buoy sizing and there is a lack of consideration of PTO sizing. In addition, the sizing methods based on the Budal diagram and Froude scaling can only be used to conduct sizing of buoy but the influence of PTO sizing cannot be covered. Numerical simulation can be applied to take into account both effects of buoy sizing and PTO sizing, but it is usually associated with low computational-efficiency. As sizing can be regarded as a kind of optimization which normally requires a number of iterations, an efficient method is beneficial for accelerating the design process of WECs. Followed up by the literature review, Chapter 3 to Chapter 7 of this thesis are dedicated to accomplishing two main research objectives.

Establish a systematic sizing method for WECs

The first step of this study is to build a framework of the systematic size optimization method for a generic point absorber. The collective influence of buoy sizing and PTO sizing are covered in the framework, and the optimization is aiming at minimizing the LCOE. In the framework, frequency domain modeling is adopted to calculate the power production of WECs in different sizes, since it has high efficiency. The influence of the PTO size is simplified as force constraints, and the constraints are complied by tuning the PTO parameters. A preliminary economic model is established to calculate the cost of the WEC. A case study carried out based on the established sizing method shows that both buoy sizing and PTO sizing are significant to the LCOE. Downsizing the PTO size is beneficial for the reduction of the LCOE. In the considered case, it could reduce the LCOE by 24 % to 31 %. In addition, the size determination is highly resource-specific. The wave resource with higher mean wave power is not necessarily associated with a larger buoy or PTO size, but it contributes to the lower LCOE.

The second step of this study is to enhance the systematic size optimization, since the nonlinear effect of PTO sizing on the power estimation was not considered in the framework. A spectral domain model incorporating the PTO force saturation is then developed. It allows for the inclusions of nonlinearity by statistical linearization but maintains high computational efficiency. Verified against the results from nonlinear time domain model,

the proposed spectral domain model shows adequate accuracy. Compared with the frequency domain model, the spectral domain model remarkably reduces the relative errors in predicting the power performance of WECs with force constraints, while the computational demand is much lower than the nonlinear time domain model. Furthermore, a case study is conducted to size the PTO capacity in a chosen wave site. The frequency domain, nonlinear time domain and spectral domain models are applied respectively. The frequency domain model could lead to a poor estimate of the optimal PTO capacity, with a maximum relative error on the prediction of the annual energy production (AEP)of 24 %. In contrast, the spectral domain model indicates the same optimal PTO size with the time domain modeling, and its relative errors on the prediction of the AEP are within 4.3 %.

To make the sizing method more concrete, the third step shifted the focus from the power absorption stage to power conversion stage of WECs. As a dominating type of PTO system in wave energy conversion, the linear permanent magnet (PM) generator is chosen as the research object. The influence of the variation of the PTO size on the efficiency of linear PM generator is analyzed. Three different methods for sizing the linear generator are applied and compared. The results show that the overall power conversion efficiency has a notable dependence on the size of generators. Thus, the assumption of a constant generator efficiency leads to an obviously poor estimate on the AEP, LCOE and the PTO size determination. In particular cases, its relative errors on the estimation of the AEP and the optimal PTO size reaches 10 % and 29 %. Compared with the method based on the scaling law, the scaling with implementing the optimization of main machine parameters could better reflect the techno-economic potential of WECs when conducting PTO sizing. Therefore, it is highly recommended to take into account the variation of the generator efficiency.

Investigate the performance of the adjustable draft system on improving power production of point absorbers with constrained PTO capacities

Downsized PTO capacities are proved to be beneficial for reducing the LCOE in the investigation attributed to the first objective. A novel design, namely the adjustable draft system, is then proposed in this thesis to further improve the power production of point absorbers with constrained PTO capacities. Both a frequency domain model and a nonlinear time domain model are established to reveal the performance of the concept. From the frequency domain analysis, two potential advantages are identified by installing the adjustable draft system. Firstly, the excitation force can be controlled by adjusting the buoy draft, which could be utilized to reduce the required PTO force. This is helpful for downsizing the PTO capacity. Secondly, the relevant natural frequency of the point absorber can be adapted to the operating wave states by varying the buoy draft, which improves the power absorption. A nonlinear approach is adopted specifically for the spherical buoy to include the nonlinear Froude–Krylov force and viscous drag force. The results show that the nonlinear forces have a significant influence on the power absorption when operating close to resonance regions. However, the advantages resulting from the proposed system still can be observed while considering the nonlinear forces. The power absorption can be improved by 27 % and 12 % in particular cases of regular and irregular wave states respectively.

The draft adjustment of the buoy changes the dynamics of the device, which could also make a difference to the performance of the PTO system. Thus, a wave-to-wire model is established to provide an in-depth insight into the systematic performance of the adjustable

draft point absorber integrated with a linear PM generator. Based on the established model, wave-to-wire responses of the novel concept are obtained and analyzed. The results show that, on the one hand, the draft adjustment results in negative effects on the power production, since it varies the symmetry of the stroke and the overlap between the stator and translator of the generator. On the other hand, the draft adjustment leads to the increased buoy speed, which contributes to the improvement of the generator efficiency. For the WEC considered in this thesis, the advantage of the adjustable draft system is more dominating than the disadvantage with regard to the power production. At particular operating conditions, the delivered electrical power of the adjustable-draft WEC is over 20 % and 10 % higher than that of the conventional fixed-draft WEC for regular and irregular wave conditions respectively.

SAMENVATTING

Oceaangolfenergie heeft een enorm potentieel om een bijdrage te leveren aan de wereldwijde energietransitie. De hoge Levelized Cost of Energy (LCOE) is momenteel echter een grote hindernis voor de ontwikkeling van golfenergieconverters (WEC's). Dit proefschrift is gemotiveerd om het technisch-economische concurrentievermogen van WEC's te verbeteren. Het richt zich op de effecten van de grootte van WEC's. Het hoofddoel van dit proefschrift is dus gedefinieerd als:

Verbeter de technisch-economische prestaties van WEC's vanuit het perspectief van systematische dimensionering.

"Systematische maatvoering"wordt in dit proefschrift weerspiegeld door de effecten van maatvoering op de twee hoofdcomponenten van WEC's, namelijk de boei en het aftakassysteem, te beschouwen.

Het hoofdgedeelte van dit proefschrift begint met een literatuuronderzoek. Ten eerste is het bedoeld om een overzicht te geven van de huidige golfenergietechnologieën en de toepassing van PTO-systemen. Ten tweede worden de onderzoeken die relevant zijn voor de dimensionering van WEC's beoordeeld en worden de in de context gebruikte meetmethoden besproken en vergeleken. Het geeft aan dat de bestaande onderzoeken zich voornamelijk richten op de effecten van de maatvoering van boeien en dat er onvoldoende rekening wordt gehouden met de maatvoering van de aftakas. Bovendien kunnen de maatbepalingsmethoden op basis van het Budal-diagram en Froude-schaling alleen worden gebruikt om de maatbepaling van de boei uit te voeren, maar de invloed van de aftakasmaatbepaling kan niet worden afgedekt. Numerieke simulatie kan worden toegepast om rekening te houden met zowel de effecten van de grootte van de boei als van de grootte van de aftakas, maar wordt meestal geassocieerd met een lage rekenefficiëntie. Aangezien dimensionering kan worden beschouwd als een soort optimalisatie die normaal gesproken een aantal iteraties vereist, is een efficiënte methode gunstig om het ontwerpproces van WEC's te versnellen. Gevolgd door het literatuuronderzoek, zijn Hoofdstuk 3 tot Hoofdstuk 7 van dit proefschrift gewijd aan het bereiken van twee hoofdonderzoeksdoelen.

Stel een systematische dimensioneringsmethode op voor WEC's

De eerste stap van deze studie is het bouwen van een raamwerk van de systematische methode voor grootte-optimalisatie voor een generieke puntabsorbeerder. De collectieve invloed van de maatvoering van de boei en de maatvoering van de aftakas wordt behandeld in het raamwerk, en de optimalisatie is gericht op het minimaliseren van de LCOE. In het raamwerk wordt frequentiedomeinmodellering toegepast om de stroomproductie van WEC's in verschillende groottes te berekenen, omdat het een hoog rendement heeft. De

invloed van de PTO-afmetingen wordt vereenvoudigd als krachtbeperkingen, en aan de beperkingen wordt voldaan door de PTO-parameters af te stemmen. Er wordt een voorlopig economisch model opgesteld om de kosten van het WEC te berekenen. Een case study die is uitgevoerd op basis van de gevestigde maatmethode laat zien dat zowel de maatvoering van de boeien als de maatvoering van de aftakas belangrijk zijn voor de LCOE. Het verkleinen van de aftakas is gunstig voor de verlaging van de LCOE. In het beschouwde geval zou het de LCOE met 24 % tot 31 % kunnen verminderen. Bovendien is de bepaling van de grootte zeer resource-specifiek. De golfbron met een hoger gemiddeld golfvermogen is niet noodzakelijkerwijs geassocieerd met grotere boei- of aftakasafmetingen, maar draagt bij aan de lagere LCOE.

De tweede stap van deze studie is het verbeteren van de systematische optimalisatie van de grootte, aangezien het niet-lineaire effect van PTO-afmetingen op de vermogensschatting in het raamwerk niet werd overwogen. Vervolgens wordt een spectraal domeinmodel ontwikkeld waarin de PTO-krachtverzadiging is opgenomen. Het maakt het opnemen van niet-lineariteit mogelijk door statistische linearisatie, maar handhaaft een hoge rekenefficiëntie. Geverifieerd tegen de resultaten van het niet-lineaire tijddomeinmodel, toont het voorgestelde spectrale domeinmodel voldoende nauwkeurigheid. Vergeleken met het frequentiedomeinmodel, vermindert het spectrale domeinmodel opmerkelijk de relatieve fouten bij het voorspellen van de vermogensprestaties van WEC's met krachtbeperkingen, terwijl de rekenvraag veel lager is dan het niet-lineaire tijddomeinmodel. Verder wordt een case study uitgevoerd om de PTO-capaciteit in een gekozen golflocatie te bepalen. De frequentiedomein-, niet-lineaire tijdsdomein- en spectrale domeinmodellen worden respectievelijk toegepast. Het frequentiedomeinmodel zou kunnen leiden tot een verkeerde inschatting van de optimale PTO-capaciteit, met een maximale relatieve fout op de voorspelling van de jaarlijkse energieproductie (AEP) van 24 %. Daarentegen geeft het spectrale domeinmodel dezelfde optimale PTO-grootte aan met de tijdsdomeinmodellering, en de relatieve fouten bij de voorspelling van de AEP liggen binnen 4.3 %.

Om de dimensioneringsmethode concreter te maken, verlegde de derde stap de focus van de stroomabsorptiefase naar de stroomconversiefase van WEC's. Als dominerend type PTO-systeem bij golfenergieconversie, is de lineaire permanente magneet (PM) generator gekozen als onderzoeksobject. De invloed van de variatie van de PTO-grootte op de efficiëntie van de lineaire PM-generator wordt geanalyseerd. Drie verschillende methoden voor het dimensioneren van de lineaire generator worden toegepast en vergeleken. De resultaten laten zien dat de algehele efficiëntie van de stroomconversie sterk afhankelijk is van de grootte van de generatoren. De aanname van een constant generatorrendement leidt dus tot een duidelijke misschatting van de AEP-, LCOE- en de PTO-afmetingsbepaling. In bepaalde gevallen bereiken de relatieve fouten op de schatting van de AEP en de optimale PTO-grootte 10 % en 29 %. Vergeleken met de methode op basis van de schaalwet, zou de schaalvergroting met het implementeren van de optimalisatie van de belangrijkste machineparameters het technisch-economische potentieel van WEC's beter kunnen weerspiegelen bij het uitvoeren van PTO-maatvoering. Daarom wordt het ten zeerste aanbevolen om rekening te houden met de variatie in het generatorrendement.

Onderzoek de prestaties van het instelbare treksysteem bij het verbeteren van de stroomproductie van puntabsorbers met beperkte aftakascapaciteiten

In het onderzoek dat aan de eerste doelstelling werd toegeschreven, is bewezen dat verkleinde aftakascapaciteiten gunstig zijn voor het verminderen van de LCOE. In dit proefschrift wordt vervolgens een nieuw ontwerp, namelijk het instelbare treksysteem, voorgesteld om de energieproductie van puntabsorbers met beperkte PTO-capaciteiten verder te verbeteren. Zowel een frequentiedomeinmodel als een niet-lineair tijddomeinmodel zijn opgesteld om de prestaties van het concept te onthullen. Uit de analyse van het frequentiedomein worden twee potentiële voordelen geïdentificeerd door het installeren van het regelbare treksysteem. Ten eerste kan de excitatiekracht worden gecontroleerd door de diepgang van de boei aan te passen, die kan worden gebruikt om de vereiste aftakaskracht te verminderen. Dit is handig voor het verkleinen van de aftakascapaciteit. Ten tweede kan de relevante eigenfrequentie van de puntabsorbeerder worden aangepast aan de golftoestanden in bedrijf door de diepgang van de boei te variëren, wat de vermogensopname verbetert. Specifiek voor de sferische boei wordt een niet-lineaire benadering gevolgd om de niet-lineaire Froude-Krylov-kracht en viskeuze weerstandskracht te omvatten. De resultaten laten zien dat de niet-lineaire krachten een significante invloed hebben op de vermogensopname bij het werken in de buurt van resonantiegebieden. De voordelen die voortvloeien uit het voorgestelde systeem kunnen echter nog steeds worden waargenomen wanneer rekening wordt gehouden met de niet-lineaire krachten. De vermogensopname kan in bepaalde gevallen van respectievelijk regelmatige en onregelmatige golftoestanden met 27 % en 12 % worden verbeterd.

De diepgangaanpassing van de boei verandert de dynamiek van het apparaat, wat ook een verschil kan maken voor de prestaties van het aftakassysteem. Zo is een wave-to-wire-model opgesteld om eendiepgaand inzicht te geven in de systematische prestaties van de instelbare diepgangspuntabsorber die is geïntegreerd met een lineaire PM-generator. Op basis van het gevestigde model worden wave-to-wire-reacties van het nieuwe concept verkregen en geanalyseerd. De resultaten tonen aan dat enerzijds de diepgangaanpassing negatieve effecten heeft op de stroomproductie, aangezien deze de symmetrie van de slag en de overlap tussen de stator en de vertaler van de generator varieert. Aan de andere kant leidt de aanpassing van de diepgang tot een hogere boeisnelheid, wat bijdraagt aan de verbetering van het generatorrendement. Voor de in dit proefschrift behandelde WEC is het voordeel van het instelbare treksysteem meer overheersend dan het nadeel met betrekking tot de stroomproductie. Onder bepaalde bedrijfsomstandigheden is het geleverde elektrische vermogen van de WEC met instelbare trekkracht meer dan 20 % en 10 % hoger dan dat van de conventionele WEC met vaste trekkracht voor respectievelijk regelmatige en onregelmatige golfomstandigheden.

NOMENCLATURE

Below follows a list of the most frequently used symbols and notations in this thesis.

ROMAN SYMBOLS

a	acceleration in heaving direction	(m/s^2)
A_{Cus}	cross-sectional area of a phase winding	(m^2)
A_D	characteristic area of the buoy	(m^2)
b_p	magnet pole pitch	(m)
b_s	slot width	(m)
b_t	tooth width	(m)
B_0	magnetic flux density at the calibrated condition	(T)
$\hat{B}_{gm}$	fundamental space harmonic of the magnetic flux density in the air gap	(T)
B_{rm}	remanent flux density of the magnets	(T)
$\hat{B}_{st}$	fundamental space harmonic of the magnetic flux density in the stator teeth	(T)
$\hat{B}_{sy}$	fundamental space harmonic of the magnetic flux density in the stator yoke	(T)
C_D	drag coefficient	(−)
C_{Mass}	mass-related capital cost	(Euros)
C_{Power}	power-related capital cost	(Euros)
C_P	cost of PTO system	(Euros)
C_S, C_F, C_I, C_C	cost of the structure, foundation, installation and grid connection of the WEC	(Euros)
C_{mat}, C_{man}	cost of active material and manufacture of the generator	(Euros)
C_{Fe}, C_{Cu}, C_{pm}	unit cost of iron, copper and permanent magnet used in the generator	(Euros/kg)
D	water depth	(m)
E_p	No-load voltage	(V)
f_e	excitation force coefficient	(N/m)
f_{ele}	electrical generator frequency	(Hz)
f_0	electrical generator frequency at the calibrated condition	(Hz)
F_e	excitation force in heaving direction	(N)
$F_{e,i}$	excitation force in mode i	(N)
F_r	radiation force in heaving direction	(N)
F_{hs}	hydrostatic force in heaving direction	(N)
F_{vis}	viscous drag force in heaving direction	(N)
F_{pto}	PTO force	(N)
F_{FK}	Froude-Krylov force in heaving direction	(N)

$F_{FK_{st}}$	static Froude-Krylov force	(N)
$F_{FK_{dy}}$	dynamic Froude-Krylov force	(N)
$F_{FK_{dy(re)}}$	dynamic Froude-Krylov force in regular waves	(N)
$F_{FK_{dy(irr)}}$	dynamic Froude-Krylov force in irregular waves	(N)
F_D	diffraction force in heaving direction	(N)
F_{es}	end-stop force in heaving direction	(N)
F_{max}	maximum generator force	(N)
F_{ge}	generator force	(N)
F_m	PTO force limit	(N)
F_{limit}	designed maximum generator force	(N)
g	gravitational acceleration	(m/s^2)
g_l	air gap length	(m)
G	characteristic length	(m)
h_0	buoy draft in still water	(m)
h_a	the range of the adjustable buoy draft	(m)
h_s	slot height	(m)
h_{sy}	slot yoke height	(m)
H	wave height	(m)
H_s	significant wave height	(m)
H_D	wave height in the representative wave state	(m)
I_s	stator phase current	(A)
I_{sq}	quadrature component of the stator phase current	(A)
I_{sd}	direct component of the stator phase current	(A)
I_{sm}	maximum generator side phase current of the converter	(A)
I_{conm}	rated phase current of the converter	(A)
J_{re}	wave power transport per unit frontage of regular waves	(W/m)
J_{irr}	wave power transport per unit frontage of irregular waves	(W/m)
J_T	wave power threshold of the concerned sea site	(W/m)
k	wave number	(1/m)
k_w	winding factor	(−)
k_{sfill}	copper fill factor	(−)
K_{hs}	hydrostatic stiffness	(N/m)
K_{pto}	PTO stiffness	(N/m)
K_{es}	stiffness of end-stop spring	(N/m)
K_{rad}	radiation impulse response function	(Ns/m)
K_{diff}	diffraction impulse response function	(N/m)
l_{act}	actual length of the overlap between the translator and stator	(m)
l_{Cus}	phase winding length	(m)
l_s	stack length of the generator	(m)
l_m	magnet thickness	(m)
L_m	magnet length	(m)
L_{sta}	stator length of the generator	(m)
L_{tra}	translator length of the generator	(m)
L_t	stator inductance of the generator	(H)

m	phase number of the generator	(−)
M	mass of the buoy	(kg)
M_r	added mass in heaving direction	(kg)
M_{Cu}	mass of copper	(kg)
M_{Fe}	mass of iron	(kg)
M_{pm}	mass of permanent magnets	(kg)
M_{Fest}	mass of the stator teeth	(kg)
M_{Fesy}	mass of the stator yoke	(kg)
$\mathbf{n}$	normal vector to the surface	(−)
N_p	number of pole pairs	(−)
N_s	number of conductors per slot	(−)
N_Y	lifespan of the WEC	(year)
p	pressure	(Pa)
P	power	(W)
P_a	absorbed power	(W)
$P_{adjustable}$	absorbed power of the adjustable draft WEC	(W)
P_A	high-frequency power limit in the Budal diagram	(W)
P_B	low-frequency power limit in the Budal diagram	(W)
P_{copper}	copper losses	(W)
P_{con}	converter losses	(W)
P_{conm}	converter losses at the rated power	(W)
P_e	electrical power	(W)
P_{exc}	excitation power	(W)
P_{fixed}	absorbed power of the fixed draft WEC	(W)
P_r	radiation power	(W)
$P_{a,max}$	maximum absorbed power	(W)
P_{Fes}	iron losses of the generator	(W)
P_{Fes0}	iron loss per unit mass at a frequency f_0 and flux density B_0	(W)
P_{rated}	rated power of the electrical machine	(kW)
P_{wd}	power taken by the generator winding	(W)
q	probability density function of Gaussian distribution	(−)
Q	exceedance probability	(−)
r	discount rate	(−)
R	radius of the spherical buoy	(m)
R_r	hydrodynamic damping in heaving direction	(Ns/m)
R_{pto}	PTO damping	(Ns/m)
R_t	stator phase resistance	(Ω)
$R_{pto,min}$	minimal PTO damping complying with constraints	(Ns/m)
$R_{pto,max}$	maximum PTO damping complying with constraints	(Ns/m)
$R_{pto,opt}$	optimal PTO damping	(Ns/m)
$R_{eq,pto}$	equivalent PTO damping	(Ns/m)
$R_{eq,vis}$	equivalent viscous damping	(Ns/m)
s	displacement	(m)
s_m	maximum motion amplitude	(m)
S	stroke	(m)
S_{wl}	water-plane area	(m^2)

S_{ζ_a}	wave energy spectrum	(m^2/Hz)
S_u	spectral density of the velocity	$[m^2/(s^2Hz)]$
S_{conm}	rated apparent power of the scaled converter	(W)
t	time	(s)
T	wave period	(s)
T_p	peak period	(s)
T_e	energy period	(s)
T_z	zero-crossing period	(s)
T_{tot}	total time of the appearance of a certain sea state	(hours)
u	velocity	(m/s)
u_i	velocity in mode i	(m/s)
u_m	maximum velocity of the buoy	(m/s)
u_0	undisturbed flow velocity	(m/s)
u_{max}	maximum velocity of the translator	(m/s)
U_s	terminal voltage	(V)
U_{conm}	rated terminal voltage of the converter	(V)
V	volume	(m^3)
X_m	mechanical reactance	(Ns/m)
X_{pto}	PTO reactance	(Ns/m)
Y	the evaluated year	(−)
Z_m	mechanical impedance	(Ns/m)
Z_{pto}	PTO impedance	(Ns/m)
z	vertical position	(m)
$z^{'}$	corrected vertical position	(m)

GREEK SYMBOLS

$\alpha_S, \alpha_{F\&M}, \alpha_I$	percentage of cost of structure, foundation mooring and installation in the total capital expenditure	(−)
α_C, α_P	percentage of cost of grid connection and power take-off system in the total capital expenditure	(−)
β	phase angle of excitation force to the incoming wave	(rad)
δ	phase angle between the current and terminal voltage	(rad)
γ	phase difference between the excitation force and the body velocity	(rad)
ζ_a	wave amplitude	(m)
η	wave elevation	(m)
θ, σ	angular coordinate and coordinate of the longitudinal axis in cylindrical coordinate system	(rad, m)
κ	weighting factor	(−)
λ	scale factor of the buoy	(−)
λ_e	scale factor of the generator	(−)
μ	overall conversion efficiency	(−)
μ_{rm}	recoil permeability of the magnets	(−)
ρ	material density	(kg/m^3)

ρ_{force}	force density of electrical machine	(N/m^2)
$\sigma_{\zeta a}$	standard deviation of wave elevation	(m)
σ_u	standard deviation of velocity	(m/s)
σ_F	standard deviation of PTO force	(N)
τ	intermediate variable in convolution	(−)
ϕ	phase angle of the incoming wave to the origin	(rad)
χ	operation availability of the WEC	(−)
ω	wave frequency	(rad/s)
ω_o	natural frequency of the WEC	(rad/s)
ω_e	generator frequency	(rad/s)
ω_j	wave frequency of j_{th} wave component	(rad/s)

LIST OF MATHEMATICAL OPERATORS

The following mathematical operation are used in this thesis:

$\hat{x}$	complex amplitude of x
Re$\{\hat{x}\}$	real part of x
$\overline{x}$	time-averaged value of x
$\lvert x \rvert$	absolute value of x
$\boldsymbol{x}$	vector of x
$< x >$	expected value of x

LIST OF ABBREVIATIONS

The following abbreviations are used in this thesis:

AEP	Annual energy production
AWS	Archimedes' Wave Swing
BIMEP	Biscay Marine Energy Park
CAPEX	Capital expenditure
CFD	Computational Fluid Dynamics
DK 2	DK North Sea Point 2
FD	Frequency domain
LCOE	Levelized cost of energy
OPEX	Operating expenditure
OWC	Oscillating water column
PM	Permanent-Magnet
SD	Spectral domain
SPD	Submerged pressure differential
TD	Time domain
PTO	Power take-off
RAO	Response amplitude operator
WEC	Wave energy converter

1

INTRODUCTION

Threatened by global warming and energy crisis, developing renewable energy is becoming a topic of utmost importance to our human-being in the next decades. Ocean waves carry a huge mount of clean energy, and exploiting energy from waves is expected to make a significant contribution to the energy transition. After being investigated and developed more than two hundred of years, most wave energy technologies are still not approaching a stage of being commercial.

This chapter gives a background of the energy transition and ocean wave energy, and the history of wave energy technologies is briefly introduced. As the high levelized cost of energy is hindering the commercialization of wave energy technologies, the research motivation is then presented and a primary research goal is defined as improving the techno-economic performance of wave energy converters from the perspective of systematic sizing. Particularly, systematic sizing in this thesis covers both buoy and power take-off sizing. In order to accomplish the primary research goal, two main research objectives are identified. Furthermore, the principal contributions, research scope, outline and approach of this thesis are presented in this chapter.

1

1.1. BACKGROUND: THE ROLE OF OCEAN WAVE ENERGY TOWARDS ENERGY TRANSITION

WITH the development of human society and industry, the global demand of energy has increased sharply during the last 70 years, as is shown in Figure 1.1. Currently, energy from fossil resources still plays the most important role in energy supply worldwide. For instance, in 2019, fossil fuels still account for 84 % of the global primary energy sources [1]. However, there are an amount of issues connected to fossil fuels, such as air pollution, climate change, energy crisis and sea level rise. In order to handle these problems and find a sustainable solution for human beings, it is necessary to put more efforts on the development of renewable energy.

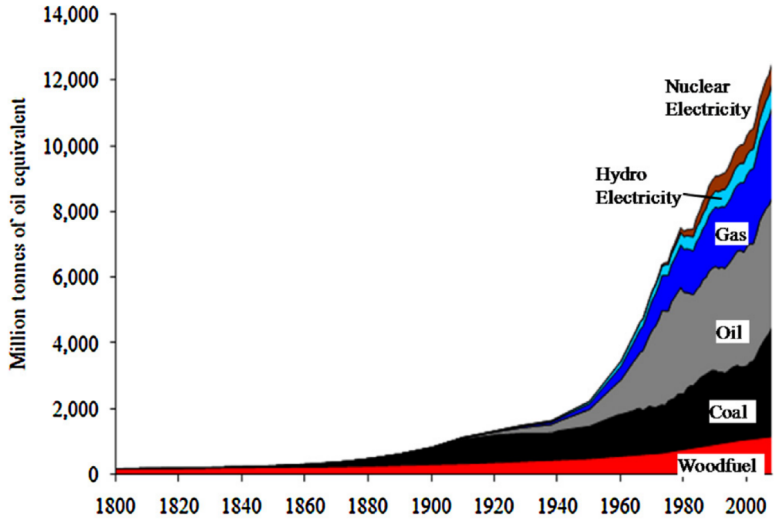


Figure 1.1: Global Primary Energy Consumption [2].

Over 70 % surface area of our planet is covered by seas and oceans. The oceans contain a variety of renewable energy resources, including offshore wind energy, tidal energy, ocean thermal energy, ocean salinity energy and wave energy. As stated in [3], the global potential of electricity generation from ocean energy is estimated to be between 20, 000 TWh and 80, 000 TWh per year, while the current annual energy consumption is around 16, 000 TWh worldwide. Thus, the exploitation of ocean energy is of significance to the global energy transition. Among these resources, ocean wave energy has a number of attractive properties. First, with an estimated worldwide theoretical potential around 8, 000 - 80, 000 TWh/year, ocean wave energy is one of the highest energy dense renewable resource [4]. Secondly, wave energy can be regarded as a kind of continuous input regardless of daytime or nighttime, which could be used as a supplementary resource to solar energy. Thirdly, wave energy is widely distributed across the world, which makes it generally accessible. The distribution of the global ocean wave energy resource is depicted in Figure 1.2.

The history of the human beings attempting to exploit ocean wave energy is long, and the first patented wave energy converter (WEC) is traced back to 1799 [6]. In modern times, wave energy has been receiving international attention since 1974 when Stephen Salter

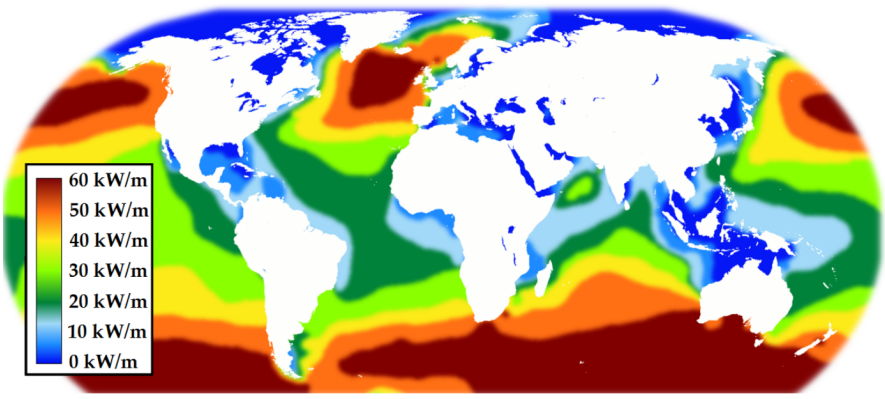


Figure 1.2: The global annual average wave energy transport [5].

demonstrated the feasibility of absorbing energy from ocean waves and proposed a concept of WEC known as "Salter Duck" in [7]. Later on, the exploitation of wave energy resource attracted much interest because of the global energy crisis that happened in the 1970s. Various wave energy converter concepts were proposed and patented at that time [8]. Entering 1980s, the dropping price of petroleum oil significantly slowed down the pace of wave energy research since the relevant funding was reduced [9]. After 2000, under the concern of climate change, the global society started to pay more attention to the development of renewable energy. Wave energy communities, therefore, received financial support to further investigate and test their concepts. Recently, towards the target of energy transition, developing wave energy technologies has been highlighted in the energy development plans of various countries, and a set of supporting policies were released nationwide or worldwide. For instance, both Wave Energy Scotland (WES) in UK and Department of Energy (DOE) in USA indicated that they are aiming at advancing wave energy technologies toward commercial viability by continuing funding relevant projects [10]. In the Netherlands, the Wadden Fund which is backed by the government has also provided financial support to demonstrate a wave energy pilot, namely the Slow Mill, in Texel island which is off the Dutch coast [11].

1.2. RESEARCH MOTIVATION: SIZING MATTERS TO THE TECHNO-ECONOMICS OF WECS?

A number of WEC concepts have been patented and some of the wave energy projects have reached the prototype stage and performed sea trial. However, the techno-economic competitiveness of WECs is much lower than other renewable energy technologies, such as wind, solar and tidal energy [12]. As estimated in *Ocean energy technology development report 2018* [13], the levelized cost of energy (LCOE) of wave energy ranged between 0.47 Euros/kWh and 1.4 Euros/kWh, with a reference value of 0.72 Euros/kWh; The LCOE of tidal energy was estimated to range between 0.47 and 1.02 Euros/kWh, with a reference value of 0.62 Euros/kWh. In [14], the LCOE of floating offshore wind technologies was estimated to be around 0.095 to 0.135 Euros/kWh. The high price of wave energy technologies is hin-

dering their advance towards the large-scale commercialization. In addition, as stated in the EU Offshore Renewable Energy Strategy [15], the targets of the LCOE for wave energy are 0.20 Euros/kWh by 2025 and 0.15 Euros/kWh by 2030. It clearly shows that wave energy technologies still have a long way to go toward the reduction of the LCOE.

In [16]–[18], it has been suggested that sizing is influential to the techno-economic performance of WECs. For WEC technologies, sizing or scaling refers to the procedure of determining the suitable scale of an individual WEC device for a given wave resource. Different from design optimization in the research and development phase, sizing hardly accounts for the variation of the buoy geometry or the principle of system components. Sizing is more relevant to the stages of commercialization or pre-commercialization of WECs. For instance, even for a mature technology, it is necessary to implement sizing before deployment. Because the characteristics of wave resources differ with the geographical location, the original scale of the device is only optimized for a specific sea site or a limited number of sea states. In addition, device-site paring is an important procedure prior to deployment [19], in which the techno-economic metrics of various WECs are evaluated for the sea sites and the optimal pair is then searched. However, the performance of WECs could vary with their size. Thus, in pursuit of a fair evaluation, it is important to conduct sizing of WECs for each wave resource during the evaluation. In this sense, the potential of each type of WEC can be better reflected.

Independently or integrated with other studies, sizing of WECs has been discussed in recent literature [17], [18], [20]–[25], in which the importance of sizing was identified for WECs which work as wave activated bodies. However, there is still a lack of analysis and methods of systematic sizing of WECs. The operating process of WECs is composed of two main stages: the power absorption stage and power conversion stage. The first stage is accomplished by the captor (or the buoy), in which the captor interacts with the incoming waves and absorbs the wave power typically as mechanical energy. The second stage is mainly achieved by the power take-off (PTO) system, where the absorbed power is converted into usable electricity during this stage. But the above-mentioned literature regarding sizing of WECs concentrated mainly on buoy sizing and the effects of PTO sizing are hardly considered. This inevitably weakens the effect of sizing on the improvement of techno-economic performance of WECs. On the one hand, as a core component in charge of power conversion, the PTO size is associated with the maximum force and power limits that the system could sustain. These limits could directly affect the power production. On the other hand, the PTO system accounts for a considerable proportion of the total capital expenditure (CAPEX), and it was normally estimated to be over 20 % [12], [26]. To improve the contribution of sizing to the techno-economic performance, it is essential to include both buoy and PTO sizing in a systematic manner.

To conclude, the core motivation of this thesis is to improve the feasibility of WECs because the current techno-economic competitiveness of WECs is clearly lower than other renewable technologies. Despite various factors affecting the techno-economic performance, this research focuses on the effects of sizing of WECs.

1.3. RESEARCH OBJECTIVES

In response to the motivation, the primary research goal of this thesis is defined as

To improve the techno-economic performance of WECs from the perspective of systematic

sizing.

The method is called "systematic sizing" because both the buoy and the PTO sizing are covered and implemented independently. The LCOE is used as the indicator for evaluating the techno-economic performance in this thesis. To accomplish the primary goal, two main research objectives need to be addressed:

Objective 1: Establish a systematic sizing method for WECs

In order to specify such a systematic sizing method, several challenges have to be addressed. First, since the buoy sizing and the PTO sizing have hardly been considered collectively in the techno-economic analysis, the first challenge is to build up a framework of the systematic sizing method for reducing the LCOE. Secondly, sizing could be considered as a kind of optimization requiring a number of iterations, where fast numerical models are preferred for saving computational time. To maintain both high efficiency and adequate accuracy, an alternative modeling technique, namely spectral domain (SD) modeling [27], to conventional time domain (TD) and frequency domain (FD) modeling is adopted for PTO sizing in this thesis. SD modeling can be regarded as an extension of FD modeling, is established based on statistical linearization and random phase assumption [28]. It could efficiently take nonlinear effects into account, and it is highly suitable for estimating statistical responses. But the particular nonlinear effects related to PTO sizing have not been considered in existing SD modeling. Thus, the second challenge is to further develop SD modeling to incorporate the nonlinear effect of PTO force constraints. Thirdly, PTO sizing will not only affect the dynamics of the device but also influence the electric generator efficiency and therefore this can make a difference to the delivered power output. Thus, the third challenge is to reveal the influence of the variation of the PTO size on its power conversion efficiency and further the PTO size determination. Therefore, corresponding to these three challenges, the first main objective can be divided into three sub-objectives:

- Establish a framework of the systematic sizing method of WECs to minimize the LCOE.
- Establish a computational-efficient numerical model for PTO sizing.
- Analyze the influence of PTO sizing on the power conversion stage.

Objective 2: Investigate the performance of the adjustable draft system on the power production of point absorbers with constrained PTO capacities.

This objective follows up the first objective, and it is intended to explore the possibility of improving the power production while maintaining the constraints of PTO capacity. Because the importance of downsizing PTO capacities has been suggested in the findings of the first objective.
In response to the second objective, a novel concept, namely the adjustable draft system, is proposed for point absorbers to improve the power production with constrained PTO capacities. This system enables the variation of the dynamic properties by regulating the buoy draft, which expands the suitability of WECs to different wave conditions. As a novel design, its impacts on the dynamics and power production of WECs remains to be studied.

In this thesis, the effects on both the power absorption and the power conversion stages of the novel concept are covered.

1.4. PRINCIPAL CONTRIBUTIONS

The main contributions of this thesis can be summarized as

- Analysis of the collective influence of buoy sizing and PTO sizing on the techno-economic performance of WECs.
- Development of spectral domain modeling to incorporate the nonlinear effect of the PTO sizing in an efficient manner.
- Analysis of the PTO sizing effects on the power conversion efficiency of linear PM generators in WECs.
- Proposal and investigation of the adjustable draft system for improved power production of point absorbers with constrained PTO capacities.

1.5. RESEARCH SCOPE

The main scope of this research is defined as follows. First, despite the variation of wave energy technologies, this work focuses on heaving point absorbers. Thus, the main discussions and conclusions drawn in this thesis are limited to this particular type of device. However, the sizing method proposed in this thesis is applicable to other types of WECs. Secondly, this thesis is intended to investigate the sizing of a single WEC. The hydrodynamic interaction between WECs in wave farms and the influence of the device number on the economic modeling are not taken into account. However, a good understanding of a single WEC sizing is crucial to the sizing of WEC farms. Thirdly, the linear PM generator is the main interest of this thesis when investigating the influence of sizing on the power conversion efficiency of PTO systems. The variation of the application of PTO systems is not considered. Fourthly, only a simplified economic model is applied in this thesis. The influence of economic parameters on the sizing of WECs is not considered, but it is realized that economic modeling could play a role in size determination. Fifthly, the numerical models applied in this work focus on the operational regions of WECs. Thus, the representation of wave resources is simplified to be unidirectional linear waves. The hydrodynamic coefficients of WECs are derived based on linear potential flow theory, in which the fluid is assumed to be irrotational, inviscid and incompressible [29].

1.6. OUTLINE AND APPROACH

Figure 1.3 illustrates the outline of this thesis. Chapter 1 introduces the background, motivation, research objectives, questions and structure of this thesis. Chapter 2 reviews the development and challenges of wave energy technologies. Chapter 3 to 5 are constructed to achieve the first main objective, and Chapter 6 to 7 are concentrated on the second main objective. The following text details the functions of each chapter.

- **Chapter 2: Wave Energy Technology and Sizing of Wave Energy Converters**
  The main purpose of this chapter is to present an overview of wave energy conversion,

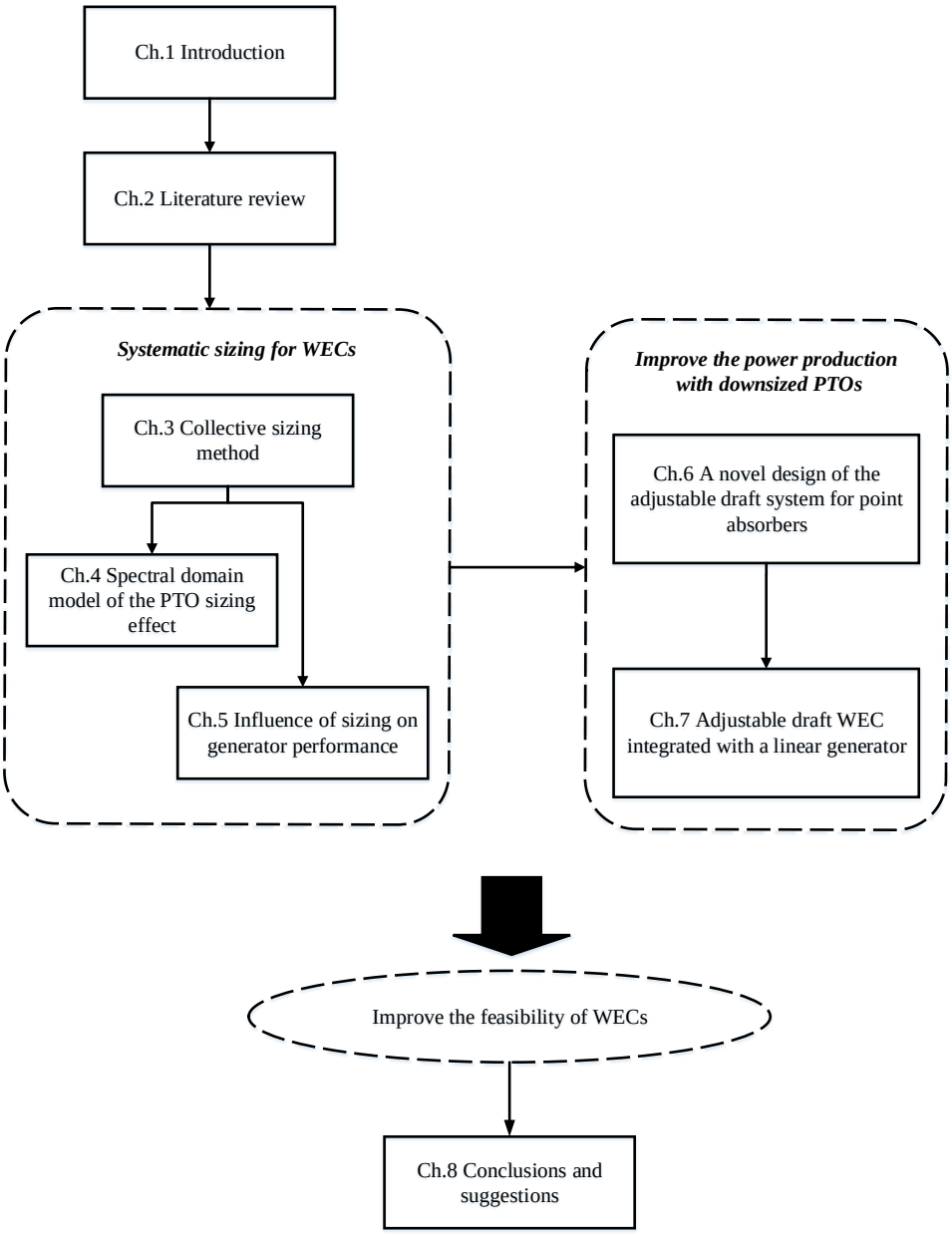


Figure 1.3: The outline of this thesis.

in which the wave energy concepts and PTO systems are reviewed respectively. The second purpose is to review the recent studies related to sizing of WECs.

- **Chapter 3: A Collective Sizing Method for WECs**
  In this chapter, the effect of sizing on the techno-economic performance will be discussed with a focus on a generic spherical point absorber. A collective sizing method is proposed to minimize the LCOE of the WEC, in which the PTO sizing and buoy sizing are simultaneously considered. The benefits of PTO downsizing are identified. Furthermore, a comparison between the proposed method and existing sizing methods is made.

- **Chapter 4: A Spectral Domain Model for PTO Sizing**
  In the previous chapter, PTO sizing was performed based on the FD approach which is efficient but not able to contain nonlinear terms. To improve the accuracy of the PTO sizing and retain the computational efficiency at the same time, a spectral domain model is developed in this chapter to incorporate the PTO force saturation. The proposed model is verified against the results obtained from the nonlinear TD model. Furthermore, a case study is made to demonstrate the performance of this model in the application of a techno-economic analysis. The chapter aims to provide an efficient and accurate tool for the PTO sizing.

- **Chapter 5. The Influence of PTO Sizing on the Power Conversion Efficiency**
  This chapter is dedicated to improving the accuracy of the proposed sizing method. In previous chapters, PTO sizing has been discussed and its importance to the techno-economic performance has been shown. However, the effects of PTO sizing on the power production of WECs contain two aspects. First, the PTO sizing implies the physical limits like force, power and stroke constraints which actually limit the maximum energy absorbed by WECs. Secondly, for electrical generators, the PTO sizing also has an influence on their conversion efficiency. The last aspect is not considered in the previous chapters where the PTO efficiency is assumed to be constant regardless of its size. Focusing on the linear permanent magnet (PM) generator, this chapter investigates the influence of linear generator sizing on its conversion efficiency and finally the techno-economic performance.

- **Chapter 6: Improving the Power Production with a Downsized PTO Capacity: Adjustable Draft System**
  The previous chapters indicate that suitably downsizing PTO capacity is beneficial for improving the techno-economic performance of WECs. The work in this chapter is dedicated to improving the power production of point absorbers especially with the downsized PTO capacities. A novel design, namely the adjustable draft system, is proposed for point absorbers. This chapter covers the conceptual design and numerical analysis of the power production. In the numerical analysis, a FD model and a nonlinear TD model are implemented respectively, and their results then are compared. The power production of this proposed design is calculated for different wave conditions.

- **Chapter 7: The Performance of the Adjustable Draft Point Absorber Integrated with a Linear PM Generator**

As an extension of the previous chapter, this chapter is intended to exploring the performance of the adjustable draft point absorber coupled with a linear PM generator. A wave-to-wire model is established to comprehensively evaluate the usable power delivered to grid and the overall efficiency of the WEC. Subsequently, a close look on the negative effects resulting from the draft adjustment on the power production of WECs is presented. Furthermore, the power production of the integrated system with downsized PTO capacities is identified for both regular and irregular waves. Finally, a power comparison is performed between the integrated system and conventional point absorbers.

- **Chapter 8. Conclusions and recommendations**
  This chapter summarizes all the work in this thesis and indicates the future work of interest in the closely related research directions.

2

WAVE ENERGY TECHNOLOGY AND SIZING OF WECS

In this chapter, two main aspects are addressed. Firstly, WEC technologies are reviewed and classified. The operating principle of each type of WEC is introduced. Subsequently, PTO mechanisms commonly utilized in wave energy conversion are briefly reviewed. The advantages and disadvantages of each category of PTO systems are summarized. Particularly, a literature review of the application of linear generators in wave energy conversion is presented, since in the following up chapters the influence of PTO system sizing on its power conversion efficiency is investigated with regard to linear generators. Secondly, as an approach to improve the techno-economic performance, the function and importance of sizing of WECs are introduced. Three common methods applicable for sizing are reviewed and compared.

Parts of this chapter have been published in the paper: Tan J, Polinder H, Wellens P, et al. The Fair Evaluation of Wave Energy Converters [C]//The 39th International Conference on Offshore Mechanics and Arctic Engineering (OMAE). American Society of Mechanical Engineers, 2020. [30].

2.1. INTRODUCTION

As introduced in Chapter 1, the history of research and development of wave energy conversion has been more than two hundred of years. However, compared with other renewable technologies, wave energy technologies haven't shown a tendency of convergence. For instance, it is known that the technical development way of wind turbines has quickly converged to the current technology of three blades. Comparatively, as reported in [31], over one thousand of WEC concepts have been patented worldwide. As the design of the PTO system is inherently related to the principle of power capture of the technology, various types of PTO systems exist. To have an insight into wave energy conversion, it is necessary to provide an overview on the classification and working principles of the typical wave energy technologies and PTO systems. Thus, a brief review of wave energy technologies is given in subsection 2.2.

It has been introduced in Chapter 1 that the high LCOE is hindering the development of WECs. With an aim to improve the feasibility, this thesis is intended to investigate the influence of sizing on the techno-economic performance of WECs. The effects of sizing should be considered from two perspectives:

- On the dynamics of WECs
  Sizing could make a difference to the motion of WECs under the excitation of ocean waves. Natural frequency is an important parameter reflecting the dynamic characteristics of a system. It is described as the frequency at which the system tends to oscillate in the absence of any driving or damping force. For a floating heaving buoy consisting of a rigid body, its natural frequency is proportional to the square root of the hydrostatic stiffness and inversely proportional to the square root of the mass. Further, the hydrostatic stiffness is proportional to the water-plane area of the buoy, while mass is proportional to the volume if assuming a constant buoy density. Then, if the device is resized based on geometrical similarity principles, the scaling ratios for the volume and area are different. In this sense, the natural frequency is also changed. In addition, sizing varies the buoy volume as well as the wetted surface, which leads to changes in hydrodynamics of WECs, including excitation force, added mass and radiation damping. As electricity generation of WECs relies on their movement, the changes in dynamics are subsequently reflected in the power production.

- On the cost of WECs
  It can be expected that the cost is strongly related to the size of the devices. For the same technology, the larger size of devices implies more materials, labour, a higher requirement on transportation and deployment. As a result, the cost is correspondingly higher.

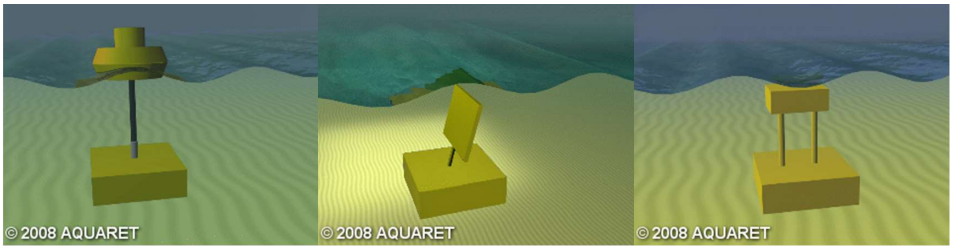
The influence of sizing on the economic viability of WECs has been discussed in the existing literature. In [17], [18], the techno-economic indicators of different types of WECs were investigated and compared, and various sea sites were considered. It was indicated that the sizing could make a notable difference to the economies of WECs, and the optimal size of the WEC is dependent on the wave resource, principle of the technology and the estimation of the operational expense (OPEX). Recent studies [32], [33] suggest that smaller WECs are more likely to contribute to economic success. Because the response nature of downsized WECs could better match the inherent oscillatory characteristic of ocean waves,

the capacity factor which is defined as the average power production by the rated power of the WEC [23] can be increased by downsizing. To include sizing into the techno-economic assessment of WECs, it is essential to adopt an efficient approach to estimate the power performance of WECs in a range of scales. Thus, subsection 2.3 of this chapter presents a review of sizing methods applied in the field of WECs.

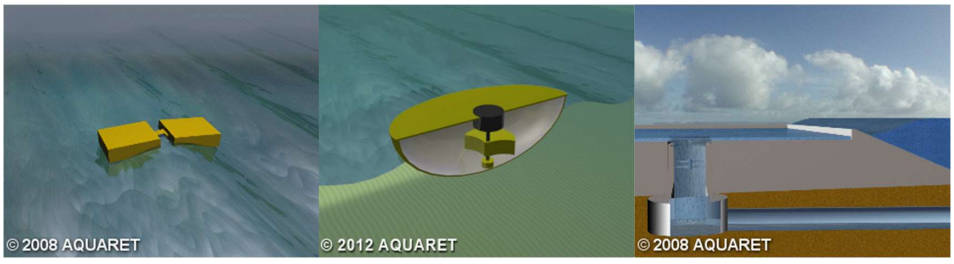
2.2. REVIEW OF WAVE ENERGY TECHNOLOGIES

2.2.1. OVERVIEW OF WAVE ENERGY CONVERTERS

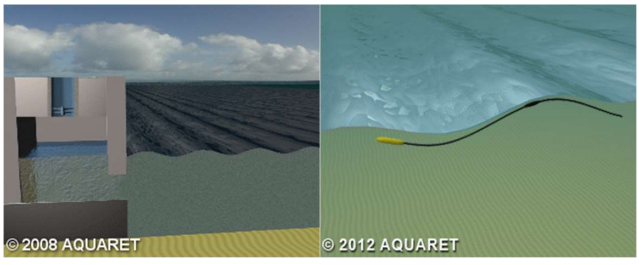
The classification of WECs has been discussed in a number of papers, and existing WECs can be categorized by various criteria [9], [35]–[37]. Based on the working principle and orientation of devices to the incoming waves, WECs can be categorized as eight different types of devices, and their schematics are illustrated in Figure 2.1. It should be acknowledged that first five types of WECs shown in the figure are also often categorized as one more type of



(1) Point absorber (2) Oscillating surge converter (3) Submerged pressure differential



(4) Attenuator (5) Rotating mass (6) Overtopping device



(7) Oscillating water column (8) Bulge wave

Figure 2.1: The classification of WECs [34]. (Images from The European Marine Energy Center LTD)

devices, namely "oscillating bodies" [36]. Each type of devices is introduced in more detail in the following text.

- Point absorber
  The horizontal dimension of point absorbers' captors is small compared with the incoming wavelength, and therefore they are not sensitive to the wave direction. The relative motion between the captor and PTO system is converted to useful energy. Depending on the operating region with regard to the sea surface, point absorbers can be further divided into the floating type and submerged type. CETO is a typical submerged point absorber [38] and Wave Star is an example of floating point absorbers [39]. Figure 2.2 and 2.3 illustrate these two WECs.

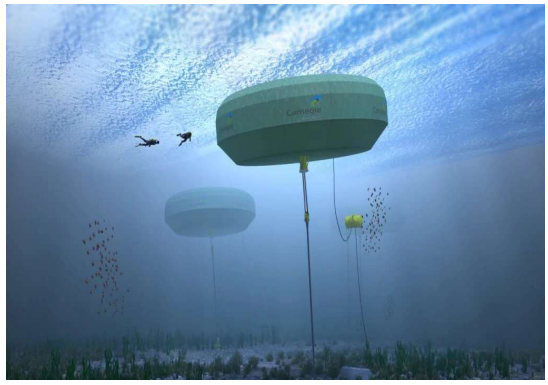


Figure 2.2: Artist impression of CETO 6 WECs [40].



Figure 2.3: Artist impression of Wave Star WECs [41].

- Oscillating surge converter
  Oscillating wave surge converters extract energy from the surge motion of waves. The arm of the device rotates as a pendulum mounted on a joint in response to the action of waves. This type of WECs is thought of as a solution for nearshore regions. Oyster is an example of oscillating wave surge converters [42], which is shown in Figure 2.4.

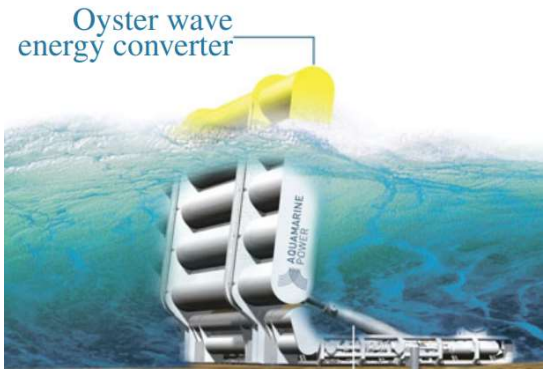


Figure 2.4: Artist impression of Oyster WEC [42].

- Submerged pressure differential
  SPD (Submerged pressure differential) WECs could also be regarded as a kind of point absorbers. SPD devices are operating under the sea surface. In ocean waves, the free surface is oscillating, which leads to a pressure change on the top cap of the captor. As a result, the pressure difference between the inside and outside surfaces of the buoy drives the captor to move up and down. Archimedes' Wave Swing (AWS) is a SPD device [43], which is shown in Figure 2.5.



Figure 2.5: AWS WEC [44].

- Attenuator
  Attenuators are a kind of WECs in which the floater is parallel to the dominant incoming wave direction. This type of devices could absorb energy from the relative motion between their pitching bodies when waves pass through. Pelamis is an example of the attenuator [45], which is shown in Figure 2.6.

- Rotating mass
  Rotation mass devices usually contain two main components: a hull and a rotating



Figure 2.6: Pelamis WEC [45].

mass object inside the hull. Subjected to incoming waves, the dynamic coupling of these two parts results in the gyroscope-like or pendulum-like movement of the inside mass. This movement drives the electric generator to produce electricity. Wello Penguin, shown in Figure 2.7, is a typical rotating mass wave energy converter [46].



Figure 2.7: Wello Penguin WEC [46].

- Overtopping device
  Overtopping devices capture water as incoming waves break into their storage reservoir. The water is then returned to the sea passing through a conventional low-head hydro turbine, by which electricity is generated. WaveDragon is known as one type of overtopping WECs [47], and it is shown in Figure 2.8.

- Oscillating water column
  Oscillating water column converters comprise two key elements: a collector chamber and an air turbine. When the incoming waves approach the devices, the water is driven into the chamber and air in the chamber is compressed. Then the air inside the chamber is forced to pass through the turbine, in which the energy can be converted.



Figure 2.8: WaveDragon WEC [47].

OWC converters can be either integrated with a fixed structure or a floating platform [48]. Figure 2.9 shows the OWC wave power plant integrated into a breakwater located in Mutriku.



Figure 2.9: OWC power station of Mutriku [40]

- Bulge wave WEC
  The main body of a Bulge WECs is a flexible rubber tube filled with water. The pressure change resulting from incoming waves creates a bulge wave inside the tube. The bulge wave propagates as the incoming wave moves, and the rectified flow is then built. The PTO system is located at the end of the tube to capture the kinetic energy gathered by the flow [49].

Figure 2.10 depicts the proportion of different categories of WECs worldwide. It suggests that the point absorber is the most popular type of WECs [50]. Compared to other technologies, this type of WECs has the main advantages of low design complexity and high absorption efficiency [51]. Therefore, in the following chapters of this thesis, the point absorber is considered as a suitable research reference.

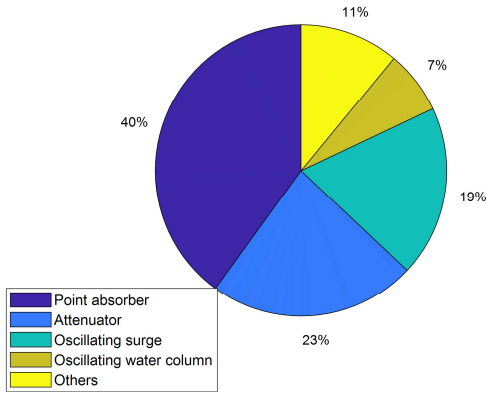


Figure 2.10: Distribution of existing WEC projects by the classification [50].

In addition to the above classification, WECs can also be sorted by other criteria. Depending on the location of deployment, WECs can be classified as onshore, nearshore and offshore devices [52]. According to the orientation of the WECs to the incoming waves, WECs can be classified as terminators, attenuators and point absorbers [31]. WECs can also be categorized up to the adopted PTO systems, in which pneumatic, hydro, hydraulic and direct drive PTO systems are included [37]. Although the classification differs in scientific publications, this thesis is not intended to address or compare the classification criteria.

2.2.2. OVERVIEW OF POWER TAKE-OFF SYSTEMS

The PTO system is in charge of converting the absorbed power to usable electricity in wave energy conversion. The PTO systems in WECs can be divided into five types according to the characteristics of their transmission stages. Figure 2.11 is commonly used to illustrate the power flow in different PTO systems. A general overview of these PTO systems is given below.

- Hydraulic PTO
  In hydraulic PTO systems, the motion of a buoy drives the hydraulic piston to increase the pressure of the working medium. Then the pressure of the medium is raised sufficiently high in an accumulator to rotate the hydraulic motor. The hydraulic PTO is robust and able to provide large forces at low frequencies, which highly matches the dynamic characteristics of WECs. Hydraulic PTO systems were widely used in WECs, such as Pelamis and Edinburgh Duck [53]. However, hydraulic PTO systems contain plenty of moving parts, which results in their complex structure. As a consequence, regular system maintenance and inspection are normally required, which is time-consuming and costly [37]. In addition, conversion efficiency of hydraulic PTO systems are relatively low with regard to mechanical PTO systems and linear generators [54].

- Hydro PTO
  The hydro PTO mainly refers to the hydro turbines. This type of PTO systems is commonly employed in overtopping devices, such as WaveDragon [47]. The water collected by the device is stored in the reservoir and flow back to the ocean through

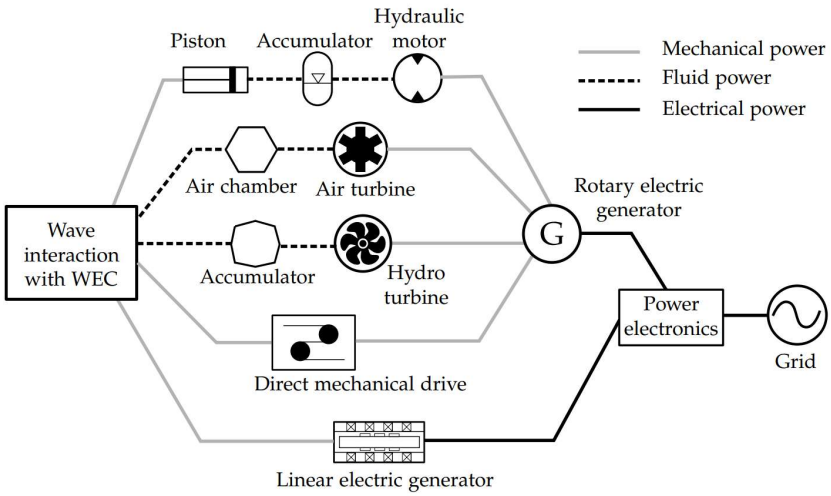


Figure 2.11: Typical PTO mechanisms applied in wave energy conversion [5].

the hydro turbine. Although medium-head to high-head hydro turbines have been adopted in the field of power conversion over a long time and their technologies are mature, the main applications in WEC are low-head hydro turbines which are currently associated with low technological maturity. [37], [55]. Another big challenge of the hydro PTO based systems is not related to itself but the low power capture efficiency of overtopping devices [24].

- Pneumatic PTO
  The pneumatic PTO systems refer to air turbines, and they are generally employed in OWC converters. The air turbines are driven by the oscillating air pressure in the air chamber [56], and the generator coupled with the turbines is rotated to produce electricity. Similar with the hydro PTO systems, air turbines are also a mature technology. However, due to the bi-directional air flow, traditional air turbine can not be directly used in OWC converters. To solve this problem, non-return valves could be applied to rectify the air flow. However, the addition of non-return valves increases the complexity of the system and make the maintenance of the system harder. Another limitation of the non-return valve systems is that they are not suitable for devices with large power rating. Alternatively, self-rectifying air turbines can be implemented as the pneumatic PTO system in OWC converters. This kind of air turbines can rotate in the same direction regardless of air flow directions. Among self-rectifying turbines, Wells turbines and impulse turbines are two commonly reported ones.

- Mechanical PTO
  In the mechanical PTO system, a gearbox is used to convert the linear movement of the buoy to rotary motion for fitting conventional rotary generators. The oscillation

of the buoy of WECs is of low speed due to the characteristics of ocean waves. For improving the efficiency, another important function of the gearbox is to increase the speed of motion. In [57], a point absorber equipped with a bidirectional gearbox and rotary generator was introduced.

- Direct-drive linear generator
  The linear generator could be used as the direct-drive PTO system in the oscillating body WECs, and they are usually used in point absorber wave energy converters, such as AWS [58]. In direct-drive linear generators, intermediate transmission interfaces, such as gearbox and hydraulic motors, are not necessary. Instead, the oscillating buoy is directly coupled with the translator of the linear generator. The linear generators are commonly associated with higher efficiencies compared with other PTO systems. This is because there are fewer transmission losses resulting from a reduced number of energy conversion steps [37], [58]. In addition, the reduced number of components in the PTO system increases the reliability of the whole WEC system [59]. The linear generator has been thought of as an appealing solution for wave energy technologies among all types of PTO systems because of the mentioned advantages. Hence, this thesis concentrates on the WECs with a linear generator when investigating the influence of PTO sizing on power conversion efficiency in Chapter 5.

2.2.3. LITERATURE REVIEW OF LINEAR GENERATORS IN WAVE ENERGY CONVERSION

The focus of this thesis is on the linear generator among different PTO systems when investigating the influence of the PTO sizing on the overall sizing and the techno-economic performance in the following chapter. Therefore, the application of linear generators in wave energy conversion is particularly reviewed here. Linear generators have been investigated and developed for application in WECs over many years. Several WEC prototypes equipped with a linear generator have been successfully designed and tested in real oceanic environments [60], [61]. So far, three full-scale WEC technologies equipped with the linear generator, excluding their updated versions, have been successfully tested in real oceanic climates. The key information of their prototypes is presented in Table 2.1.

Table 2.1: WECs applying the linear generator tested in the oceanic environment.

Parameters	AWS	Uppsala concept	SeaBeavI
Rated power	2 MW	10 kW	10 kW
WEC type	Submerged PA	Floating PA	Floating PA
Generator structure	Bottom founded	Bottom founded	Floating
Generator topology	Flat and double sided	Flat and four sided	Tubular
First tested time	2004	2006	2007
Testing site	Portugal	Sweden	USA

The AWS was the first large-scale WEC project using the linear generator [58]. It is a fully submerged WEC device, and it produces energy relying on the pressure difference on the moving part of the device when the ocean wave passes above. The linear generator in the AWS was designed to be doubled-sided to avoid huge attractive forces between the stator

and translator. The first full-scale AWS prototype was tested in 2004 in Portugal, as shown in Figure 2.5 [44]. The maximum peak power of the tested prototype was 2 MW, which is remarkably high in the field of wave energy conversion [61]. Uppsala university developed a floating point absorber WEC concept, and the first full-scale prototype was deployed and tested at the Lysekil research site in Sweden in 2006. Figure 2.12 shows the prototype prior to installation. Since then, thirteen follow-up prototypes have been deployed [62]. This WEC consists of a floating buoy and a linear generator founded on the seabed. The buoy is connected to the translator of the generator through a connection line. In the generator, the translator moves vertically along the rail, and four stator packages are mounted on a pillar fixed at the foundation structure [60]. Oregon State University developed a dual-body WEC in which a linear generator was incorporated, called SeaBeavI Project [63]. The ocean testing of its 10 kW prototype was performed in Yaquina Bay in 2007, and the photo of the prototype just before installation is shown in Figure 2.13. This WEC includes a moored cylindrical spar and a floating buoy. The heave motion of the spar is restrained by the mooring system, but the buoy is free to move vertically relative to the spar. In this concept, the spar and buoy act as the translator and stator of the linear generator respectively. The coils are wound on the interior surface of the spar and permanent magnets are placed on the buoy. Furthermore, this generator was configured as a tubular geometry [59]. These three linear generators share some common features. First, all of them are permanent-magnet (PM) synchronous machines. Second, they are all longitudinal flux machines. Since the successful tests of these three concepts, a series of extensive studies have been performed. They were mainly intended to address the negative characteristics of linear generators when serving WECs.

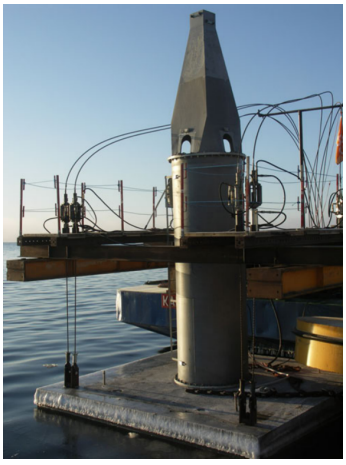


Figure 2.12: The first prototype of Uppsala concept before it was installed at Lysekil research site [64].

The application of linear generators in wave energy conversion also faces some challenges. Firstly, the dimensions of linear generators are much larger than standard electrical machines for sustaining a similar power level. This results from the low typical speed of WECs. One solution to reduce the dimension is the use of transverse flux linear machines. The advantage of the transverse flux machines is the high force density, which results from the flux concentration and decoupled magnetic and electrical circuits [65]. In [66]–[68],



Figure 2.13: The prototype of SeaBeavI project prior to installation in Yaquina Bay [63].

WECs with transverse flux linear generators were investigated, in which a lower cost of permanent magnets and higher force/power density were indicated. However, their fabrication is much more complex than the longitudinal flux machines, and their leakage paths also lead to low power factors [65]. As a consequence, they have not been as of much interest as the longitudinal flux machines in the field of WECs. Another possible solution is to increase the movement speed of WECs. For example, a speed amplified linear generator was proposed for a WEC concept in [69], and the relative speed between the stator and translator was therefore increased. The second challenge is a general one for all PTO systems applied in WECs, that is, the power conversion efficiency is still limited. This is because the motion of the object excited by ocean waves is normally in low speed. In linear generators, the induced voltage is also low because of the low motion speed of the captor, and then a large current is required to produce the desired generator force. In this case, the resistive losses on the conductors are high. In [70]–[72], superconducting linear generators were studied to improve it. The results showed that superconducting generators could clearly contribute to the high efficiency and force density. This is because they are associated with less resistivity and a stronger magnetic field compared to conventional machines. However, the difficulty and high expense of making the cryogenic temperature in an oceanic environment are still hurdles in practice.

2.3. REVIEW OF SIZING METHODS OF WECS

The relevant sizing methods have been discussed independently or integrated with evaluation studies. In 1978, an analytical method was first derived to depict the relation of the theoretical power limit of point absorbers with the buoy volume, and it is known as Budal diagram [73]. By means of this method, the power capture potential of a certainly sized WEC can be approximated, which could be supportive for the size determination [20], [21]. In the techno-economic assessment or site-matching studies, the power performance of the considered WECs in their original scales is normally given explicitly by previous work and described in the form of a power matrix. Therefore, Froude similarity can be applied to efficiently obtain power production of scaled devices. Then, combining with economic models to estimate the cost, the techno-economic metrics are revealed for differently sized WECs [17], [18]. Sizing has also been taken into account in studies addressing geometry op-

timization and performance identification, in which numerical modeling is majorly used to predict the power performance of WECs in each size. The biggest advantage of using the numerical simulation for each device size is to enable the incorporation of the variation of design parameters during sizing. In this subsection, literature related to the above-mentioned three sizing methods is reviewed.

2.3.1. FROUDE SIMILARITY

Froude scaling is commonly used in the field of ocean engineering to achieve the dynamic similarity between full-scale prototypes and scaled models. During Froude scaling, the Froude number of the concerned models should be maintained consistent. The Froude number (F_r) is a dimensionless quantify which is defined as the ratio between inertial force and gravitational force imposed on the object [74]. The Froude number is calculated as

$$F_r = \frac{u}{\sqrt{gG}} \tag{2.1}$$

where u is the local flow velocity, g is the gravitational acceleration and G is the characteristic length of the object.

If the power performance of originally sized WECs has been identified and the WECs are scaled following Froude scaling, the power performance of resized devices can be directly predicted based on Froude similarity. Mostly, the performance of the originally sized WECs is characterized by the form of a power matrix [75]. This method enables efficient estimates of power matrices of WECs at various scales. If scale factor is $\lambda = G_c/G_o$, in which G_c and G_o represent the characteristic lengths of scaled and original WEC respectively, other parameters could be related as shown in (2.2) to (2.6) [74].

$$\text{Force}: \quad \frac{F_c}{F_o} = \lambda^3 \tag{2.2}$$

$$\text{Velocity}: \quad \frac{u_c}{u_o} = \lambda^{0.5} \tag{2.3}$$

$$\text{Power}: \quad \frac{P_c}{P_o} = \lambda^{\frac{7}{2}} \tag{2.4}$$

$$\text{Wave height}: \quad \frac{H_c}{H_o} = \lambda \tag{2.5}$$

$$\text{Wave period}: \quad \frac{T_c}{T_o} = \sqrt{\lambda} \tag{2.6}$$

where subscripts c and o embody the scaled model and original model respectively. Given its high efficiency, this method has been widely applied to conduct sizing of WECs in techno-economic studies. In Table 2.2, an overview of the literature of using Froude similarity to account for sizing effects of WECs is presented.

However, this method is associated with some limitations. Firstly, the environment parameters in the power matrix, which are normally T_z and H_s, are accordingly scaled during Froude scaling. In order to calculate the power production, the scaled power matrix needs to match the scatter diagram of the concerned wave resource, and then data fitting techniques, namely the interpolation or extrapolation, have to be applied [18]. This inevitably

Table 2.2: Sizing studies of applying Froude similarity to calculate the power performance.

Authors	Year	WEC type	Sizing range	Sea sites
M. O'Connor, et al. [18]	2012	Pelamis and WaveStar	250 to 1000 kW	6 European sites
S. Bozzi, et al. [76]	2014	AquaBuOY, Pelamis and Wave Dragon	Scaling factor of 0.1 to 1	2 sites in Italian offshore
C. Iuppa, et al. [77]	2015	10 devices	Scaling factor of 0.1 to 1	West side of Sicily
A. de Andres, et al. [17]	2016	Floating PA	25 to 2000 kW	6 European sites
S. Bozzi, et al. [78]	2018	8 devices	Scaling factor of 0.1 to 1	Mediterranean coastline
M. Majidi Nezhad, et al. [79]	2018	WaveStar, Oyster, Wave Dragon and AWS	290 kW to 2400 kW	Western coast of Sicily
W. Monteiro, et al. [80]	2018	Wave Dragon , Pelamis and AquaBuoy	Scaling factor of 0.2 to 1	Leeward islands of Cabo-Verde
Joao Morim, et al. [81]	2019	10 devices	Scaling factor of 0.1 to 1	Central coastal shelf of New South Wales in Southeast Australia
S. Oliveira-Pinto, et al. [82]	2020	CETO, Langlee, Pelamis and Wavebob	± 30 % deviating from 1	Global Oil and Gas offshore platform site
A. Majidi, et al. [33]	2021	15 devices	Scaling factor of 0.1 to 1	Southwestern coast of the Black Sea

brings some uncertainties, especially when the scaling ratio is largely deviating from one. Secondly, Froude scaling is not typically applicable for losses in power conversion stages, such as mechanical bearing losses and electrical losses in generators or power electronic components. It could be argued that these losses don't account for a significant portion, but it also depends on the design and sizing of electric machines [83]. Thirdly, the rated force and power of the scaled devices are inherently assigned during Froude scaling, and consequently, the adaptation of PTO rating to different wave resources is strongly limited.

In this sense, the PTO rating of the scaled devices is dependent on the original rating, but the original PTO system is only sized for a specific wave resource. PTO systems cannot only make a difference to energy absorption and conversion but also make up a notable proportion of the total CAPEX. As a result, the lack of considering the PTO system sizing could lead to a poor estimate of the overall sizing of devices and further unfair evaluation of WECs.

2.3.2. BUDAL DIAGRAM

The Budal diagram was originally proposed to describe the power absorption bounds of point absorbers. It consists of two bounds in regular wave conditions, namely P_A and P_B. P_A bound is related to the maximum amount of energy that could be extracted from the incoming wave, while P_B reflects the bound of energy that could be absorbed by realistically sized WECs. The derivation is briefly introduced below, and more details are given in [21], [84]

In harmonic waves, the excitation force, displacement and velocity of the moving buoy of a WEC could be expressed as

$$F_{e,i}(t) = \mathrm{Re}\{\hat{F}_{e,i} e^{i\omega t}\} \tag{2.7}$$

$$s_i(t) = \mathrm{Re}\{\hat{s}_i e^{i\omega t}\} \tag{2.8}$$

$$u_i(\mathrm{t}) = \mathrm{Re}\{\hat{u}_i e^{i\omega t}\} \tag{2.9}$$

where $\hat{F}_e$, $\hat{s}$ and $\hat{u}$ are complex amplitudes of the excitation force, displacement and velocity of the body respectively, and ω is the angular frequency of incoming waves. In addition, i represents the degree of freedom, equations (2.7), (2.8) and (2.9) describe the motion of the buoy in mode i. Assuming the device is only moving in heaving direction (along z-axis), hereafter the derivation is only discussed in this degree of freedom. Then, the time-averaged absorbed power of the moving body could be expressed as (2.10).

$$\overline{P}_a = \overline{P}_{exc} - \overline{P}_r = \frac{1}{2}\left|\hat{F}_e\right||\hat{u}|\cos\gamma - \frac{1}{2}R_r|\hat{u}|^2 \tag{2.10}$$

where $\overline{P}_a$ is time-averaged absorbed power, $\overline{P}_{exc}$ is time-averaged excitation power, and $\overline{P}_r$ is time-averaged radiated power. $\left|\hat{F}_e\right|$, $|\hat{u}|$ and γ are the amplitude of the excitation force, the amplitude of the body velocity, and the phase difference between the excitation force and the body velocity respectively. R_r is the hydrodynamic damping of the body. If the optimum phase is selected, the phase difference is 0 with $\cos\gamma$ =1, and the global optimal velocity amplitude could be expressed as

$$|\hat{u}|_{OPT} = \frac{\left|\hat{F}_e\right|}{2R_r} \tag{2.11}$$

Hence, in this optimal condition, the relation between $\overline{P}_a$, $\overline{P}_{exc}$ and $\overline{P}_r$ could be expressed as

$$\overline{P}_{a,max} = \frac{\left|\hat{F}_{exc}\right|^2}{8R} = \left(\overline{P}_r\right)_{OPT} = \frac{1}{2}\left(\overline{P}_{exc}\right)_{OPT} \tag{2.12}$$

here, $\overline{P}_{a,max}$ is the maximum absorption power. Corresponding to the conditions of high wave frequency and low wave frequency, two theoretical power limits P_A and P_B can be further derived based on (2.10) and (2.12).

- P_A: power limit in high frequency waves
  At high frequency wave conditions, the $|\hat{u}|_{OPT}$ can easily be reached. This is because the maximum velocity amplitude of the oscillating body is related to the wave frequency and the maximum motion amplitude $|\hat{s}_m|$, which can be expressed as

$$|\hat{u}_m| = \omega|\hat{s}_m| \tag{2.13}$$

  where ω is the wave frequency, $|\hat{u}_m|$ is the maximum velocity amplitude of the oscillating body. With the optimal velocity $|\hat{u}|_{OPT}$, the optimal absorbed power could be obtained as expressed in equation (2.12). Based on Haskind relation [21], the heaving excitation force of an axisymmetric body relates to the hydrodynamic damping in heaving direction as

$$R_r = (\frac{k}{8J_{re}})|\hat{F}_e|^2 \tag{2.14}$$

  where k is the wave number; J_{re} is the wave-power transport per unit frontage of the incident regular waves. Then, if the deep water condition is assumed, the first power bound P_A for heaving point absorbers could be expressed as

$$P_A{=}\overline{P}_{a,max}{=}\frac{J_{re}}{k} = \frac{\rho g^3 H^2 T^3}{128\pi^3} \tag{2.15}$$

  here, ρ is the water density; g is the gravity acceleration; H is the wave height, and T is the wave period.

- P_B: power limit in low frequency waves
  In low frequency wave conditions, according to (2.13), it can be deduced that the maximum velocity amplitudes would be too low to meet the optimal velocity $|\hat{u}|_{OPT}$ in (2.11). Then, the maximum velocity that the buoy could actually achieve plays a role in the estimation of the power limit. The maximum velocity is dependent on the designed motion limit (maximum motion amplitude) which is associated with the size of the buoy. A fair assumption can be made that the heaving motion amplitude of the buoy is designed to be lower than the half of its vertical dimension [84]. Assuming a constant cross-sectional area of the buoy in vertical direction, the maximum motion limit and the maximum heaving velocity can be reasonably approximated as

$$|\hat{s}_m| < \frac{V}{2S_{wl}}, \quad |\hat{u}_m| = \omega\frac{V}{2S_{wl}} \tag{2.16}$$

  where S_{wl} and V embody the water-plane area and the volume of the buoy. In low frequency waves, the wavelength is also large relative to the body, and the diffraction force is negligible. Then, the small-body approximation [85] can be applied to estimate the excitation force as

$$|\hat{F}_e| < \rho g S_{wl}\zeta_a \tag{2.17}$$

  where ζ_a is the wave amplitude. In low frequency waves, only a little power is dissipated in radiation, and thus the radiation power $\overline{P}_r$ is much smaller than the excitation power $\overline{P}_{exc}$. Then, according to (2.10), the time-averaged power $\overline{P}_a$ can be

approximated by the excitation power $\overline{P}_{exc}$. Combining (2.16) and (2.17) gives an approximation of the excitation power, namely the power bound in low wave frequencies, as

$$P_B \approx \overline{P}_{exc} = \frac{\pi \rho g H V}{4T} \tag{2.18}$$

The schematic of the Budal diagram is depicted in Figure 2.14. Relying on the Budal diagram, the theoretical power limits of a point absorber with a given size throughout various wave frequencies can be efficiently characterized.

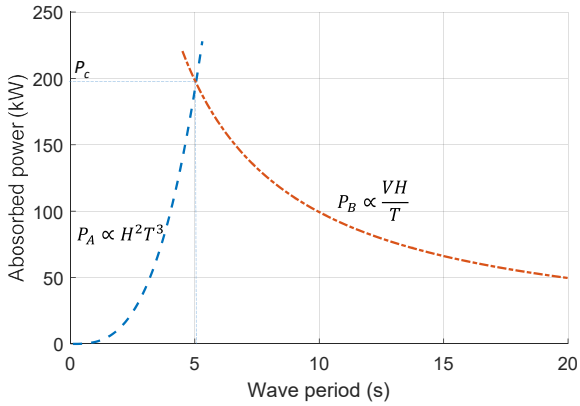


Figure 2.14: Schematic of the Budal diagram for a floating vertical cylinder.

As the effect of the size on the power absorption of WECs can be reflected in the Budal diagram, it is possible to be applied in sizing WECs. In [84], the Budal diagram was introduced as a tool to conduct the sizing of WECs for the first time. More recently, in [20], the Budal diagram was further developed to be applicable for submerged WECs, and it was used to investigate and compare the effects of sizing on the submerged WECs and floating WECs. The size of WECs is reflected in the Budal diagram as the volume V in P_B of (2.18). In order to calculate the volume V, the designed working condition (H and T) has to be explicitly defined. In [20], [84], WECs were assumed to be commercially viable if the amount of working time at full capacity exceeds one third of the annual time. So the size of WECs should match the so-called "one third wave power threshold" of the given wave resource. Based on the power threshold, a representative wave state, including the wave height H_D and wave period T_D , can be derived as the designed working condition for sizing the buoy. More specifically, the selection of the suitable size of WECs is conducted as following procedures [20].

1. Calculate the wave power threshold J_T (W/m) which is being exceeded one-third of the annual time in the concerned wave climate;
2. Choose the most frequent wave period in scatter diagram as the T_D in P_A and P_B;
3. Since T_D and J_T are already known from step 1 and 2, in harmonic waves, the wave height H_D can be calculated;

4. The suitable volume of WECs, V in P_B, can be calculated by solving P_A=P_B;

5. According to different control strategies and types of PTO systems, the PTO capacity is selected as the maximum absorbed power of WECs at the representative wave condition (H_D and T_D).

Relying on the Budal diagram, the suitable size of WECs can be approximated for a particular sea site in a significantly efficient way, since it doesn't require the identification of the power performance of WECs of different sizes. In addition to buoy sizing, the selection of the PTO capacity can also be included in this method, as stated in the fifth of the sizing procedures shown above. However, there are some limitations associated with the method. First, the sizing result is dependent on the selection of the representative wave state. However, using a representative wave state to represent the wave resource clearly simplifies the variability of the characteristics of ocean waves. In other words, a WEC successfully designed for a particular wave state is not necessarily viable in a realistic sea site consisting of various wave states. In addition, the selection of the representative wave state is associated with such an assumption that to be viable, the WEC has to operate at full capacity over a certain amount of time, such as the above-mentioned "one third wave power threshold". This is a big simplification of the economics of WECs. Secondly, the Budal diagram can only be used to estimate the absorbed power but not the losses in other conversion phases. For instance, PTO conversion efficiency is highly related to the operating conditions of WECs, and therefore the tendency of the actual delivered power curves might be different from the bounds predicted by the Budal diagram. Then, the intersection of actual power curves could shift from that of P_A and P_B in the Budal diagram, which results in an erroneous estimate on the size determination. Thirdly, the Budal diagram was derived based on harmonic wave conditions, which cannot indicate the ability of the sized WECs to respond to irregular waves. However, sizing could play a role in the ability, since the size of WECs generally increases the resistive term and further the absorption bandwidth [86]. For instance, as reported in [87], increasing the diameter of a floating cylinder (with a draft of 7.5 m) from 4 m to 9 m could extend the absorption bandwidth by approximately 1.8 times. From this point of view, the relatively larger sized WECs are preferred in realistic wave conditions, and the sizing method based on the Budal diagram tends to underestimate the optimal size of WECs. Moreover, the Budal diagram was derived based on the assumption of deep water conditions, and its current form is not applicable for incorporating the shallow water effect on the power absorption of WECs.

2.3.3. NUMERICAL SIMULATION

Alternatively, numerical simulation can be used to identify the power performance of WECs in different sizes. Compared with Froude scaling and the Budal diagram, the numerical simulation could offer the information of the power performance with higher fidelity. For differently sized WECs, it is possible to incorporate the variation of other design parameters and the effect of sizing on power conversion stages in numerical modeling. For instance, different PTO forces and power limits can be implemented in numerical modeling to represent the effect of the PTO sizing on the power performance of WECs. However, numerical simulation is not commonly used in sizing studies of WECs. The first reason is that numerical modeling is more computationally time-demanding compared to the above-mentioned methods, but the sizing normally requires a large number of iterations. The second reason

is that most WECs are not yet at a stage of being mature and commercial. Consequently, the main research focus is still located on the technological improvement, but the overall sizing of WECs has not been widely treated as a mandatory procedure in the current phase. With the increasing development of WECs towards commercialization, the sizing is expected to be in larger demand for improving the economic competitiveness. At that point, a more refined sizing method will be needed, in which numerical simulation would be a more suitable tool than the two above-mentioned methods.

The most commonly used numerical models in the field of WECs can be classified as FD models, TD models and Computational Fluid Dynamics (CFD) models. Their computational efficiency decreases in the sequence, while the fidelity increases. CFD models are a kind of fully nonlinear numerical models, in which Navier-Stokes equations are solved numerically. Navier-Stokes equations are derived from the conservation of mass and momentum and is generally considered to be the most fundamental fluid flow equations. Thus, viscous effects and turbulence are taken into account in CFD models. On the other hand, CFD models are significantly more time-consuming compared to nonlinear TD models, which is the main limitation of extensive application of CFD models. Therefore, CFD models are mostly used in the assessment of the survivability of WECs in severe wave conditions, but they are hardly used to estimate the power production. Instead, the power performance of WECs is commonly estimated by FD models and TD models.

In the context of WECs, FD models and TD models are commonly established based on linear potential theory [88]. The linear potential flow theory has been used to solve wave-structure interaction problems in offshore engineering over decades. In the theory, fluid is assumed to be inviscid, irrotational and incompressible, and thus vortexes and viscosity are neglected. In addition, in order to simplify the problem, the boundary conditions of the free surface and body are linearized as the mean free surface and the mean wetted surface. Linear potential flow theory is computationally efficient to derive hydrodynamic coefficients. Given the explicit coefficients, FD models can be easily formulated according to physical principles to estimate the dynamics of WECs. External forces can be taken into account, but all the components in the conventional FD models are required to be linear. The most important advantage of FD models is their simplicity and thus high efficiency. Further, based on the Cummins equation [89] describing the memory effects of radiation forces, TD models can be established and the time-dependent responses of WECs can be solved. In TD models, nonlinear external force components can be considered, such as the nonlinear mooring force, PTO force and viscous drag force. It is also possible to extend TD models to cover weakly nonlinear hydrodynamics. For instance, the mean wetted surface assumption can be corrected by integrating incident pressure over instantaneous wetted surface when calculating the nonlinear Froude-Krylov force and nonlinear hydrostatic force [90], [91]. The mean free surface assumption can be corrected by Wheeler Stretching theory to rebuild the wave pressure field in each time step [92]. Even though TD models are associated with higher fidelity than FD models, the computational demand of TD models is typically three orders of magnitude higher than that of FD models [93]. In scenarios requiring a large amount of iterations, such as design optimization and sizing, FD models are more appealing, since the application of TD models could make the process significantly time-consuming.

As an alternative to FD models and TD models, spectral domain models have only been proposed to estimate the statistical responses of WECs in recent years [27]. They can be

regarded as an extension of FD models, but they are capable of including nonlinear force components. Therefore, it combines high computational efficiency and adequate reliability. As a newly proposed numerical technique, it has not been widely used in the field of WECs. However, considering its characteristics, spectral domain models have high potential to be used in the sizing of WECs.

2.4. SUMMARY AND CONCLUSIONS

Based on the review of WECs, it can be concluded that the operational principles and designs are rather divergent with regard not only to the aspect of the power capture technology but also to the application of PTO systems. As wave resources also vary from one sea site to another, towards the commercialization of WECs, the divergence makes it challenging to evaluate and subsequently compare the techno-economic performance of different WECs at the sea sites potential for the deployment. Sizing of WECs could not only make a difference to the dynamics but also to the cost of the WEC devices, and further to the evaluation of the techno-economic performance. The sizing of WECs is commonly conducted based on the Budal diagram and Froude similarity since their computational loads are significantly low. However, these two methods have limited capacities in accounting for the effect of PTO sizing, which implies that the consideration of the PTO sizing is lacking in the existing sizing studies. As an alternative, WECs sizing can also be implemented based on numerical simulation, in which the flexible variation of PTO sizes can be incorporated. Compared with the Budal diagram and Froude scaling, the numerical simulation is associated with lower computational efficiency, which is hindering its extensive application in the sizing of WECs where a large number of iterations is normally required. Among numerical models applicable for WECs, FD models are characterized by their high efficiency, but it is constrained by linear theory limitations. Its accuracy would be challenged when nonlinear effects are not negligible. Therefore, developing a numerical model combining both high efficiency and adequate accuracy could make a significant contribution to the sizing of WECs. As a recently proposed modeling technique in the context of WECs, the application of the spectral domain model is still limited but it is expected to be a promising numerical tool in supporting the sizing of WECs.

3

A Collective Sizing Method for WECs

As discussed in Chapter 2, sizing could make a difference to the techno-economic performance of WECs. However, in existing literature, sizing of the PTO system was hardly considered in overall sizing of WECs. In this chapter, a collective sizing method is established based on the numerical simulation for a generic point absorber, in which the buoy and the PTO system can be sized independently to reduce the LCOE. FD modeling is adopted to estimate the power production of WECs in different sizes. FD modeling neglects nonlinear effects but it is associated with high computational efficiency. Force constraints are used to represent the effects of PTO sizing on the absorbed power, in which passive and reactive control strategies are considered respectively. Furthermore, an economic model is established to estimate the cost of WECs. The proposed method is implemented for three realistic sea sites, and the dependence of the optimal size of WECs on wave resources and control strategies is analyzed. Moreover, a comparison is made between the proposed method and other sizing methods with respect to the determination of the optimal size and the lowest LCOE of WECs. The importance of PTO sizing on the reduction of the LCOE is identified.

Parts of the chapter have been published in the paper: Tan J, Polinder H, Laguna A J, et al. The Influence of Sizing of Wave Energy Converters on the Techno-Economic Performance[J]. Journal of Marine Science and Engineering, 2021, 9(1): 52. [94].

3.1. INTRODUCTION

IN Chapter 2, the importance of sizing to the techno-economic performance of WECs was highlighted, and the related literature was reviewed. However, those studies concentrated mainly on buoy sizing without addressing PTO system sizing. As a core component, PTO systems are significantly influential to the performance of WECs [95]. On the one hand, its cost normally accounts for over 20% of the total CAPEX [26]. On the other hand, the PTO size is highly related to the rated power and the force constraint, which could directly affect the power absorption [95]–[98]. To the author's knowledge, there is a lack of studies considering both PTO and buoy sizing of WECs. Thus, the aim of this chapter is to investigate the influence of PTO sizing on the overall sizing and the LCOE.

In this chapter, a size optimization method considering both buoy and PTO sizing is established, and it is applied to a generic heaving point absorber. The optimization is performed based on an exhaustive search algorithm. Firstly, FD modeling is used to calculate the power performance of WECs with different buoy and PTO sizes. The implementation of the PTO sizing using passive and reactive control is demonstrated, respectively. In addition, a preliminary economic model is described to build a cost function with the aim to minimize the LCOE. Next, based on the proposed method, size optimization of WECs is carried out for three realistic sea sites. The interaction between buoy and PTO sizing is analyzed, and the dependence of size determination on wave resources and control strategies is presented. Furthermore, a comparison between this proposed size optimization method and other methods is performed. Finally, conclusions are drawn based on the obtained results.

3.2. WEC CONCEPT AND CONCERNED SEA SITES

A generic heaving point absorber [99], [100] is used as a WEC reference throughout this thesis. The diameter of the buoy in the original size is 5.0 m. The average density of the buoy in all sizes is assumed to be identical and with a value of half of the water density (1025 kg/m^3). The schematic of the concept is shown in Figure 3.1. In practice, the amplitude of the buoy motion has to be limited to protect the mechanical structure, and the displacement limit of this WEC is set as 0.8 times the radius of the buoy. In addition, WECs have to be stopped from operating at severe sea states. Thus, there must be a maximum operational wave height for protection. A similar prototype to the WEC in this work is WaveStar, which is a semi-spherical heaving point absorber [39]. The maximum operational wave height of WaveStar is 6 m and the diameter of WaveStar is 5 m. Therefore, the maximum operational wave height for the original WEC, in this case, is estimated as H_s = 5 m , in a conservative way.

In this chapter, three realistic sea sites are selected to investigate the techno-economic performance of WECs. They are Yeu Island, in the oceanic territory of France, Biscay Marine Energy Park (BIMEP) in Spain, and DK North Sea Point 2 (DK2) in Denmark. The scatter diagrams of these sea sites are taken from Reference [17], which are shown in Figure 3.2–3.4. In these scatter diagrams, H_s and T_z represent the significant wave height and the mean zero-crossing wave period, respectively, and the time of the corresponding occurrence are depicted in each cell as the number of occurrence hours in a year for that particular sea state. It should be pointed out that Yeu, BIMEP, and DK2 are geographically far from each other and their most frequent wave heights and periods differ significantly. Hence, these three sea sites are chosen to be the representatives of European wave characteristics. The

scatter diagrams of hours of the occurrence of wave states of Yeu island, DK 2 and BIMEP are shown below.

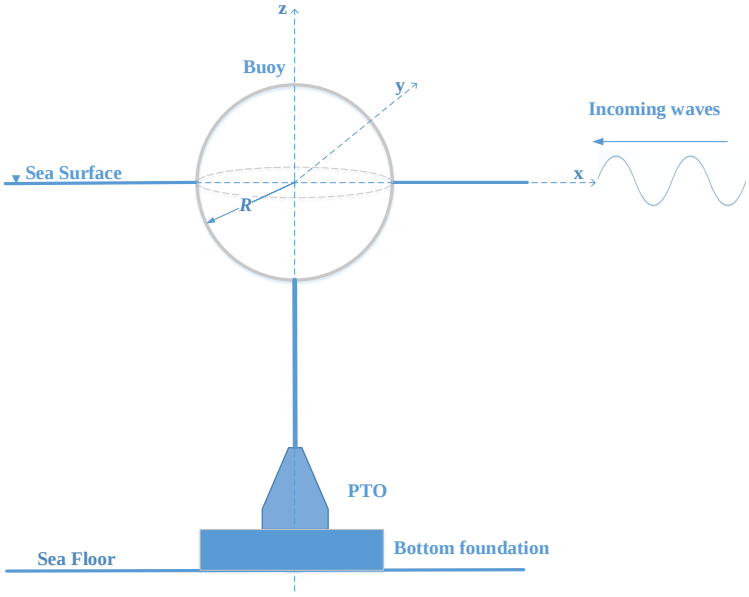


Figure 3.1: Schematic of the heaving point absorber concept.

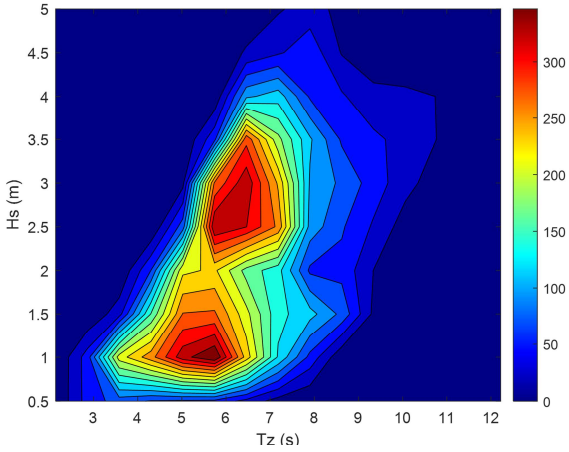


Figure 3.2: Hours of occurrence of each wave state of Yeu island [101].

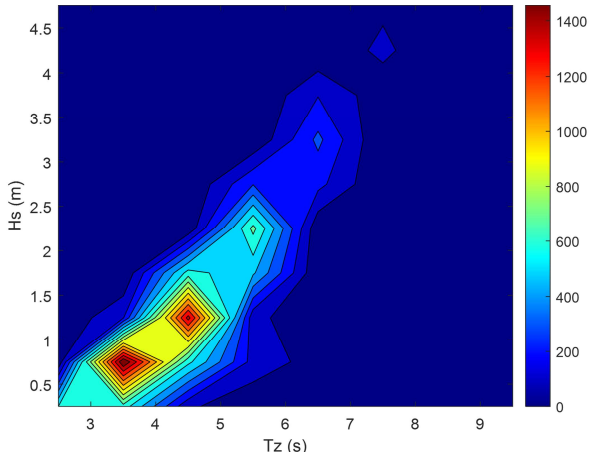


Figure 3.3: Hours of occurrence of each wave state of DK 2 [17].

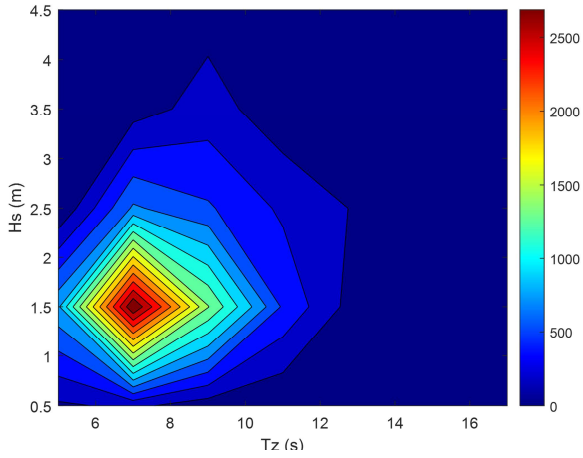


Figure 3.4: Hours of occurrence of each wave state of BIMEP [17].

3.3. METHODOLOGY

This section starts with the framework of the collective sizing method. Next, the equations of motion and FD modeling of WECs are presented, and the approaches to incorporate the effects of buoy and PTO sizing are introduced. Finally, a preliminary economic model is established to predict the cost of WECs.

3.3.1. COLLECTIVE SIZING METHOD

The framework of the collective sizing method is presented in this part. The flowchart of this sizing method is shown in Figure 3.5. This method aims at improving the techno-economic performance of WECs through the combined contribution of the buoy and PTO size optimization. The cost function of the size optimization adopted in this thesis is the LCOE. The method is mainly composed of two models: a FD model is applied to estimate the power

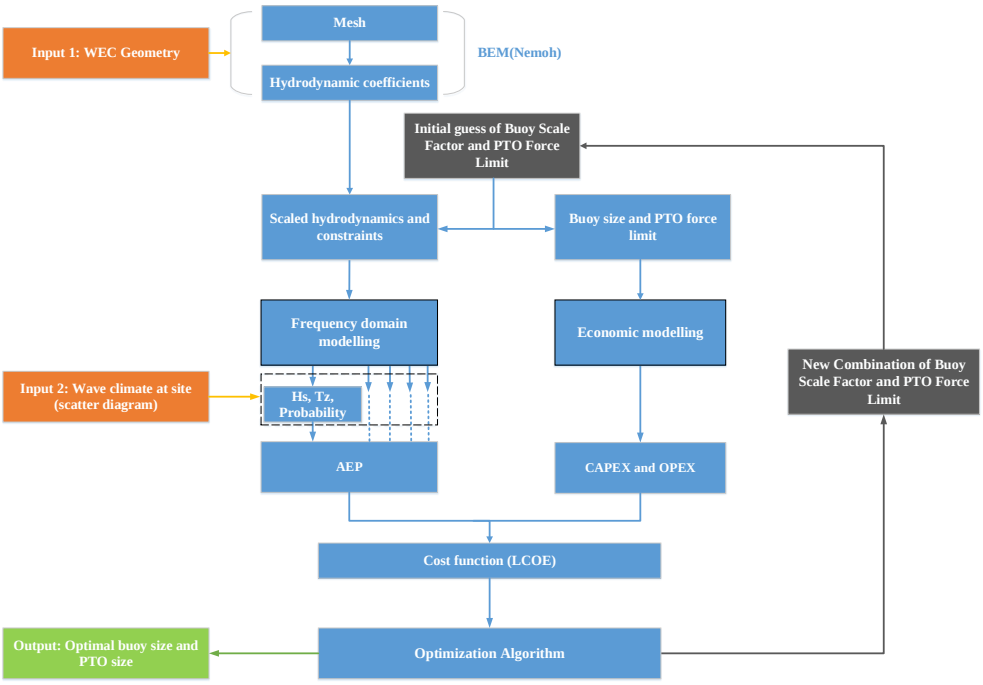


Figure 3.5: Flowchart of the size optimization method of Wave Energy Converters (WECs).

production of WECs in each buoy and PTO size, and an economic model is established to calculate the corresponding costs. These two models are explained in more detail in the following subsections.

An exhaustive search algorithm is used in the optimization. The buoy scale factor λ and a normalized factor for PTO sizing, namely PTO sizing ratio, are treated as the optimization variables. The buoy scale factor λ is specified as

$$\lambda = \frac{G_c}{G_o} \tag{3.1}$$

where G is the characteristic length of the WEC, and the subscript c and o represent the "scaled device" and the "original device", respectively. The specification of the original device has been described in Subsection 3.2, in which the diameter of the spherical buoy is decided as 5 m. The PTO sizing ratio is defined as

$$\text{PTO sizing ratio} = \frac{\text{PTO force limit}}{\text{Maximum required PTO force}} \tag{3.2}$$

where the relevant terms are explained as follows.

- PTO force limit: the nominal force that the chosen PTO system could sustain during operation.
- Maximum required PTO force: the PTO force required to maximize the annual energy production (AEP) of the WEC at the given sea site. It is calculated as the largest

value of unconstrained PTO forces within all the operational sea states of the sea site. Where the unconstrained PTO force corresponds to the maximum theoretical power absorption without any force limits for a given sea state.

It can be deduced that the maximum required PTO force occurs at the operational sea state with the largest wave power density. It varies with the wave resource, the buoy size, and the control strategy. Thus, in each case, the maximum required PTO force is pre-calculated for each sea site and buoy scale factor λ. In the following section, Figure 3.10a will illustrate the relation of the unconstrained PTO force to the sea states, and Figure 3.10b will presents the values of the maximum PTO force obtained for different buy scale factors at the three different sea sites.

During the size optimization, the initial searching bounds of the buoy scale factor λ and PTO sizing ratio are set as [0.3,2.0] and [0.1,1.0], respectively. If the the optimal solution is not found within these ranges during iterations, the bounds would be automatically extended until a solution is obtained. A discrete iteration step of 0.1 is used in the exhaustive searching algorithm for both buoy scale factors λ and PTO sizing ratios. The proposed size optimization method is also compatible with other optimization algorithms, which may provide more precise solutions or save computational costs. However, it is beyond the scope of this work to discuss the relative impacts of optimization algorithms in detail.

3.3.2. FREQUENCY DOMAIN MODELING

In this subsection, a FD model of WECs is presented based on linear wave theory. For a single rigid floating body subjected to ocean waves, its motion can be described based on Newton' second law as

$$\boldsymbol{M}\boldsymbol{a}(t) = \boldsymbol{F_{hs}}(t) + \boldsymbol{F_e}(t) + \boldsymbol{F_{pto}}(t) + \boldsymbol{F_r}(t) \tag{3.3}$$

where $\boldsymbol{M}$ represents the 6×6 inertial matrix of the oscillating buoy, $\boldsymbol{a}$ is the 1×6 vector of the buoy's acceleration, $\boldsymbol{F_{hs}}$ is the 1×6 vector of hydrostatic force, $\boldsymbol{F_e}$ is the 1×6 vector of wave excitation force, $\boldsymbol{F_r}$ is the 1×6 vector of wave radiation force, $\boldsymbol{F_{pto}}$ is the 1×6 vector of PTO force.

In this thesis, the device is assumed to oscillate only in heave motion, the FD model of the WEC is only discussed for the heaving degree of freedom. Then, if the body is assumed to perform harmonic motion and a linear PTO model is used to simulate the behavior of the PTO system, (3.3) could be rewritten in the form of complex amplitudes [21], as

$$\hat{F}_e(\omega) = [R_r(\omega) + R_{pto}]\,\hat{u} + \mathrm{i}\omega\,\hat{u}[M + M_r(\omega)] + \mathrm{i}\,\hat{u}[-\frac{K_{pto}}{\omega} - \frac{K_{hs}}{\omega}] \tag{3.4}$$

where $R_r(\omega)$ is the hydrodynamic damping coefficient, R_{pto} is the PTO damping coefficient, ω is the wave frequency, $M_r(\omega)$ is the added mass of the WEC, $\hat{u}$ is complex amplitude of the vertical velocity, K_{pto} is the PTO stiffness coefficient, and K_{hs} is the hydrostatic stiffness. The intrinsic impedance of the heaving buoy and PTO impedance can be introduced as

$$Z_m(\omega) = R_r(\omega) + \mathrm{i}X_m(\omega) \tag{3.5}$$

$$X_m(\omega) = \omega[M + M_r(\omega)] - \frac{K_{hs}}{\omega} \tag{3.6}$$

where $Z_m(\omega)$ is the intrinsic impedance of the heaving buoy, and $X_m(\omega)$ is the intrinsic reactance. Similarly, the impedance of PTO can be given as:

$$Z_{pto}(\omega) = R_{pto}(\omega) + \mathrm{i}X_{pto}(\omega) \tag{3.7}$$

$$X_{pto}(\omega) = -\frac{K_{pto}}{\omega} \tag{3.8}$$

where $Z_{pto}(\omega)$ is the PTO impendence, and $X_{pto}(\omega)$ is the PTO reactance. So, (3.4) is rewritten as

$$\hat{F}_e(\omega) = [Z_m(\omega) + Z_{pto}(\omega)]\,\hat{u} \tag{3.9}$$

The hydrodynamic characteristics of WECs, including $M_r(\omega)$, $R_r(\omega)$, and $F_e(\omega)$, are calculated using the Boundary Element Method through the open source software Nemoh [102]. The mesh convergence analysis of the hydrodynamic calculation and the corresponding hydrodynamic coefficients used in this work are presented in Appendix A.1 and A.2. Then, by solving (3.9), the complex amplitude of velocity $\hat{u}$ could be obtained as

$$\hat{u}(\omega) = \frac{\hat{F}_e(\omega)}{Z_m(\omega) + Z_{pto}(\omega)} \tag{3.10}$$

Then, the complex amplitude of the motion displacement is expressed as

$$\hat{s}(\omega) = \frac{\hat{F}_e(\omega)}{i\omega\big[Z_m(\omega) + Z_{pto}(\omega)\big]} \tag{3.11}$$

For regular wave conditions, the time averaged absorbed power can be obtained and expressed as

$$\overline{P}_a = \frac{1}{2}R_{pto}\,|\hat{u}|^2 \tag{3.12}$$

The above analysis is based on the assumption of harmonic motion, but incoming waves in real sea states are always irregular. In this work, the calculation of power absorption in irregular waves is conducted based on the superposition of regular waves [103]. If the ocean wave inputs are assumed to be Gaussian processes, then the stochastic waves can be represented by the linear superposition of a set of frequency components with a random phase. Hence, the wave elevation is expressed as

$$\eta(t) = \sum_{j=1}^{N} \zeta_a(\omega_j)\cos(\omega_j t + \varphi(\omega_j)) \tag{3.13}$$

where t is time, ω_j is the wave frequency of j_{th} wave component; $\zeta_a(\omega_j)$ and $\varphi_(\omega_j)$ are the wave amplitude and phase of the regular wave component corresponding to ω_j. In a predefined wave spectrum, the amplitude of the wave component is related to the wave energy spectrum S_{ζ_a}, as

$$\zeta_a(\omega_j) = \sqrt{2S_{\zeta_a}(\omega_j)\Delta\omega} \tag{3.14}$$

The variance of the wave elevation $\sigma^2_{\zeta a}$ is calculated as

$$\sigma^2_{\zeta a} = \sum_{j=1}^{N} S_{\zeta_a}(\omega_j)\Delta\omega \tag{3.15}$$

where $\sigma_{\zeta a}$ is the standard deviation of the wave elevation. Similarly, as the velocity amplitude of WEC corresponding to each wave component can be obtained by (3.10), the standard deviation and spectral density of the WEC response can be calculated. Then, the mean absorbed power can be derived as

$$\overline{P}_a = \sum_{j=1}^{N} \frac{1}{2} R_{pto} \left|\hat{u}(\omega_j)\right|^2 = \sum_{j=1}^{N} R_{pto} S_u(\omega_j) \Delta\omega = R_{pto} \sigma_u^2 \tag{3.16}$$

where S_u and σ_u denote the spectral density and standard deviation of the velocity of the WEC. In this thesis, the irregular waves are considered to be unidirectional. In addition, JONSWAP spectrum, together with the peakedness factor of 3.3, is used to represent the irregular waves in this thesis [104].

It must be acknowledged that FD modeling has limited applicability. Firstly, it is restricted to the linear theory. The accuracy of this approach around the resonance of WECs is limited where the motion amplitude is too high and the linear assumption is violated [105]. However, the displacement limit is considered here, which could ease this problem [22]. Secondly, FD modeling does not allow the implementation of real-time control strategies by which PTO parameters can be adjusted instantaneously with the PTO force saturation and buoy displacement constraints [106], [107]. Although there are limitations in FD modeling, it is considered reasonable given the purpose of this chapter to provide an insight into the role of the PTO sizing on the techno-economic performance. FD models are more computationally efficient compared to TD approaches, which makes it highly suitable in optimization studies that require a large number of iterations. In addition, the energy production of WECs in different buoy and PTO sizes is calculated based on the same FD model, which is fair for the size determination and techno-economic analysis.

BUOY SIZING

During the iterations of the size optimization, the buoy size of WECs are scaled following geometrical similarity. Therefore, the hydrodynamic coefficients of buoys in different sizes and the corresponding wave conditions can be obtained by means of Froude scaling [74],

$$\begin{aligned} \omega_c &= \omega_o \lambda^{-0.5} \\ H_c &= H_o \lambda \\ F_{e_c} &= F_{e_o} \lambda^3 \\ R_{r_c} &= R_{r_o} \lambda^{2.5} \\ M_{r_c} &= M_{r_o} \lambda^3 \end{aligned} \tag{3.17}$$

where ω is the wave frequency and H is the wave height; F_e, R_r and M_r are the excitation force, the radiation damping, and the added mass coefficients, respectively. Hence, this allows the hydrodynamic coefficients of the original buoy to be transferred to the scaled buoy instead of using BEM approach to calculate the hydrodynamic coefficients in each iteration. In this way, the computing efficiency can be significantly improved. The density of the buoy structure in different sizes are assumed to be same. The maximum operation wave height and the displacement limit of WECs are scaled with the buoy scale factor λ.

PTO SIZING

PTO sizing implies the implementation of determining the optimal PTO size for different sea sites. The PTO size is directly related to the rated power, PTO force limits, displacement limits, and PTO peak power constraints of WECs [59]. In this work, the PTO force limit is used to characterize the PTO size. According to (3.7) and (3.10), the PTO force amplitude can be expressed as

$$\left|\hat{F}_{pto}\right| = \left|\hat{u}Z_{pto}\right| = \frac{\left|Z_{pto}\right|}{\left|Z_m + Z_{pto}\right|}\left|\hat{F}_e\right| = \left|\hat{F}_e\right| \frac{\sqrt{R_{pto}^2 + X_{pto}^2}}{\sqrt{(R_{pto}+R_r)^2 + (X_m + X_{pto})^2}} \tag{3.18}$$

As is shown in (3.18), the PTO force amplitude is a function of R_{pto} and X_{pto}. Therefore, one approach to restrict the PTO force amplitude is to adjust PTO parameters. Reactive control and passive control are typical control strategies in WECs. In the reactive control, both the PTO reactance and the PTO damping coefficient could be varied to tune the device. However, in the passive control, only the PTO resistance load (damping force) is provided. Next, the methods to determine the PTO parameters for limiting the PTO force amplitude in the passive control strategy and the reactive control strategy are explained, respectively.

- The determination of PTO parameters in passive control:
  Here, the PTO force amplitude is constrained by means of adjusting the PTO parameters. Furthermore, the PTO parameters are also expected to be determined to limit the stroke and maximize the absorbed power.
  First, let us discuss the PTO force constraints. In the passive control strategy, only PTO damping can be varied and the PTO reactance equals zero. Therefore, the PTO force amplitude expressed in (3.18) can be simplified as

$$\left|\hat{F}_{pto}\right| = \left|\hat{F}_e\right| \frac{R_{pto}}{\sqrt{(R_{pto}+R_r)^2 + X_m^2}} \tag{3.19}$$

  To reveal the relationship between $|\hat{F}_{pto}|$ and R_{pto}, the derivation of (3.19) with respect to R_{pto} is calculated and gives

$$\frac{\mathrm{d}(|\hat{F}_{pto}|)}{\mathrm{d}R_{pto}} = \left|\hat{F}_e\right| \frac{R_{pto}R_r + X_m^2 + R_{pto}^2}{\left[(R_{pto}+R_r)^2 + X_m^2\right]^{\frac{3}{2}}} \tag{3.20}$$

  It can be deduced that (3.20) is always positive as R_{pto} and R_r are greater than 0, which also implies that $\left|\hat{F}_{pto}\right|$ is a monotonic function of R_{pto}. In other words, decreasing the PTO damping coefficient can directly constrain the PTO force amplitude. During size optimization, the PTO sizing ratio and buoy scale factor λ are used as optimization variables. However, to determine PTO parameters with the force limit, the PTO force limit should be derived to be explicit. According to the definition of the PTO sizing ratio, the PTO force limit can be calculated by multiplying the given PTO sizing ratio with the maximum required PTO force for the particular buoy scale factor and considered sea site. Therefore, the PTO force limit is directly related to each set of

optimization variables. Here, the PTO force limit is represented by F_m, and the maximum allowed PTO damping $R_{pto,max}$ can be obtained by solving (3.21), in which only the positive solution should be retained.

$$\left|\hat{F}_e\right| \frac{R_{pto,max}}{\sqrt{(R_{pto,max}+R_r)^2+X_m^2}} = F_m \tag{3.21}$$

Therefore, for constraining the PTO force amplitude, R_{pto} should satisfy

$$R_{pto} \leq R_{pto,max} \tag{3.22}$$

Secondly, except PTO force constraints, the displacement limit should be considered during the selection of PTO parameters. It can be deduced from (3.10) that the $|\hat{u}|$ decreases with R_{pto} increasing. If the stroke constraint of the buoy, S_m, comes to play, the PTO resistance should be increased to limit the velocity amplitude, which is shown as

$$|\hat{u}| = \frac{\left|\hat{F}_e\right|}{\left|R_{pto}+Z_m\right|} \leq |u_m| \tag{3.23}$$

In this way, for constraining the stroke amplitude, R_{pto} should satisfy

$$R_{pto} \geq \sqrt{(\frac{\hat{F}_e}{u_m})^2 - X_m^2)} - R_r = R_{pto,min} \tag{3.24}$$

where u_m is the velocity limit of the buoy, which is equal to ωs_m. Therefore, it can be seen from (3.22) and (3.24) that the upper bound and the lower bound of the available PTO damping are decided by the PTO force limit and the stoke limit, respectively, which could also be expressed as

$$R_{pto,min} \leq R_{pto} \leq R_{pto,max} \tag{3.25}$$

Thus, the PTO damping should be selected from the range expressed in (3.25) to satisfy the constraints.

According to Reference [106], in regular waves, the optimal PTO damping for maximizing the absorbed power without any constraint is expressed as

$$R_{pto,opt} = |Z_m| = \sqrt{R_r^2 + X_m^2} \tag{3.26}$$

To maximize the absorbed power of WECs, R_{pto} should be as close to $R_{pto,opt}$ as possible. So, the principle of PTO damping selection in PTO sizing can be presented as:

- If $R_{pto,min} \leq R_{pto,opt} \leq R_{pto,max}$, the optimal R_{pto} should be selected as $R_{pto,opt}$.
- If $R_{pto,opt} < R_{pto,min}$ or $R_{pto,opt} > R_{pto,max}$, the optimal R_{pto} should be selected as the one of $R_{pto,min}$ and $R_{pto,max}$ which is closer to $R_{pto,opt}$.

– In case $R_{pto,max} < R_{pto,min}$, there is no feasible PTO damping coefficient satisfying both of the constraints. This case would happen when the PTO force limit is very low or the wave power is very high, which realistically means the device has to be stopped from operation for protecting itself from frequently violating the physical constraints.

- The determination of PTO parameters in reactive control:
  Unlike PTO sizing in passive control, both R_{pto} and X_{pto} can be varied to meet the requirement of the motion and PTO force constraints. Given the complexity of the multivariable optimization with nonlinear constraints, a numerical optimization tool is used to select the optimal combination of R_{pto} and X_{pto}, and it can be expressed in the form as

$$\begin{aligned} &maximize \ \ f = \overline{P}_a(R_{pto}, X_{pto}) \\ &subject\ to \begin{cases} |\hat{F}_{pto}(R_{pto}, X_{pto})| \leq F_m \\ |\hat{u}(R_{pto}, X_{pto})| \leq u_m \\ R_{pto} \geq 0 \\ X_{pto} \in \mathbb{R} \end{cases} \end{aligned} \tag{3.27}$$

  The optimization is performed based on the "interior point" algorithm in MATLAB environment, and the tolerance of the function is set as 1e-4. To avoid the local optimal solution, the "MultiStart" solver is adopted. In this solver, iterations start with multiple random points, in which the global optimal solution is expected to be found [108]. In this work, the number of multiple starting points is set as 20, and the bounds of the PTO damping and PTO reactance are set as [0,10 $R_r(\omega)$] and [-10$X_m(\omega)$, 10$X_m(\omega)$] for each sea state. In case that no feasible solution is found in the optimization, the PTO absorbed power would be treated as 0. To make sure the selected number of starting points in the optimization is sufficient in this case, a verification has been conducted and shown in Appendix A.3.

Based on the above method, PTO parameters subjected to different PTO force constraints can be obtained for each wave condition. Then, the corresponding power performance of WECs can be calculated. In this sense, the effects of PTO sizing on the power performance of WECs are taken into account. However, it has to be clarified that the above PTO sizing method is established based on regular wave conditions. To constrain the buoy displacement and PTO force in irregular wave conditions, it is necessary to calculate their instantaneous solutions, in which TD modeling is required. However, the inefficiency of TD simulation would make the iteration process much more time consuming, which is not preferable for the optimization problem. To simplify this problem, in this chapter PTO parameters are selected only to suit the typical characteristics of irregular wave conditions, referring to Reference [98]. According to Reference [21], the time-averaged power transport per unit length of wavefront of incoming waves at regular wave conditions and irregular wave conditions can be calculated as

$$J_{re} = \frac{1}{32\pi}\rho g^2 H^2 T \tag{3.28}$$

$$J_{irr} = \frac{1}{64\pi}\rho g^2 H_s^2 T_e \tag{3.29}$$

By equating (3.28) to (3.29) at the case of the same energy period, namely T equating T_e, the corresponding wave height in regular wave condition is solved as $H_s/\sqrt{2}$. To transfer the T_z in scatter diagrams to T_e, the wave period ratio between T_e and T_z is selected as 1.18 given the JONSWAP spectrum and the peakedness factor of 3.3 [109]. Then, PTO parameters for irregular wave conditions can be selected to suit regular wave conditions whose period and height correspond to T_e and $H_s/\sqrt{2}$, respectively [98]. The purpose of the transfer between irregular wave conditions and regular wave conditions is to simplify the determination of PTO parameters for PTO sizing. However, the selected PTO parameters based on regular wave conditions cannot strictly guarantee that the PTO force and stroke constraints would not be violated at the corresponding irregular wave conditions. Considering the purpose of this study to investigate the impacts of sizing on the techno-economic performance, it is considered to be acceptable. In this work, all the power absorption of WECs are calculated based on irregular wave conditions, and the PTO parameters are optimized for each sea state. As an example, the optimized PTO parameters of WEC in the original buoy size for different sea states are shown in Figures 3.6 and 3.7.

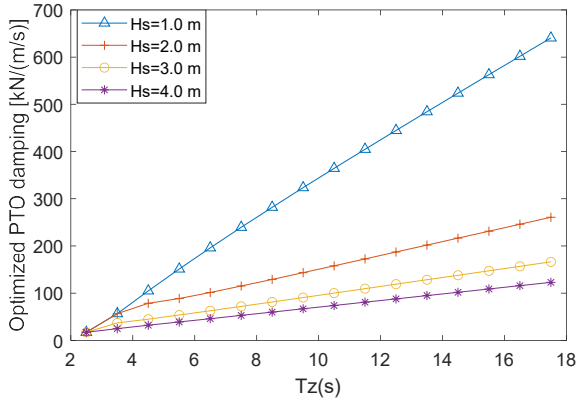
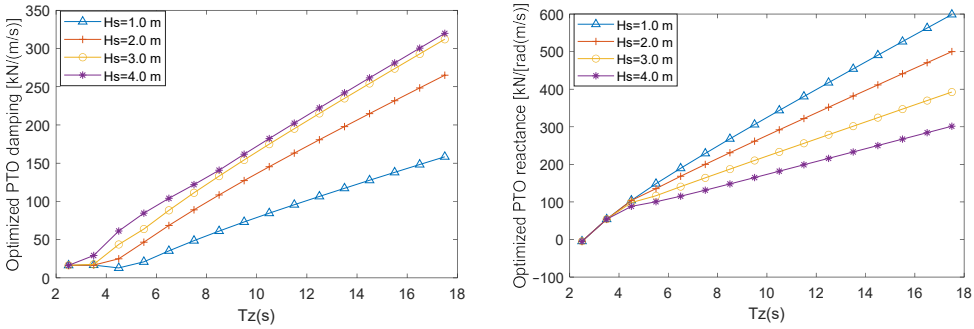


Figure 3.6: Optimized Power Take-Off (PTO) damping of the WEC with passive control for various sea states ($\lambda = 1$ and PTO force limit = 50 kN).

Therefore, as the PTO parameters are determined, the absorbed power of WECs at each sea state can be obtained and the AEP (Annual Energy Production) at the specific sea site is calculated as

$$AEP = \sum_{x=1}^{x=n} \mu \cdot \chi \cdot \overline{P}_a(x) \cdot T_{tot}(x) \tag{3.30}$$

where μ is the overall conversion efficiency from the annual absorbed energy to the AEP and is assumed 70% [110]; χ is the availability of WECs to work, and it is set as 90% due to the necessary operation and maintenance [39]; T_{tot} represents the total hours of the appearance of a certain sea state, which is presented in the scatter diagram in Figures 3.2–3.4; x represents the sea state in scatter diagrams.



(a) PTO damping

(b) PTO reactance

Figure 3.7: Optimized PTO parameters of the WEC with reactive control for various sea states (λ = 1 and PTO force limit = 250 kN).

ECONOMIC MODELING FOR COST ESTIMATION

LCOE is an important techno-economic metric of WECs. For evaluating the LCOE, it is of essence to establish an economic model to estimate the CAPEX and OPEX of WECs. Following Reference [12], the steel price is selected as 1.6 British Pounds (GBP)/kg and the structure cost is calculated by assuming that all the structure cost comes from the steel cost. Based on the inflation calculator tool [111], the cumulative inflation rate of GBP from 2017 to 2020 is 5.89% and the exchange rate of Euros to GBP is set as 0.87. Referring to Reference [12], the statistical percentages of CAPEX-related components in total LCOE can be found. The percentage values are recalculated as the average percentage in total CAPEX, shown in Table 3.1. According to Table 3.1, the cost of "Foundation and Mooring" and "Installation" accounts for 19.1% and 10.2% averagely of CAPEX, respectively. Comparatively, the cost of the structure accounts for 38.2% of CAPEX in average. Therefore, mass-related capital cost can be calculated as

$$C_{Mass} = C_S + C_F + C_I = (\frac{\alpha_{F\&M}}{\alpha_S} + \frac{\alpha_I}{\alpha_S} + 1)C_S \tag{3.31}$$

where C_{Mass} represents the Mass-related-capital-cost; C_S, C_F, and C_I are the cost of the structure, foundation, and the installation, respectively, and α_S, $\alpha_{F\&M}$, and α_I are their corresponding percentages in the total LCOE . It can be seen from Table 3.1 that the cost of "Connection" and "PTO" averagely accounts for 8.3% and 24.2% of CAPEX, respectively. Similarly, power-related capital cost can be calculated as

$$C_{Power} = C_{PTO} + C_C = (\frac{\alpha_C}{\alpha_P} + 1)C_{PTO} \tag{3.32}$$

where C_{Power} represents the power-related capital cost; C_P and C_C are the cost of the PTO and the connection, respectively; and α_P and α_C are their corresponding percentages in the total LCOE. Therefore, the CAPEX is calculated as

$$CAPEX = C_{Mass} + C_{Power} \tag{3.33}$$

In this work, PTO is assumed to be a direct drive generator and all PTO costs come from the generator. The generator cost is divided into the cost of the active material and the cost

Table 3.1: Percentages of Capital Expenditure (CAPEX)-related components of WECs in total CAPEX.

CAPEX	Categories	Average Percentage
Mass-related capital cost	Structure	α_S =38.2%
	Foundation and mooring	$\alpha_{F\&M}$=19.1%
	Installation	α_I =10.2%
Power-related capital cost	PTO component	α_P =24.2%
	Connection	α_C =8.3%

of manufacturing. The amount of active material required is approximately related to the PTO force limit and the force density of generators. Referring to Reference [112], the maximum force density in this work is assumed as 44 kN/m^2, which generally ranges from 30 to 60 kN/m^2 depending on the design. The cost of active material of this generator in series production is estimated as 12,000 Euros/m^2 based on the currency value in 2006. The cumulative inflation rate from 2006 to 2020 is 22.1% [111]. Taking the inflation into account, the active material of this generator in this work is estimated as 14,655.31 Euros/m^2. Regarding the manufacturing cost, it is approximately assumed as half of the total cost of the generator [113]. So, the cost of PTO can be expressed as

$$C_{PTO} = C_{Mat} + C_{Man} \tag{3.34}$$

where C_{mat} and C_{man} represent the cost of required material and manufacturing. In this work, the annual OPEX is assumed as 8% of the CAPEX, and the discount rate r is assumed as 8% with the lifespan of 20 years, referring to Reference [17]. Then, the LCOE of WECs is calculated as

$$LCOE = \frac{CAPEX + \sum_{Y=1}^{N_Y} \frac{OPEX_Y}{(1+r)^Y}}{\sum_{Y=1}^{N_Y} \frac{AEP_Y}{(1+r)^Y}} \tag{3.35}$$

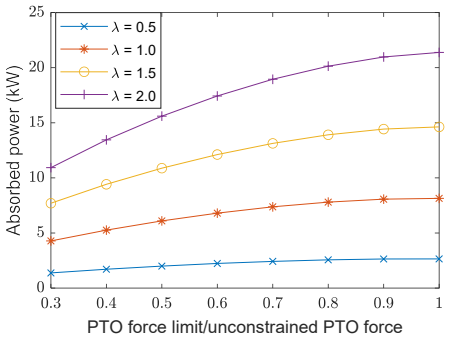
where N_Y represents the total years of the lifespan, and Y represents the evaluated year.

It has to be clarified that it is a preliminary economic model, and the parameters in the model differ from one to another project in practice. For instance, reactive control is associated with negative power flow, which could lead to larger losses and related wear. Therefore, control strategies in practice are able to affect the OPEX and conversion efficiency. However, the specific effects are related to the PTO design and maintenance strategy, which is outside the scope of this chapter. Given the purpose of this work to identify the influence of sizing on the techno-economic performance, the assumption on the constant OPEX percentage and conversion efficiency for both control strategies is considered reasonable. Furthermore, the survivability of WECs in practice is complex and related to many affecting factors. For instance, the increase of the buoy size results in the larger exerted force and input power flow, which could make the WEC more vulnerable. However, it is also dependent on the mooring design, material and even control strategies of WECs. For simplicity, the lifespan for WECs in all sizes is assumed to be constant. Nevertheless, our aim based on the economic analysis is not to give a final judgment of the optimal size of the WEC but to use the LCOE as an indication for providing an insight into the effects of sizing on the techno-economic performance. Overall, the proposed size optimization method has pure theoretical characteristics, and a more complex size optimization study is required in practical applications.

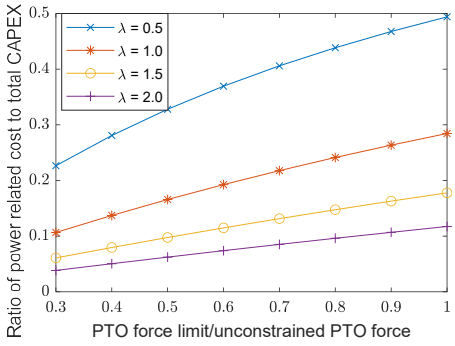
3.4. RESULTS

This section starts with a discussion about the effects of buoy sizing and PTO sizing on the performance of the WEC. Next, the size optimization results for the sea sites are presented. The interaction between PTO sizing and buoy sizing and the benefits of downsizing PTO size for decreasing LCOE are analyzed. Finally, a comparison between this proposed method and other existing methods for the size optimization is performed.

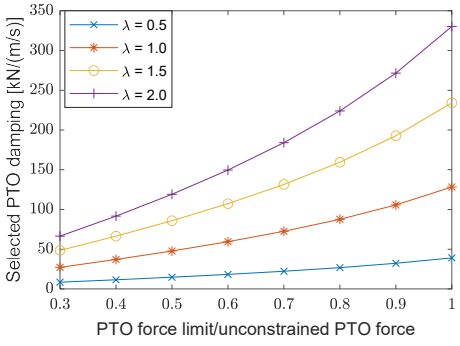
3.4.1. THE EFFECTS OF SIZING ON THE PERFORMANCE OF THE WEC



(a) PTO absorbed power



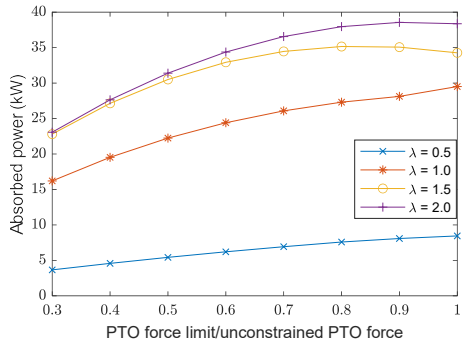
(b) Proportion of power-related cost to total cost



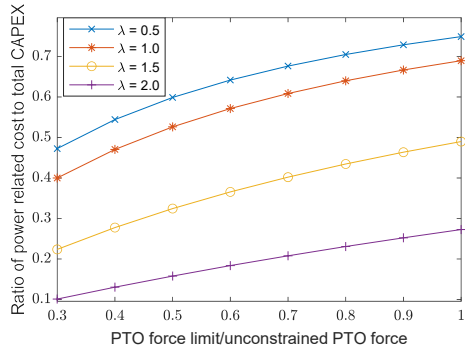
(c) Selected PTO damping

Figure 3.8: Performance of the WEC with passive control under different PTO sizes and buoy scale factor λ, at $H_s = 1.5$ m and $T_z = 5$ s.

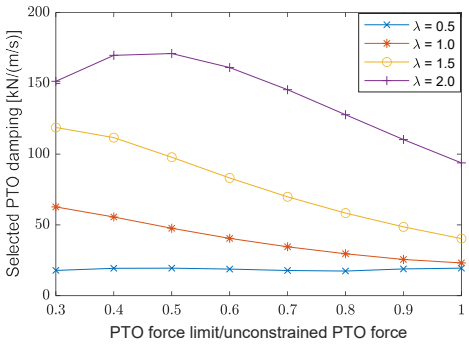
Taking one single sea state ($H_s = 1.5$ m, $T_z = 5$ s) as an example, the effects of PTO sizing and buoy sizing on the performance of the WEC are investigated. In Figures 3.8 and 3.9, the effects on the absorbed power, economic performance and PTO parameters of the WEC with passive control and reactive control are presented, respectively. The horizontal axis in Figures 3.8 and 3.9 is expressed as "PTO force limit/unconstrained PTO force". Here, the unconstrained PTO force corresponds to the PTO force required to maximize the power absorption for the considered sea state ($H_s = 1.5$ m, $T_z = 5$ s). The PTO parameters corresponding to each PTO size and buoy size were calculated following the method described in Section 3.3.2. From Figures 3.8 and 3.9, it is noted that both the power performance and



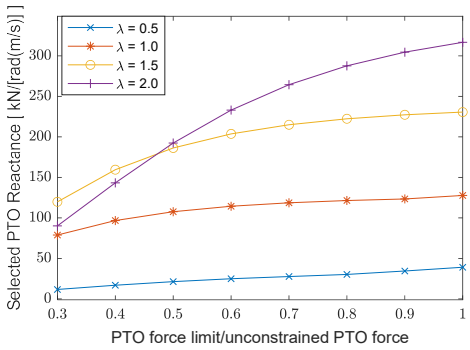
(a) Absorbed power performance



(b) Proportion of power-related cost to total cost.



(c) Selected PTO damping



(d) Selected PTO reactance

Figure 3.9: Performance of the WEC with reactive control under different PTO sizes and buoy scale factor λ, at $H_s = 1.5$ m and $T_z = 5$ s.

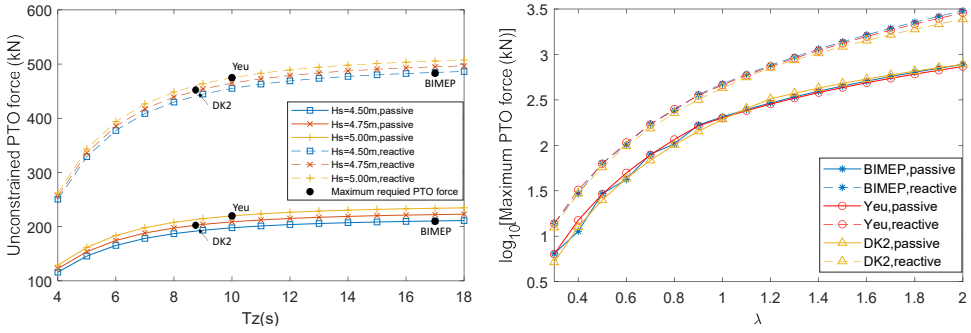
the economic performance are highly related to the sizing of the WEC. In Figures 3.8a and 3.9a, it can be seen that the absorbed power of the WEC increases with the PTO size and the buoy size. In Figures 3.8b and 3.9b, the proportion of the power-related capital cost to the total CAPEX increases with the PTO size, but it decreases with the rise of the buoy scale factor λ. Therefore, at a certain PTO sizing ratio, the CAPEX would be more dominated by the mass-related capital cost than power-related capital cost with the increase of the buoy scale factor λ. Comparing Figures 3.8 and 3.9, it can be found that the effects of sizing on the WEC are also related to the control strategy. Firstly, the absorbed power of the WEC with reactive control is significantly higher than that in the passive control. Secondly, the proportion of power-related capital cost to the total CAPEX in the WEC with reactive control is much higher than that with passive control. This phenomenon can be explained by that the reactive control strategy is associated with higher PTO force limits than the passive control strategy. The higher PTO force then leads to the increase of the proportion. Thirdly, the trends of PTO parameters changing with the force limit depend on the control strategy. In Figure 3.8c, the PTO damping coefficient increases with the ratio "PTO force limit/unconstrained PTO force" when the passive control strategy is used. This is logical as the PTO force monotonically increases with the PTO damping, which has been explained

in (3.20). Comparatively, it can be seen from Figure 3.9c,d, with the increase of "PTO force limit/unconstrained PTO force", the PTO damping coefficient tends to decrease, while the PTO reactance increases. The reason is that the PTO in reactive control would act more like a pure damper to reduce its required force when the force constraint becomes tighter.

3.4.2. SIZE OPTIMIZATION FOR TYPICAL REALISTIC SEA SITES

RESULTS OF SIZE OPTIMIZATION

Based on the proposed method, the size optimization of the WEC for three sea sites is performed. First, to define the PTO sizing ratio, it is necessary to obtain the maximum required PTO forces corresponding to each buoy size. They are calculated by (3.18), and the results are shown in Figure 3.10. Figure 3.10a shows the relation of unconstrained PTO forces of the WEC in original buoy size to sea states, and the maximum required PTO forces for different sea sites are picked. It can be found from Figure 3.10b that the maximum required PTO force increases dramatically with the increase of the buoy size. In addition, the maximum required PTO forces in the WEC with reactive control are much higher than those with passive control. This is to be expected as PTO forces in reactive control consist of PTO damping-induced forces and PTO reactance-induced forces, while there are only PTO damping-induced forces in the case of passive control.



(a) Unconstrained PTO force vs T_Z ($\lambda = 1$)

(b) Maximum required PTO force vs buoy scale factor λ

Figure 3.10: Maximum required PTO forces for various sea sites and buoy scale scale factor λ.

The size optimization results of the WEC using passive and reactive control for the three sea sites are depicted in Figures 3.11 and 3.12, respectively. It can be clearly seen from these figures that both the LCOE and the AEP can be significantly influenced by sizing of the WEC, no matter in which sea site or with what kind of control strategies. Therefore, for improving the viability of the WEC, it is highly suggested to conduct size optimization of the WEC for the considered wave resources. Next, it can be noted that upscaling buoy size is able to improve the AEP, while it cannot necessarily reduce the LCOE of the WEC. Similarly, the AEP is highly sensitive to the PTO sizing ratio, and the increase of the PTO size can make a significant contribution to the improvement of the AEP. However, from the techno-economic point of view, enlarging PTO size does not necessarily result in a lower LCOE. In this case, it can be noted that downsizing the PTO size to a suitable level is beneficial for reducing the LCOE. Hence, to improve the techno-economic performance, it is significant to conduct PTO sizing for compromising the AEP and the cost.

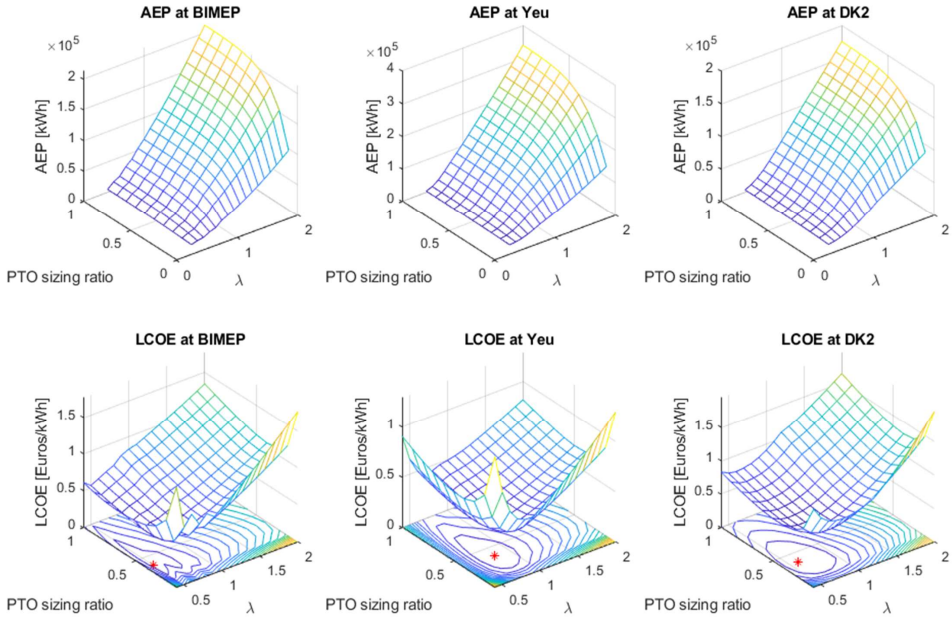


Figure 3.11: Size optimization of the WEC with passive control.

In Figure 3.13, the dependence of size optimization of the WEC on wave resources and control strategies is shown. From Figure 3.13a,d, it can be found that there is not a direct relationship between the buoy size determination and the mean wave power density of wave resources. In other words, the optimal buoy size cannot be indicated by the mean wave power density. For instance, the mean wave power density in BIMEP is almost twice as much as that in DK2, but DK2 corresponds to a higher optimal buoy scale factor λ. As is seen in Figure 3.13a, control strategies do not have a notable influence on the buoy size determination for a given sea site. The reason is that the trends of the AEP changing with the buoy scale factor λ are comparable in both cases of reactive and passive control. Though control strategies lead to a notable difference in the absolute values of the AEP. Regarding PTO sizing, it can be found from Figure 3.13b that the optimal PTO sizing ratios in the WEC with the reactive control are slightly higher than those with passive control in BIMEP and Yeu. The only exception occurs in DK2 where the reactive and the passive control are associated with the same optimal PTO sizing ratio. In addition, it is noteworthy that the optimal PTO sizing ratio is relatively independent of wave resources, and it converges at around 0.4 to 0.5.

Different from the size determination, the optimized LCOE is highly related to wave resources and control strategies. It can be found from Figure 3.13c that the LCOE of the WEC with reactive control is much lower than the WEC with passive control, and the reduction can reach 35 % on average for these sea sites. The optimized LCOE of the WEC with reactive control ranges around 0.2 to 0.35 Euros/kWh, while this value ranges around 0.35 to 0.55

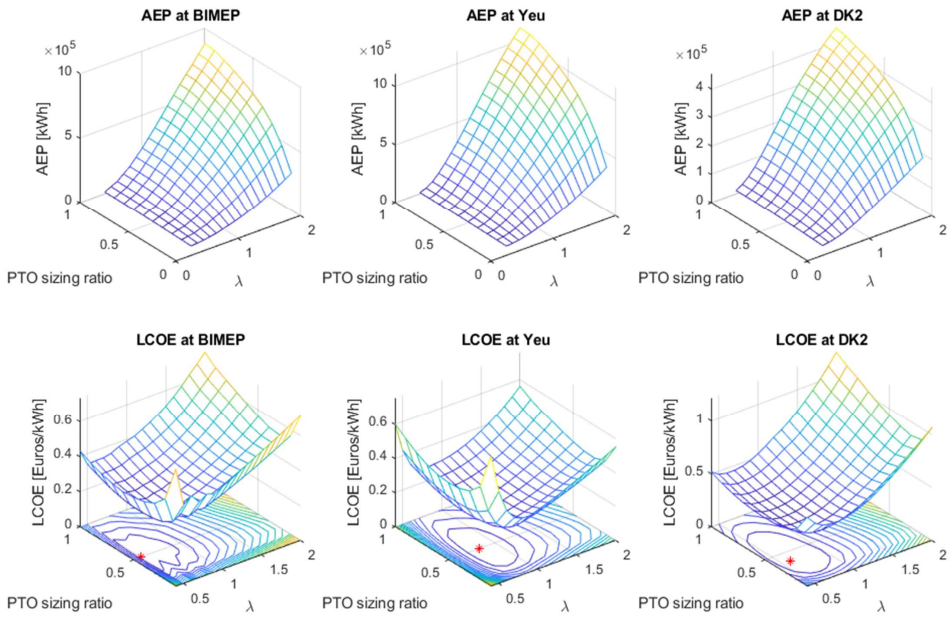
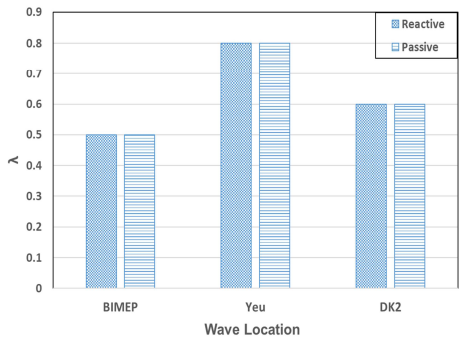


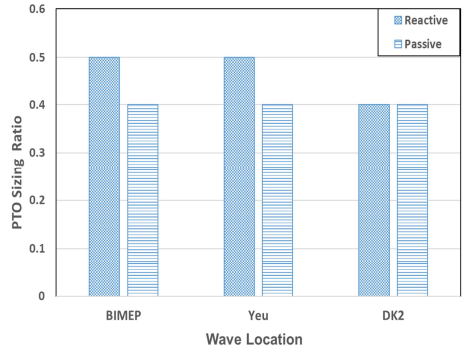
Figure 3.12: Size optimization of the WEC with reactive control.

Euros/kWh in the case of passive control. This is to be expected since the WEC with reactive control produces much more power than the WEC with passive control at the same sea state. From Figure 3.13c,d, it can be found that the higher the mean wave power density, the lower the optimal LCOE.

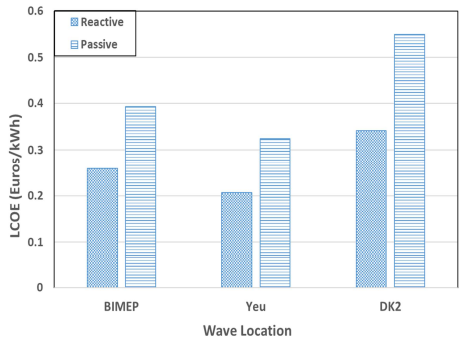
After the optimal buoy and PTO size have been determined for each sea site, the optimal cost proportion of the WEC can be obtained. The proportion of the PTO cost to the total CAPEX at the optimal sizing condition is shown in Figure 3.14. It can be seen that this cost proportion tends to be relatively independent of wave resources, while it is highly related to the control strategy of the WEC. In this case, the PTO cost of the WEC with reactive control accounts for 45% to 50% of the total CAPEX. Comparatively, for the WEC with passive control, this proportion decreases dramatically to around 30%. This can be explained by the fact that the required PTO forces in the WEC with reactive control are much higher than those with passive control. It also implies that the PTO size in the WEC with reactive control should be designed larger than that with passive control. Furthermore, it is noticed that the optimized cost proportion of PTO is much higher than the statistical value of 24.2% depicted in Table 3.1. The reason is that the WECs investigated in the literature [12] are generally in large scales, and the costs of the structure are dominating. However, the optimized buoy size of the WEC, in this case, is relatively small, with the diameter ranging around 2.5 m to 4 m ($\lambda = 0.5 - 0.8$). As a consequence, the PTO cost is more weighted compared with the structure cost. This phenomenon has also been explained in subsection 3.4.1 as the proportion of power-related capital cost decreases with the buoy scale factor λ.



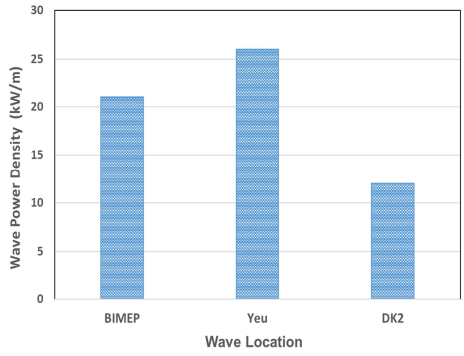
(a) Optimal buoy size



(b) Optimal PTO size



(c) Lowest LCOE



(d) Mean wave power density

Figure 3.13: The dependence of size optimization on wave resources and control strategies.

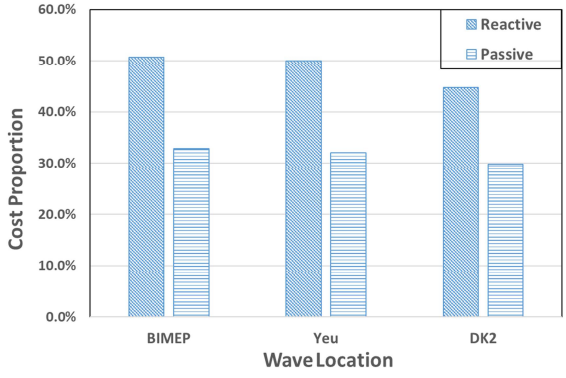


Figure 3.14: The proportion of cost on PTO to total CAPEX at the optimal buoy size and PTO size.

THE BENEFITS OF PTO DOWNSIZING FOR THE TECHNO-ECONOMIC PERFORMANCE

Increasing the PTO sizing ratio could reduce the negative effect of the PTO force limit on the power production of the WEC but it is clearly associated with the rise of the total CAPEX. A good illustration is shown in Figure 3.15. It is visible that the AEP increases up dramatically with the PTO sizing ratio at the range of relatively small values of the PTO sizing ratio. However, with the increase of the PTO sizing ratio, the increasing tendency becomes slower and the margin of the AEP is limited. Comparatively, the CAPEX is proportional to the PTO sizing ratio. Hence, from the economic point of view, downsizing the PTO sizing ratio to a certain extent is expected to be more beneficial.

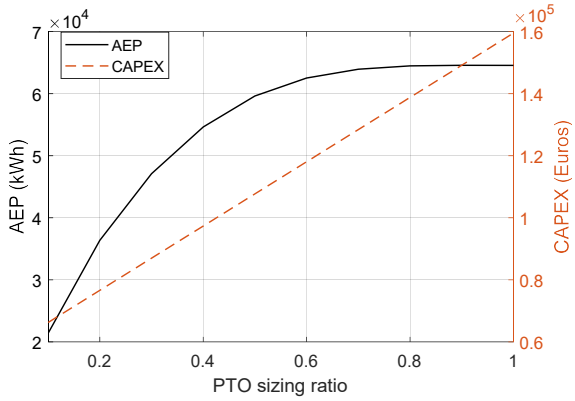
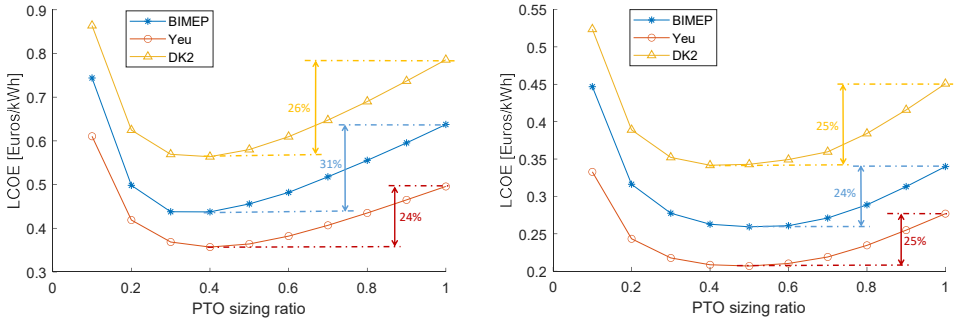


Figure 3.15: The variation of the AEP and the total CAPEX of the WEC with the PTO sizing ratio in Yeu island. The buoy scale factor λ is 0.8 which has been optimized for the sea site, and the passive control strategy is considered.



(a) The WEC with passive control

(b) The WEC with reactive control

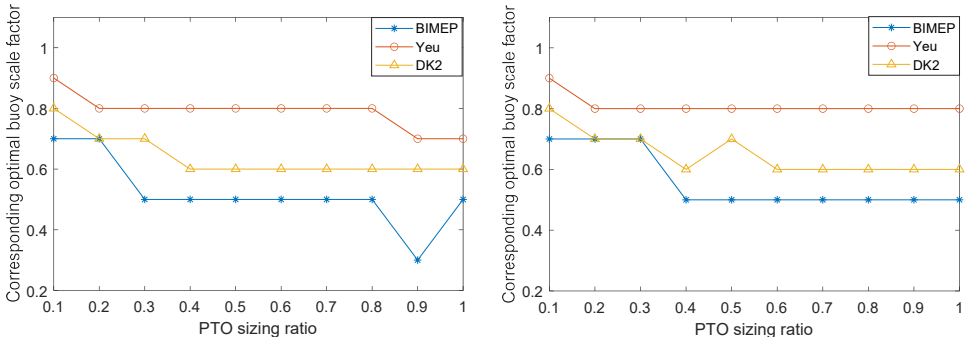
Figure 3.16: The effects of PTO downsizing on the Levelized Cost Of Energy (LCOE) of the WEC at the optimal buoy size.

To better illustrate the benefit of PTO sizing on the LCOE of the WEC, Figure 3.11 and Figure 3.12 could be presented in a different way with only looking at the results of the WEC at the optimal buoy sizes, shown as Figure 3.16. It can be seen that the LCOE can be significantly reduced by downsizing the PTO size even though the buoy sizes have been

optimized. In this case, downsizing the PTO sizing ratio to around 0.4 to 0.5 is preferable to minimize the LCOE. For the WEC with the passive control, downsizing the PTO size is able to reduce the LCOE by 24% to 31%, and it could reduce the LCOE by 24% to 25% in the case of reactive control. Hence, it is essential to take PTO size optimization into account when conducting sizing of the WEC. It also indicates that the techno-economic performance of WECs is generally underestimated due to the absence of PTO sizing in evaluation studies.

THE INTERACTION BETWEEN PTO SIZING AND BUOY SIZING

The interaction between PTO sizing and buoy sizing is shown in Figure 3.17. It can be seen that the optimal buoy size generally declines with the corresponding PTO sizing ratio. However, this effect is limited and the optimal buoy size tends to be constant as the PTO sizing ratio is higher than 0.3 or 0.4. Hence, in this case, it can be noted that the buoy size optimization can be influenced by PTO sizing, but only to a limited extent. However, it should be pointed out that the interaction between PTO sizing and buoy sizing is related to wave resources, WEC principles, and economic parameters. Therefore, for avoiding a poor estimate of the optimal buoy size, it is suggested to conduct PTO sizing simultaneously with buoy sizing. Furthermore, comparing Figure 3.17a,b, it is observed that there is no notable difference between the WEC with passive control and reactive control regarding the impact of PTO sizing on the buoy size determination.



(a) The WEC with passive control

(b) The WEC with reactive control

Figure 3.17: The interaction between PTO and buoy sizing.

3.4.3. THE PROPOSED METHOD VERSUS OTHER SIZE OPTIMIZATION METHODS

BUDAL DIAGRAM

As introduced in Chapter 2, Budal diagram is a useful tool to estimate the theoretical absorbed power of the WEC. According to Budal diagram, there are two upper absorbed power bounds in regular wave conditions, namely P_A and P_B. P_A bound is related to the maximum amount of power that could be extracted from incoming waves, while P_B reflects the bound of power that could be absorbed by the realistically sized WEC [20], [22]. P_A corresponds to the maximum absorbed power at the high wave frequency limit and is expressed as

$$P_A = J_{re}/k = \frac{\rho g^3 H^2 T^3}{128\pi^3} \tag{3.36}$$

Another power bound P_B corresponds to the maximum absorbed power at the low wave frequency limit and is expressed as

$$P_B = \frac{\pi \rho g H V}{4T} \tag{3.37}$$

where V is the volume of the buoy.

The size of WECs should match the wave resource to enable viability. Therefore, combined with the information of wave resources, Budal diagram could be used to select the suitable size of the WEC [20], [22]. However, for calculating V in (3.37), the designed working condition (H and T) should be explicit. In Reference [22], the WEC is assumed to be commercially viable if the amount of working time at full capacity exceeds one third of the annual time. Thus, the size of the WEC should match "one third wave power threshold" of the wave resource. Based on the power threshold, the wave height H_D and wave period T_D in the designed wave condition can be calculated. The detailed procedures using Budal diagram in sizing have been described in Chapter 2. With the defined designed wave condition, V can be easily calculated by equating (3.36) and (3.37) as the most suitable size of the WEC. However, it should be realized that, in this method, the calculation of volume V depends on the assumption of viable conditions, such as working at full capacity over one third of the annual time" [22]. In this case, the size selection of the WEC is shown in Table 3.2.

Table 3.2: Size selection based on Budal diagram.

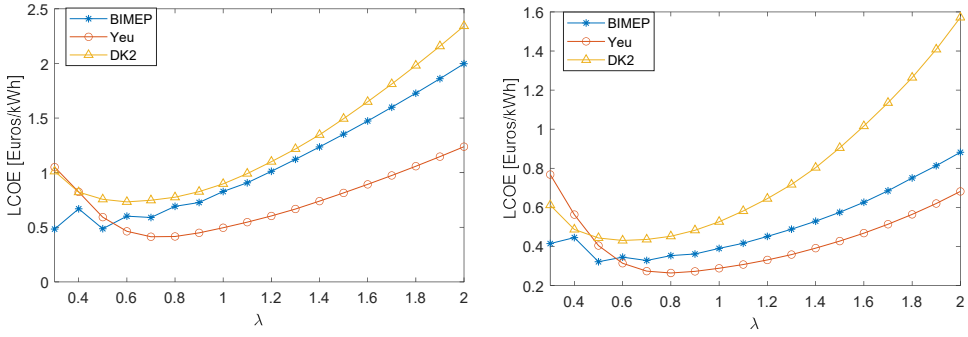
Sea Site	Wave Power Density Threshold	T_D	H_D	Buoy Volume	PTO Force Limit	
					Reactive	Passive
Yeu Island	30.4 kW/m	7.8 s	2.00 m	224 m^3	985 kN	216 kN
BIMEP	14.6 kW/m	8.4 s	1.33 m	206 m^3	946 kN	145 kN
DK2	8.2 kW/m	5.4 s	1.24 m	33 m^3	142 kN	36 kN

THE SIZE OPTIMIZATION WITHOUT PTO DOWNSIZING

As has been reviewed, the majority of existing literature regarding size optimization of WECs focused only on buoy sizing without considering PTO sizing. In those studies, the buoy size was optimized for the chosen sea sites, but the PTO size was simply scaled with the buoy scale factor λ [17], [18]. This kind of buoy size optimization is conducted based on Froude scaling. With the aim to compare different size optimization methods, the size optimization without PTO sizing is conducted as a reference in this work. The original buoy diameter is still defined as 5 m, the original PTO size is selected to sustain the maximum required force for the considered sea site, namely without PTO downsizing. Then, PTO force limits of the WEC in other buoy scale factors λ are scaled following Froude scaling, as (3.38).

$$F_{m_c} = F_{m_o} \lambda^3 \tag{3.38}$$

The power performance and the cost of the WEC at each buoy size are calculated by FD modeling and economic modeling, respectively. Therefore, the LCOE of the WEC at each buoy scale factor λ can be obtained. The optimization results are shown in Figure 3.18.



(a) LCOE vs buoy scale factor λ, passive control

(b) LCOE vs buoy scale factor λ, reactive control

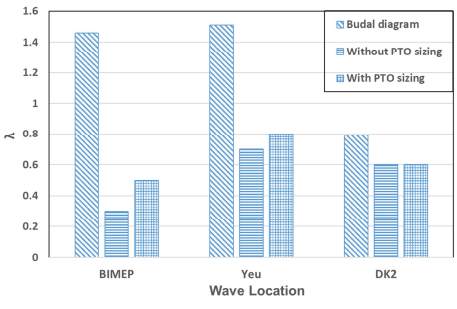
Figure 3.18: The size optimization of the WEC without PTO sizing.

COMPARISON OF SIZE OPTIMIZATION METHODS

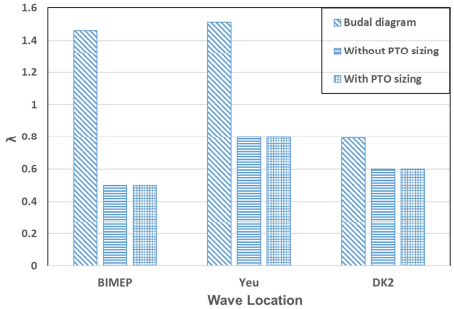
As is explained above, there are several methods available to conduct size optimization for improving the techno-economic performance of the WEC. A comparison among these methods is performed and the results are shown in Figure 3.19. Firstly, from Figure 3.19a,b, it can be observed that Budal diagram is not capable of determining the suitable sizes of the WEC. The deviation of the selected size between Budal diagram and the proposed method differs with wave resources, and this deviation tends to be random. For instance, the selected buoy scale factor λ for BIMEP is three times as much as that estimated by this proposed method, while the difference of selected sizes for DK2 is relatively small. However, as a theoretical and efficient approach, Budal diagram can be used to narrow the scope of size selection for potential sea sites. Secondly, compared with Budal diagram, size optimization without PTO downsizing shows a better ability to estimate the suitable buoy size of the WEC. Generally, without PTO sizing, the buoy size optimization can still acquire the suitable buoy size. This phenomenon also verifies the finding in Section 3.4.2. Thirdly, it can be seen from Figure 3.19c,d that the LCOE of the WEC optimized by this proposed method is clearly lower than those by the other two methods, no matter which control strategy is adopted. Hence, it can be concluded that this proposed method is able to result in a further improvement on the techno-economic performance of the WEC.

3.5. DISCUSSION

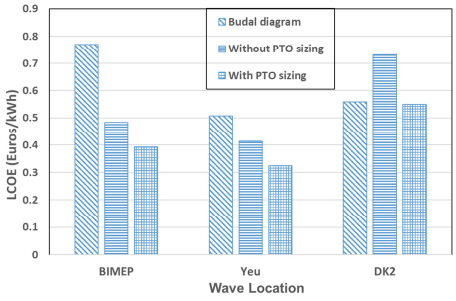
From an economic perspective and for the sake of simplicity, this study is limited to the analysis of a single device using general values of OPEX costs derived from existing literature. It should be acknowledged that one of the important factors affecting the LCOE is related to the system survivability and safety of WECs. Therefore, the techno-economic performance in practice is strongly related to the recurrence of extreme conditions, such as the roughest sea state for 50 or 100 years in the deployment site. In this way, the total LCOE could be significantly higher than the optimized value based on the current study, which could mitigate the effects of sizing on the techno-economic performance. However, a better understanding of the collective influence of buoy and PTO sizing of WECs can clearly contribute to a more suitable WEC design. In addition, sizing of a single WEC could make



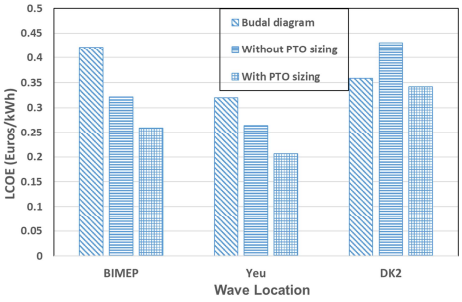
(a) Buoy size determination, passive control



(b) Buoy size determination, reactive control



(c) Lowest LCOE, passive control



(d) Lowest LCOE, reactive control

Figure 3.19: Comparison among different size optimization methods.

a difference in the total number of units selected for a wave farm or array, where the operation and maintenance costs are directly influenced by the number of WECs. For instance, a wave farm with a large number of small individual WECs is expected to result in an increased number of operation and maintenance activities, leading to higher operation and maintenance costs. On the other hand, larger WECs can reduce the number of units in the wave farm, but their requirements for service operation vessels could be higher [17]. Thus, as stated in Reference [114], estimating an accurate value for OPEX is a difficult task since there is not enough available information in practical projects.

In this thesis, two types of PTO control strategies are taken into account, namely the passive control and reactive control. However, they are not implemented in a real-time scale when calculating the power absorption. Instead. the PTO parameters are tuned to constant values for each sea state. It is realized that applying real-time control strategies allows instantaneous tuning of PTO parameters, and it could improve the power absorption of WECs particularly in irregular wave conditions. In this sense, the techno-economic performance of WECs can be better reflected. In recent years, real-time control strategies have been extensively studied and tested for the use in WECs. In [115], [116], the real-time passive control strategy was implemented for point absorbers, in which the PTO damping was adapted instantaneously to the frequency of the excitation force of the incoming waves.

In the studies, the velocity and displacement constraints were taken into account in the control methods. The reference indicated that the real-time passive control could increase the power absorption by 21 % compared to conventional tuning method with a constant PTO damping [116]. Even though the passive control strategies are only sub-optimal with respect to the reactive control strategies in principle, the passive control strategies were characterized by simpler implementation, lower peak-to-average power ratios, and avoidance of the negative power flow. The reactive control strategies make it possible for WECs to achieve both the optimal phase and amplitude of the velocity [106]. The application of real-time reactive control strategies to WECs has also been investigated [117]–[120]. Both the PTO damping and the PTO stiffness are tuned in the reactive control, from which even higher power absorption can be expected as compared with the passive control strategies. However, the use of the reactive control strategies is associated with drawbacks including:

- complex PTO mechanisms due to additional actuators or electronic components;
- negative power flow which reduces the power conversion efficiency;
- larger rated PTO systems, which could lead to higher cost;
- higher computational loads to obtain the optimal solutions for controllers in irregular wave conditions.

As an alternative, the latching control strategy can also be used to match the phase of the WEC with the incoming waves but without resulting in negative power flow. Real-time latching control strategies applied in irregular wave conditions have been investigated in [121]–[124]. These studies implied that the maximum capture width of WECs can be increased by 70 % in particular cases through applying the latching control strategies. But a major issue resulting from the latching control is the remarkable increase of the structural fatigue on the WEC [23], [124]. In addition, a general challenge in the real-time control of WECs is the prediction of the incoming wave forces, which significantly affects the control performance. As discussed above, real-time control strategies can be expected to improve the power production of WECs, but it still faces challenges towards a reliable, maintenance-friendly and cost-effective solution in practical application [23]. Thus, the performance of WECs with the constant PTO parameters tuned for each sea site can be thought as a simple but realistic reflection of current development level of wave energy technologies.

3.6. SUMMARY AND CONCLUSIONS

In this chapter, a size optimization method of the WEC is proposed for improving the techno-economic performance and applied to a spherical heaving point absorber. Both buoy sizing and PTO sizing are taken into account. Based on the proposed method, A case study is carried out for three typical sea sites. Both buoy sizing and PTO sizing are able to affect the techno-economic performance of the WEC. To improve the techno-economic performance, it is highly suggested to perform the buoy size optimization and PTO size optimization collectively. A comparison between the proposed method and other size optimization methods is performed. The following conclusions are drawn:

- The optimal buoy size differs with wave resources, but it is not necessarily proportional to the mean wave power density. In this case, the optimal buoy scale factor λ

ranges from 0.5 to 0.8. Furthermore, in most sea sites, the optimal PTO sizing ratios in the WEC with reactive control are slightly higher than those with passive control. The optimal PTO sizing ratios converge at around 0.4 to 0.5 for different sea sites. Moreover, the higher mean wave power density and reactive control can clearly contribute to the reduction of the LCOE.

- Downsizing the PTO size would penalize the AEP, but it is beneficial for reducing the LCOE. In this case, the LCOE can be reduced by 24% to 31% through downsizing the PTO sizing ratio from 1 to around 0.4 to 0.5.
- The corresponding optimal buoy size tends to slightly decrease with the PTO sizing ratio, but the influence of PTO sizing on the buoy size determination is limited.
- The sizing method based on Budal diagram relies on the definition of the designed wave condition, and it could result in an obvious deviation in the determination of the buoy size. The size optimization without PTO sizing can provide a relatively accurate prediction of the buoy size. Compared with these two methods, a further reduction in the LCOE can be achieved by including PTO sizing.

This chapter suggested the significance of PTO sizing, but there are two major limitations in addressing the effects of the PTO size. Firstly, nonlinear effects are neglected because of the application of FD modeling. Particularly, PTO sizing is highly associated with the PTO force limits, which can be characterized as the effect of PTO force saturation and is influential to the power absorption. Secondly, the PTO efficiency was considered to be constant regardless of the variation of the PTO size. In the following two chapters these two issues will be discussed and addressed in sequence, for a further improvement of the collective sizing method.

4

A Spectral Domain Model for PTO Sizing

In Chapter 3, the importance of PTO sizing was identified in reducing the LCOE of WECs, in which the power production of differently sized WECs was predicted by FD modeling. But FD modeling is not able to cover the relevant nonlinear effects, which limits the accuracy of the sizing method. As an extension, this chapter is intended to develop a computationally-efficient SD model incorporating a nonlinear component highly related to PTO sizing, namely the PTO force saturation. Compared with the FD model, the SD model remarkably reduces the relative errors in predicting the power performance of WECs with force constraints, while the computational demand is much lower than the nonlinear TD model. Furthermore, a case study is conducted in this chapter to size the PTO capacity for reducing the LCOE in a chosen wave site. The three different models are applied respectively, and a comparison is made with respect to their accuracy and efficiency in PTO sizing.

Parts of the chapter have been published in: Tan J, Polinder H, Laguna A J, et al. The application of the spectral domain modeling to the power take-off sizing of heaving wave energy converters[J]. Applied Ocean Research, 2022, 122: 103110. [93].

4.1. INTRODUCTION

THE PTO size implicitly indicates the maximum force it could sustain during normal operation. Therefore, it has to be considered as a physical constraint in the numerical modeling when calculating the power performance of WECs with differently sized PTO systems. In mild wave states with sufficiently large PTO sizes, the violation of the force constraint is limited, and the dynamic response of the WEC can be thought linear. For linear systems, the conventional FD modeling is considered to be a suitable numerical tool. When the force constraint comes to play, the force saturation becomes relevant and the system then is nonlinear. In this case, the TD modeling is required to include nonlinear behavior. However, the TD modeling is much more computationally time-demanding than the FD models. In this sense, the TD modeling is not an appealing solution since the PTO size optimization requires a large number of iterations through different wave states. To deal with the force constraint and save the computational efforts simultaneously, some assumptions were made in previous studies. For instance, a PTO sizing method based on the FD modeling was presented in [94], in which the irregular wave states were transferred to harmonic waves by equating the wave power transport. Then, the PTO parameters were tuned to make the PTO force amplitude in the corresponding harmonic waves lower than the defined constraint. In [125], a hydrodynamic optimization of a point absorber was conducted subjected to different physical constraints based on the FD modeling. The constraints were handled based on probabilistic analysis. The probability of exceeding the constraints was calculated by assuming that the responses obey a Rayleigh distribution. In the formulation of the Rayleigh distribution, the probability can be related to the standard deviation of the considered response. Therefore, given a defined tolerance on the exceedance probability, the PTO parameters were optimized to maximize the extracted power within the allowed range of the standard deviation of the response. Although these two methods ease the FD modeling's problem of lacking the consideration of the force constraint, they are still insufficient to model the contribution of the constraints to the power absorption. As an alternative, the SD modeling can be used to take nonlinear components into account, while its computational demands are significantly less than the TD modeling. The SD modeling could be regarded as an extension of the FD modeling, and the nonlinear terms are incorporated by statistical linearization. Therefore, the SD modeling is not able to predict the transient response, such as the peak displacement and extreme loads. However, it could effectively provide the estimates of statistical parameters, such as the mean absorbed power, which makes it highly suitable for the early-stage conceptual design and performance evaluation of WECs.

Although statistical linearization has been widely used in dynamic engineering for long time, the SD modeling was only introduced into the field of wave energy in 2010 [27]. In the work, a SD model considering the quadratic damping and wave force decoupling was derived for a flap-type WEC. Afterwards, follow-up studies were conducted to develop the SD modeling for taking more types of nonlinear components into account. In [126], a SD model including nonlinear damping terms for oscillating water column WECs was developed and validated by physical wave tank tests. In [127], a SD model of nonlinear hydrostatic stiffness was established for a semi-sphere point absorber. Recently, in [128]–[131], the SD modeling was further developed to incorporate the linearized representations of the end stop force, mooring force, viscous drag force, Coulomb damping and partial overlap effect between the stator and translator of the direct-drive PTO.

To the author's knowledge, a SD model considering the PTO force saturation has not been reported yet, but it is expected to serve as an powerful tool in PTO sizing. In addition, most of previous literature regarding the SD modeling mainly focused on model development or validation, and there is limited practical application of the SD modeling reported in the field of wave energy. Hence, the objective of this chapter is to develop a SD model of the PTO force saturation and demonstrate its relevance to the application of PTO sizing.

In this chapter, the representation of the PTO force saturation is derived for the SD modeling by statistical linearization. Next, for comparison, a FD model and nonlinear TD model are established. The proposed SD model is verified by the nonlinear TD modeling along various PTO force limits and wave states. Furthermore, the estimates of the power capture from three models are compared, in which the relative errors and computational efficiencies are presented. Moreover, the proposed SD model is applied to a case study of reducing the LCOE by optimizing the PTO size. A realistic wave site and preliminary economic model are considered. The impact of the numerical modeling on the tuning of PTO damping coefficients is analyzed. The reliability of the SD model on the prediction of the AEP, LCOE and optimal PTO size is demonstrated.

4.2. NUMERICAL MODELING

This section first presents the formulations of the FD modeling, TD modeling and SD modeling respectively. Then, the representations of the PTO force saturation are derived for these models. Finally, the three models are applied to a case study relevant to PTO sizing, in which the accuracy and efficiency of the SD modeling are identified.

4.2.1. FREQUENCY DOMAIN MODELING

FD modeling has been introduced in Chapter 3, the equations are briefly presented here for a clearer comparison with the TD and SD modeling. In FD, the motion of the WEC could be described as

$$\hat{F}_e(\omega) = [R_r(\omega) + R_{pto}]\hat{u} + \mathrm{i}\omega\hat{u}[M + M_r(\omega)] + \mathrm{i}\hat{u}(-\frac{K_{hs}}{\omega}) \tag{4.1}$$

Then, by solving (4.1), the complex amplitude of velocity $\hat{u}$ could be obtained as

$$\hat{u}(\omega) = \frac{\hat{F}_e(\omega)}{R_r(\omega) + R_{pto} + \mathrm{i}\omega[M + M_r(\omega)] - \mathrm{i}\frac{K_{hs}}{\omega}} \tag{4.2}$$

In irregular waves, the mean absorbed power can be derived as

$$\overline{P}_a = \sum_{j=1}^{N} \frac{1}{2} R_{pto} \left|\hat{u}(\omega_j)\right|^2 = \sum_{j=1}^{N} R_{pto} S_u(\omega_j)\Delta\omega = R_{pto}\sigma_u^2 \tag{4.3}$$

where S_u and σ_u denote the spectral density and standard deviation of the velocity of the WEC.

4.2.2. TIME DOMAIN MODELING

The above FD modeling is built based on the assumption that the system is fully linear. In the TD modeling, nonlinear terms can be taken into account. In the TD modeling, the

Cummins equation [89] is applied to describe the dynamic response of the floating body by the expression:

$$(M + M_r(\infty))a(t) = F_e(t) + F_{pto}(t) + F_{hs}(t) + \int_0^t K_{rad}(t-\tau)u(t)d\tau \tag{4.4}$$

where $M_r(\infty)$ is the added mass evaluated at the infinite frequency and K_{rad} is the radiation impulse function, and they can be calculated based on the results of $R_r(\omega)$ and $M_r(\omega)$ [89], [132]. The representation of wave excitation force F_e is expressed according to the predefined incident wave spectrum and random phase assumption, as

$$F_e(t) = \sum_{j=1}^{N} f_e(\omega_j)\zeta_a(\omega_j)\cos(\omega_j t + \varphi(\omega_j) + \beta(\omega_j)) \tag{4.5}$$

where f_e represents the excitation force coefficient which is the excitation force normalized to the wave amplitude of the harmonic wave component, ζ_a is wave amplitude of each frequency component, and $\beta(\omega_j)$ is the phase angle of the excitation force to the corresponding wave component.

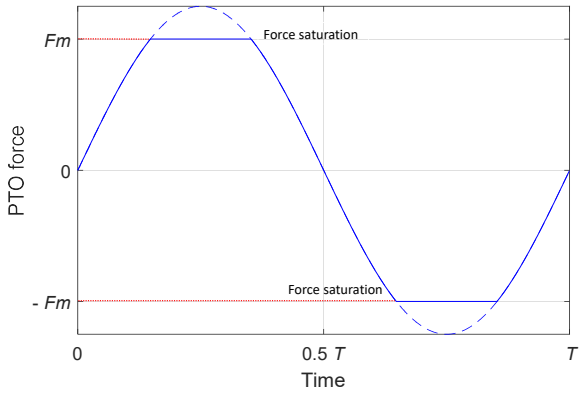


Figure 4.1: An example of the time-dependent PTO force response with the saturation.

The PTO force saturation can be included, and a typical force saturation effect is depicted in Figure 4.1. Once the PTO force limit is set to F_m, the F_{pto} is expressed as

$$F_{pto}(t) = \begin{cases} -R_{pto}u(t), & for \quad |R_{pto}u(t)| \le F_m \\ \text{sign}[-R_{pto}u(t)]F_m, & for \quad |R_{pto}u(t)| > F_m \end{cases} \tag{4.6}$$

The time averaged absorbed power is calculated as

$$\overline{P}_a = \frac{1}{t_0}\int_{t=0}^{t_0} -F_{pto}(t)u(t)dt \tag{4.7}$$

The only nonlinear behavior addressed in this TD model is the PTO force saturation, and all the other force components are considered to be linear. It is realized that the nonlinear hydrodynamic and hydrostatic forces would also be relevant to the reliability of the

modeling when wave heights are large relative to the diameter of the WEC. However, this paper is intended to demonstrate the relevance of PTO force saturation and therefore other nonlinearities are omitted.

4.2.3. SPECTRAL DOMAIN MODELING

As an extension of FD modeling, SD modeling is formulated based on the assumption that the system is linear and that the inputs and outputs are uncorrelated among different frequency components. Therefore the superposition principle is valid. Furthermore, all the dynamic responses of the system are assumed to have a Gaussian distribution. The SD modeling introduces quasi-linear coefficients to include the considered nonlinear effects. The derivation of the quasi-linear coefficients is based on statistical linearization, in which the contributions resulting from the nonlinear effects of the considered frequency components are taken into account.

The derivation of the quasi-linear coefficients in the SD modeling is briefly introduced here, and more details can be found in [27], [28], [126]. Assuming a general differentiable nonlinear function $f(x)$ and its linear equivalent function $f_e(x)$ are given as

$$f(x) = g(x) \tag{4.8}$$

$$f_e(x) = cx + b \tag{4.9}$$

where a and b are the quasi-linear coefficients, and $g(x)$ denotes a general nonlinear function with respect to x. Then, the error of the linearization can be expressed as

$$\epsilon = f(x) - f_e(x) = g(x) - cx - b \tag{4.10}$$

The average value of errors can be calculated in the statistical form of expected value, denoted as $<\cdot>$. By definition, the expected value of a random variable is the weighted average of all its possible outcomes. In statistical theory, the weight is represented by the probabilities of realizing each outcome. The expected value of the error squared is expressed as

$$<\epsilon^2> = <(g(x) - cx - b)^2> \tag{4.11}$$

To minimize the squared error, c and b should satisfy

$$\frac{\partial}{\partial c} <\epsilon^2> = 0 \quad \text{and} \quad \frac{\partial}{\partial b} <\epsilon^2> = 0 \tag{4.12}$$

The solutions to (4.12) are derived as

$$c = \frac{<xg(x)>}{<x^2>} \quad \text{and} \quad b = <g(x)> \tag{4.13}$$

If the nonlinear function $g(x)$ satisfies the zero-mean Gaussian distribution, its expected value is as zero and then only c to be solved.

According to the derivation of statistical linearization, the quasi-linear damping to represent the PTO force saturation can be calculated as

$$R_{eq,pto} = \frac{<uF_{pto}(u)>}{<u^2>} \tag{4.14}$$

where $< \cdot >$ denotes the expected value of a variable.

As the upper and lower limits of the PTO force in expressed in (4.6) are symmetric with regard to the horizontal axis, then substituting (4.6) into (4.14) gives

$$R_{eq,pto} = 2\int_0^{F_m/R_{pto}} \frac{R_{pto}u^2 q(u)\mathrm{d}u}{\sigma_u^2} + 2\int_{F_m/R_{pto}}^{\infty} \frac{F_m u q(u)\mathrm{d}u}{\sigma_u^2} \tag{4.15}$$

where $q(u)$ is the probability density function of Gaussian distribution, which is expressed as

$$q(u) = \frac{1}{\sigma_u\sqrt{2\pi}}\exp(-\frac{u^2}{2\sigma_u^2}) \tag{4.16}$$

where σ_u is the standard deviation of the buoy velocity. Then, (4.15) can be solved as

$$R_{eq,pto} = \frac{2R_{pto}}{\sigma_u^3\sqrt{2\pi}}[\frac{\sqrt{\pi}\sigma_u^3\mathrm{erf}(\frac{u_1}{\sqrt{2}\sigma_u})}{\sqrt{2}} - \sigma_u^2 u_1\exp(\frac{-u_1^2}{2\sigma_u^2})] + \frac{2R_{pto}u_1\sqrt{2\pi}}{\sigma_u}\exp(\frac{-u_1^2}{2\sigma_u^2}) \tag{4.17}$$

where “erf" represents the error function, and u_1 is the ratio between the PTO force limit and the PTO damping coefficient, expressed as

$$u_1 = \frac{F_m}{R_{pto}} \tag{4.18}$$

Therefore, (4.1) in the SD modeling is adjusted in order to include the quasi-linear damping coefficient $R_{eq,pto}$, as

$$\hat{F}_e(\omega) = [R_r(\omega) + R_{eq,pto}]\hat{u} + \mathrm{i}\omega\hat{u}[M + M_r(\omega)] + \mathrm{i}\hat{u}(-\frac{K_{hs}}{\omega}) \tag{4.19}$$

However, (4.19) cannot be solved directly since the standard deviation σ_u in (4.17) is unknown, and an iteration process is required. As demonstrated in [86], a relatively simple iteration solver is normally sufficient for the SD modeling of WECs to achieve the convergence. Because the nonlinear effects are not dominating in the operation of WECs and the responses of WECs are conditioned. Detailed discussion about the application of the iterative process in the SD modeling can be found in [86].

During the iteration of this work, the standard deviation of the velocity calculated by the FD modeling is taken as the initial guess to estimate the the quasi-linear damping coefficient $R_{eq,pto}$ used in the first iteration of the SD modeling. Then, the revised responses solved by (4.19) are updated in each iteration and a new value of the standard deviation of the velocity σ_u^+ can be calculated. Next, a refined approximation of σ_u is obtained as the weighted sum of the previous estimate σ_u^- and the renewed estimate σ_u^+, as

$$\sigma_u = \kappa\sigma_u^+ + (1-\kappa)\sigma_u^- \tag{4.20}$$

where κ is the weighting factor. The refined approximation σ_u is then used to formulate a updated value of $R_{eq,pto}$ for the next iteration. The iteration continues until the difference between the previous and iterative value converges within a certain margin. The convergences are checked for the all simulation cases implemented in this work.

After (4.19) is solved by iteration, the standard deviation of the velocity can be derived and the mean absorbed power in the SD modeling is then calculated as

$$\overline{P}_a = R_{eq,pto}\sigma_u^2 \tag{4.21}$$

4.2.4. IMPLEMENTATION OF SIMULATION

The simulation set-up is presented in this subsection. This chapter is focused on the PTO sizing, thus the variation of the buoy size is not addressed. The diameter of the floating spherical buoy is fixed to be 5 m in this chapter. A JONSWAP spectrum together with peakedness factor of 3.3 is applied to represent the irregular waves. For each wave state, 500 individual harmonic wave components with a random phase between frequency components are considered. The angular frequencies of the wave components are uniformly spaced from 0.05π to 4π rad/s.

In the TD modeling, directly computing the convolution integral of radiation force in (4.2) is computationally expensive [28]. However, it can be represented using an state-space approximation. In this paper, the FD identification method [133] is used to determine the state-space parameters and $M_r(\infty)$ as well. The TD simulation was implemented in the commercial Matlab environment and solved using a numerical integration scheme based on the ODE45 solver. The initial displacement and velocity of the buoy are set to zero. The simulation time duration and time step are set to 200 times and 0.01 times the considered peak period T_p respectively. A ramp function is used to avoid strong transient flow at earlier time steps, and the ramp time is chosen as 25 T_p [134]. The duration of the ramp time is not included in the calculation of the average power absorption. To mitigate random errors, the TD model is re-run 10 times for each case, and the mean values are calculated. In the SD simulation, as the iterative process is required to solve the standard deviation of the buoy velocity, a convergence criteria of 0.01 % is selected [126], [130].

4.3. VERIFICATION OF SPECTRAL DOMAIN MODELING

The TD modeling is used as the verification reference in this chapter. The SD modeling is established based on Gaussian assumption, but the addition of nonlinear force components makes the assumption less valid. Hence, it is necessary to have an insight into the validity of the assumption when the considered nonlinear components take effect. Figure 4.2 and 4.3 show the normalized probability density of the buoy velocity calculated by the nonlinear TD modeling for different wave heights and PTO force limits. Furthermore, in these figures, the probability density of the Gaussian distribution with the standard deviation calculated by the TD modeling accordingly is also shown as the reference. In general, the responses of the WEC remain Gaussian to a suitable extent. However, the Gaussian assumption tends to be relatively less valid when the wave height turns higher or the PTO force limits become stricter, which implies a reduction of the reliability of the SD modeling. For instance, in Figure 4.3, the difference of the probability density for the PTO force limit of 30 kN is larger than those for the PTO force limit of 50 kN and 100 kN. This happens since the highly constrained force limit makes the PTO force frequently saturated, in which the nonlinearity is highly intensified. This results in a decrease of the validity of the Gaussian assumption, even though the quantitative difference is hardly noticeable at the low PTO force limit of 30 kN. Nevertheless, the SD modeling is commonly applied for the performance evaluation or early-stage design of WECs, where the contribution of the highly powerful wave states and strong force saturation is limited. Therefore, the use of Gaussian assumption is thought to be reasonable.

To verify the SD modeling, its calculated power spectral density, standard deviation of the responses are compared with those obtained by the nonlinear TD modeling. For the results of the TD modeling, Fourier analysis is used to obtain the response components

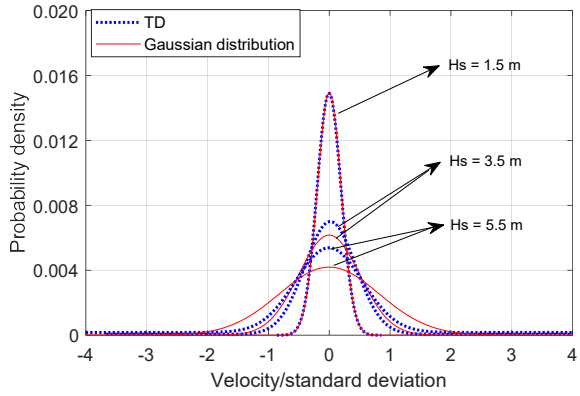


Figure 4.2: The probability density of velocity of the WEC for different wave heights, T_p = 12.87 s, F_m = 50 kN and R_{pto} = 100 kNs/m.

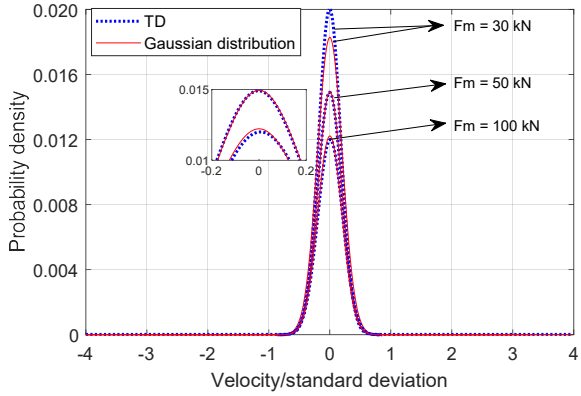


Figure 4.3: The probability density of velocity of the WEC for different PTO force limits, T_p = 12.87 s, H_s = 1.5 m and R_{pto} = 100 kNs/m.

in different frequencies. Figure 4.4 shows the power spectral density of the buoy velocity obtained by three different models. The shaded area in Figure 4.4 represents the standard deviation of TD results by running the model multiple times. It can be seen that the SD modeling has a good agreement with the TD modeling, and its accuracy is clearly better than the FD modeling. Figure 4.5 and 4.6 show the standard deviations of the buoy velocity calculated by the TD and SD modeling, and different wave states and PTO force constraints are considered. In Figure 4.5 and 4.6, the standard deviations predicted by the SD and TD modeling tend to converge as the PTO force limit keeps increasing to the point when the system can be considered linear. Furthermore, it can be found that changes in the standard deviations predicted by the SD modeling are more notbale from those calculated by the TD modeling with the increase of H_s and the decrease of the PTO force limit. In Figure 4.5, the maximum difference is 2.4 % occurring at T_p of 7.28 s and H_s of 5 m, and it is 3.2 % at the PTO force limit of 20 kN and H_s of 3.5 m in Figure 4.6. In mild wave states and PTO force

constraints, the difference is even more limited. Therefore, the proposed SD modeling is thought to be reliable for the use in the PTO sizing.

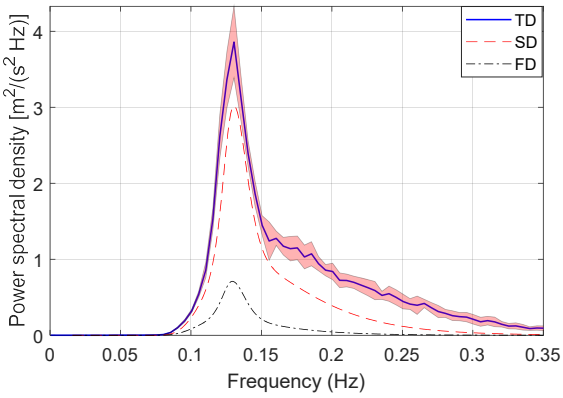


Figure 4.4: The power spectral density of velocity of the WEC ($H_s = 2$ m, $T_p = 7.28$ s), $F_m = 20$ kN and $R_{pto} = 400$ kNs/m. The shaded area is used to represent the standard deviation of the TD domain results.

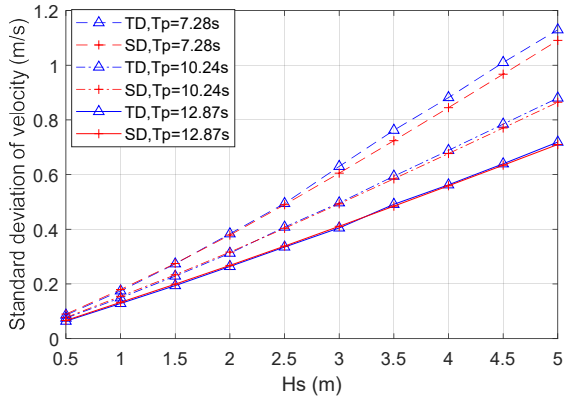


Figure 4.5: The standard deviation of velocity of the WEC at different wave states, $F_m = 50$ kN and $R_{pto} = 100$ kNs/m.

4.4. COMPARISON OF THREE MODELS ON THE PREDICTION OF THE POWER ABSORPTION

In this section, the accuracy and computational efficiency of three models are compared. Figure 4.7 and 4.8 depict the capture width ratio (CWR) predicted by the three models and the average relative errors of the FD and SD modeling with respect to the TD modeling. Different wave heights and PTO force constraints are taken into account. In Figure 4.7b and 4.8b, the resulting errors are averaged over the three considered wave periods. The CWR is defined as the absorbed power divided by the wave power per unit length of wavefront and

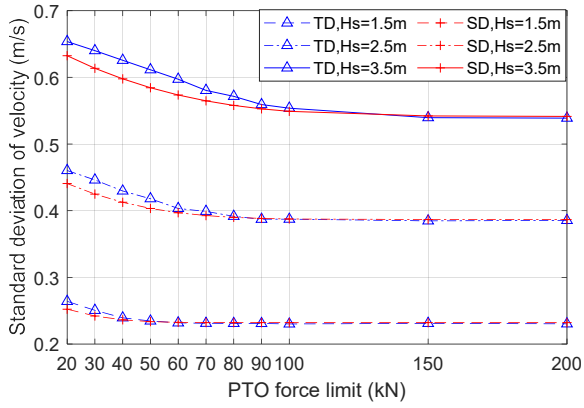
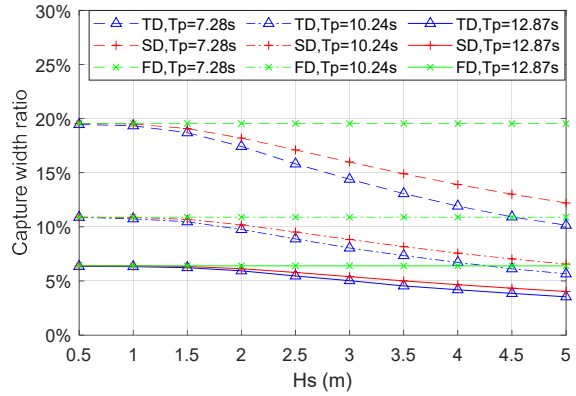


Figure 4.6: The standard deviation of velocity of the WEC for different PTO force limits, T_p = 10.24 s and R_{pto} = 100 kNs/m.

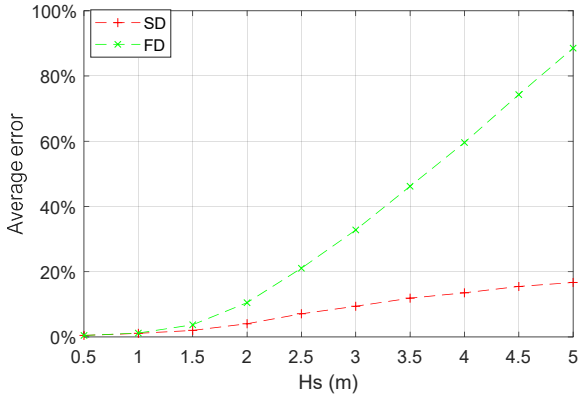
characteristic length of the WEC. It can be seen from Figure 4.7 and 4.8 that the FD modeling has an acceptable reliability at low wave heights or large PTO force limits even though the force constraint effect is not included at all. This is because the PTO force constraint is not significant in these cases. When the force limit turns tighter or the wave height becomes higher, the force saturation occurs more often, and then the FD modeling can hardly give a reliable prediction. For instance, when H_s is 5 m and T_p is 7.28 s in Figure 4.7a, the CWR predicted by the TD modeling is approximately only half of that given by the FD modeling. In Figure 4.7b and 4.8b, the average relative error of the FD modeling even reaches 100 % and 200 % when the H_s is 5 m and the PTO force limit is 20 kN respectively. As for the SD modeling, it presents comparable results with the TD modeling throughout all the considered conditions. At relatively low wave heights and large force limits, the prediction difference on CWR between the SD and TD modeling is negligible. It can be noted that the accuracy of the SD modeling tends to decrease with the wave height and the strictness of the PTO force limit where the nonlinearity is stronger. However, the relative errors of the SD modeling are dramatically lower than those of the FD modeling, and the maxima is around 20 % which only occurs at the extreme PTO force limit of 20 kN. This is an obvious improvement on the accuracy compared with the FD modeling. Furthermore, it can noticed that the CWR shown in these two figures are relatively lower than the reported values for point absorbers in literature [101]. This is because the PTO damping coefficient is not optimized here for the considered operating conditions.

The relative computational time of the three models is compared in Table 4.1, and all the simulations are run in the same machine with an Intel i7/2.80 GHz processor. The TD modeling computational time is counted as the time of running one single simulation. It is seen that the computational efficiency of the SD modeling remains in a similar level with the FD modeling, and the TD modeling is dramatically more time-demanding. Therefore, compared with the FD and TD modeling, the SD modeling could clearly improve the accuracy of power prediction and still retain sufficient computational efficiency. It should be clarified that the computational time of the TD modeling depends on the run length and time step length of the simulation. However, the setup of these two parameters is important

to the accuracy of the modeling. One comparable example is given in [134] where the run length was set to 125 T_p with a time step of 0.01 T_p in the TD modeling for calculating the motion response and power production while the run length in this paper is set to 200 T_p. Nevertheless, the computational time of the TD modeling is several orders of magnitude higher than the SD modeling.



(a) Capture width ratio predicted by different models

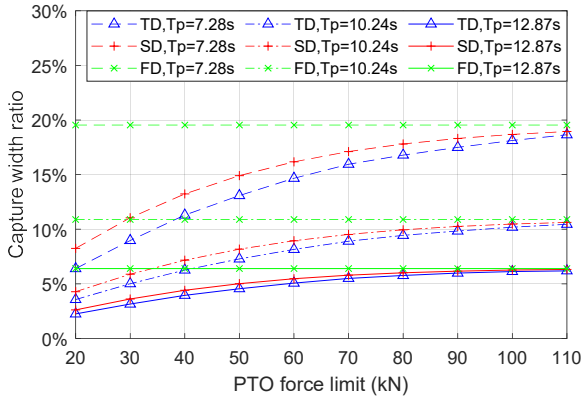


(b) The average errors of the FD and SD modeling to the TD modeling over three wave periods (T_p = 7.28 s, T_p = 10.24 s and T_p = 12.87 s)

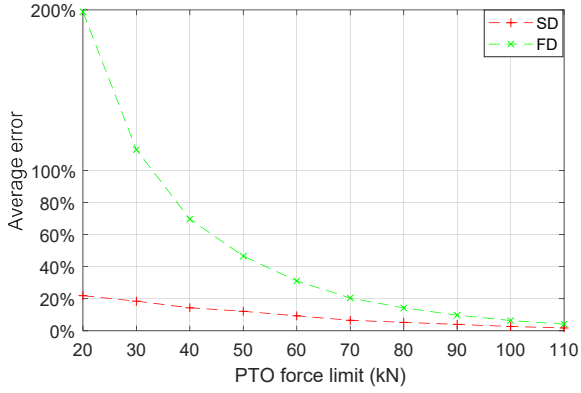
Figure 4.7: Comparison of capture width ratio predicted by three models along different wave heights, F_m = 50 kN and R_{pto} = 100 kNs/m.

Table 4.1: Comparison of the computational time in the simulation case with H_s = 1.5 m, T_p = 10.24 s and F_m = 50 kN.

Numerical modeling	FD	SD	TD (single-run)
Computational time (s)	$1.88 \cdot 10^{-3}$	$3.22 \cdot 10^{-3}$	6.71



(a) Capture width ratio predicted by different models



(b) The average errors of the FD and SD modeling to the TD modeling over three wave periods (T_p = 7.28 s, T_p = 10.24 s and T_p = 12.87 s)

Figure 4.8: Comparison of capture width ratio predicted by three models along different PTO force limits, F_m = 50 kN, H_s = 3.5 m and R_{pto} = 100 kNs/m.

4.5. CASE STUDY: DETERMINING THE OPTIMAL PTO SIZE FOR YEU ISLAND

In this section, three models are implemented to do the PTO sizing for Yeu island. It is intended to demonstrate the performance of the SD modeling in a practical application. The impacts of the numerical modeling on tuning of the PTO damping coefficients, techno-economic performance and determination of the PTO size are identified.

4.5.1. INCORPORATION OF VISCOUS DRAG FORCE

In the AEP calculation, the viscous drag force is taken into account in the SD and TD modeling for better accuracy of the techno-economic assessment. In the TD simulation, the

viscous drag force can be represented by a quadratic damping term [130] as

$$F_{vis} = -\frac{1}{2}\rho C_D A_D |u| u \tag{4.22}$$

where ρ is the water density, C_D is the drag coefficient and A_D is the characteristic area of the buoy perpendicular to the moving direction. The drag coefficient is selected as 0.6 to minimize the error of the power estimate based on the investigation reported in [135], in which the research reference is also a sphere.

For the SD modeling, the linearized viscous damping has been derived in [27], [126], [130], and it is expressed as

$$R_{eq,vi} = \frac{1}{2}\rho C_D A_D \sigma_u \sqrt{\frac{8}{\pi}} \tag{4.23}$$

Then (4.19) can be updated as

$$\hat{F}_e(\omega) = [R_r(\omega) + R_{eq,pto} + R_{eq,vi}]\hat{u} + \mathrm{i}\omega\hat{u}[M + M_r(\omega)] + \mathrm{i}\hat{u}(-\frac{K_{hs}}{\omega}) \tag{4.24}$$

After including the viscous drag force into the SD and TD modeling, other set-ups and the solution process remain identical as demonstrated in Section 4.2. The CWR calculated by the models with and without considering the viscous drag forces are compared in Figure 4.9. It is clearly reflected in the SD and TD modeling that the incorporation of the viscous drag force decreases the power absorption. In addition, the SD modeling still presents fairly close results to the TD modeling even though two nonlinear effects, namely the PTO force saturation and nonlinear viscous drag force, are taken into account at the same time. It also indicates that more nonlinear effects can be effectively considered in the SD modeling to further improve the accuracy. However, this is out of the scope of this work which is intended to focus on the effect of the PTO force saturation. The derivation of other commonly concerned nonlinear effects in the SD modeling can be found in [27], [127], [130].

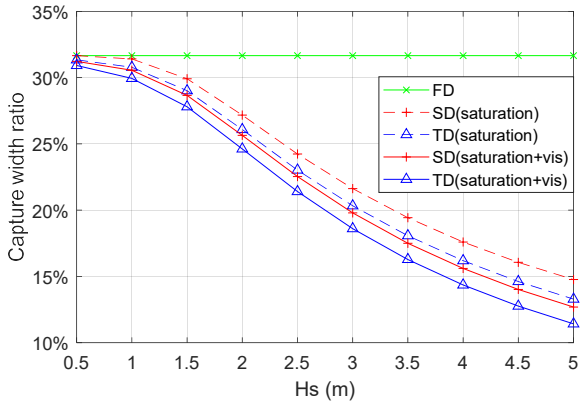


Figure 4.9: Comparison of capture width ratio predicted by different models, F_m = 30 kN, R_{pto} = 70 kNs/m and T_p = 5.15 s. In the legend, 'saturation' represents the models including PTO force saturation as the only nonlinearity, and 'saturation + vis' represents the models with both nonlinear effects of the PTO namely force saturation and viscous drag force.

4.5.2. THE TUNING OF PTO PARAMETERS

The PTO damping coefficients are significant to the power absorption of WECs. To provide an insight into the dependence of the optimization of the PTO damping coefficients on the numerical modeling, a comparison is made among the models. In addition to maximizing the power capture, the probability of occurrence of the PTO force saturation also needs to be considered in the determination of the PTO damping coefficients. Taking the direct-drive generator as an example, the PTO force saturation is associated with large currents, and the highly frequent PTO force saturation might lead to overheating conditions. Two methods are introduced below to incorporate the probability of occurrence when tuning the PTO parameters of WECs.

- Probabilistic method

  As the WEC is subjected to random wave inputs, the probability of occurrence can be estimated by the probabilistic analysis. If the dynamic process is assumed to be Gaussian with zero mean, the amplitude of the variables can be characterized by Rayleigh distribution [104]. Hence, the probability of PTO force saturation can be calculated by

$$Q(s) = \exp\left(\frac{-F_m^2}{2\sigma_F^2}\right) \tag{4.25}$$

  where σ_F represents the standard deviation of PTO force. Then, a tolerance on the probability should be defined, and it is tackled as a constraint in the optimization of PTO parameters. This method has been used in [125] for the hydrodynamic optimization of WECs. However, the tolerance on the probability is dependent on plenty of factors, such as the PTO type and design, scale of the WEC, severity of the load, material strength, maintenance frequency and so on. It is expected that the tolerance on the probability of the PTO force saturation would differ from one project to another in practice. Therefore, it is challenging to properly determine the tolerance due to the lack of information from practical WEC projects.

  The relation of the absorbed power and probability of the force saturation to the PTO damping coefficient is calculated by the three models respectively, as depicted in Figure 4.10. It is noticed that the selection of the numerical model makes a notable difference to the PTO damping optimization. For instance, the PTO damping coefficient with the highest power absorption is 75 kNs/m in the FD modeling. Comparatively, in the SD and TD modeling, the power absorption tends to be saturated with the increase of the PTO damping without reaching a certain peak point. This is because the PTO force is highly limited by the saturation effect when the PTO damping coefficient is large. The further increase of the PTO damping has a limited effect on the standard deviation of the PTO force or the system dynamics. Furthermore, it is observed that the maximum power predicted by the FD modeling is higher than other models, and this can be explained by the existence of the viscous drag force in the SD and TD modeling. In addition, compared with the SD and TD modeling, the FD modeling overestimates the probability of the PTO force saturation. The reason is that the PTO force saturation does not take effect in the FD modeling, and hence the resulting PTO forces are accordingly higher. Moreover, the difference between the probabilities cal-

culated by the SD and TD modeling is negligible, which implies the good reliability of the SD modeling on predicting the standard deviation of the PTO force.

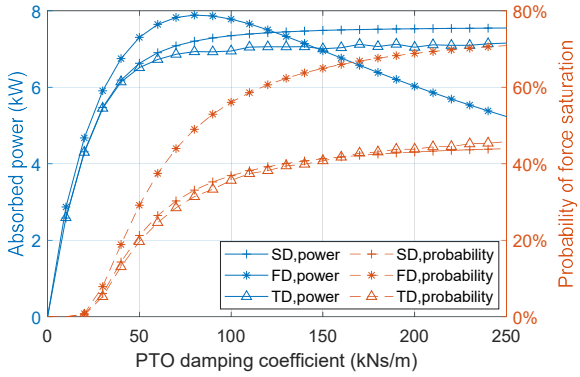


Figure 4.10: The absorbed power and probability of PTO force saturation as a function of PTO damping coefficient, $H_s = 1.5$ m, $F_m = 30$ kN and $T_p = 5.15$ s.

Figure 4.11 shows the PTO damping and absorbed power optimized by the three models, and different allowable probabilities of the PTO force saturation are considered. It can be seen that both the optimal PTO damping and absorbed power increase with the allowable probability. In addition, the PTO damping optimized by the FD modeling is lower than those corresponding to the SD and TD modeling, and the difference becomes larger with the increase of the probability. For instance, the optimal PTO damping of the SD and TD modeling is around twice the value of the FD modeling when the probability is 40%. The reason is that the FD modeling overestimates the standard deviation of the PTO force as well as the probability of the exceedance, thus its optimized PTO damping should be correspondingly lower under certain tolerance. Comparatively, the SD and TD modeling result in similar optimal PTO damping coefficients throughout all the considered allowable probabilities.

It is noticed in Figure 4.11 that the FD modeling only presents a slightly higher power estimate than the SD and TD modeling, although its optimal PTO damping is very different. This observation can be explained by analyzing how the optimal PTO damping is found during the optimization. In most of cases, the optimal absorbed power is obtained when the allowable probability of the PTO force is reached. Then, the standard deviations of the PTO force at the optimal conditions are identical for the SD and FD modeling, and the standard deviations of the PTO force are expressed as

$$\sigma_F = R_{pto}\sigma_u, \text{ for FD modeling} \tag{4.26}$$

$$\sigma_F = R_{eq,pto}\sigma_u, \text{ for SD modeling} \tag{4.27}$$

As the PTO force is significantly more dominating than the viscous drag force in the SD modeling, the equivalent PTO damping $R_{eq,pto}$ in (4.27) is close to R_{pto} in (4.26) after the PTO damping optimization. In this way, the dynamics estimated by the two models tend to be similar. Then, the absorbed power of the SD and FD modeling are

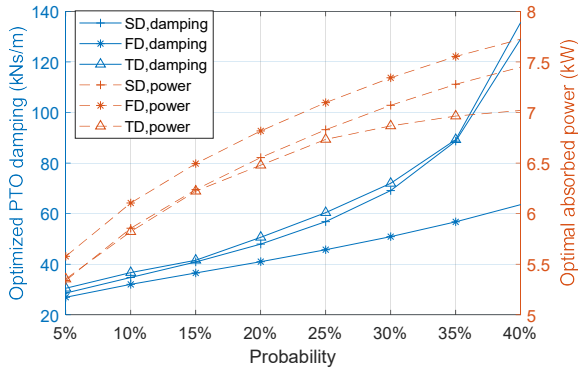


Figure 4.11: The optimized PTO damping coefficients and absorbed power as a function of the allowable probability of the PTO force saturation, $H_s = 1.5$ m, $F_m = 30$ kN and $T_p = 5.15$ s.

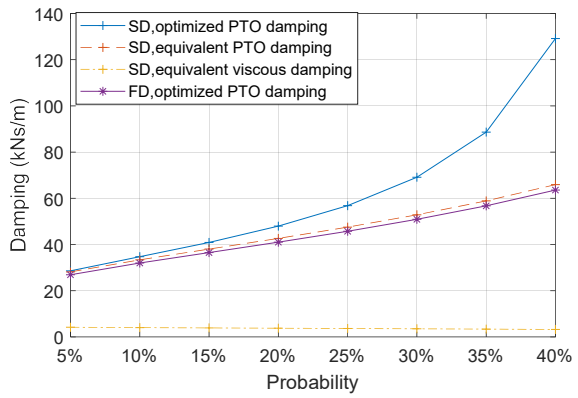


Figure 4.12: The PTO damping coefficients optimized by the FD and SD modeling, the corresponding equivalent PTO and viscous damping in the SD modeling as a function of the allowable probability of the PTO force saturation, $H_s = 1.5$ m, $F_m = 30$ kN and $T_p = 5.15$ s.

also comparable, and the slight difference results from the viscous drag force. This explanation can be verified by Figure 4.12, which depicts the $R_{eq,pto}$ for the SD modeling and R_{pto} for the FD modeling after the PTO damping optimization. It is seen that the equivalent viscous damping is highly limited in this case. Furthermore, the equivalent PTO damping $R_{eq,pto}$ is very similar with the PTO damping R_{pto} optimized by the FD modeling, even though the value of the optimized PTO damping by the SD modeling is much larger. This explains why the values of the optimal absorbed power of the three models are close after the PTO damping optimization. However, it should be noted that this observation is limited to this particular case. When other nonlinear effects are considered or the viscous damping is more influential, the difference in dynamics estimated by the SD and FD modeling could become higher with the optimized PTO damping coefficients. As a result, the values of the optimal absorbed

power from the FD and SD modeling are also expected to have higher variations. However, further investigation is out of the scope of the present paper.

- Transferred method

  A simplified method can also be used to determine the PTO coefficients without defining the tolerance and calculating the exceedance, and this method has been used in [94], [98]. Specifically, in this method, the irregular wave states are transferred to corresponding regular wave states by equating their time-averaged power transport per unit length of wave front. Then, the PTO parameters are selected to suit the transferred regular wave states, namely energy period T_e and $H_s/\sqrt{2}$. As the PTO force amplitude and time average power can be explicitly derived for the regular wave states, the optimal PTO damping coefficient can be obtained to maximize the absorbed power and guarantee the PTO force amplitude to be lower than the PTO force constraint. For convenience, it is called the transferred method in the following text. It is realized that this tuning method is only an approximation. Therefore, in irregular wave states, the maximization of the power absorption cannot be guaranteed and the violation probability of the force constraint is not necessarily within a certain tolerance either.

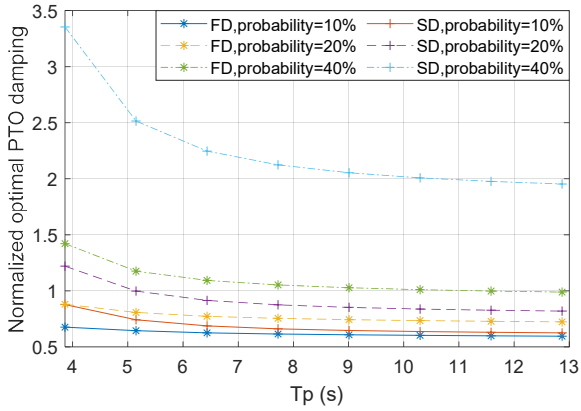


Figure 4.13: The optimal PTO damping coefficients with different probabilities of force saturation obtained by the FD and SD modeling normalized to those obtained by the transferred method, H_s = 3.5 m, F_m = 50 kN.

In Figure 4.13, the optimal values of PTO damping obtained by the probabilistic method are normalized to those obtained by the transferred method. For comparison, the SD and FD modeling are applied in the probabilistic method respectively. Different wave periods and tolerances on the probability of the force saturation are considered. It is seen from Figure 4.13 that the tolerance has a remarkable impact on the PTO damping determination, and easing the tolerance increases the selected optimal damping coefficients. In this case, the transferred method implies a tolerance on the probability of approximately 20 %, if the results of the SD modeling are taken as the reference. In addition, the PTO damping optimization is highly dependent on the numerical modeling, and the difference between the optimal damping coefficients selected by the FD and SD modeling increases proportionally to the tolerance. In particular cases,

the difference reaches up to 100 %.

4.5.3. THE TECHNO-ECONOMIC ANALYSIS

To search for the optimal PTO size, the techno-economic performance of the WEC is calculated for different PTO force limits. The step length of the PTO force limit is selected to be 10 kN. In the AEP calculation of the techno-economic analysis, both of the above methods are used to tune the PTO parameters for comparison. The PTO parameters are updated for each sea state.

LCOE USING THE PROBABILISTIC METHOD

In this method, the PTO parameters are optimized by each model independently, and hence the effect of the numerical modeling on tuning the PTO is reflected in the AEP and LCOE calculation. The allowable probability of the PTO force saturation acts as a constraint during optimization, and it is defined as 20 % here for a preliminary assessment. Regarding the PTO damping optimization by the SD and FD modeling, the "interior point" algorithm in Matlab environment is used, and the tolerance of the function is set as 1e-5. The bound of the PTO damping is set as $[0,20R_r(\omega_p)]$ for each sea state, in which ω_p is the peak frequency of the irregular wave state.

Table 4.2: The comparison of AEP (MWh) predicted by three models and the relative errors of the FD and SD modeling to the TD modeling, and PTO parameters are tuned based on the probabilistic method.

PTO force limit F_m (kN)	TD (standard deviation)	FD	SD	Errors of FD	Errors of SD
20	27.29 (0.19)	28.31	27.63	3.7 %	1.2 %
30	38.78 (0.14)	40.08	39.22	3.4 %	1.2 %
40	48.80 (0.27)	50.50	49.50	3.5 %	1.4 %
50	57.26 (0.18)	59.68	58.54	4.2 %	2.2 %
60	64.86 (0.33)	67.78	66.52	4.5 %	2.6 %
70	71.69 (0.45)	74.86	73.47	4.4 %	2.5 %
80	77.53 (0.44)	80.99	79.50	4.5 %	2.5 %
90	81.87 (0.51)	86.26	84.66	5.4 %	3.4 %
100	86.25 (0.51)	90.71	89.02	5.2 %	3.2 %
110	89.67 (0.66)	94.36	92.59	5.2 %	3.3 %
120	92.22 (0.71)	97.30	95.45	5.5 %	3.5 %
130	95.15 (0.70)	99.60	97.70	4.7 %	2.7 %
140	97.07 (0.69)	101.38	99.44	4.4 %	2.4 %

As for the optimization using the TD modeling, an exhaustive searching process is used for a range around the optimal PTO damping optimized by the SD modeling $R_{opt,sd}$, namely $[0.9R_{opt,sd},1.1R_{opt,sd}]$, and the searching step is selected to be $0.01R_{opt,sd}$. The selected searching range is thought to be fair, since the deviation between the PTO damping optimized by the SD modeling and by the TD modeling is observed to be limited, as shown in Figure 4.11. This is intended to save the optimization time given the low computational efficiency of the TD modeling.

Table 4.2 and Figure 4.14 present the AEP and LCOE of the WEC with different PTO force limits respectively. It can be seen that the relative errors of the SD modeling to the TD mod-

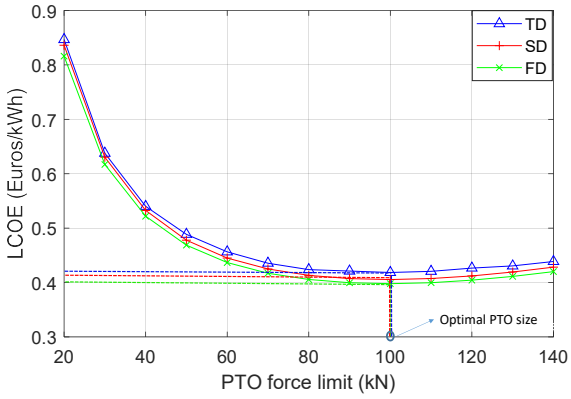


Figure 4.14: LCOE of the WEC predicted by three different models, and PTO parameters are tuned based on the probabilistic method.

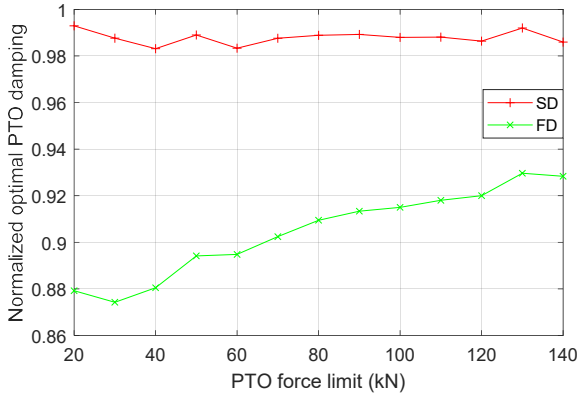


Figure 4.15: The weighted mean values of the PTO damping optimized by the FD and SD modeling normalized to those obtained by the TD modeling.

eling are less than those of the FD modeling. Regarding the AEP prediction, the maximum error of the SD modeling is 3.5 % while it is 5.5 % for the FD modeling. However, the three models generally indicate similar results, and they also lead to the same optimal PTO sizing in this case. This can be expected, because the difference of the absorbed power of the three models is limited when using the probabilistic method to tune the PTO parameters. The detailed explanation can be found in subsection 4.5.2. However, this conclusion could not be simply extended to other scenarios, particularly when other nonlinear effects are more influential than the PTO force saturation.

To provide an insight into the difference among the three models on the determination of the PTO parameters, the weighted mean values of the optimal PTO damping coefficients are calculated. In the calculation, the value of hours of the occurrence of each sea state is considered as the weight. Figure 4.15 shows the weighted mean of the optimized PTO damping coefficients estimated by the FD and SD modeling normalized to that estimated

by the TD modeling. It is noticed that the SD modeling has a good reliability on tuning PTO parameters, and the discrepancies are limited to 2 %. In contrast, the optimal PTO damping estimated by the FD modeling is much lower, with an error of more than 12 % relative to the TD modeling when the PTO force limit ranges from 20 to 30 kN. This implies that the FD modeling is insufficient to identify the optimal PTO parameters.

LCOE USING THE TRANSFERRED METHOD

In the transferred method, the PTO damping coefficients applied in the three models are kept identical, and they are updated to each sea state. In the sense, the relative errors on the AEP and LCOE estimates of the FD and SD modeling only result from the modeling itself.

The AEP of the WEC predicted by different models is shown in Table 4.3. It can be seen that both the FD modeling and SD modeling result in an overestimation of the AEP compared with the TD modeling. However, the predication deviation between the FD modeling and TD modeling is significant, and the relative error increases as the PTO force limit turns stricter. When the PTO force limit is 20 kN, the deviation is over 24 %. In this sense, the reliability of the FD modeling in tackling cases where the PTO force saturation is relevant is clearly insufficient. In contrast, the SD modeling presents a much better accuracy on the prediction of the AEP, the relative errors are observed to be no more than 4.3 %, ranging from 2.0 % to 4.3 %, along all the considered cases.

Table 4.3: The comparison of AEP (MWh) predicted by three models and the relative errors of the FD and SD modeling to the TD modeling, and PTO parameters are tuned based on the transferred method.

PTO force limit F_m (kN)	TD (σ)	FD	SD	Errors of FD	Errors of SD
20	29.35 (0.11)	36.50	29.95	24.4 %	2.0 %
30	41.01 (0.21)	49.93	42.06	21.8 %	2.6 %
40	50.99 (0.22)	61.20	52.60	20.0 %	3.2 %
50	59.87 (0.19)	70.70	61.80	18.1 %	3.2 %
60	67.29 (0.38)	78.65	69.80	16.9 %	3.8 %
70	73.56 (0.42)	85.27	76.70	16.0 %	4.3 %
80	79.66 (0.29)	90.69	82.62	13.9 %	3.7 %
90	84.39 (0.46)	94.99	87.60	12.6 %	3.8 %
100	88.33 (0.52)	98.29	91.66	11.3 %	3.8 %
110	91.45 (0.61)	100.74	94.88	10.2 %	3.8 %
120	93.85 (0.67)	102.50	97.39	9.2 %	3.8 %
130	95.76 (0.63)	103.73	99.30	8.3 %	3.7 %
140	97.36 (0.79)	104.55	100.68	7.4 %	3.4 %

Figure 4.16 shows the LCOE predicted by these three models. The FD modeling shows an over-optimistic result, and its corresponding lowest LCOE is around 0.362 Euros/kWh which is 11.3 % lower than that predicted by the TD modeling, namely 0.408 Euros/kWh. The SD modeling presents a close result with that obtained by the TD modeling, and its resulted lowest LCOE is 0.394 Euros/kWh, with a deviation of 3.4 % from the TD modeling. In addition, it is seen that the FD modeling indicates a slightly lower optimal PTO size than the SD modeling and TD modeling do. The FD modeling corresponds to the optimal PTO size of 80 kN while the SD modeling and TD modeling are associated with 90 kN. In this case,

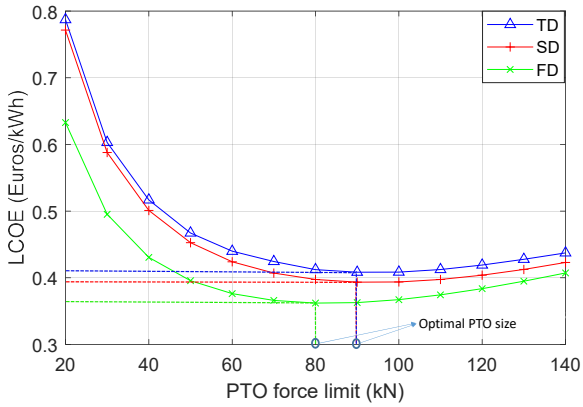


Figure 4.16: LCOE of the WEC predicted by three different models, and PTO parameters are tuned based on the transferred method.

considering the step length of the PTO force limit, the difference between the FD modeling and TD modeling on the PTO size determination is not significant. However, the PTO sizing differs with the wave resource and types of WECs, and the insufficient accuracy of the FD modeling might lead to an unacceptable poor estimate of the optimal PTO size in other scenarios.

Regardless of the PTO tuning method, the SD modeling always presents a good agreement with the TD modeling on estimating the AEP and LCOE. At the same time, the application of the SD modeling contributes to a huge reduction in computational time in the techno-economic assessment. Specifically, with the explicit PTO parameters, the FD and SD modeling consume 1.02 s and 2.11 s to complete the AEP calculation for the considered thirteen PTO force limits in this case. However, the TD modeling takes more than 1.6 hours if the simulation is run single time for each sea state, and this is approximately 3000 times the duration for the SD modeling. Regarding the optimization time in the probabilistic method, it takes over 30 hours with counting the single-run time for the TD modeling to find all the necessary optimal PTO parameters, but it is only 75 s for the SD modeling.

4.6. DISCUSSION

This chapter suggests that the PTO force saturation can be incorporated into the SD modeling of WECs. As SD modeling combines the high efficiency and adequate reliability, it could make a contribution to the WEC optimization related to the PTO sizing. However, in this work, the PTO force saturation is only derived for the ideal PTO system behaving as a passive component or damper. In practice, the modeling of practical PTO systems could be more complicated depending on their designs and types, which might lead to different linearization solutions. For instance, in hydraulic PTO systems, the coupling of the hydraulic circuit with the rest of the components makes the PTO force profile highly nonlinear even without the force saturation [136], [137]. Therefore, further development is needed to incorporate the effect of the force limit in SD modeling for more realistic PTO systems, and then the accuracy and computational efficiency also remain to be investigated.

In this work, only a single WEC is considered in the case study for a preliminary as-

sessment. Given the high computational efficiency when compared to other approaches, it is attractive to apply SD modeling to the optimization or design of WEC farms, which are characterized by large computational loads. The reliability of SD modeling in predicting the performance of a WEC farm has been validated in [138]. Thus, the next phase of this work is to extend the representation of the PTO force saturation to SD modeling for WEC farms. In addition, the present SD model has only been developed for a point absorber with a single degree of freedom, but it is feasible to extend the modeling to multiple degrees of freedom, as demonstrated in [130].

The current SD model is formulated based on linear wave theory with a Gaussian process, which limits the method to be used extensively. For instance, the relevance of the wave nonlinearity becomes more important in large wave heights, and then Gaussian assumption would be challenged. Although the assumption of the Gaussian distribution can be thought adequately valid in most operational regions of WECs, the source of the error resulting from the assumption is still unavoidable. To ease the limitation, as stated in [28], the consideration of non-Gaussian responses will be a promising future work, which could contribute to a more accurate estimation.

4.7. SUMMARY AND CONCLUSIONS

To improve the accuracy of PTO sizing, a SD model is developed in this chapter to include the effect of the PTO force saturation. The SD model is constructed based on the framework of the FD modeling, and the nonlinear effect is incorporated by a quasi-linear term. The quasi-linear term is derived by statistical linearization, which is based on the assumption that all the responses of the system follow Gaussian distribution. Based on the investigation, the following concluding remarks are drawn.

- The assumption of Gaussian distribution is fair for most operating conditions of the WEC even thought the validity decreases with the increase of wave height and tightness of the PTO force limit. The proposed SD model is verified against the nonlinear TD modeling, and a reliable accuracy is identified over a range of relevant wave conditions and force constraints.

- A comparison among the FD, SD and TD modeling is conducted regarding the prediction of power performance. In low significant wave heights or large PTO force limits, three models present similar power performance. With the increase of the significant wave heights and strictness of the PTO force limit, the FD modeling tends to be insufficiently reliable and the highest error can reach values up to 200 % relative to the nonlinear TD modeling. However, the SD modeling shows a good reliability, and its error relative to the nonlinear TD modeling is only around 20 % even at the strict PTO force constraint. At the same time, the computational efficiency of the SD modeling is comparable with the FD modeling and significantly higher than the TD modeling.

- A case study of the PTO sizing is performed to demonstrate the potential of the SD modeling in practical applications. A realistic sea site and preliminary economic modeling are considered. The SD modeling proves to be a desired alternative for the PTO sizing and other similar applications of performance evaluation or early-stage design optimization. It combines the high computational efficiency and the high accuracy on the performance prediction. Its errors on the prediction of the AEP are no

more than 4.3 % relative to the TD modeling, and it shows an agreement on the optimal PTO size with respect to the TD modeling. In contrast, the FD modeling could lead to a poor estimate on the PTO sizing, and its prediction of the AEP and LCOE is questionable, especially with strict PTO force limits. The relative error of the FD modeling on the predication of the AEP is over 24 % in the particular case. In addition, with considering nonlinear effects, the SD modeling suggests an adequate reliability on tuning the PTO parameters, while the FD modeling is found to be insufficient.

To improve the systematic sizing method of WECs, a SD model of the PTO force saturation was developed and verified in this chapter. It combines adequate accuracy and efficiency, which is highly suitable for the application of PTO sizing. But this model addresses the prediction of the energy absorption. In the next chapter, the influence of sizing on the energy conversion will be identified to further consolidate the sizing method.

5

THE INFLUENCE OF PTO SIZING ON THE POWER CONVERSION EFFICIENCY

In the previous chapters, the numerical models were developed to incorporate the effect of PTO sizing on the power absorption. But, the effect on the power conversion is not addressed. Thus, this chapter shifts the focus from the power absorption to the power conversion stage. The influence of PTO sizing on the generator efficiency and further the techno-economic performance are investigated, in which a PM linear generator is considered as the research reference for the PTO system.

Parts of the chapter have been published in: Tan J, Wang X, Laguna A J, et al. The Influence of Linear Permanent Magnet Generator Sizing on the Techno-Economic Performance of a Wave Energy Converter[C]//2021 13th International Symposium on Linear Drives for Industry Applications (LDIA). IEEE, 2021: 1-6. [83]
Tan J, Wang X, Polinder H, et al. Downsizing the Linear PM Generator in Wave Energy Conversion for Improved Economic Feasibility[J]. Journal of Marine Science and Engineering, 2022, 10(9): 1316. [139].

5.1. INTRODUCTION

In Chapter 3, a collective sizing method considering both buoy and PTO sizing was proposed, and the importance of PTO sizing was emphasized. In Chapter 4, to improve the accuracy of PTO sizing, a SD model was established to account for the nonlinear effect of the PTO force limit. However, some assumptions in the last two chapters need to be further studied when evaluating the power performance of WECs with differently sized PTO capacities. The influence of PTO sizing could play a role at two conversion stages in the power extraction. Firstly, the PTO capacity is highly related to the physical limits, which determines the maximum absorbed power. Secondly, the PTO sizing inevitably brings changes to its design, which might make a difference to the conversion efficiency from the absorbed power to the electrical power. The second aspect was not taken into account in chapters discussing the PTO sizing, in which the PTO efficiency was assumed to be constant regardless of its size. Hence, a better understanding of the effect of the sizing on PTO conversion efficiencies is expected to make contribution to the sizing of WECs.

Among various types of PTO systems in WECs, linear generators have received significant attention because of the high efficiencies and low maintenance demands [37], [140]. However, there is limited literature addressing the influence of the sizing on the performance of linear generators of WECs even though downsizing the PTO capacity has shown the potential to reduce the LCOE. Therefore, the objective of this chapter is to identify the impact of the sizing on the generator efficiency and techno-economic performance of WECs with a linear permanent magnet (PM) generator.

The present chapter starts with the description of the linear PM generator reference are presented. Next, an analytical generator model is presented to calculate the generator performance. Rather than designing a complete new generator, the scaling principle is applied to resize generator with respect to different designed maximum forces. For a fair comparison, several main design parameters are optimized for each sized generator to minimize the LCOE. The effects of the PTO sizing on the generator efficiency, as well as the techno-economic performance of the WEC are analyzed. Moreover, the dependence of the generator efficiency on the characteristics of wave resources is discussed. Finally, conclusions are drawn.

5.2. CONCEPT DESCRIPTION

In this section, the WEC concept and the design of the reference linear PM generator are described. Figure 5.1 illustrates the concept of the investigated heaving point absorber, and the PTO mechanism of the concept is considered to be a linear PM generator. Figure 5.1 also depicts the connection scheme of the PM generator with the electrical converter and the grid. A three-phase back-to-back voltage source converter is applied here to regulate the stator current and terminal voltage because of its high efficiency [61]. The converter is connected to the output side of the linear generator. In the concept studied in the present paper, the translator of the bottom-founded machine is directly connected to the floating buoy. The radius of the spherical floater was designed to be 2.5 m, and the buoy draft is 2.5 m as well in still water. During operation, the incoming wave force excites the floater to oscillate in the heaving direction. The stroke of the point absorber is set as 4 m, and the maximum allowed velocity u_{max} is 1.25 m/s. To avoid excessive motion, the generator has end stop mechanisms mounted on both the top and bottom. More details about modeling,

design and the sea trial test of the reference generator can be found in [61], [141].

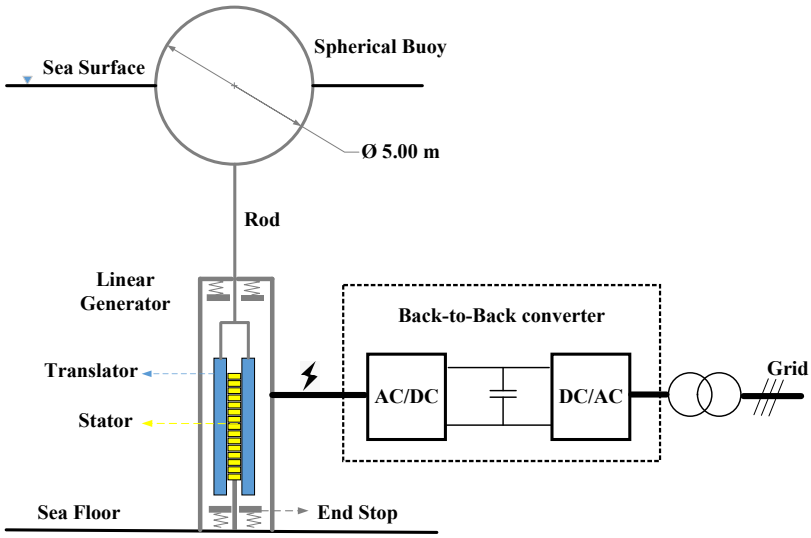
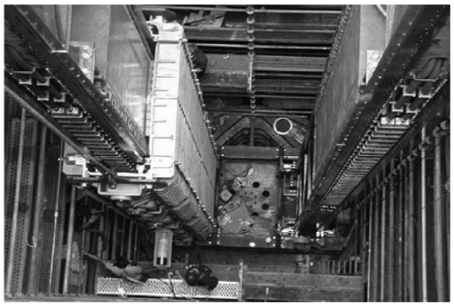


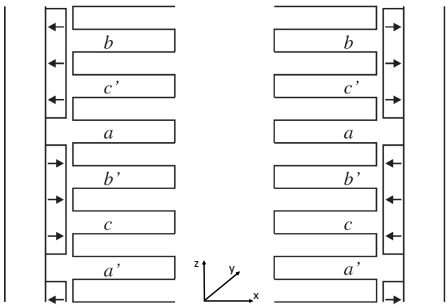
Figure 5.1: Schematic of the heaving point absorber WEC, and the connection scheme of the PM linear generator with the back-to-back converter and the grid.

In Figure 5.2a, a photo of the reference linear PM machine applied in the prototype of the AWS wave energy converter is shown. Figure 5.2b illustrates the cross-section of the reference linear PM generator, which indicates that it is a three-phase machine. The machine was designed to be double-sided so as to counteract the force of attraction between the translator and stator [43]. Magnets are placed on the translator segments, and coils are wound on the stator segments. Different from rotary electrical machines, the partial overlap between the translator and stator could happen to the linear generator. This phenomenon makes a part of the material of the machine unproductive during operation, which is negative to the conversion efficiency. It is known that a longer translator is able to reduce the occurrence of the partial overlap, but it could clearly increase the cost. Hence, a compromise always has to be made, and the translator was 3 m longer than the stator in the design of the reference machine.

The key design parameters of the reference linear PM generator are specified in Table 5.1. As the design parameters of the original reference machine were not fully disclosed, some parameters (including the air gap length, slot width, pole width, tooth width and magnet thickness) were referred to the design of a direct-drive wind turbine generator design [112]. The referred generator has a similar power rating and maximum designed force to the reference machine studied in this paper. It is considered fair since this work is focused on the effect of the generator sizing instead of its design phases.



(a) Photo of the reference machine



(b) Cross-Section of the machine

Figure 5.2: The photo of the reference linear electrical machine in the pilot of the AWS WEC, and the cross-section of the linear PM generator of the AWS plant. In subfigure (b), a/a', b/b' and c/c' are the current directions [43], and the "z" axis in the coordinate is perpendicular to the ground plane.

Table 5.1: SPECIFICATION OF THE REFERENCE GENERATOR.

Parameters	Symbol	Reference machine
Rated power	P_{rated}	1 MW
Maximum force	F_{max}	933 kN
Maximum velocity	u_{max}	2.2 m/s
Stroke	S	7 m
Translator length	L_{tra}	8 m
Stator length	L_{sta}	5 m
Air gap length	g_l	5 mm
Slot width	b_s	15 m
Stack length	l_s	1 m
Magnet pole width	b_p	79 mm
Tooth width	b_t	19 mm
Magnet thickness	l_m	15 mm
Number of conductors per slot	N_s	6

5.3. GENERATOR MODELING

The performance of variously sized generators is calculated based on an analytical generator model. The model has been validated by a full-scale experiment [141]. As magnetic saturation only plays a very limited role in this linear generator design [97], and the effect is neglected in this study.

The fundamental space harmonic of the magnetic flux density in the air gap due to the magnets is calculated as

$$\hat{B}_{gm} = \frac{l_m}{\mu_{rm} g_{eff}} B_{rm} \frac{4}{\pi} \sin\left(\frac{\pi b_p}{2\tau_p}\right) \tag{5.1}$$

where l_m is the magnet length in the magnetization direction, g_{eff} is the effective air gap, μ_{rm} is the recoil permeability of the magnets and B_{rm} is the remanent flux density of the

magnets. The no-load phase voltage induced by this flux density in the stator winding is

$$E_p = \sqrt{2} N_p l_s N_s k_w u \hat{B}_{gm} \frac{l_{act}}{L_{sta}} \tag{5.2}$$

where u is the floater velocity, N_p is the number of pole pairs, l_{act} is the actual length of the overlap between the stator and translator, and k_w is the winding factor. l_{act} is a function of translator displacement, and it can be calculated as,

$$l_{act}(s) = \begin{cases} L_{sta}, & for \quad |s| < 0.5(L_{tra} - L_{sta}) \\ 0, & for \quad |s| > 0.5(L_{tra} + L_{sta}) \\ 0.5(L_{tra} + L_{sta}) - |s|, & else \end{cases} \tag{5.3}$$

where s is the displacement of the translator (or the floater). The stator phase resistance is calculated from the machine dimensions, the number of turns in a slot and the cross-section of a slot:

$$R_t = \rho_{Cu} \frac{l_{Cus}}{A_{Cus}} = \rho_{Cu} \frac{2N_s^2(l_s + 2\tau_p)}{N_p h_s b_s k_{sfil}} \tag{5.4}$$

where R_t is the resistivity of copper, and k_{sfil} is the copper fill factor of the slots. l_{Cus} and A_{Cus} are the phase winding length and the cross-sectional area of a phase winding. The iron losses are calculated as

$$P_{Fes} = P_{Fe0}\left(m_{Fest}\left(\frac{\hat{B}_{st}}{B_0}\right)^2 + m_{Fesy}\left(\frac{\hat{B}_{sy}}{B_0}\right)^2\right)\frac{f_{ele}}{f_0} \tag{5.5}$$

where P_{Fe0} is the iron loss per unit mass at a frequency f_0 and flux density B_0, m_{Fest} and m_{Fesy} are the mass of the stator teeth and the stator yoke respectively, and f_{ele} is the electrical generator frequency. $\hat{B}_{st}$ and $\hat{B}_{sy}$ embody the fundamental space harmonic of the magnetic flux density in the stator teeth and yoke respectively. This is a rough approximation of the iron losses, in which the iron losses are assumed to be only proportional to the frequency.

After the PTO damping coefficient is derived, the required generator force F_{ge} (or F_{pto}) is calculated based on (3.19). Then, the power taken by the generator winding is calculated as

$$P_{wd} = F_{ge} u - P_{Fes} \tag{5.6}$$

For the sake of higher system efficiency, the operating points of the generator are determined by the method demonstrated in [61]. The current I_s can be divided into quadrature (or force making) component I_{sq} and direct (or flux making) component I_{sd}. The current I_s is initially assumed to be in phase with the no-load voltage E_p, which implies that there is no direct component as seen in the first phasor diagram in Figure 5.3. To extract this power, the current can be calculated as

$$I_s = I_{sq} = \frac{P_{wd}}{mE_p} \tag{5.7}$$

When the current is greater than the maximum current of the converter I_{conm}, the current is limited to the maximum current. As a result, the actual generator force is decreased

to be lower than the required generator force. In this sense, the terminal voltage is derived as

$$U_s = \sqrt{(E_p - I_{sq}R_t)^2 + (\omega_e L_t I_{sq})^2} \tag{5.8}$$

where L_t is the stator inductance of the machine.

If the terminal voltage is about to violate the rated converter voltage U_{conm}, it would be limited by a direct component I_{sd} separated from the current, as shown in the second phasor diagram of Figure 5.3. If the resulting current under this condition is larger than the maximum converter current, the operating point is defined by the maximum converter current and voltage. In these situations, the actual generator force would also be penalized.

The converter losses are dependent on three factors. The first one is the constant power dissipation, resulting from control, cooling and power supplies. The second is proportional to the current, representing the switching losses and conduction losses. The third is related to the current squared, including conduction losses. Besides, only the losses from the generator side are considered in this model. Therefore, the converter losses can be calculated as

$$P_{con} = \frac{P_{conm}}{31}\left[1 + 20\frac{I_s}{I_{sm}} + 10\left(\frac{I_s}{I_{sm}}\right)^2\right] \tag{5.9}$$

where P_{conm} is the dissipation in the converter at the rated power, which is assumed to be 3% of the converter's rated power [142]; I_{sm} is the maximum generator side current of the converter, which is set to be equal to I_{conm}. The rated power of the converter for the reference generator (single double-sided machine) equals to the rated power of the plant, namely 1 MW, and the maximum line voltage and phase current are 1500 V and 400 A respectively [61].

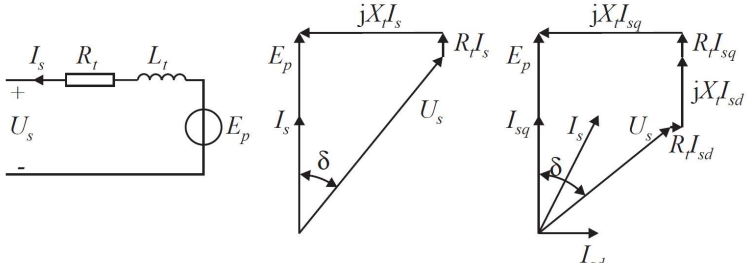


Figure 5.3: Equivalent circuit of the generator and the phasor diagram with the converter [61]. R_t, Lt and X_t embody the stator phase resistance, stator phase inductance and stator phase reactance.

5.3.1. GENERATOR SIZING

As characteristics of wave climate vary with locations, sizing of WECs could result in devices better fitting the local wave resource. In the existing literature, PTO systems are commonly sized by the same scaling ratio as the buoy, in which PTO sizing is only playing a limited role. To allow for independently sizing of the PTO system, three sizing methods different in complexity are applied in this chapter for comparison.

- Method 1: Scaling law

In this method, the generator is resized based on the principle that the force density (the force acting per unit surface area of the air gap) is rather constant for differently sized machines [112]. Two factors affect the force density: the air-gap flux density and the linear current density. The former is limited by the saturation of magnetic flux and the latter is limited by the maximum allowed heat dissipation. In this chapter, the machine is resized to suit different designed maximum forces. The force density of resized machines remains identical to the reference machine.

For convenience, a scale factor λ_e for electrical machines is introduced here as

$$\lambda_e = \frac{G_c}{G_o} \tag{5.10}$$

where G_c and G_o embody the geometrical lengths of the scaled machine and the original machine. In this method, stator, translator and stack length are sized based on an identical scale factor. But, in principle, they can be sized independently as implemented in the method 2 introduced in the following text. In this work, only the stator, translator and stack lengths are considered in scaling, and other geometrical parameters of the machine are kept identical. For a fair comparison of differently sized generators, the stroke and speed limits are maintained to be the same. Then the other parameters are scaled as follows:

$$\text{Force}: \quad \frac{F_{max_c}}{F_{max_o}} = {\lambda_e}^2 \tag{5.11}$$

$$\text{Velocity}: \quad \frac{u_{max_c}}{u_{max_o}} = 1 \tag{5.12}$$

$$\text{Current}: \quad \frac{I_{conm_c}}{I_{conm_o}} = 1 \tag{5.13}$$

where F_{max} is the maximum generator force, u_{max} is the maximum translator velocity, and I_{conm} is the maximum phase current of the converter; subscripts "c" and "o" indicate the scaled machine and original machine.

The rating of the converter is accordingly scaled for each machine. The rated apparent power, current and terminal voltage should be selected during the rating. As the linear current density is assumed to remain identical for differently sized machines, the maximum phase current of the scaled converter is selected to be unchanged, namely I_{conm} of 400 A. At the rated operating condition, the velocity of the buoy is u_{max} of 1.25 m/s, and then the resulting no-load voltage can be obtained by (5.2). Furthermore, the no-load voltage at the rated point is assumed to be in phase with the current. As a consequence, the rated terminal voltage of the scaled converter, U_{conm_s}, and the phase angle between the current and terminal voltage, namely δ, can be calculated according to the first phasor diagram in Figure 5.3. Therefore, the rated apparent power of the scaled converter is obtained as

$$S_{conm_c} = mI_{conm}U_{conm_c} \tag{5.14}$$

- Method 2: Scaling with optimization

  In this method, the main parameters of the machine, including the translator length, stator length and stack length are optimized during sizing for the lowest LCOE. The optimization for each designed maximum generator force is expressed as

$$subject\,to \begin{cases} minimize\ \ f = LCOE(L_s, L_{tra}, l_{sta}) \\ 2\rho_{force_ref} L_{sta} l_s = F_{limit} : constraint\ 1 \\ 1.2 L_{sta} \leq L_{tra} : constraint\ 2 \end{cases} \tag{5.15}$$

  where ρ_{force_ref} is the force density of the reference machine, and F_{limit} is the designed maximum generator force. In (5.15), constraint 1 is associated with the force density. The force density adopted here is considered as 46 kN/m^2 which is calculated based on the performance identification of the AWS generator in [61]. A factor of 2 is included on the left side of the constraint 1 because the machine is double-sided. Constraint 2 indicates that the translator length is required to be larger than 1.2 times the stator length, which is used to mitigate the effect of partial overlap between stator and translator. The maximum phase current, voltage and the rated apparent power of the scaled converter are calculated based on the same way as introduced in Method 1. As the objective function is computationally expensive in this case, the surrogate algorithm is adopted. In the algorithm, the objective function is approximated by a surrogate function, and therefore the optimization speed can be significantly improved [143]. The optimization is implemented in Matlab environment (version 2020). The tolerance of the function and the maximum iteration steps are set to $1e^{-5}$ and 3000 respectively, and the iteration process is terminated when any of the criteria is crossed.

- Method 3: Scaling with assuming a constant generator efficiency

  For simplification, in studies discussing the effects of sizing of WECs, sizing of WECs was commonly implemented in the absence of the consideration of the variation of generator efficiencies. Instead, a constant energy conversion efficiency from the absorption stage to the grid was assumed. In this method, the generator size acts simply as a PTO force constraint in the hydrodynamic modeling. This method is discussed in this chapter for a comparison with the other two above methods to demonstrate the effects of this simplification on the generator size determination and the LCOE estimation. In this chapter, this constant efficiency is considered to be 70 %, as usually used in literature [12], [144]. Moreover, as the design of the generator is not taken into account in this method, the cost could not be derived explicitly. To evaluate the techno-economic performance of WECs, the PTO related cost in this method is assumed to be the same as that estimated in the method 2 for each designed maximum generator force limit.

5.3.2. COST ESTIMATION OF THE LINEAR GENERATOR

The techno-economic metrics are calculated based on the economic model established in Chapter 3. All the economic parameters in this chapter remain same as the chapter 3 except

the PTO cost. This is because the detailed generator design has been considered and the required material of the generator can be estimated for a more accurate cost calculation. Regarding this WEC concept, the PTO cost totally comes from the linear generator cost, which is calculated as

$$C_{PTO} = 2(C_{Fe}M_{Fe} + C_{Cu}M_{Cu} + C_{pm}M_{pm}) \tag{5.16}$$

where a factor 2 is considered to include the manufacturing cost and converter cost; M_{Fe}, M_{Cu} and M_{pm} are the mass of iron, copper and permanent magnet respectively; C_{Fe}, C_{Cu} and C_{pm} are the unit price of iron, copper and permanent magnet respectively.

5.4. GENERATOR PERFORMANCE

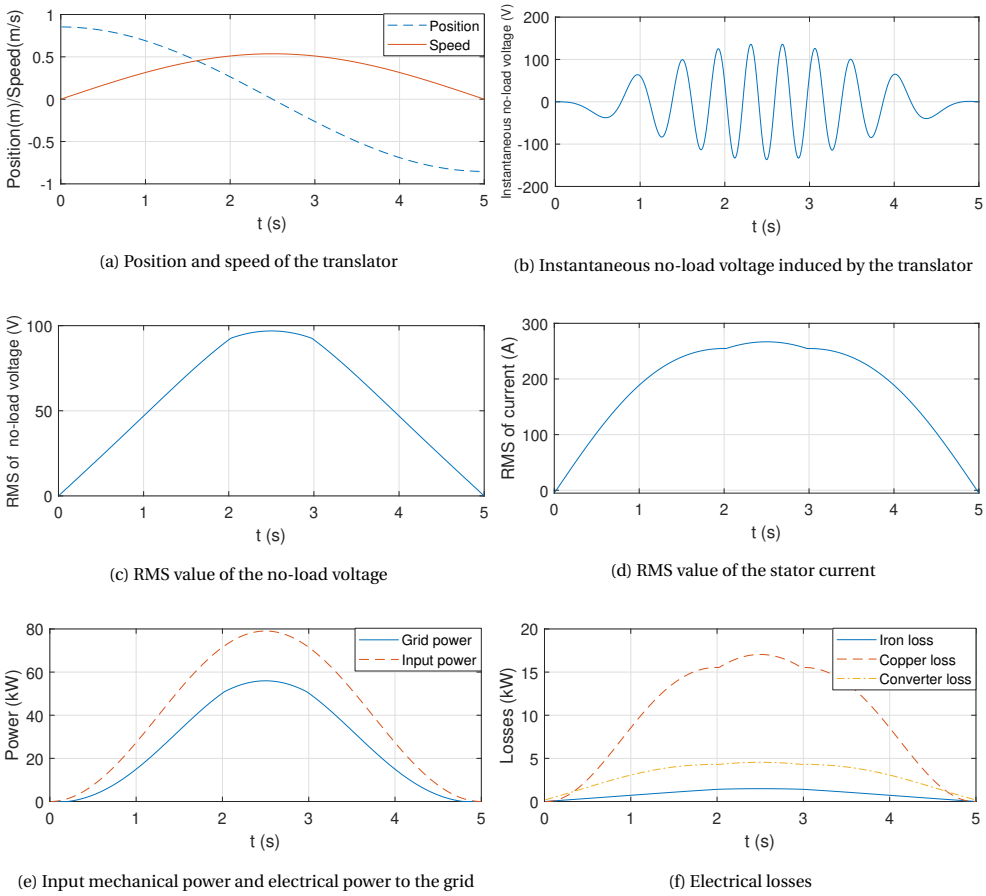
The performance of the linear PM generator is calculated for a particular regular wave state, which is depicted in Figure 5.4. The concerned generator is sized by method 2 with a maximum designed generator force of 200 kN, and the resized parameters will be shown in Figure 5.5 and discussed in the following text. It is seen from Figure 5.4 that the root mean square (RMS) of the no-load voltage doesn't present a sinusoidal curve, which results from the partial overlap between the translator and stator. A negative effect of the partial overlap can be observed as that the stator current is driven relatively higher for maintaining the required generator force. Consequently, the copper and converter losses are also increased.

5.5. COMPARISON OF SIZING METHODS

5.5.1. ON THE GENERATOR PERFORMANCE

The reference linear generator is resized corresponding to the designed maximum generator forces ranging from 60 kN to 280 kN. The machine parameters scaled by method 1 and method 2 are compared in Figure 5.5. It can be seen that all of the translator, stator and stack lengths show a trend to increase with the designed maximum generator force regardless of the sizing method. However, these two methods result in very different machine parameters. The stack lengths obtained using the method 2 are clearly longer than those by the method 1, but the translator and stator lengths resulting from the method 2 are shorter. Noteworthy, based on the method 2, the length difference between the translator and the stator is limited if compared to the cases using the method 1. This indicates that the negative effect of the partial overlap is not significant for the combination of the machine and the considered wave resource. This can be interpreted as the fact the displacement of the WEC is relatively small in the wave states dominating energy production.

Figure 5.6 shows the efficiency maps of linear generators with the designed maximum force of 100 kN, 160 kN and 200 kN respectively, in which regular wave states are considered. Sizing method 1 and method 2 are both applied for comparison. The efficiency at each wave state is calculated as the ratio between the electrical power and the absorbed power of the floater. It is visible in Figure 5.6 that larger generators generally correspond to higher efficiencies. Furthermore, the efficiency tends to increase with the wave height and decline with the wave period. For the generator with a designed maximum force of 100 kN, a few empty cells can be noticed at low wave periods and very high wave heights. This is because the buoy velocity tends to be high in these operating conditions. Then, the PTO damping has to be increased to lower the velocity, but the larger PTO damping values are necessarily



(a) Position and speed of the translator

(b) Instantaneous no-load voltage induced by the translator

(c) RMS value of the no-load voltage

(d) RMS value of the stator current

(e) Input mechanical power and electrical power to the grid

(f) Electrical losses

Figure 5.4: Generator performance over a half of wave period with a displacement of 0.85 m and a wave period of 10.0 s. The considered machine is sized with a maximum designed generator force of 200 kN based on sizing method 2.

related to the larger PTO force. Therefore, with a relatively strict designed maximum force, it is not feasible to satisfy both the defined force constraint and velocity constraint.

The overall conversion efficiency of the differently sized generators operating in Yeu island are shown in Figure 5.7, which is defined as the yearly energy yield delivered to the grid divided by the yearly energy absorbed by the buoy. First, the overall efficiency has a clear dependence on the generator size no matter which sizing method is applied. Generally, larger generators present higher conversion efficiencies. In this particular case, the overall conversion efficiencies are around 60 % to 65 % for the generator sized with a designed maximum force of 60 kN, while they increase to be higher than 75 % for generators with a designed maximum force of 280 kN. This observation clearly reflects the inaccuracy of the assumption used in previous sizing studies [17], [33], [144] that the generator efficiency is not changing during PTO sizing. Secondly, even though the optimization procedure is incorporated in method 2, it does not necessarily lead to higher efficiency. For instance, the

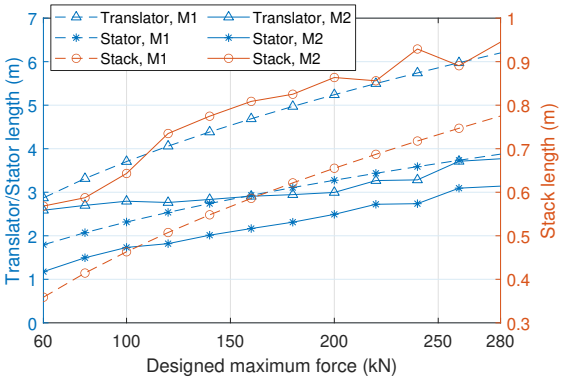


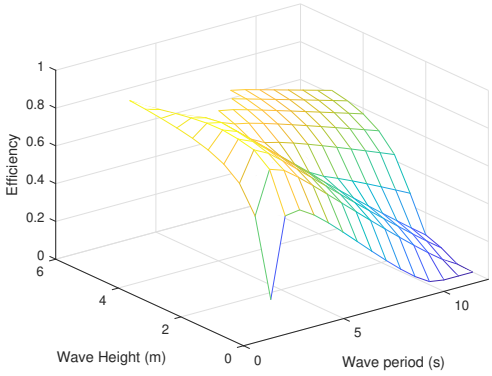
Figure 5.5: Scaled translator, stator and stack lengths for different designed maximum generator forces. 'M1' and 'M2' embody the method 1 and method 2 for generator sizing.

overall efficiency of the generator scaled based on the method 2 is associated with slightly lower efficiency compared to that using the method 1 when the designed maximum force is larger than 250 kN. Nevertheless, the contribution of the optimization can be found in Figure 5.8 as the method 2 gives a lower PTO cost when the designed maximum force is higher than 100 kN. For instance, the PTO cost of the generator with a designed maximum force of 280 kN is 160,000 Euros and 12,000 Euros for the method 1 and 2 respectively, while their generator efficiencies are comparable.

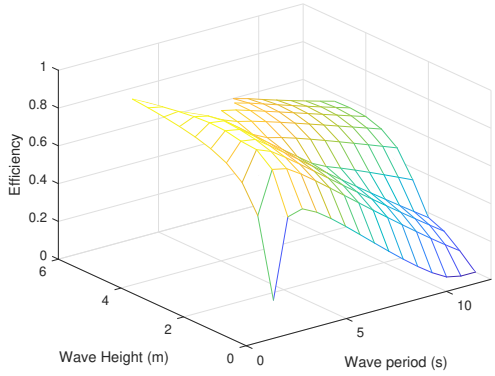
5.5.2. ON THE TECHNO-ECONOMICS AND THE PTO SIZE DETERMINATION

The AEP and the LCOE of the WEC with differently sized generators are depicted in Figure 5.9 and Figure 5.10, in which three different sizing methods are applied respectively. From Figure 5.9, it is visible that the method 1 and method 2 result in similar values of the AEP, but the relative discrepancy of the method 3 is noticeable. For example, when the designed maximum force is 280 kN the AEP is approximately 130 MWh for the method 1 and method 2, but the AEP is calculated to be around 117 MWh by using the method 3. In this sense, the relative error reaches 10 %. However, unlike the trends of the AEP, these three methods results in very different values of the LCOE, as shown in Figure 5.10. For instance, when the designed maximum force of the generator is 280 kN, the LCOE is estimated to be around 0.45 Euros/kWh, 0.38 Euros/kWh and 0.42 Euros/kWh for the method 1, 2 and 3 respectively. In this sense, the optimization of generator parameters leads to the reduction of the LCOE of around 15 % and 10 % with regard to method 1 and 3. In addition, as a consequence of the optimization of the main parameters, the method 2 is always related to a lower value of the LCOE compared to the method 1. Furthermore, the selection of the generator sizing method is significant to the PTO size determination. In this case, the optimal PTO force limit corresponding to the lowest LCOE is 120 kN, 140 kN and 100 kN for the method 1, 2 and 3 respectively. In this sense, the relative error resulting from the assumption of a constant generator efficiency on the PTO size determination is around 29 %. It can be concluded that the method 3, which assumes the constant generator efficiency during sizing, could lead to a notably erroneous estimate of the AEP, LCOE and the optimal PTO size. Thus, it is highly recommended to take the effect of sizing on the generator efficiency into account when

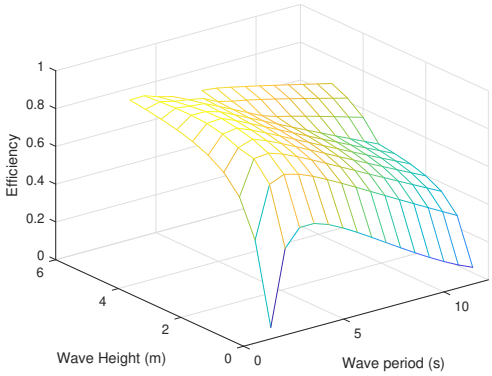
conducting PTO sizing. The method 2, namely scaling with the optimization of the main



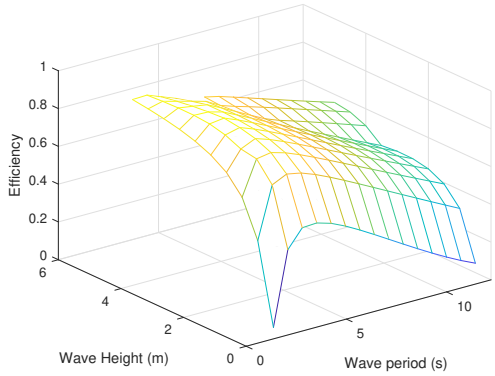
(a) Designed maximum force is 100 kN, based on method 1.



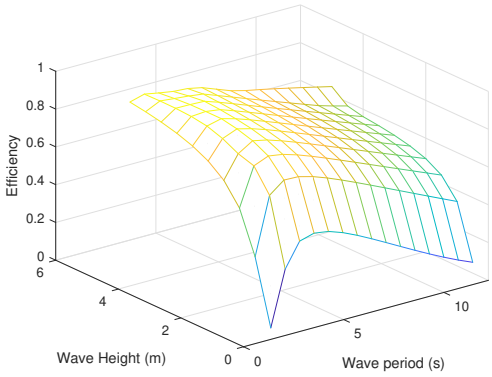
(b) Designed maximum force is 100 kN, based on method 2.



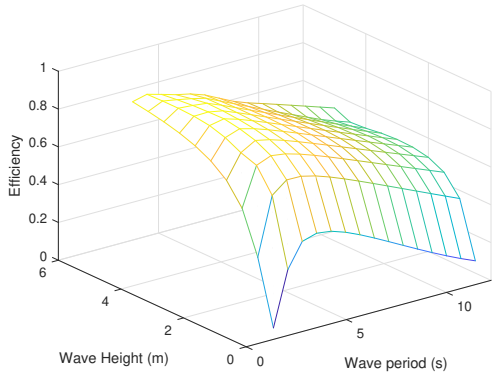
(c) Designed maximum force is 160 kN, based on method 1.



(d) Designed maximum force is 160 kN, based on method 2.



(e) Designed maximum force is 200 kN, based on method 1.



(f) Designed maximum force is 200 kN, based on method 2.

Figure 5.6: Comparison between efficiency maps of generators scaled based on different methods.

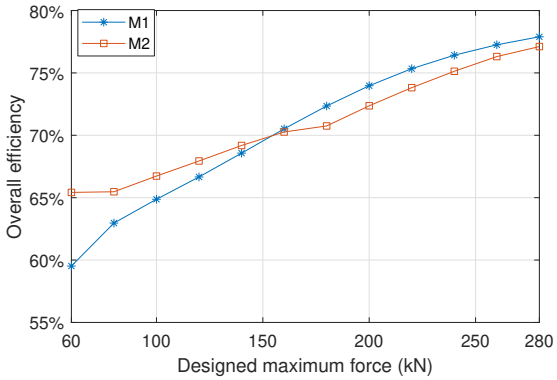


Figure 5.7: The overall conversion efficiency of the generator with different designed maximum generator forces.

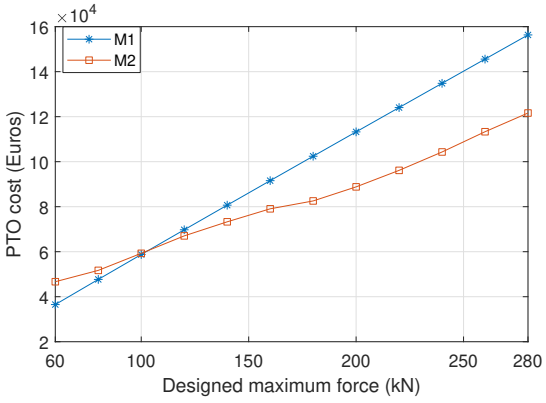


Figure 5.8: The PTO related cost of generators scaled by different methods.

parameters could better reflect the techno-economic potential of the WEC, since it presents a lower LCOE compared to the method 1 which is based on the scaling law. However, it has to be acknowledged that the optimization requires higher computational efforts, while the scaling law requires negligible computational loads with a given reference machine.

5.6. DEPENDENCE OF THE GENERATOR SIZING ON WAVE RESOURCES

To demonstrate the dependence of the generator sizing and techno-economic performance of the WEC on different characteristics of wave resources, two more wave sites are considered as a comparison in this subsection. They are DK North Sea Point 2 (DK2) and Biscay Marine Energy Park (BIMEP) located in the oceanic territory of Denmark and Spain respectively. Their detailed information can be found in [144]. The mean wave power density of Yeu island, DK 2 and BIMEP are 26 kW/m, 12 kW/m and 21 kW/m respectively. Only the method 2 is applied in this subsection for PTO sizing. Figure 5.11 shows the optimized design parameters of the linear generator in different wave sites, and the parameters are normalized to the optimized values for Yeu island. It can be found that the wave resource

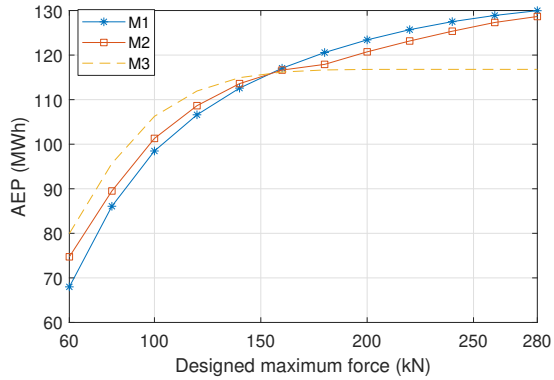


Figure 5.9: The AEP of the WEC as a function of the designed maximum generator force. 'M3' embodies the method 3 for generator sizing.

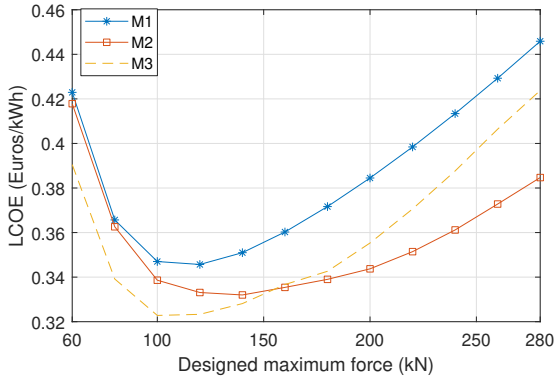


Figure 5.10: The LCOE of the WEC as a function of the designed maximum generator force.

makes a difference to the optimization of the design parameters.

Figure 5.12 shows the overall efficiencies of the differently sized linear generators in the three wave sites. It can be seen that the overall efficiency is highly related to the wave resource. The overall efficiencies in Yeu island and DK 2 are clearly higher than that in BIMEP. For instance, when the designed maximum generator force is 60 kN, the efficiencies in Yeu island and DK 2 are around 65 % while it is only 45 % in BIMEP. This can be explained by the fact that the wave states in BIMEP are concentrated in relatively long wave periods which are associated with low translator velocities. Therefore, it is seen that the efficiency of the linear generator is not only related to the generator size but also to the wave resource, and it is unrealistic to be represented by a constant value. Figure 5.13 depicts the LCOE of WECs in different wave sites. The LCOE in Yeu island is the lowest among the three. The LCOE in DK 2 is lower than that in BIMEP while BIMEP corresponds to a higher mean wave power density. Hence, more powerful wave resources do not necessarily contribute to better techno-economic performance. In addition, the optimal generator size differs with wave resources. The lowest LCOE values in Yeu island, DK 2 and BIMEP correspond to the designed maximum generator force of 120 kN, 100 kN and 160 kN respectively.

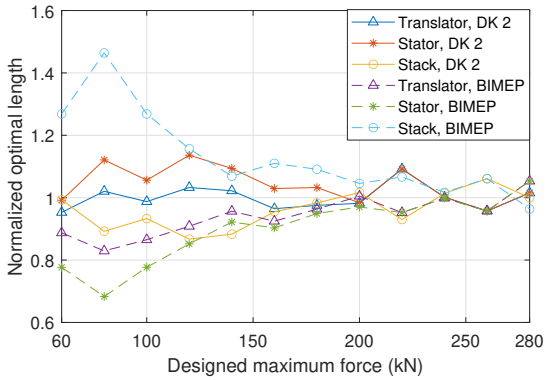


Figure 5.11: The optimized design parameters for DK 2 and BIMEP, which are normalized to the corresponding values in Yeu island.

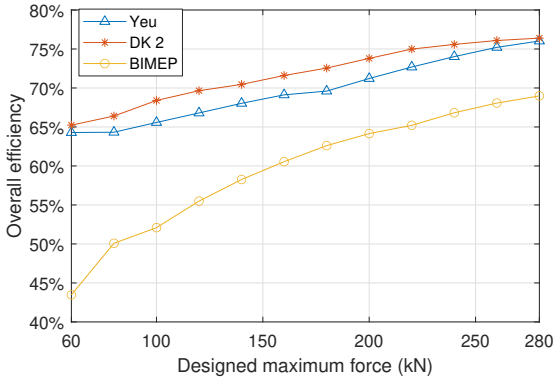


Figure 5.12: The overall efficiency of the linear generator as a function of the designed maximum generator force in different wave sites.

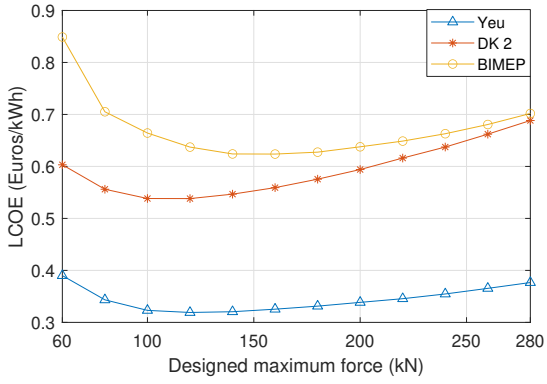


Figure 5.13: The LCOE of the WEC as a function of the designed maximum generator force in different wave sites.

5.7. CONCLUSION

This chapter studies the effects of the PTO sizing on generator efficiencies and the techno-economic performance of WECs. Both hydrodynamic modeling and generator modeling are presented. Different methods are applied to sizing the linear PM generator for various designed maximum generator forces. Based on the results, the following conclusions are drawn.

- The sizing of the generator is important to the LCOE of WECs. The overall conversion efficiency has a notable dependence on the size of generators. Thus, the assumption of a constant generator efficiency leads to an obvious poor estimate on the AEP, LCOE and the PTO size determination. In particular cases, the relative errors on the estimation of the AEP and the optimal PTO size reaches 10 % and 29 %.
- Compared with the method based on the scaling law of electrical machines, the scaling with implementing the optimization of main machine parameters could better reflect the techno-economic potential of WECs when conducting PTO sizing. In particular cases, the LCOE can be reduced by 15 % by optimizing the generator parameters.
- The overall generator efficiency and the LCOE are notably related to the wave resource. The wave resource has a clear influence on the LCOE and overall efficiencies of the linear generator. As the overall efficiency of the generator is far from being constant, it is highly suggested to consider the variation of the generator performance when performing PTO sizing for WECs in different wave sites.

The influence of sizing on the generator efficiency is not negligible, and it is highly suggested to consider the detailed efficiency map of the generator when performing PTO sizing of WECs. Based on the results obtained in Chapter 3 to 5, it indicated that downsizing the PTO system is beneficial for reducing the LCOE. In response to this finding, in the next two chapters, the focus will be put on the exploration of improving the power production of WECs with downsized PTO capacities.

6

IMPROVING THE POWER PERFORMANCE WITH A DOWNSIZED PTO CAPACITY: ADJUSTABLE DRAFT SYSTEM

Previous chapters have indicated that downsizing the PTO capacity to a suitable level is beneficial for improving the techno-economic competitiveness of WECs. However, it is clear that the improvement results from the compromise between the cost and power production, and the reduced PTO capacity inevitably penalizes the power production. To mitigate the negative effect of the downsized PTO capacity on the power performance, a novel WEC, namely the adjustable draft system, is proposed in this thesis. In this chapter and next chapter, the potentials of the design are explored by a numerical study. This chapter focuses on the hydrodynamic performance, and the investigation is performed based on the FD model and an algebraic nonlinear TD model. In the next chapter, a wave-to-wire model will be established to further study how the addition of the novel system affect the overall performance of the WEC.

The results in this chapter show that the relevant natural frequency of the point absorber can be adapted to the operating wave states by varying the buoy draft, which amplifies the RAO and the buoy velocity. With the constrained PTO force, the increased velocity is necessarily associated with the higher power absorption. In addition, the results from the nonlinear TD model show that the nonlinear forces have a significant influence on the power absorption when operating close to resonance regions. However, the advantages resulting from the proposed system can still be observed in both regular and irregular waves while considering the

Parts of the chapter have been published in:
Tan J, Polinder H, Wellens P, et al. A feasibility study on downsizing of power take off system of wave energy converters[C]//Developments in Renewable Energies Offshore. CRC Press, 2020: 140-148.[145]
Tan J, Polinder H, Laguna A J, et al. A numerical study on the performance of the point absorber Wave Energy Converter integrated with an adjustable draft system[J]. Ocean Engineering, 2022, 254: 111347.[146]

nonlinear forces.

6.1. INTRODUCTION

The impact of PTO sizing on the techno-economic performance of WECs has been investigated in previous chapters. It is indicated that suitably downsizing the PTO capacity could result in a good compromise between the power production and the cost, and further lead to a lower LCOE. However, the downsized PTO capacities are inevitably associated with tighter force constraints, which could penalize the power absorption. To further reduce the LCOE, it is reasonable to mitigate the negative effect of the downsized PTO capacity on the power absorption. Possibilities for improving the power performance of WECs subjected to constraints of the PTO capacity have been explored. The first type of methods concentrates on the aspect of PTO control strategies. Elisabetta Tedeschi and Marta Molinas [95], [98], [100], [147] investigated the impacts of control strategies on the PTO rating of WECs. A generic point absorber was used as the research object. It was found that the reactive control strategy clearly improves the power absorption but requires higher PTO capacities. In contrast, the passive control strategy could reduce the required PTO capacities while it corresponds to low power absorption. In order to reach a suitable PTO rating and retain an adequate level of the power production at the same time, they came up with a trade-off tactic by adapting the PTO control strategy to different wave states. The second type of methods is to increase the speed of the buoy by means of adding an intermediate transmission mechanism, such as a gearbox. For instance, a linear generator coupled with a speed amplifying gearbox was designed for a WEC concept in [69], and the relative speed between the stator and translator was therefore increased. In this sense, a smaller PTO force is sufficient to supply a similar output power level with the low-speed PTO systems. However, the addition of transmission stages in the PTO system could decrease the reliability and conversion efficiency. Alternatively, an adjustable draft system is proposed in this thesis to improve the power performance of point absorbers operating in conditions with constrained PTO forces [145]. The system was deigned to implement the buoy draft adjustment by changing the ballast water inside the buoy. In this way, both the hydrostatic stiffness and mass of the buoy can be regulated, which enables the variation of the buoy's natural frequency. Then, the increased displacement and speed of the buoy can be achieved over a range of wave periods. As a consequence, the power absorption of WECs coupled with the ADD system tends to be less affected by the downsized PTO capacity with regard to the conventional fixed-draft point absorbers.

A key feature of the adjustable draft system is to enable the regulation of the hydrostatic stiffness and mass of the buoy through the draft adjustment. To create a strong dependence of the hydrostatic stiffness on the buoy draft, it is reasonable to have a varying horizontal cross-sectional area in the vertical direction such as the spherical geometry considered in this thesis. The effect of the buoy draft on the performance of WECs has been investigated in literature [148]–[153]. Generally, the effect was discussed in studies focusing on geometry optimization of the WEC's floating buoy. In most cases, the buoy draft has been proven to be related to the energy absorption efficiency and the absorption bandwidth of WECs, although the specific effect differs with the buoy geometry and size [148]–[152], [154]. Furthermore, the influence of the buoy draft adjustment on the hydrodynamic performance of WECs was investigated in [153], which was intended to explore the possibility for limiting the heaving motion of WECs in extreme waves by the buoy draft adjustment with upper surface immersion. Their results showed that the increase of the buoy draft causes the increase of both the natural period and the hydrodynamic damping, and the buoy motion

can be reduced efficiently by increasing the floater's mass. In [153], a valuable insight about the possibilities of making the hydrodynamic performance of WECs variable by the buoy draft adjustment was provided, which also inspired the work in this paper. However, the utilization of the buoy draft adjustment for downsizing the PTO capacity and improving the power performance has not been widely discussed. In the work [145] related to this thesis, the adjustable draft system for the use of PTO downsizing was introduced for the first time.

This chapter aims at investigating the power performance of a point absorber integrated with an adjustable draft system by means of a numerical approach. For this purpose, this chapter first provides an insight into the influence of the buoy draft adjustment on the hydrodynamic performance of a spherical heaving point absorber. Then, it reveals the contribution of the adjustable draft system to the adjustment of the required PTO force. Finally, this chapter looks at the improvement resulting from integrating the adjustable draft system with a point absorber on the power absorption.

This chapter starts with the description of the point absorber concept and the adjustable draft system. Both FD modeling and nonlinear TD modeling are used to investigate the performance of the adjustable draft WEC. Based on the FD analysis, the effects of the draft adjustment on PTO performance and natural frequencies of the buoy are discussed. The variation of the required PTO force and absorbed power with the buoy draft is presented. In addition, a comparison between power performance of the adjustable draft WEC and fixed draft WEC is made. Furthermore, in the nonlinear TD analysis, the nonlinear Froude-Krylov force and viscous force are taken into account. The impact of the nonlinear forces on the absorbed power of the adjustable draft WEC is shown. The improvement on the power performance resulting from the adjustable draft system is evaluated based on the nonlinear TD model, and both regular and irregular wave states are considered.

6.2. CONCEPT DESCRIPTION

This section describes the concept of the adjustable draft WEC. A generic heaving point absorber is used as the WEC reference in this study. The geometry of the floating buoy is a sphere with a diameter of 5.0 m. The schematic of the adjustable draft WEC concept is shown in Figure 6.1. In this concept, a ballast pump is installed inside the buoy for implementing the buoy draft adjustment. The minimal and the maximal adjusted buoy draft are defined as 0.50 and 0.75 times the buoy diameter respectively. In principle, it is possible to extend the adjustable draft to a wider range by this adjustable draft system. However, further increasing the buoy draft could result in the occurrence probability of the floating buoy's being fully submerged and breaching the water surface during the operation, which could bring in excessive losses due to surface tension. On the contrary, by means of the adjustable draft system, it is possible to decrease the draft to less than 0.5 times the diameter. But the lower buoy drafts improve the chances of the buoy leaving and then impacting on the water, causing slamming loads harmful to the structure [125]. As a consequence, both these two phenomena should be avoided as much as possible in designing WECs. In addition, both the effects are coupled with highly nonlinear behaviours [20], which are outside the scope of this study. Thus, the adjustable range of the buoy draft is defined between 2.50 m and 3.75 m in the present study and the adjustable range of the draft h_a is 1.25 m. This designed range could be varied according to the buoy geometry and size.

The total mass of the buoy can be changed by varying the ballast water inside the buoy. It is assumed that the buoy without ballast water naturally floats at the minimum draft of

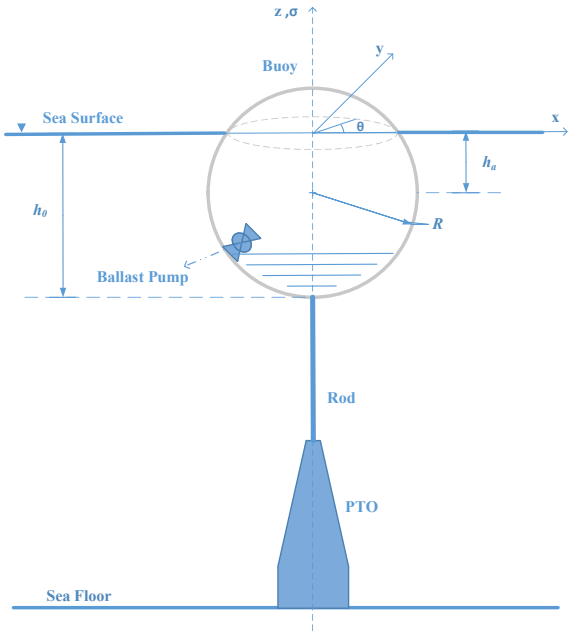
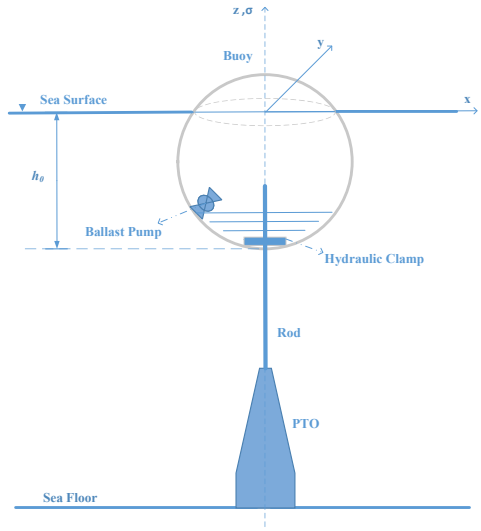


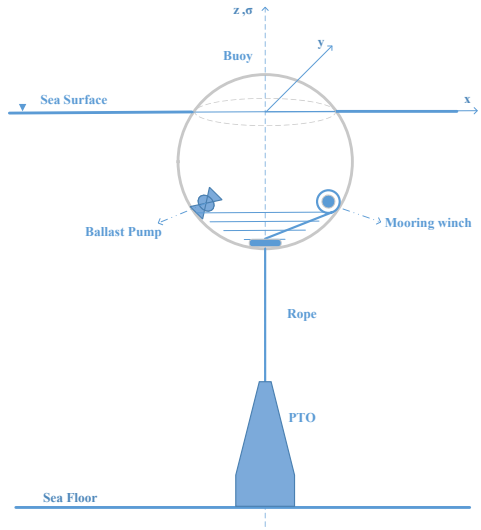
Figure 6.1: Schematic of the spherical point absorber with the adjustable draft system. R, h_a and h_0 represent the buoy radius, the adjustable draft range and the buoy draft.

2.50 m in still water. To reach each desired buoy draft, the ballast water inside the buoy is regulated by the pump to make the buoy float in equilibrium. It is realized that the ballast water inside the buoy could cause sloshing during the movement of the buoy. Sloshing affects the dynamics of the buoy, which might reduce the stability and controllability of the system. To avoid this issue, one possible solution is to install multiple ballast segments inside the buoy. To implement the buoy adjustment, each segment can only be fully loaded or drained out. In this way, sloshing inside the buoy can be expected to be mitigated.

The floating buoy is connected to the moving part of the PTO system, and the moving part could be a piston or generator translator depending on the PTO type. However, the draft adjustment varies the equilibrium position of the buoy and moving part of the PTO system. Since the PTO position is fixed, the draft variation could make a difference to the symmetry of the buoy stroke during the movement. As a result, the allowable stroke of the buoy would be limited at one side, which might affect the power absorption. This issue can be avoided by two ways, which are depicted in Figure 6.2. If the buoy and the PTO are rigidly connected, such as by a rod, a hydraulic clamp could be used, as shown in Figure 6.2a. When the buoy draft varies, the clamp adjusts the rod length correspondingly and stores the additional part of the rod inside the buoy. If they are connected by a rope, a mooring winch can be applied to play a same role as the hydraulic clamp, as shown in Figure 6.2b. However, it should be realized that the addition of the auxiliary equipment increases the complexity of the whole system. This negative effect of the draft adjustment on the symmetry will be investigated in detail in the next chapter, and the power performance of the system with



(a) With a hydraulic clamp



(b) With a mooring winch

Figure 6.2: Schematic of two possible revised designs for avoiding the non-symmetry of the PTO stroke.

non-symmetric PTO stroke will be discussed. Nevertheless, in the present chapter, it is assumed that a good symmetry of the buoy stroke can be maintained by two ways when the buoy draft changes. Furthermore, the control strategy and efficiency of the ballast pump and hydraulic clamp have in practice an influence on performance of the adjustable draft system, but it is assumed that the draft could always be adjusted to the expected value in

each wave state. In addition, the displacement of the buoy is limited to protect the structure, and it is limited to 0.4 times the diameter of the buoy in this paper. Moreover, a passive control strategy is implemented for the studied point absorber, which implies that only a force proportional to buoy velocity is applied by the PTO system.

6.3. NONLINEAR TIME DOMAIN MODEL

Scientific literature [155], [156] has indicated that the non-uniform buoy cross-sectional area could make the effect of the nonlinear Froude–Krylov force pronounced. In addition, the draft adjustment of the buoy is expected to affect the significance of the nonlinear Froude-Krylov force. Therefore, it is necessary to investigate the influence of the nonlinear Froude–Krylov forces on the performance of the studied WEC. In [155], a computationally efficient nonlinear model was proposed for axisymmetric and prismatic geometries, and the model uses an algebraic solution to the Froude–Krylov force integral. The proposed nonlinear Froude–Krylov model is adopted in the present paper for the adjustable draft WEC. Regarding more complex geometries, numerical approaches can be applied to compute the nonlinear Froude-Krylov force [88]. For example, in the open-source software WEC-Sim, the nonlinear Froude-Krylov force is calculated by integrating the pressure over each pre-meshed panel of the instantaneous wetted surface [157]. However, compared with the analytical model, the numerical routines are inevitably associated with higher computational times. The formulation of the analytical nonlinear Froude-Krylov model is briefly presented in the following text, and more details can be found in [155].

In the model, the incoming waves are represented based on the linear wave theory, and all the considered waves are assumed to be unidirectional. The responses of the WEC in both regular and irregular wave conditions are investigated. The regular wave input is described as harmonic waves which can be expressed as

$$\eta(t) = \zeta_a \cos(kx - \omega t) \tag{6.1}$$

where t is time, k is the wave number, ω is the angular frequency of the incoming wave and ζ_a is the wave amplitude. Given the linear wave theory, irregular waves can be represented by the superposition of a set of regular wave components, as

$$\eta(t) = \sum_{j=1}^{N} \zeta_a(\omega_j) \cos(k(\omega_j)x - \omega_j t + \varphi(\omega_j)) \tag{6.2}$$

where $k(\omega_j)$, $\zeta_a(\omega_j)$ and $\varphi_(\omega_j)$ are the wave number, wave amplitude and phase of the regular wave component corresponding to the frequency component ω_j. Regarding irregular wave conditions, the JONSWAP spectrum together with peakedness factor of 3.3 is applied [109]. For each wave state, 500 individual harmonic wave components with a random set of phases between frequency components are considered. The angular frequencies of the wave components are uniformly spaced from 0.1 to 4.0 rad/s.

The Froude–Krylov force can be divided into static and dynamic terms. The static Froude–Krylov force is equivalent to the hydrostatic force, and calculated by the balance between the gravity force and the buoyancy force:

$$\boldsymbol{F}_{\boldsymbol{FK_{st}}} = M\mathbf{g} - \iint_{S(t)} p_{st}\mathbf{n}\,\mathrm{d}S \tag{6.3}$$

where $\boldsymbol{F_{FK_{st}}}$, $S(t)$, p_{st} and $\mathbf{n}$ represent the static Froude–Krylov force, submerged surface, hydrostatic pressure and normal vector to the geometry surface. The dynamic Froude–Krylov force is expressed as:

$$\boldsymbol{F_{FK_{dy}}} = -\iint_{S(t)} p_{dy}\mathbf{n}\,\mathrm{d}S \tag{6.4}$$

where $\boldsymbol{F_{FK_{dy}}}$ and p_{dy} represent the dynamic Froude–Krylov force and the dynamic pressure. The excitation force in (3.3) in heaving direction is calculated by the sum of the dynamic Froude–Krylov force and the diffraction force. The viscous drag force is also considered in the nonlinear TD model. Therefore, the equation of motion of the buoy in heaving direction can also be expressed as

$$Ma(t) = F_{FK_{st}} + F_{FK_{dy}} + F_D + F_r + F_{pto} + F_{vis} \tag{6.5}$$

where F_D is the diffraction force.

According to [21], in deep water condition, the pressure resulting from the regular wave can be obtained based on Airy wave theory as

$$p(x,z,t) = \rho g \zeta_a e^{kz}\cos(\omega t - kx) - \rho g z \tag{6.6}$$

where the positive x-axis is the direction of wave propagation. For axisymmetric geometries, parametric cylindrical coordinates can be used to describe the geometry surface:

$$\begin{cases} x(\sigma,\theta) = f(\sigma)\cos(\theta) \\ y(\sigma,\theta) = f(\sigma)\sin(\theta),\ \theta \in [0,2\pi) \wedge \sigma \in [\sigma_1,\sigma_2] \\ z(\sigma,\theta) = \sigma \end{cases} \tag{6.7}$$

where $f(\sigma)$ is the function describing the geometry profile. For the heaving point absorber, only the force in the vertical direction is considered. In regular waves, the magnitude of the total Froude–Krylov force in vertical direction can be expressed as

$$\begin{aligned} F_{FK} &= \int_0^{2\pi}\int_{\sigma_1}^{\sigma_2} p(x(\sigma,\theta),z(\sigma,\theta),t) f^{'}(\sigma) f(\sigma)\mathrm{d}\sigma\mathrm{d}\theta \\ &= \int_0^{2\pi}\int_{\sigma_1}^{\sigma_2} \left(\rho g \zeta_a e^{k\sigma}\cos(\omega t - k f(\sigma)\cos(\theta)) - \rho g \sigma\right)\cdot f^{'}(\sigma) f(\sigma)\mathrm{d}\sigma\mathrm{d}\theta \end{aligned} \tag{6.8}$$

The integral limits of the wetted surface is defined as

$$\begin{cases} \sigma_1 = s(t) - h_0 \\ \sigma_2 = \eta(t) \end{cases} \tag{6.9}$$

where η is the elevation of the free surface at $x = 0$ and h_0 is the draft of the buoy. The dependence of the pressure on x in (6.6) can be neglected in the long wave approximation which assumes that the wave length is much longer than the characteristic dimension of the buoy. Then the term $\cos\theta$ in (6.8) can be neglected correspondingly. The integral calculation of (6.8) for the heaving point absorber with centroid at the still water level has been explicitly derived in [155]. In regular waves, the static and dynamic Froude-Krylov force in heaving direction for the spherical geometry with a given draft can be calculated as

$$F_{FK_{st}} = \int_0^{2\pi}\int_{\sigma_1}^{\sigma_2} p_{st}\mathrm{d}\sigma\mathrm{d}\theta = -2\pi\rho g\left[\frac{\sigma^3}{3} + \big(s(t) - h_0 + R\big)\frac{\sigma^2}{2}\right]_{\sigma_1}^{\sigma_2} \tag{6.10}$$

$$\begin{aligned} F_{FK_{dy(re)}} &= \int_0^{2\pi}\int_{\sigma_1}^{\sigma_2} p_{dy}\mathrm{d}\sigma\mathrm{d}\theta \\ &= -\frac{2\pi}{k}\rho g\zeta_a(\cos\omega t)\left[\big(s(t) - h_0 + R\big) + \frac{1}{k} - \sigma\right)e^{k\sigma}\Big]_{\sigma_1}^{\sigma_2} \end{aligned} \tag{6.11}$$

where R is the radius of the buoy. The superposition theory can be applied to calculate the dynamic Froude-Krylov force in irregular waves, while it is noted that (6.10) is also applicable for the calculation of the static Froude-Krylov force in irregular waves. In addition, the formulation for computing other forces remain same in irregular waves. According to (6.2) and (6.11), in irregular waves, the dynamic Froude-Krylov force in heaving direction can be expressed as

$$\begin{aligned} F_{FK_{dy(irr)}} = \sum_{j=1}^{N} -\frac{2\pi}{k(\omega_j)}\rho g\zeta_a(\omega_j)\big(\cos(-\omega_j t + \varphi(\omega_j))\big) \\ \left[\Big((s(t) - h_0 + R) + \frac{1}{k(\omega_j)} - \sigma\Big)e^{k(\omega_j)\sigma}\right]_{\sigma_1}^{\sigma_2} \end{aligned} \tag{6.12}$$

According to Cummins equation [89], the radiation force is calculated as

$$F_r(t) = -\int_{-\infty}^{t} K_{rad}(t-\tau)u(\tau)\mathrm{d}\tau - M_r(\infty)a(t) \tag{6.13}$$

where $M_r(\infty)$ is the added mass evaluated at the infinite frequency, K_{rad} is the radiation impulse function, and they can be calculated based on the results $R_i(\omega)$ and $M_r(\omega)$ obtained from Nemoh. To compute the convolution integral efficiently, the state-space approximation is used [133]. According to [155], the diffraction force is calculated as

$$F_D(t) = -\int_{-\infty}^{\infty} K_{diff}(t-\tau)\eta(\tau)\mathrm{d}\tau \tag{6.14}$$

where K_{diff} is the diffraction impulse function.

In the nonlinear TD simulation, an end-stop mechanism is applied to limit the excessive displacement. The end-stop force is expressed as

$$F_{es}(t) = \begin{cases} 0, & |s(t)| \le s_m \\ -K_{es}\frac{s(t)-s_m}{|s(t)-s_m|}|s(t) - s_m|, & |s(t)| > s_m \end{cases} \tag{6.15}$$

where K_{es} is the stiffness coefficient of the end stop spring, and it is set as 500 kN/m in this work.

The viscous drag force is represented by a quadratic damping term which is similar to the drag component in Morison's equation [101], as

$$F_{vis} = -\frac{1}{2}\rho C_D A_D|u - u_0|(u - u_0) \tag{6.16}$$

where ρ is the water density, C_D is the drag coefficient, A_D is the characteristic area of the buoy, and u_0 is the undisturbed flow velocity at the centroid of the buoy. The drag coefficient is selected as 0.6 to minimize the error of the power estimate based on the investigation reported in [135], in which the research reference is also a sphere.

During the calculation of the nonlinear Froude-Krylov force, the static and dynamic pressures are integrated over the wetted surface of the buoy. The pressure is obtained based on linear wave theory, and the pressure field is described by (6.6). It is clear that the values of the pressure would be overestimated when the surface area of interest moving above the mean free surface, since z is in the exponential term in (6.6). To enhance the accuracy of the model, Wheeler stretching theory is used to correct the pressure expression. In this sense, the flow velocity and pressure at the initial vertical position z is replaced by those in a corrected vertical position $z^{'}$, and it can be expressed as

$$z^{'} = \frac{D(D+z)}{D+\eta} - D \tag{6.17}$$

where D is the water depth. D is set as a sufficiently large value of 1000 in the numerical set-up, considering the deep water assumption in this work.

As nonlinear forces are taken into account, the optimal PTO damping coefficients could not be obtained theoretically. Thus, in the nonlinear TD analysis, the PTO damping coefficients are selected through an exhaustively search approach. Specifically, the PTO damping is searched over the range $[0.01|Z_m(\omega)|, 2|Z_m(\omega)|]$ for regular waves or $[0.01|Z_m(\omega_p)|, 2|Z_m(\omega_p)|]$ for irregular waves, in which ω_p stands for the peak period of the irregular waves. The range was defined on the basis of linear hydrodynamics, $|Z_m(\omega)|$ has been proven to be the optimal damping for an unconstrained heaving point absorber with the passive control strategy in regular waves [99]. In this paper, 200 evenly spaced values are considered in the range, and the PTO damping is selected to maximize the power absorption while complying with the PTO force limits.

The TD simulation is performed based on the numerical integration scheme. The initial displacement and velocity of the buoy is set to zero. The simulation time duration and time step is set to 125 and 0.01 times the considered wave period (or peak period) respectively. A ramp function is used to avoid strong transient flow at earlier time steps, and the ramp time is chosen as 25 times the wave period [134]. The duration of the ramp time is not included in the calculation of average power absorption. To mitigate random errors in the simulation with irregular waves, the TD model is re-run ten times to calculate the mean value in each case.

6.4. RESULTS

This section is divided into two subsections. The first subsection presents the results from the calculation of FD modeling. The effects of the buoy draft adjustment on hydrodynamic performance and PTO performance are analyzed. Next, the power performance of the fixed draft WEC and the adjustable draft WEC are compared. The second subsection presents the results obtained from the nonlinear time modeling. The influence of the nonlinear Froude–Krylov force on the power absorption is discussed. Taking into account nonlinear Froude–Krylov forces, the benefits from the adjustable draft system are re-evaluated.

6.4.1. FREQUENCY DOMAIN ANALYSIS

THE INFLUENCE OF THE BUOY DRAFT ON THE HYDRODYNAMIC PERFORMANCE

Based on FD modeling, the effect of the draft adjustment on the hydrodynamic performance of the floating spherical buoy is investigated. First, the hydrodynamic coefficients of the spherical floating buoy in heave motion are calculated for different buoy drafts. The corresponding excitation force coefficients, added mass and radiation damping are depicted in the Appendix A.2. Then, in the case without the PTO force applied on the buoy, the heave response amplitude operators (RAO) of the spherical floating buoy in different drafts are shown in Figure 6.3. It can be noted that the heave RAO is highly dependent on the buoy draft. An increase of the buoy draft leads to a larger peak value of the heave RAO.

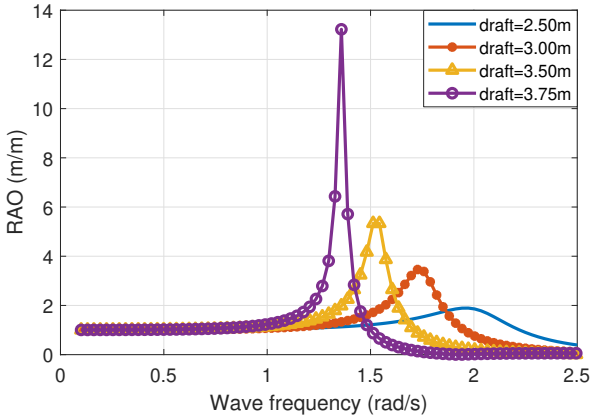


Figure 6.3: Heave RAO of the floating spherical buoy of 5.0 m diameter in different drafts without PTO force.

Figure 6.4 presents the relative power absorption of the WEC with different buoy drafts, in which the PTO damping is tuned to maximize the absorbed power at the wave period of 5.0 s. The power absorption bandwidth is defined as a frequency range within which the WEC could absorb power higher than 50 % of the maximum absorbed power. This measure effectively indicates the ability of the WEC responding to the incoming waves of frequencies rather than its natural frequency. Figure 6.4 suggests that increasing the buoy draft reduces the power absorption bandwidth and a buoy with very large drafts could result in a narrow-banded device. However, the real sea conditions are normally characterized by irregular waves, in which a range of wave frequencies is included. As a result, a compromise is needed between pursuing a higher RAO in the peak period and a wider bandwidth when adjusting the buoy draft in irregular waves.

The total mass, water plane area, natural frequency and natural period of the WEC with different buoy drafts are shown in Figure 6.5 and 6.6. It can be seen that the buoy draft adjustment makes a difference to these properties. The water-plane area and the natural frequency decrease with the increase of the buoy draft, but the total mass increases with the buoy draft.

THE INFLUENCE OF THE BUOY DRAFT ON THE PTO PERFORMANCE

In this part, the effect of the buoy draft on the PTO performance is discussed. The PTO force amplitude and average absorbed power are calculated. It can be seen from Figure 6.7 that the buoy draft significantly affects the PTO performance. Figure 6.7a shows that the

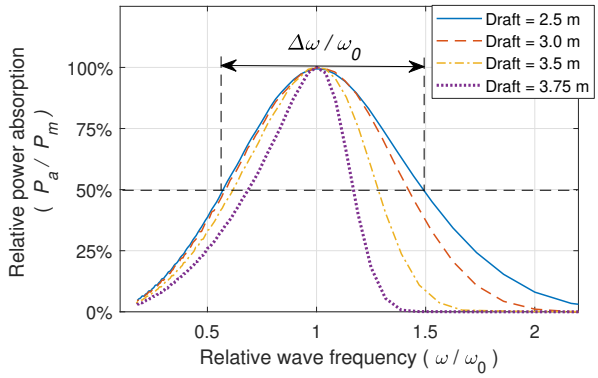


Figure 6.4: The relative power absorption of the WEC with different buoy drafts. The results are calculated in regular wave states with a wave height of 1.0 m. P_a and P_m represent the absorbed power and the maximum absorbed power along various wave frequencies. ω_0 represents the wave frequency corresponding to the maximum power absorption.

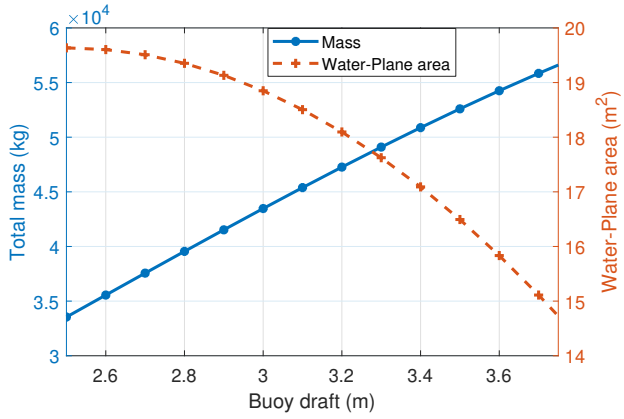


Figure 6.5: The water plane area and total mass of the buoy as a function of the draft.

required PTO force amplitude can be reduced by increasing the buoy draft. As shown in Figure 6.7b, the impact of the draft adjustment on the average power is dependent on the wave period. The buoy drafts of 3.0 m and 3.5 m and 3.75 m correspond to natural periods of 3.5 s, 4.1 s and 4.5 s respectively. Thus, their average power are higher than that of the buoy draft of 2.5 m around the range of their natural wave periods. When the wave period is higher than 5.0 s, the buoy draft of 2.5 m is associated with a higher average power than that of other larger buoy drafts. It can be deduced that the buoy draft adjustment can be used to regulate the required PTO force. Therefore, adjusting the buoy draft is expected to enable downsizing of the PTO capacity. In addition, adapting the buoy draft to wave periods is able to improve the average power, because the natural frequency of the WEC can be controlled to match the wave period. For instance, the average power of the WEC with a buoy draft of 2.5 m is higher than that of other buoy drafts over a wide range of wave periods. However,

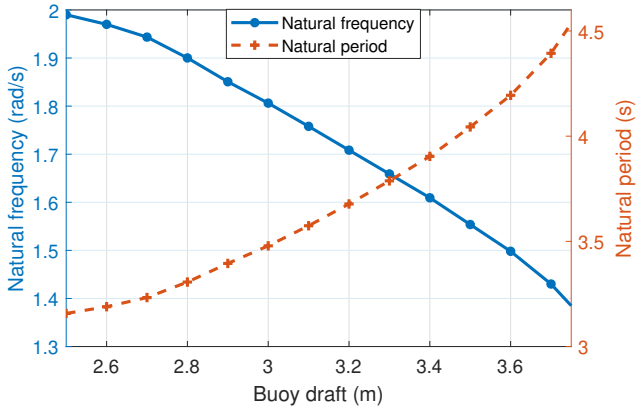


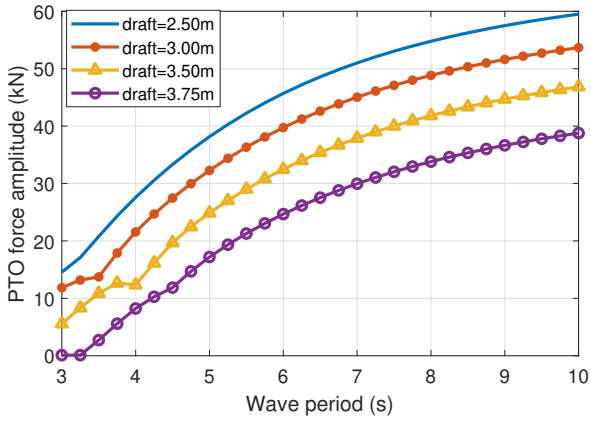
Figure 6.6: The natural frequency and corresponding period of the heaving buoy as a function of the draft.

it becomes lower than the average power of the WEC with larger buoy drafts along the wave period from 3.5 s to 4.8 s which matches the natural periods of larger buoy drafts as seen in Figure 6.6.

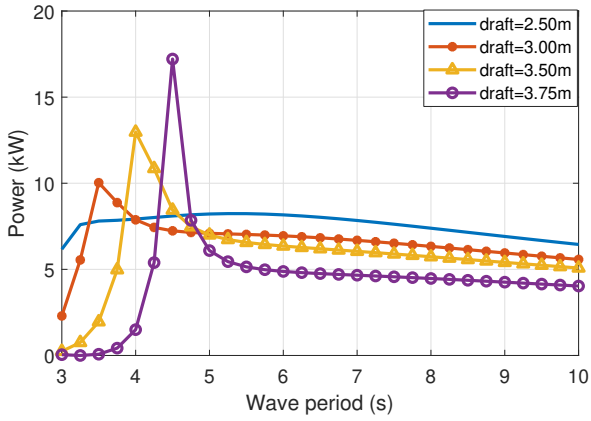
POWER PERFORMANCE WITH PTO FORCE LIMITS

As is shown before, the required PTO force of the WEC is related to the buoy draft. Thus, the effect of the PTO force constraints on power performance differs with the buoy draft. A good example is shown in Figure 6.8, which presents the relationship between the PTO force, the average power and the PTO damping coefficient. The calculation is performed based on a regular wave state, in which the wave height and wave period are 2.5 m and 5.0 s respectively. It can be noted that a buoy draft of 2.5 m corresponds to a higher average extracted power than a buoy draft of 3.75 m without PTO force constraints. However, the implementation of the PTO force constraint would limit the available range of PTO damping coefficients, and the solid curves in the middle plot of Figure 6.8 correspond to the available range of PTO damping coefficients. In this way, the absorbed power of the buoy draft of 3.75 m overtakes that with the buoy draft of 2.50 m, and they are 38 kW and 28 kW respectively with the PTO force limit of 40 kN. Therefore, it can be deduced that reasonably adjusting the buoy draft could mitigate the negative effect of PTO force limits on the power absorption.

To identify the influence of PTO force limits on the power performance of the WEC with different buoy drafts, various PTO force limits are implemented. The root mean square (RMS) value is commonly used in PTO rating, since it allows the PTO system, such as an electrical machine, to work in a sustainable condition on a longer time scale [158]. Thus, the PTO force limit is considered in the form of RMS value. Taking the wave state with a wave height of 1.0 m and wave period of 5.0 s as an example, the percentage of the absorbed power with force constrains to that without force constraints and the absorbed power per RMS of the required PTO force are presented in Figure 6.9. It can be seen from Figure 6.9a that PTO force limits have a notable negative influence on the power absorption. The percentage value increases with the PTO force limit. Furthermore, it can be seen that the percentage values of the WEC with the larger buoy drafts are generally higher than those with lower buoy drafts. This is expected since the WEC with the larger buoy drafts correspond to the lower required PTO forces at the unconstrained force condition, which has been shown



(a) PTO force amplitude (or maximum PTO force)



(b) PTO average power

Figure 6.7: PTO performance as a function of the buoy draft without force constraints, and the considered wave height is 1.0 m.

in Figure 6.7. In Figure 6.9b, it is seen that the absorbed power per RMS of the required PTO force tends to decrease with the force limit until the force limit is sufficiently high for the power absorption. It can also be noticed that the absorbed power per RMS of the PTO force differs with the buoy draft, and the buoy drafts of 3.75 m and 3.5 m are associated with higher values than that of the buoy draft of 2.5 m.

The power performance with force constraints is calculated for different wave periods, which is shown in Figure 6.10. It can be noted that increasing the buoy draft contributes to higher power absorption at low wave periods. With the increase of the wave period, the difference between the power performance of different buoy drafts tends to vanish. It should be realized that the power performance discussed in this paper is the absorbed power by the WEC instead of the grid power. This implies that the PTO efficiency is not taken into consideration. However, the force limit in reality represents the PTO size which could make a difference with respect to the PTO efficiency [159]. For instance, the relation of the PTO conversion efficiency to the size of linear generators in wave energy conversion has been

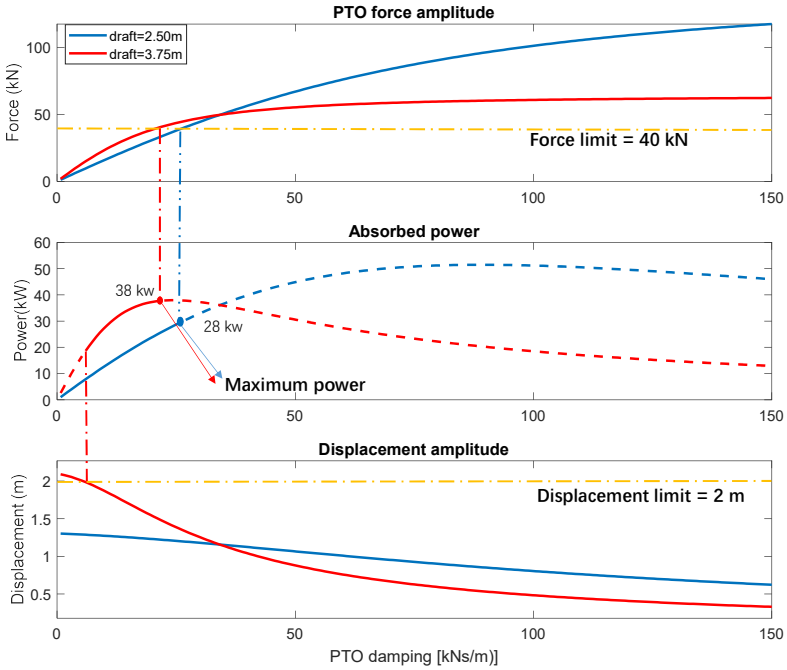
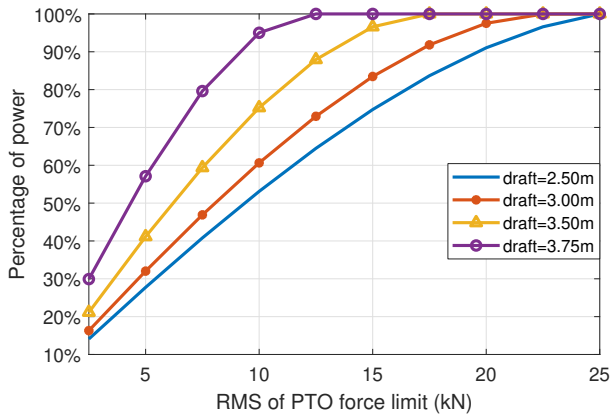


Figure 6.8: The PTO force amplitude, average power and displacement as a function of PTO damping for two different buoy drafts. The considered wave height is 2.5 m and the wave period is 5.0 s.

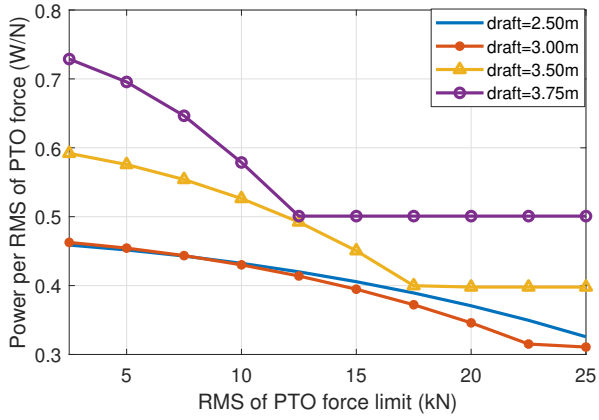
investigated in [83]. This study indicated that the overall power conversion efficiency generally increases with the dimension of linear generators, which mainly results from the reduction of copper losses in power conversion.

PERFORMANCE COMPARISON BETWEEN THE ADJUSTABLE DRAFT WEC AND THE FIXED DRAFT WEC

To present the benefits of the adjustable draft system, a comparison is made between the power absorption of the adjustable draft WEC and the fixed draft WEC. In this paper, fourteen buoy drafts evenly spaced along the adjustable range are considered when identifying the performance of the adjustable draft WEC. However, it should be realized that a continuous adjustment can be achieved in practice by the adjustable draft system. Regarding the fixed draft WEC, the buoy draft is fixed at 2.5 m. The ratios of power absorbed by the adjustable draft WEC to that by the fixed draft WEC are calculated, and the results are shown in Figure 6.11. In the calculation, three different PTO force limits are implemented, and regular wave states with a wave height of 1.0 m are considered. It can be observed from Figure 6.11 that the adjustable draft WEC is clearly associated with an improvement of the power absorption, compared with the fixed draft WEC. For instance, at the RMS of the PTO force limit being 10 kN, the absorbed power of the adjustable draft WEC is 3.5 times that of the fixed draft WEC. The improvement occurs over a wider range of wave periods with the stricter PTO force constraints. With the RMS of the PTO force limit of 10 kN, the improvement can be noticed from the wave period of 3.5 s until 6.5 s. However, it is observed



(a) Percentage of PTO absorbed power with force limits to that without force limits



(b) PTO absorbed power per RMS of the PTO force

Figure 6.9: The influence of PTO force limits on the power performance. The results are calculated in a regular wave state with the wave height of 1.0 m and the wave period of 5.0 s.

only until around 4.8 s when the RMS of the PTO force limit increases to 20 kN. Therefore, it is concluded that the adjustable draft system is beneficial for the power absorption, especially with the downsized PTO capacity. It has to be acknowledged that the improvement of power absorption concentrates on the low wave periods (from 3.0 to 6.5 s). Thus, given the considered buoy size and geometry, its contribution for realistic wave sites where long wave periods are significantly dominating is relatively limited.

THE INFLUENCE OF BUOY SIZE ON THE PERFORMANCE OF THE ADJUSTABLE DRAFT SYSTEM

The effect of the draft adjustment on the hydrodynamics and PTO performance of the system depends on the buoy geometry and size. Here, the influence of the buoy size on the performance of the adjustable draft WEC is demonstrated.

Figure 6.12 depicts how the buoy scaling affects the ratio between the power absorption of the adjustable draft WEC and the fixed draft WEC. It can be seen that the profile of the ratio does not change with the scaling factor, but the wave period changes accordingly. With

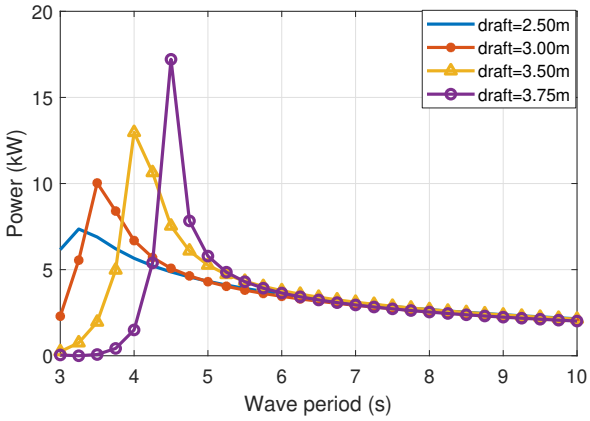


Figure 6.10: The influence of PTO force limits on the power performance, with a wave height of 1.0 m and the RMS of the PTO force limit of 10 kN.

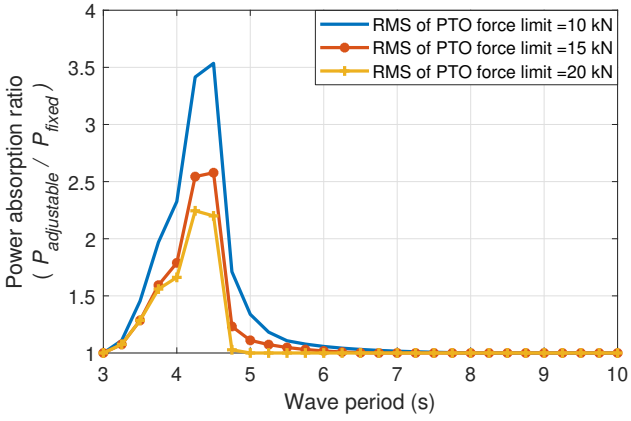


Figure 6.11: Ratio of the power absorbed by the adjustable draft WEC to that by the fixed draft WEC in different RMS of the PTO force limit. The results are calculated in regular waves with a wave height of 1.0 m. $P_{adjustable}$ and P_{fixed} embody the power absorbed by the adjustable draft WEC and the power absorbed by the WEC with a fixed draft of 2.5 m.

the increase of the buoy size, the improvement of the power absorption moves to larger wave periods. Therefore, buoy scaling can be used to adapt the adjustable draft WEC to different wave climates.

6.4.2. NONLINEAR TIME DOMAIN ANALYSIS

THE EFFECT OF NONLINEAR FORCES ON POWER PERFORMANCE

For simplification, only the buoy with a diameter of 5.0 m is discussed in the nonlinear TD analysis, although the buoy size has been proven influential in Figure 6.12. To verify the reproduced nonlinear TD model, a comparison is made between the results of RAOs from the reproduced model and the results from [155], which can be found in Appendix A.4.

To identify the influence of the nonlinear forces on power performance of WECs, the

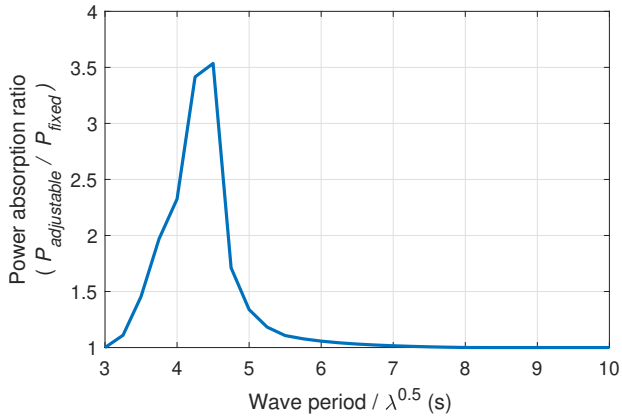


Figure 6.12: Ratio of the power absorbed by the adjustable draft WEC to that by the fixed draft WEC for different buoy sizes, the wave heights and the RMS of the PTO force limit are $1.0 \cdot \lambda$ m and $10 \cdot \lambda^3$ kN. $P_{adjustable}$ and P_{fixed} embody the power absorbed by the adjustable draft WEC and the power absorbed by the WEC with a fixed draft of $2.5 \cdot \lambda$ m.

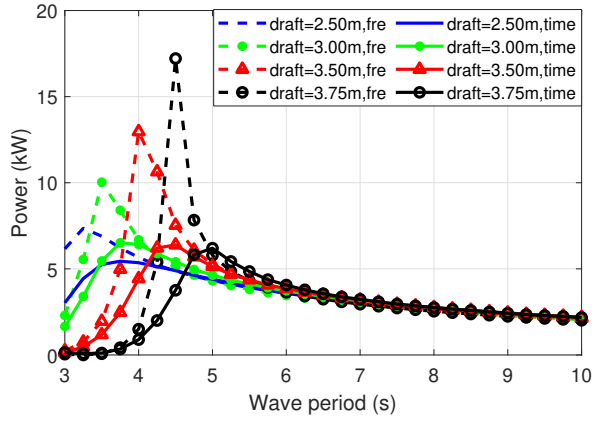


Figure 6.13: Average power calculated by the nonlinear TD model and FD model for different buoy drafts. The results are calculated in regular wave states with a wave height of 1.0 m and the RMS of the PTO force limit is 10 kN. In the legend, "fre" and "time" represent the FD model and nonlinear TD model respectively.

results of the power absorption estimated by the nonlinear TD model and linear model are compared, as shown in Figure 6.13. The considered wave height is 1.0 m, and the RMS of the PTO force limit is 10 kN. The selection of the PTO damping is different for each model, thus the influence of the numerical model response on the optimization of the PTO damping is also reflected in the figure. It can be seen from Figure 6.13 that the power estimated by the nonlinear TD model is much lower than that by the FD model around the resonance regions, but the difference is negligible at other wave periods. For instance, the buoy draft of 3.75 m is associated with 17 kW at the wave period of 4.5 s in the FD analysis, while it decreases to around 4 kW in the nonlinear TD analysis. Therefore, the linear model overestimates the power performance around the resonance. The variation of the instantaneous

wetted surface is expected to be the main contributor to the difference between the linear and nonlinear models. To reflect the variation, the standard deviations of the instantaneous displacement of the buoy relative to the wave elevation and the standard deviation of the instantaneous variation of the water-plane area are calculated for different buoy drafts, shown in Figure 6.14 and Figure 6.15. It is visible that the standard deviation of the relative displacement is clearly higher in the wave periods of resonance for each buoy draft. In addition, it is observed from Figure 6.13 that the difference of power estimation between these models turns out to be larger for larger buoy drafts. This is expected since larger buoy drafts essentially correspond to larger variations of the water-plane area, as shown in Figure 6.15. The variation of the water-plane area effectively implies the nonlinearity of the Froude-Krylov force.

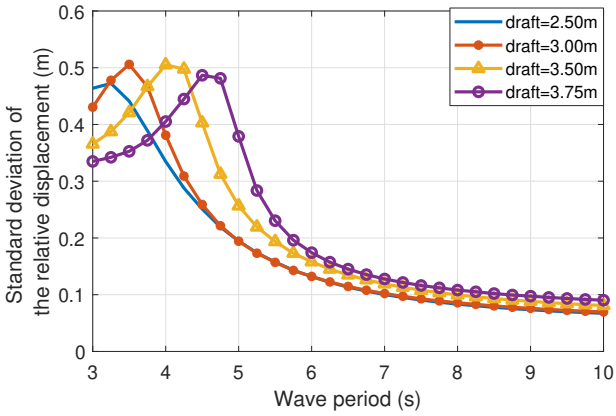


Figure 6.14: The standard deviation of the displacement of the buoy relative to the wave elevation. The results are calculated in regular wave states with a wave height of 1.0 m, and the RMS of the PTO force limit is 10 kN.

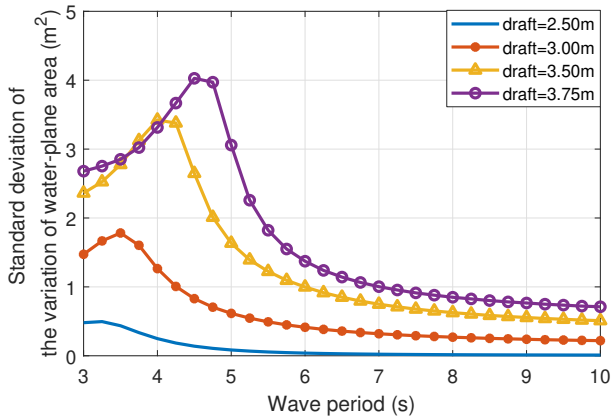


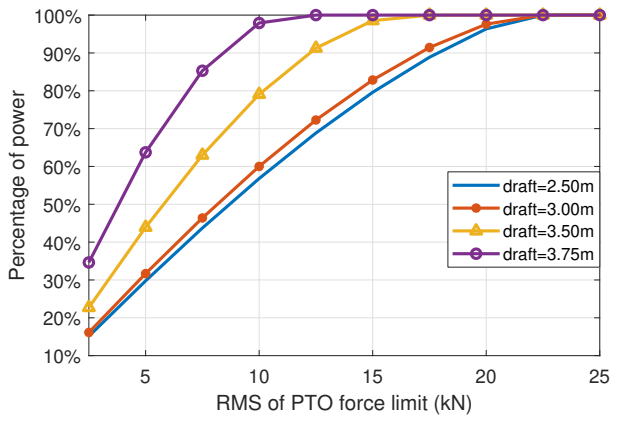
Figure 6.15: The standard deviation of the variation of the water-plane area. The results are calculated in regular wave states with a wave height of 1.0 m, and the RMS of the PTO force limit is 10 kN.

Furthermore, as a consequence of the addition of nonlinear force components, the nat-

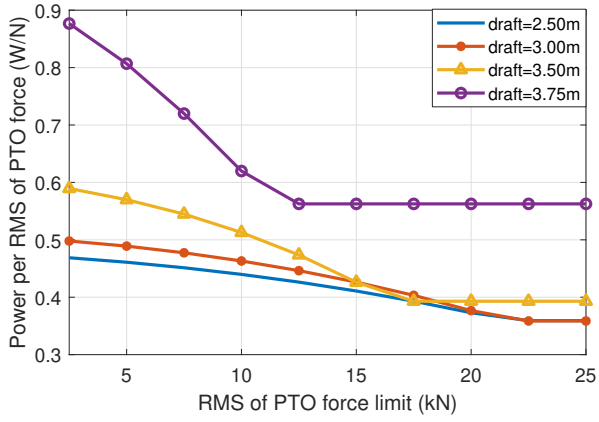
ural frequency is shifted to be lower. As can be seen in Figure 6.13, the wave periods when maximum power is obtained deviate from those presented by the FD analysis. Taking the buoy draft of 3.75 m as an example, the maximum power is obtained at 4.5 s in the FD modeling, while it is at around 5.0 s in the nonlinear TD analysis.

THE INFLUENCE OF PTO FORCE LIMITS ON POWER PERFORMANCE

The power performance of the WEC with different buoy drafts is calculated by the nonlinear TD model, and various PTO force limits are implemented. The results are shown in Figure 6.16, and the considered wave height and period are 1.0 m and 5.0 s respectively. It can be noted from Figure 6.16a that the PTO force limit reduces the power absorption, but the effect differs with the buoy draft. For example, at the RMS of the PTO force limit of 10 kN, the percentage of the buoy draft of 3.75 m reaches nearly 100% while it is only around 55% for the buoy draft of 2.50 m. This observation generally agrees with the results obtained by the FD analysis. Then, comparing Figure 6.16b and Figure 6.9b, it is seen that both their



(a) Percentage of PTO absorbed power with force limits to that without force limits



(b) PTO absorbed power per RMS of PTO force

Figure 6.16: The influence of PTO force limits on the power performance. The results are calculated in a regular wave state with the wave height of 1.0 m and the wave period of 5.0 s.

profiles suggest the similar trend, in which the power per RMS of the PTO force generally decreases with the PTO force limit. However, an obvious difference can be observed with regard to the buoy draft of 3.75 m. In the nonlinear TD analysis, its absorbed power per RMS of the PTO force is higher than that in the FD analysis. Specifically, the ultimate value stays at approximately 0.58 W/N in the nonlinear TD analysis, but it is nearly 0.5 W/N in the FD analysis. This can be supported by the fact explained in Figure 6.13 that the nonlinear components shifted its natural frequency to around 5.0 s. As a consequence, the power estimated by nonlinear TD modeling is higher than the one obtained by the FD analysis at this concerned wave period.

PERFORMANCE COMPARISON BETWEEN THE ADJUSTABLE DRAFT WEC AND THE FIXED DRAFT WEC

- *In regular waves*

  The absorbed power of the adjustable draft WEC is calculated by the nonlinear TD model for regular wave conditions, as shown in Figure 6.17. For comparison, the power performance of the semi-submerged fixed draft WEC is also presented in the figure. The calculation is performed based on the regular wave state with a wave height of 1.0 m, and the RMS of the PTO force limit is set as 10 kN. It can be seen from Figure 6.17 that the adjustable draft WEC could absorb higher power over a range of wave periods. The gain of the power resulting from the adjustable draft system is mainly observed from the wave period of 3.5 s to 6.5 s. For instance, the highest power for the adjustable draft WEC is around 7 kW at the period of 4.0 s while it is only around 5.5 kW for the fixed draft WEC. The improvement is as high as 27 %. When the wave period is below 4.0 s or above 6.5 s, the adjustable draft WEC and the fixed draft WEC tend to absorb the similar amount of power.

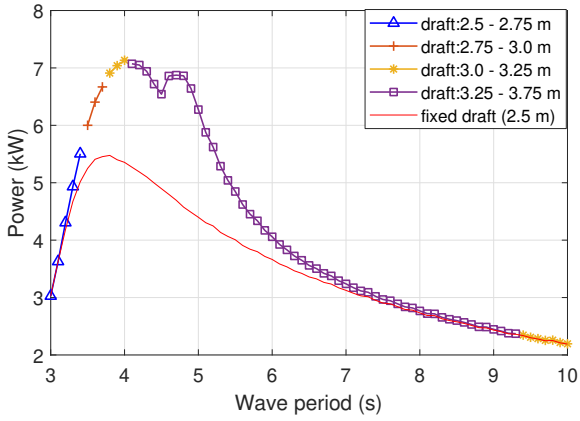


Figure 6.17: Comparison between the power absorbed by the adjustable draft WEC and that by the WEC with a fixed draft of 2.5 m, and the considered wave height is 1.0 m and the RMS of the PTO force limit is 10 kN.

Figure 6.18 shows the adjusted drafts for the maximum delivered power in different wave periods. It is clear that the draft selection is strongly dependent on the wave period. The trend of the optimal draft is generally to first increase with the wave period and then to be relatively constant. This is because the natural period of the buoy

increase with the buoy draft, which has been depicted in Figure 6.3. At their natural periods, the larger drafts are associated with higher values of the RAO as well as higher buoy velocities. When the PTO force constraint starts to be a limiting factor of the power absorption, the higher velocity could contribute to the increase of the power absorption.

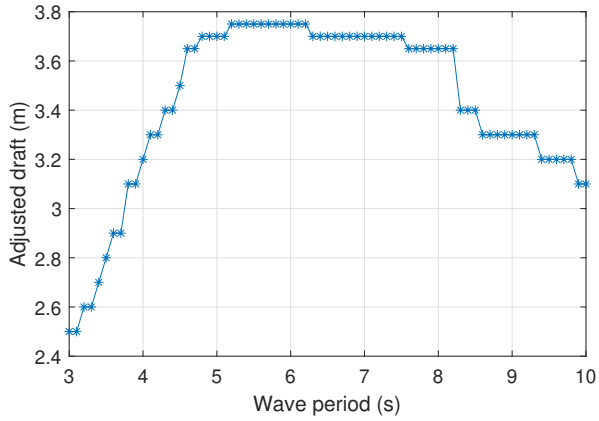


Figure 6.18: The adjusted buoy drafts corresponding to the highest power for different wave periods, and the wave height is 1.0 m and RMS of the PTO force limit is 10 kN.

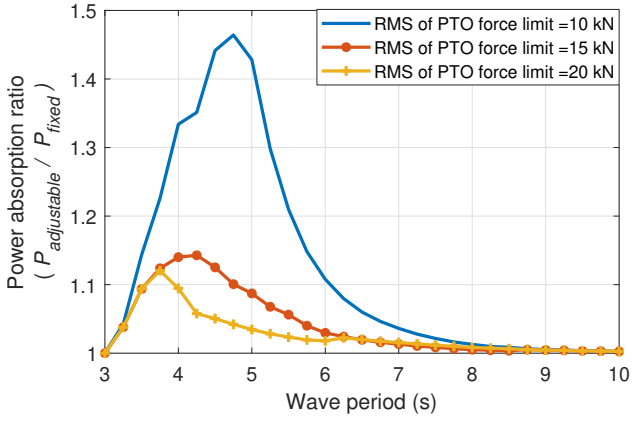


Figure 6.19: Ratio of the power absorbed by the adjustable draft WEC to that by the fixed draft WEC in different RMS of the PTO force limit. The results are calculated in regular waves with a wave height of 1.0 m. $P_{adjustable}$ and P_{fixed} embody the power absorbed by the adjustable draft WEC and the power absorbed by the WEC with a fixed draft of 2.5 m.

Figure 6.19 shows the ratios of the power absorbed by the adjustable draft WEC to that by the fixed draft WEC. The calculation is performed based on regular wave states with a wave height of 1.0 m. The corresponding ratios of power absorption in Figure 6.19 is generally lower than those predicted by the FD modeling, shown in Figure 6.19. For instance, when the RMS of the PTO force limit is 10 kN, the highest ratio reaches 3.5 in Figure 6.11 while it declines to around 1.45 in Figure 6.19. However, even with

considering nonlinear forces including the drag force, the adjustable draft WEC still suggests an obvious improvement of the power absorption, and the improvement is more significant when the PTO force limit becomes stricter. For example, when the RMS of the PTO force limit is 10 kN, the absorbed power of the adjustable draft WEC is 1.45 times that of the fixed draft WEC at the wave periods around 5.0 s. But it is only around 1.15 and 1.1 times as the RMS of the PTO force limit increases to 15 kN and 20 kN respectively. Therefore, it suggests that the adjustable draft system could improve the power performance of the spherical heaving point absorber in regular wave states, especially with the downsized PTO capacities.

- *In irregular waves*

  The power performance of the adjustable draft WEC and the fixed draft WEC in irregular wave states is calculated, shown in Figure 6.20. As the simulation with irregular waves is run ten times for each case using different seeds, the mean values and error bar of the estimated power are presented. It can be seen that the power improvement resulting from the adjustable draft system in irregular waves is less noticeable than the results from regular waves. The reason is that increasing the buoy draft reduces the absorption bandwidth of the buoy, and the narrower bandwidth reflects the incapability to respond to broad wave frequencies other than the natural frequency. Although the power absorption of the buoy with larger drafts in irregular waves is relatively weakened with regard to that in regular wave states, there is still power improvement resulting from the application of the adjustable draft system. For instance, the highest mean values of the absorbed power for the fixed draft WEC and adjustable draft WEC are approximately 5.7 and 6.4 kW, and the improvement is around 12 %. In addition, it is observed that the gain of power absorption is mainly located between the peak periods of 4.5 and 6.0 s. When the peak period is above 7.0 s, the difference between the power absorption of the adjustable draft WEC and the fixed draft WEC is negligible. One possible approach to improve the power performance of this concept in irregular waves is to optimize the buoy geometry, by which the issue of narrow absorption bandwidth is expected to be mitigated. As indicated by [86], the absorption bandwidth increases with the resistive term, and thus the buoy geometries with the radiation damping increasing with the draft might be desirable.

  The adjusted buoy drafts corresponding to the maximum power absorption for different peak periods in irregular wave states are shown in Figure 6.21. The tendency of the adjusted draft with the peak period is first to increase and then to be stabilized at around 3.2 m in spite of the small fluctuations. Comparing the results with the draft adjustment in regular waves from Figure 6.18, the values of the adjusted draft in irregular waves are accordingly lower. For instance, the adjusted draft in regular waves is higher than 3.6 m for the wave period between 4.5 and 8.2 s, while the largest adjusted draft is 3.3 m in irregular waves. This is also because the larger buoy drafts have a narrower bandwidth, which penalizes its power absorption in irregular waves.

  As suggested in Figure 6.21, the adjusted buoy draft is 2.8 m for the peak period of 4.0 s. Thus, the instantaneous responses of the WEC with the buoy drafts of 2.5 and 2.8 m are depicted in Figure 6.22 to represent the performance of the adjustable draft WEC and fixed draft WEC. For a fair comparison, the generated profile of the wave elevation is maintained identical for these two buoy drafts in the simulation. It can be seen from

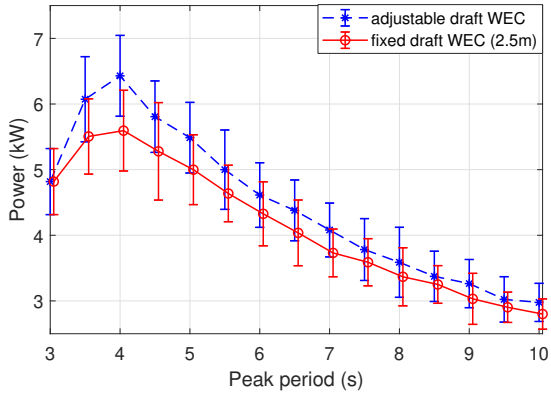


Figure 6.20: Comparison between the power absorbed by the adjustable draft WEC and that by the WEC with a fixed draft of 2.5 m, and the considered significant wave height is 1.5 m and the RMS of the PTO force limit is 10 kN.

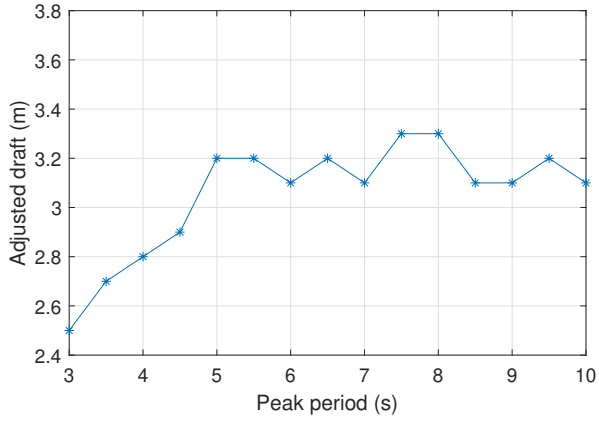
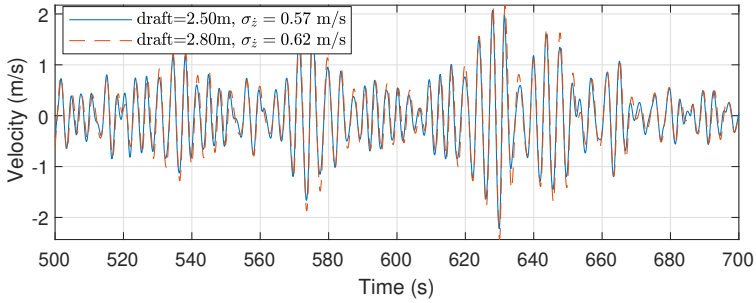


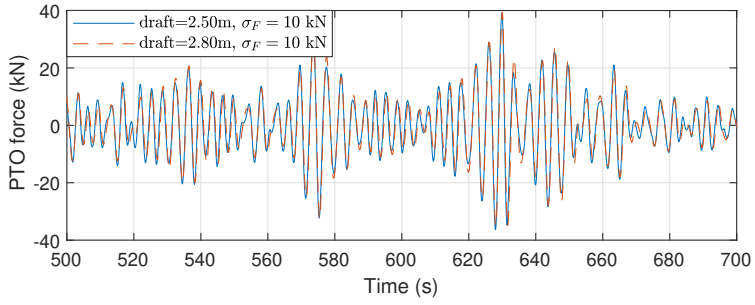
Figure 6.21: The adjusted buoy drafts corresponding to the highest power for different wave periods, and the considered significant wave height is 1.5 m and the RMS of the PTO force limit is 10 kN.

Figure 6.22a and Figure 6.22b that the buoy draft of 2.8 m is generally related to higher velocities than that of 2.5 m at the same PTO force constraint. Therefore, the power absorbed by the buoy draft of 2.8 m is accordingly higher, as shown in Figure 6.22c.

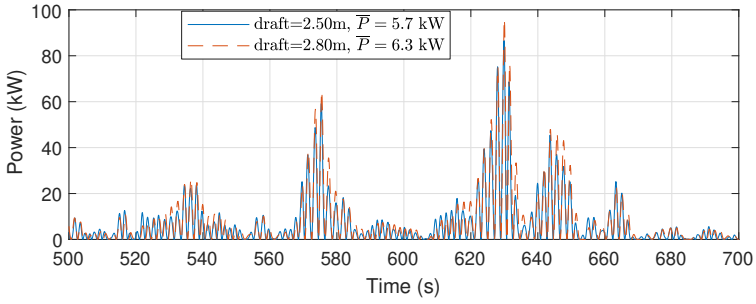
As the buoy draft increases, the possibility of the buoy being fully submerged could be higher. As a consequence, the prediction accuracy of the power performance would decrease, since the effect is not considered in the numerical model. To justify the accuracy of the performance identification, the instantaneous relative displacement of the buoy to the wave elevation is calculated for an adjusted buoy draft, shown in Figure 6.23. The adjusted buoy draft of 3.2 m in the peak period of 5.0 s is considered as a particular case. This case is sufficiently representative since the relative displacement is rather high at the wave periods between 3.5 and 5.0 s (shown in Figure 6.14), and the buoy draft of 3.2 m is almost the largest value used in the irregular



(a) Velocity



(b) PTO force



(c) Power

Figure 6.22: The TD responses of the buoy with the draft of 2.5 m and 2.8 m, corresponding to the wave elevation as input. The simulation is performed based on an irregular wave state with a significant wave height of 1.5 m and peak period of 4.0 s. The PTO damping is optimized subjected to the force constraints of RMS of 10 kN, with the values of 17600 kg/s and 16200 kg/s for the buoy draft of 2.5 m and 2.8 m. $\sigma_{\dot{z}}$ and σ_F embody the standard deviation of the velocity and PTO force.

wave states (shown in Figure 6.23). It is observed from Figure 6.23 that the relative displacement hardly gets close to the two values indicating the cases of leaving water or being fully submerged within a simulation time duration of 1000 s. Thus, the current model is thought to be verified for the considered simulation cases in the TD analysis. However, it should be realized that the possibility of the occurrence could increase if higher wave heights are considered, and then the accuracy of the current model would be challenged.

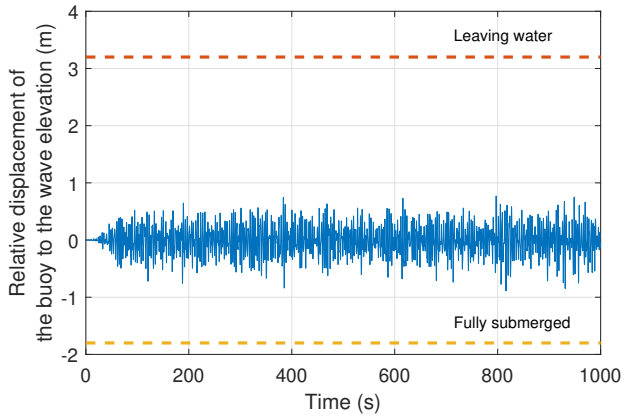


Figure 6.23: The relative displacement of the buoy to the wave elevation, and the buoy draft is adjusted to 3.2 m. The results are calculated in an irregular wave state with a significant wave height of 1.5 m and peak period of 5.0 s, and the RMS of the PTO force limit is 10 kN.

6.5. DISCUSSION

This thesis is focused on the conceptual study of the adjustable draft system. Thus, the regulation of ballast water is assumed to be implemented ideally, which means that the draft can always be instantly adjusted to the desirable level. But, loading or discharging ballast water inside the buoy takes time, which is of essence to be considered in the following development towards practical application. Considering the typical operating capacities of small and medium sized centrifugal pumps commonly used in marine engineering for ballasting [160], the consumed time of the ballasting is calculated for the flow rates ranging from 150 liter/min to 750 liter/min. The result is shown in Figure 6.24. For the flow rate of 450 liter/min, the process would take a period of time around 50, 45, 30, 25 and 10 minutes if the draft is adjusted from 2.5 m to 3.75 m, 3.5 m, 3.25 m, 3.0 m 2.75 m respectively. It should be noticed that the buoy draft adjustment is designed to be sea-state based, thus ballasting is only required in the frequency of order of hours or even longer. Furthermore, the variation of the desired buoy draft is observed gradual by the wave period as shown in Figure 6.18 and 6.21. It implies that the required change of the buoy draft is relatively limited in each adjustment operation, and the consumed time wouldn't be long. In this sense, it is expected that the buoy draft adjustment can be managed timely and effectively in reality. However, it is acknowledged the efficiency of the draft adjustment also depends on the design of the ballast management system, wave resource, buoy size and shape. Thus, a further analysis is needed in the next-stage of this conceptual design.

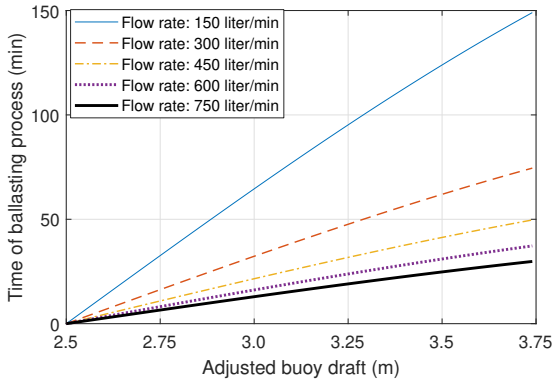


Figure 6.24: The relative displacement of the buoy to the wave elevation, and the buoy draft is adjusted to 3.2 m. The results are calculated in an irregular wave state with a significant wave height of 1.5 m and peak period of 5.0 s, and the RMS of the PTO force limit is 10 kN.

6.6. SUMMARY AND CONCLUSIONS

In this chapter, an adjustable draft system is proposed for the heaving point absorber concept. By means of this system, the buoy draft can be adapted to the wave state. First, the proposed system and the considered WEC concept are described. Next, a FD model is established to study the effect of the draft adjustment on performance of the WEC. The power performance of the adjustable draft WEC and the fixed draft WEC are compared for different PTO force constraints considerations. Furthermore, to take into account the nonlinear forces, an algebraic nonlinear TD model is used to re-evaluate the performance of the WEC integrated with the adjustable draft system, in which both regular waves and irregular waves are considered. Based on the results, the following concluding remarks are drawn.

- The draft adjustment of the spherical buoy has a significant influence on its hydrodynamic coefficients in heave mode. The excitation force can be reduced by increasing the buoy draft. The larger buoy drafts correspond to the higher peak value of the heave RAOs but the narrower bandwidth. However, this conclusion is limited to the spherical floating buoy geometry, and the dependence of the hydrodynamic performance on the draft adjustment would differ with the buoy geometry. It is therefore recommended to conduct further investigation on the relevance of the buoy geometry to the performance of the adjustable draft system.
- The PTO force amplitude and average power of WECs are highly related to the buoy draft. Adapting the buoy draft to wave states makes it possible to control the required PTO force. The required PTO force can be reduced by increasing the buoy draft. Therefore the adjustable draft system can be used to implement the downsizing of PTO capacity.
- The buoy draft adjustment varies the natural frequency of the WEC, and thus adapting the buoy draft to wave states could improve the power absorption. Reasonably adjusting the buoy draft is able to mitigate the negative effect of PTO force constraints on power performance. In addition, the performance of the adjustable draft system is related to the buoy size, and the wave periods when the power absorption can be clearly

gained is increased by scaling the buoy up. Furthermore, nonlinear forces could make a difference to power absorption of the WEC, and the power absorption from the nonlinear model is remarkably lower than that estimated in the FD analysis at the resonance regions. With regard to the fixed draft WEC, the application of the adjustable draft system is able to improve the power performance of a spherical point absorber, especially in the cases with the downsized PTO capacities. In the considered regular wave states, the power absorption could be improved around 27 % in particular cases. In irregular wave states, less power improvement is observed since the absorption bandwidth is relatively narrowed by the increase of the buoy draft. Nevertheless, in the considered irregular wave conditions, the power absorption can be improved by approximately 12 % in particular wave state.

The performance of the adjustable draft WEC was studied in this chapter, but the focus was lied on the hydrodynamic performance and power absorption. In the next chapter, the implications of the addition of the adjustable draft system on the whole system, including the electrical generator, will be identified based on a wave-to-wire model.

7

THE PERFORMANCE OF THE ADJUSTABLE DRAFT POINT ABSORBER INTEGRATED WITH A LINEAR PM GENERATOR

In the previous chapter, the effect of the draft adjustment on the power absorption was demonstrated. As an extension, a wave-to-wire model is established in this chapter to comprehensively evaluate the systematic performance of the adjustable draft point absorber integrated with a linear permanent magnet generator. The developed wave-to-wire model is capable of simulating the complete process from the wave power input through the whole system to the usable electricity produced by the generator. In addition, the negative effects of the draft adjustment on the stroke and overlap between the stator and translator are demonstrated. Subsequently, a comparison is made between this novel WEC and conventional WEC, and both regular and irregular wave states are considered. The results show that the adjustable draft system could not only increase the absorbed power but also the generator efficiency. At particular wave states, the delivered electrical power of the adjustable-draft WEC is over 20 % and 10 % higher than that of the conventional fixed-draft WEC for regular and irregular wave conditions respectively.

7.1. INTRODUCTION

ALTHOUGH the conceptual design of the adjustable draft system has been proven to be of much potential in the last chapter, it was only investigated with assuming a simplified damper-like PTO model. Thus, the effects of the draft adjustment on the PTO efficiency and overall performance of the adjustable draft WEC still remain unclear. To comprehensively evaluate the performance of WECs, a wave-to-wire model can be used as the numerical tool. It could cover all the system responses in the whole energy conversion stages, including the wave-buoy hydrodynamics, energy transmission and electricity generation. Recently, a variety of wave-to-wire models have been developed. Regarding the power absorption stage, the wave-buoy hydrodynamics can be calculated by the linear potential modeling, weakly nonlinear modeling or fully nonlinear modeling. From the perspective of the energy transmission, wave-to-wire models differ by using the pneumatic, hydraulic or mechanical PTO modeling. For the electricity generation stage, wave-to-wire models could be mainly divided by applying the rotary or linear electric generator model. For instance, a high-fidelity wave-to-wire model was proposed and validated in [161]–[163]. The nonlinear Froude-krylov force and viscous force were incorporated in the hydrodynamic model, and a hydraulic PTO model coupled with a rotary electric generator model were used to mimic the power transmission and generation stages. By means of the proposed model, the influence of the configuration of the hydraulic PTO system was investigated. In [164], a wave-to-wire model was presented for studying an array of point absorbers. It was established by a integration of a hydrodynamic model including the nonlinear hydrostatic force, a hydraulic PTO model, an induction rotary generator model and an electric network model. The interaction between electric network and the dynamic responses of the array was studied, and the importance of the wave-to-wire model in the whole system design was identified. A fully-coupled model was applied in [165] to demonstrate the power improvement of the point absorbers with a linear generator by using a field weakening control strategy in the PTO system. A linear hydrodynamic model and an electric model of linear generators are included in the wave-to-wire model, and the power production of the WECs at various wave states were revealed.

The objective of this chapter is to establish a wave-to-wire model for the adjustable draft WEC and to thoroughly evaluate its power performance. The chapter starts with the description of the integration of the adjustable draft WEC with the linear PM generator. Next, the formulation of the wave-to-wire model is presented. The algebraic nonlinear TD model, introduced in the Chapter 6, is applied to simulate the dynamic behavior of the WEC. The responses of the linear generator are calculated by the analytical model which was presented in Chapter 5. To match the wave resource of Yeu island, the diameter of the spherical buoy is increased to 3.5 m and the parameters of the linear generator are re-specified. The potential negative effects resulting from the draft adjustment on the power performance are studied, including the non-symmetry of the stroke and partial overlap between the stator and translator. The delivered electrical power and PTO conversion efficiency of the WEC are identified in both regular and irregular wave conditions. A performance comparison between the adjustable absorber and the semi-submerged fixed draft point absorber is made. Furthermore, a improved design of the adjustable draft WECs is demonstrated with an aim to reduce the negative effects associated with the draft adjustment.

7.2. SYSTEM SPECIFICATION

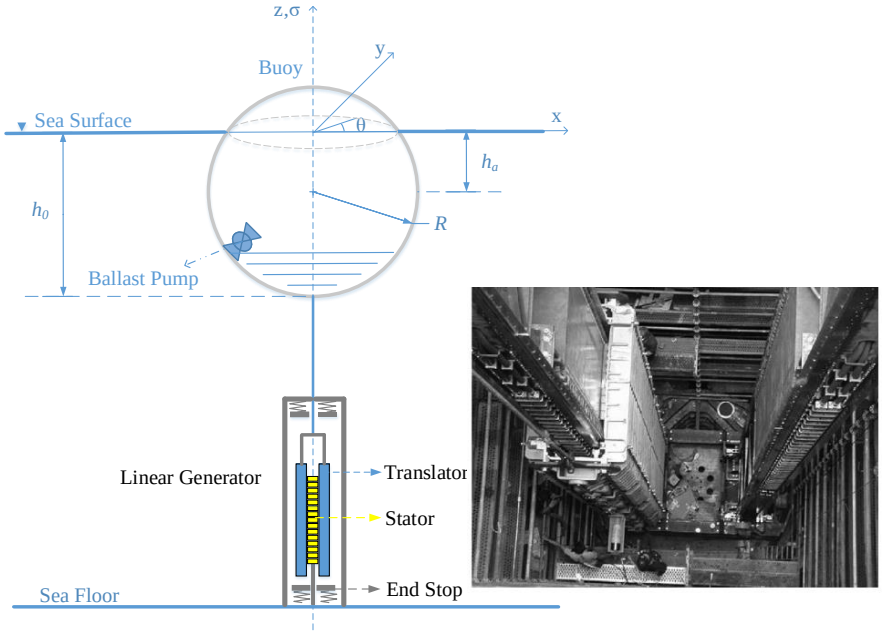


Figure 7.1: Schematic of the integration of the adjustable draft point absorber with a bottom founded linear generator.

In the last chapter, the PTO system in the adjustable draft WEC is simplified as a linear generic PTO model to mimic the behavior. In this chapter, it is further specified as a linear PM generator, and the schematic of the integration is shown in Figure 7.1. The buoy is directly connected to the translator of the generator without through any auxiliary equipment, thus the influence of the non-symmetric PTO stroke is taken into account.

7.2.1. THE SPECIFICATION OF THE BUOY SIZE AND POSITIONING

The spherical buoy is resized in this chapter to match the most frequent wave state of the sea site Yeu island. The wave state is with the crossing-zero period T_z of 5.5 s and significant wave height H_s of 1 m, as shown in Figure 3.2. The relevance of the performance of the adjustable draft WEC to the buoy size has been illustrated in Figure 6.12. For the originally sized buoy with a diameter of 5 m, the maximum ratio between the power absorbed by the adjustable draft WEC and the fixed draft WEC is located at 4.5 s. In order to increase the wave period where the maximum ratio is obtained, the buoy size needs to be scaled up and the scale factor λ can be approximated as 1.4 to make it occur at 5.5 s, based on Figure 6.12. Same with the last chapter, it is assumed that the buoy without ballast water would be naturally semi-submerged in still water.

The linear generator is bottom founded serving as the PTO system, and the translator is directly connected to the buoy. As the allowable stroke is unchangeable for a certain

generator, increasing the buoy draft reduces the lower half of the stroke. For a compromise, the translator is therefore placed at the position where the horizontal center lines of the translator and stator are aligned when the buoy draft is 4.25 m. The effects of the draft adjustment on the motion of the buoy and overlap between stator and translator will be demonstrated in more detail in the following text.

7.2.2. SPECIFICATION OF THE ELECTRIC GENERATOR

In the present chapter, the generator is rated to supply the sufficient force for maximizing the power absorption in the most frequent wave state of the sea site Yeu island. The buoy is considered to be semi-submerged during this generator rating process. Figure 7.2 shows the relationship among absorbed power, RMS value of the PTO force and PTO damping coefficient at that wave state. It can be observed that a value of the RMS PTO force of 40 kN is required to achieve the maximum absorbed power.

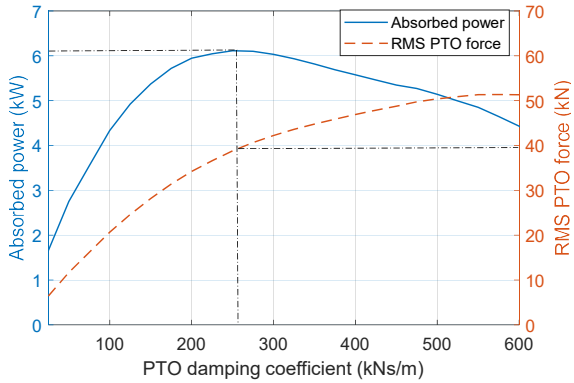


Figure 7.2: Absorbed power and RMS PTO force as a function of PTO damping coefficient, with $H_s = 1$ m and $T_z = 5.5$ s.

In irregular wave states, the dynamic response of the system is stochastic, and therefore the probability of exceeding the force limit should be reduced to a certain level. For example, the PTO force saturation is associated with large currents, and highly frequent PTO force saturation might lead to overheating conditions. Thus, defining a tolerance on the exceedance is important to the generator design. In this paper, the tolerance on the exceedance of the deigned generator force is considered as 10 %. If the dynamic process of the WEC is assumed to be Gaussian with zero mean, the amplitude of the variables can be characterized by Rayleigh distribution [104]. Hence, the probability of exceeding the PTO force limit can be calculated by

$$Q(s) = \exp\left(\frac{-F_{max}^2}{2\sigma_F^2}\right) \tag{7.1}$$

where σ_F represents the standard deviation of PTO force which is equal to its RMS value in this case, and F_{max} is the designed maximum generator force. Given the σ_F of 40 kN, the designed maximum generator force is calculated by (7.1) as 85 kN.

The size of the linear generator is determined based on the force density of the machine (the force acting per unit surface area of the air gap). The designed maximum generator force is calculated as

$$F_{max} = 2\rho_{force} L_{sta} l_s \tag{7.2}$$

where ρ_{force} is the force density of the generator, L_{sta} and l_s are the stator length and stack length, and a factor of 2 is included since the machine is double sided. The generator adopted in this paper is scaled based on the design of the linear generator of the AWS [43]. The scale factor of the generator λ_e has been introduced in (5.10). For simplification, the stator, translator and stack length are scaled together in this work while they are in practice independent sizing parameters. As stated in [112], the force density is rather constant for differently sized generators. Therefore, the designed maximum generator force is thought proportional to the surface area of the machine. Then, according to (5.11), the maximum force of the scaled machine is related to the reference machine by

$$F_{max_c} = \lambda_e^2 F_{max_o} \tag{7.3}$$

As in [61], the maximum force of the reference generator is 933 kN for two installed machines, and the translator, stator and stack length are reported as 8 m, 5 m and 1 m. As the WEC in this paper only adopts a single machine, then the scale factor λ_e is calculated as around 0.43. Therefore, the values of the translator, stator and stack length of the scaled machine can be obtained by (5.10). In addition, the rated phase current and voltage of the

Table 7.1: Specification of the sized generator.

Parameters	Symbol	Quantities
Rated power	P_{rated}	187 kW
Maximum force	F_{max}	85 kN
Maximum velocity	u_{max}	2.2 m/s
Stroke	S	5.6 m
Translator length	L_{tra}	3.5 m
Stator length	L_{sta}	2.2 m
Stack length	l_s	0.45 m
Air gap length	g_l	5 mm
Slot width	b_s	15 m
Magnet pole width	b_p	79 mm
Tooth width	b_t	18.3 mm
Pole pitch	τ_p	100 mm
Slot pitch	τ_s	33.3 mm
Stator yoke height	h_{sy}	50 mm
Slot height	h_s	85 mm
Magnet thickness	l_m	15 mm
Recoil permeability of the magnets	μ_{rm}	1.1
Remanent flux density of the magnets	B_{rm}	1.1 T at 85 °C
Iron loss per unit mass	P_{Fe0}	4.9 W/kg at 50 Hz and 1.5 T
Copper resistivity	ρ_{Cu}	0.0252 $\mu\Omega$m at 120 °C
Copper fill factor	k_{sfil}	0.6
Number of conductors per slot	N_s	6

converter of the scaled machine can be calculated based on scaling law of generator sizing, which has been presented in Method 1 of subsection 5.3.1. For the original reference generator, the rated phase current I_{conm_o} and voltage are U_{conm_o} are 400 A and 1500 V [61]. Other parameters of the scaled generator remain unchanged with respect to the reference machine, and the specification of the generator used in this paper is shown in Table 7.1.

7.3. WAVE-TO-WIRE MODELING

The wave-to-wire model established in this chapter comprises two main components: the nonlinear hydrodynamic modeling and the analytical generator modeling. The diagram of the model is shown in Figure 7.3. Regarding the hydrodynamic modeling, the nonlinear algebraic Froude-Krylov model is adopted, and the formulations have been detailed in Chapter 6. The analytical generator model presented in Chapter 5 is used here to mimic the electrical responses. The position and velocity of the buoy are taken as inputs to the generator, and the generator makes the corresponding PTO force to interact with the dynamics of the buoy.

7.4. RESULTS

This section starts with studying the effect of the draft adjustment on the hydrodynamic feature of the buoy. Then, the wave-to-wire responses of the WEC are presented. Next, the negative effects of the draft adjustment on the buoy motion and partial overlap between

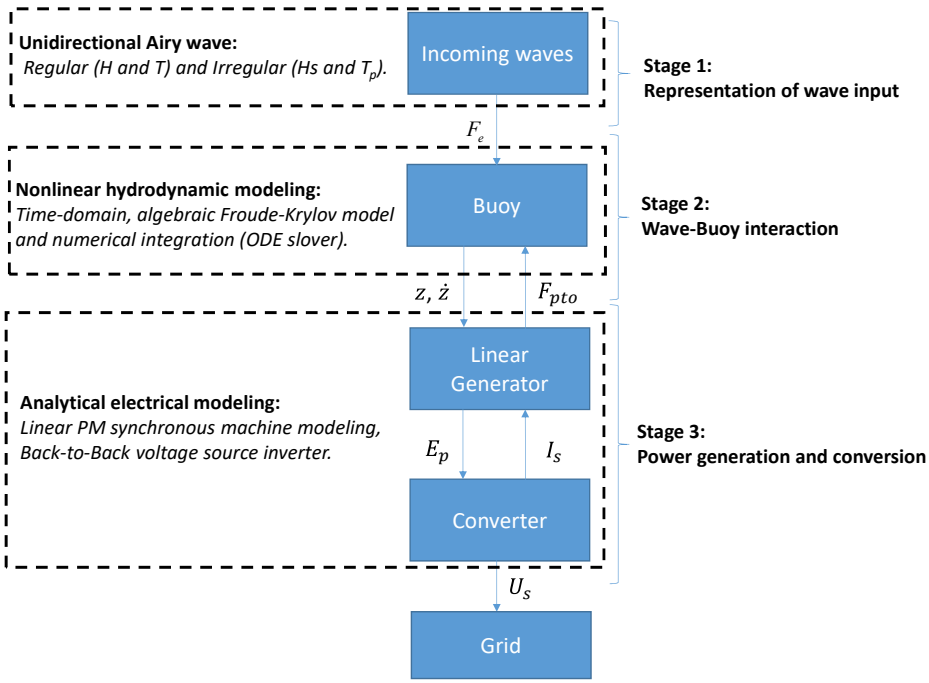
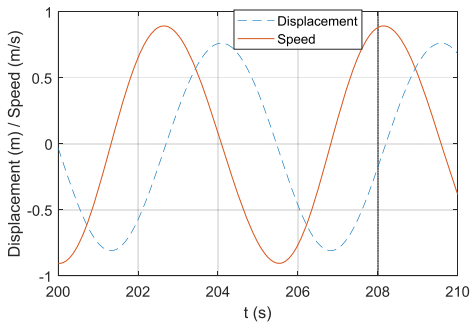
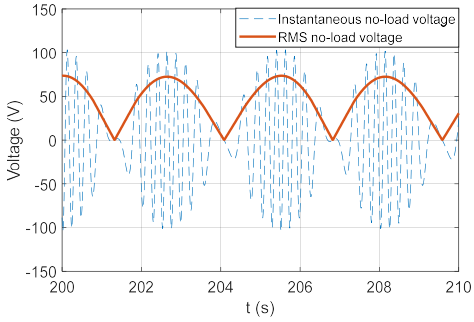


Figure 7.3: Diagram of the established wave-to-wire model.

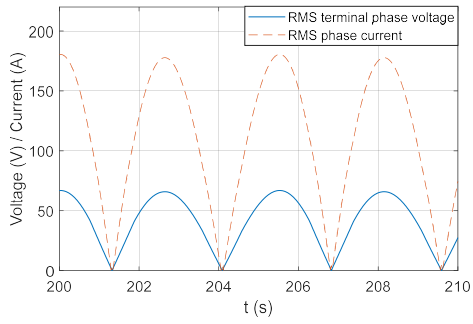
the stator and translator of the linear generator are demonstrated. Finally, the performance of the adjustable draft WEC in both regular and irregular waves is identified and compared with the conventional fixed draft WEC. The delivered electrical power, PTO conversion efficiency and the optimal buoy draft in relation with the wave state are covered in the comparison.



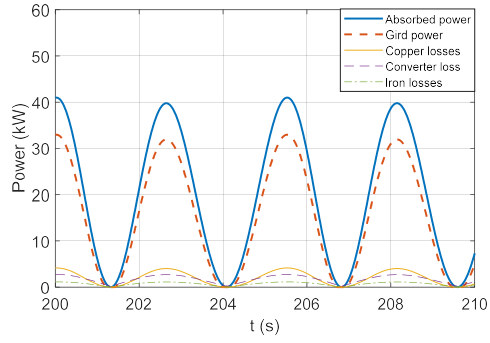
(a) Displacement and speed



(b) Instantaneous and RMS No-load voltage



(c) RMS phase current and terminal phase voltage

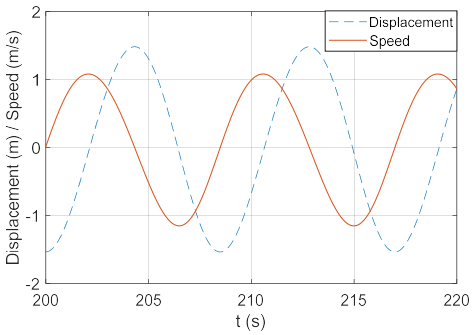


(d) Power and losses

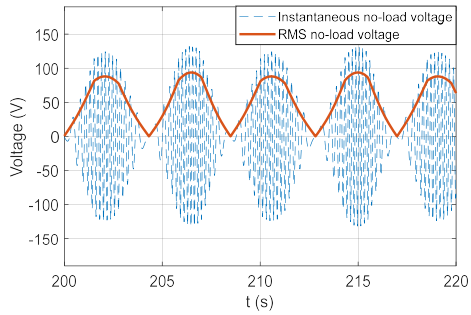
Figure 7.4: Wave-to-wire response of the WEC in a mild wave state (H = 1.5 m, T = 5.5 s), and R_{pto} = 50 kNs/m.

7.4.1. WAVE-TO-WIRE RESPONSE OF THE WEC

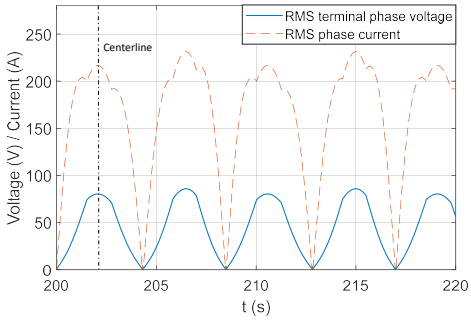
The systematic responses of the WEC calculated by the established wave-to-wire model is presented in Figure 7.4 and 7.5, in which the buoy draft is selected to be 4.0 m as an example. A mild and powerful wave states are considered respectively. The profiles of the RMS no-load voltage in Figure 7.4b and 7.5b are not sinusoidal because of the partial overlap between the stator and translator of the generator. As a consequence, the resulting phase current and terminal voltage in Figure 7.4c and 7.5c are not varying sinusoidally either. The effect is more obvious in the powerful wave state, where the amplitude of the displacement is larger. In addition, in Figure 7.5c, it is seen the profiles of the voltage and current is not symmetrical with respect to the dashed center line for a half oscillation period. The reason is that the geometry center of the translator in still water is not located in parallel with the vertical center line of the stator. This results in the difference of the partial overlap between



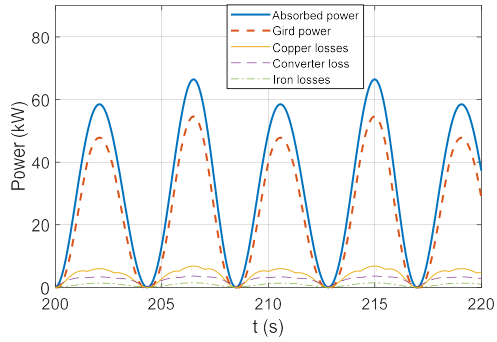
(a) Displacement and speed



(b) Instantaneous and RMS No-load voltage



(c) RMS phase current and terminal phase voltage



(d) Power and losses

Figure 7.5: Wave-to-wire response of the WEC in a powerful wave state (H = 3.0 m, T = 8.5 s), and R_{pto} = 50 kNs/m.

the buoy's moving upwards and downwards. This effect will be demonstrated in more detail in subsection 7.4.2. Furthermore, it can be found from Figure 7.4d and 7.5d that the copper losses account for a major proportion of losses during the power conversion in this case.

7.4.2. NEGATIVE EFFECTS OF THE DRAFT ADJUSTMENT

In the current concept, the buoy and translator are connected in a rigid way. Then, two effects need to be considered after the adjustable draft system is adopted. Firstly, the draft adjustment makes the stroke of the buoy non-symmetrical, and thus the end-stop force takes effect at one side earlier than at the other side. Secondly, the draft adjustment makes the duration of the partial overlap between the stator and translator non-symmetrical, which affects the profile of the induced voltage and current. Figure 7.6 illustrates how the relative position of the buoy and translator to the stator changes with the buoy draft. It can be seen that the displacement limits of the adjustable draft WEC, except for the buoy draft of 4.25 m, are not symmetrical with respect to the horizontal center line of the stroke. Thus, when the buoy draft is adjusted to be smaller than 4.25 m, the distance between the top of moving parts and the upper end of the stroke is less than that between the bottom of moving parts to the lower end of the stroke. The effect is vice-verse for cases with buoy drafts larger

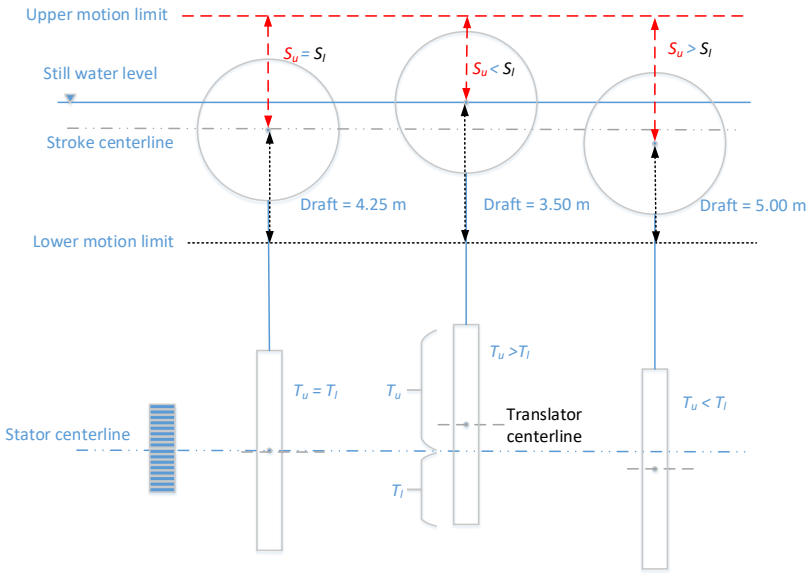


Figure 7.6: The schematic of the relative positions of the buoy, translator and stator in different buoy drafts. S_u and S_l represent the upper and lower part of the stroke relative to the buoy centroid. T_u and T_l represent the upper and lower part of the translator relative to the center line of the stator.

than 4.25 m. In addition to stroke, it is seen that if the buoy draft is smaller than 4.25 m, the overlap between the translator and stator is reduced when the buoy moves in upwards direction. The following two subsections are intended to demonstrate these two effects on the responses as well as the power performance of the WEC.

THE EFFECT ON THE STROKE

Figure 7.7 shows the ratio of the maximum displacement of the semi-submerged fixed draft WEC to that of the adjustable draft WEC with the buoy draft adjusted to 3.5 m. Figure 7.8 shows the ratio between the absorbed power of these two WECs. In the calculation, different motion limits are considered, ranging from $0.6R$ to $1.0R$. The fixed draft WEC is a good reference for comparison, since it is not subjected to the effect of non-symmetrical stroke. It can be seen that, for mild wave states or large motion limits, the influence is highly limited. However, it is noticeable for cases with short motion limits and large wave heights. The displacement ratio (in Figure 7.7) and power ratio (in Figure 7.8) even reaches 1.14 and 1.07 respectively when the motion limit is $0.6R$ and wave height is 4 m. The longer strokes could mitigate this effect, but the cost is also correspondingly higher. Thus, the motion limit is selected as $0.8R$ in the current design of the adjustable draft WEC as a compromise. However, it is acknowledged that the non-symmetry stroke effect on the response of the WEC could be more remarkable if the motion is amplified by real-time control strategies.

THE EFFECT ON THE PARTIAL OVERLAP

The buoy draft adjustment has an influence on the duration of the overlap between the stator and translator, as depicted in Figure 7.6. In Figure 7.9, the RMS no-load voltage and

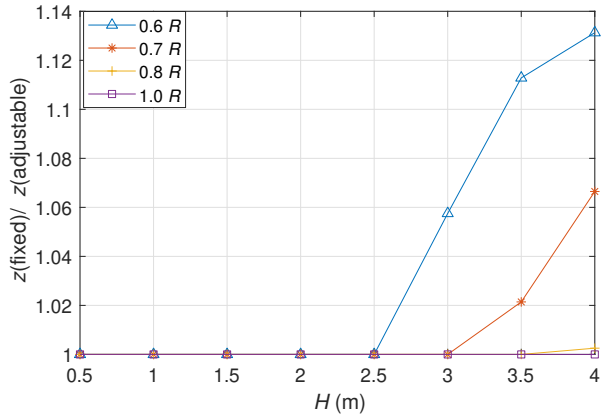


Figure 7.7: The maximum displacement of the fixed draft WEC with the draft of 3.5 m normalized to that of the adjustable draft WEC with the draft of 3.5 m at the undamped condition, and $T = 5.0$ s. The considered motion limits range from $0.6R$ to $1.0R$.

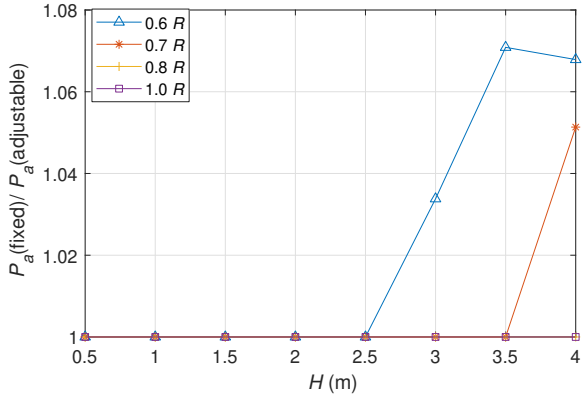
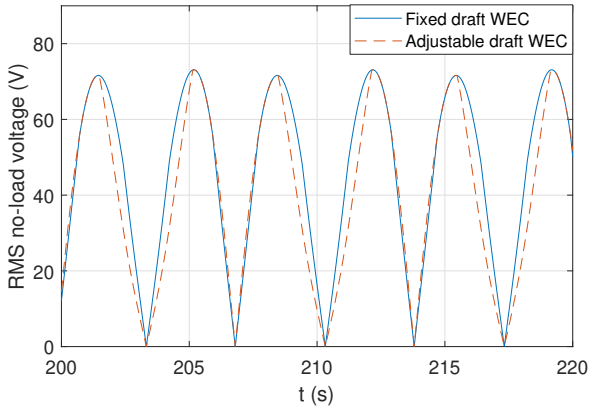


Figure 7.8: The average absorbed power of the fixed draft WEC with the draft of 3.5 m normalized to that of the adjustable draft WEC with the draft of 3.5 m, and $R_{pto} = 30$ kNs/m and $T = 7.0$ s. The considered motion limits range from $0.6R$ to $1.0R$.

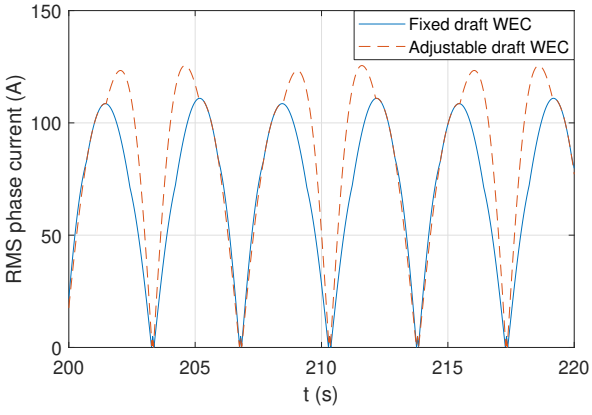
phase current profiles of the semi-submerged fixed draft WEC and adjustable draft WEC are compared, in which the buoy draft of the adjustable draft WEC is adjusted to 3.5 m in this case. It is visible in Figure 7.9a that the adjustable draft WEC has a lower RMS no-load voltage profile than the fixed draft WEC over a proportion of each oscillation. This is because the upper part of the translator T_u is larger than T_l in the case with the draft of 3.5 m as shown in Figure 7.6. The complete overlap of the adjustable draft WEC is therefore shorter when the buoy is moving in upwards direction, and then the resulting no-load voltage is lower than the fixed draft WEC. As a consequence, the phase current needs to be correspondingly increased for supplying the required generator force, as is shown in Figure 7.9b.

The effect of the non-symmetrical partial overlap on the power generation in different wave periods and heights is depicted in Figure 7.10. The electrical power of the fixed draft

WEC is normalized to that of the adjustable draft WEC. It can be seen that the effect generally tends to be stronger with the increase of the wave height. In addition, the normalized power ratio slightly decreases from the wave height of 3.5 m to 4 m for the wave period of 5 s. It can be explained by the fact that the partial overlap comes to play in both upwards and downwards buoy motion in large wave heights, and the adjustable draft WEC has a longer duration of the complete overlap in the downwards motion. Figure 7.11 suggests that enlarging the translator length could effectively mitigate the effect of the non-symmetrical overlap. For instance, increasing the translator length from 3.2 m to 4 m could reduce the normalized power ratio from 1.05 to 1.01 at the wave height of 1.5 m. However, longer translators imply more materials and thus the higher cost on the generator, and a compromise needs to be made for this issue. In the current design of the adjustable draft WEC, the translator length is determined as 3.5 m.



(a) RMS No-load voltage



(b) RMS phase current

Figure 7.9: The effect of the non-uniform partial overlap on the profile of generator responses, and $H = 2$ m, $T = 7$ s and $R_{pto} = 30$ kNs/m.

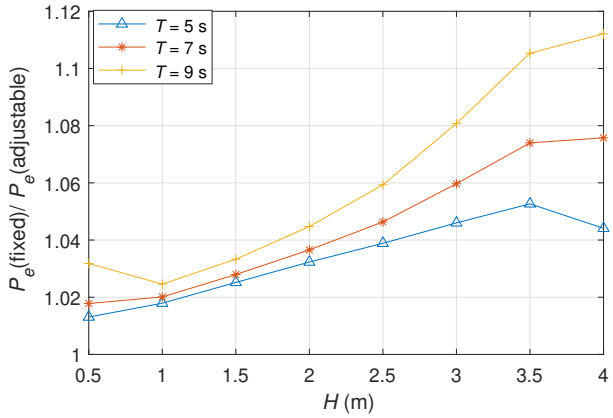


Figure 7.10: The average electrical power of the fixed draft WEC with the draft of 3.5 m normalized to that of the adjustable draft WEC with the draft of 3.5 m, and R_{pto} = 30 kNs/m.

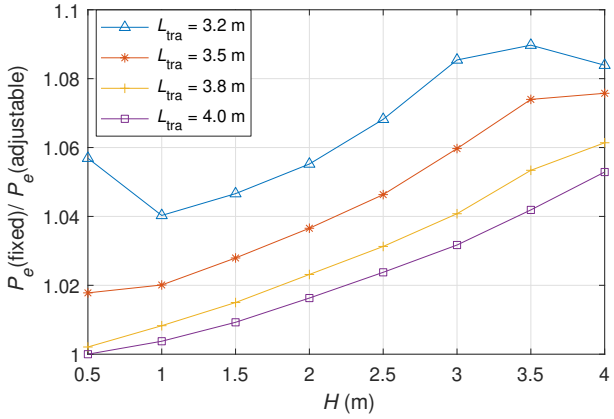


Figure 7.11: The average electrical power of the fixed draft WEC with the draft of 3.5 m normalized to that of the adjustable draft WEC with the draft of 3.5 m in wave states of T = 7.0 s, and R_{pto} = 30 kNs/m. Different values of the translator length L_{tra} are considered.

7.4.3. PERFORMANCE IDENTIFICATION

The power performance of the adjustable draft WEC is demonstrated in this part. It is assumed that the buoy draft can always be suitably and effectively adjusted to each wave state for maximizing the delivered power. The power performance of the WEC with the fixed buoy draft of 3.5 m, namely the semi-submerged WEC, is also presented for comparison.

PTO DAMPING OPTIMIZATION

The PTO damping is important to the power extraction. However, the optimal PTO damping for the absorbed mechanical power is not necessarily associated with the maximum electrical power since the influence of the PTO damping on the generator efficiency also plays a role [166]. In Figure 7.12, the relationship between the PTO damping, absorbed power, electrical power and generator efficiency is depicted. The maximum generator efficiency is 70

% and it occurs at the PTO damping of around 25 kNm/s. However, the maximum absorbed power is obtained at the PTO damping of 150 kNm/s which is associated with the generator efficiency of approximately 45 %. So, there is an obvious mismatch, and the maximization of the absorbed power doesn't necessarily result in the maximum delivered electrical power. As a collective consequence of the generator efficiency and absorbed power, the optimal PTO damping corresponding to the maximum electrical power is 100 kNm/s. In this case, the deviation of the PTO damping optimal to the absorbed power from that optimal to the electrical power reaches 50 %.

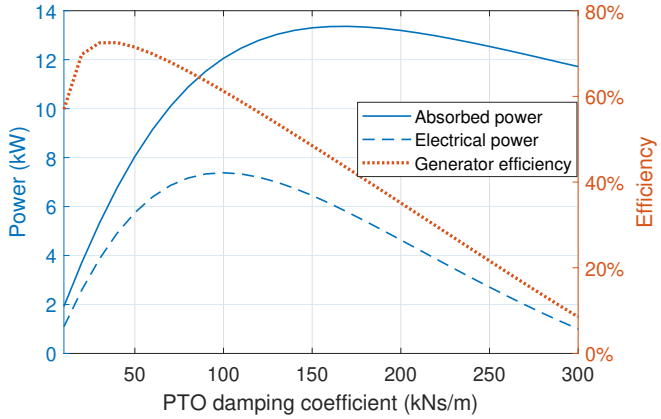


Figure 7.12: The absorbed power, electrical power and generator efficiency of the WEC with the buoy draft of 3.5 m as a function of the PTO damping coefficient, and $H = 1$ m and $T = 5.5$ s.

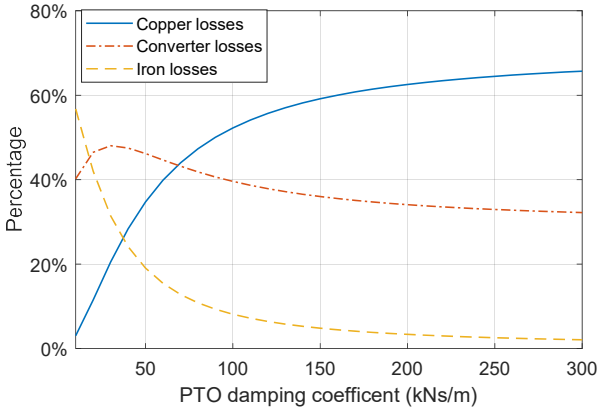


Figure 7.13: The percentage of different types of losses to the total losses of the WEC with the buoy draft of 3.5 m as a function of the PTO damping coefficient, and $H = 1$ m and $T = 5.5$ s.

Figure 7.13 shows the influence of the PTO damping on the proportion of losses. It could explain the tendency of the generator efficiency with the PTO damping shown in Figure 7.12. At very small PTO damping coefficients, the iron losses make up a major part of the

total losses. This is because the movement speed of the translator is high, which results in high generator frequencies. The iron losses are directly related to the generator frequency. With the increase of the PTO damping coefficient, the required PTO force increases, but the movement speed decreases. Thus, the no-load voltage decreases, and the current has to be improved to a higher level to supply the required generator force. In this way, copper losses tend to be more relevant. This explains why the generator efficiency tends to first increase and then decrease with the PTO damping coefficient.

It can be noticed that the generator efficiency is strongly related to the PTO parameters. Optimizing the PTO damping for the absorbed power is clearly insufficient for the maximization of the final delivered power output, namely the delivered electrical power. Hereafter, the power performance of the adjustable draft WEC is identified based on the optimized PTO damping for the delivered electrical power.

IN REGULAR WAVES

The delivered electrical power of the adjustable draft WEC is calculated for regular wave conditions, as shown in Figure 7.14. For comparison, the power performance of the semi-submerged fixed draft WEC is also presented in the figure. It can be seen that the adjustable draft WEC is associated with a higher power output over a range of wave periods. This mainly results from the increased buoy velocity, which is depicted in Figure 7.15. The gain of the power resulting from the adjustable draft system is mainly observed from the wave period of 4 s to 6 s. For instance, the highest power for the adjustable draft WEC is around 47 kW at the period of 4.5 s while it is only around 38 kW for the fixed draft WEC. The improvement is as high as 24 %. When the wave period is below 4 s or above 6 s, the adjustable draft WEC and fixed draft WEC tend to deliver a similar amount of electrical power.

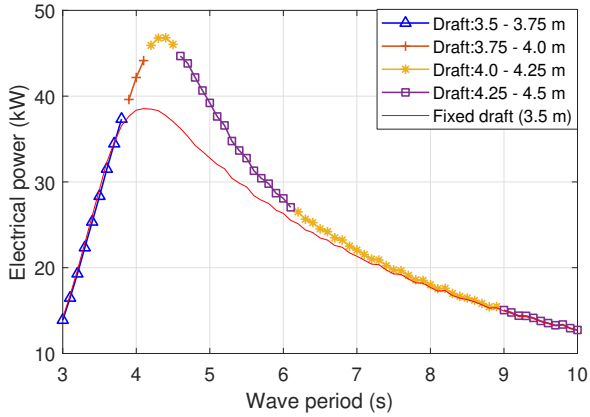


Figure 7.14: Comparison between the delivered electrical power of the adjustable draft WEC and of the fixed draft WEC, with $H = 2$ m and $\sigma_F = 40$ kN.

The electrical losses and the overall generator efficiencies in are calculated for the adjustable draft WEC and the fixed draft WEC respectively, as shown in Figure 7.16. It is reflected that the copper losses and converter losses make up the major losses in the power conversion stage of this generator. The maximum values of the copper losses, converter losses and iron losses are approximately 5 kW, 3 kW and 1 kW respectively. When the wave

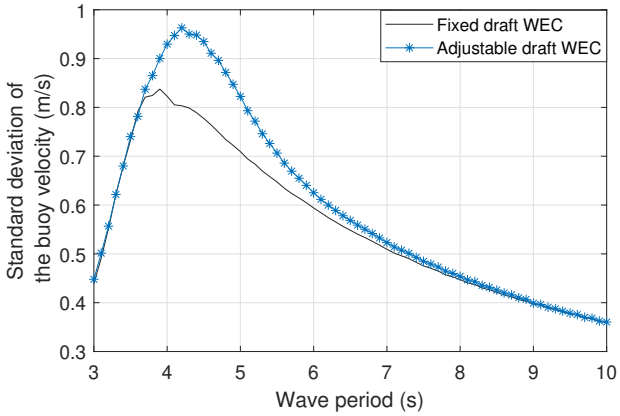
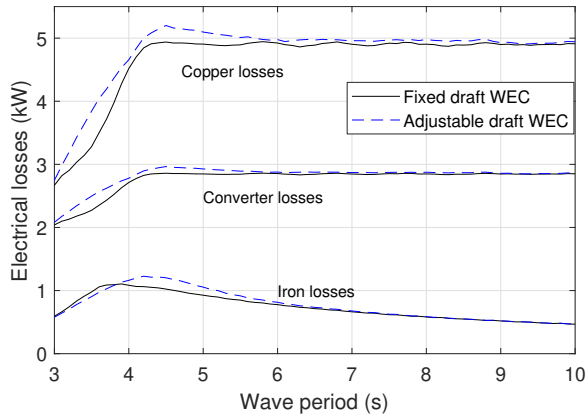


Figure 7.15: Standard deviation of the buoy velocity of the adjustable draft WEC and of the fixed draft WEC, with $H = 2$ m and $\sigma_F = 40$ kN.

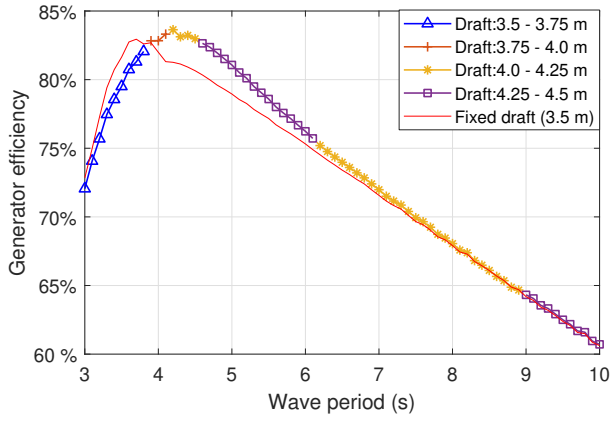
periods are below 4 s, the adjustable draft WEC presents larger copper and converter losses and the fixed draft WEC has a slightly higher generator efficiency than the adjustable draft WEC. This mainly results from the negative effects of the draft adjustment on the symmetry of the stroke and the partial overlap between the stator and translator, which causes a larger current in the generator and further larger copper and converter losses. At the wave periods from 4 s to 6.5 s, the increased generator efficiencies of the adjustable draft WEC result from the larger buoy velocity. During these wave periods, the iron losses of the adjustable draft WEC overtakes those of the fixed draft WEC due to the higher buoy velocity, and the adjustable draft WEC is associated with relatively higher copper and converter losses than the fixed draft WEC. But, given the significantly larger power absorption, the adjustable draft WEC shows a higher generator efficiency than the fixed draft WEC. For instance, at the wave period of 4.5 s, the generator efficiency of the adjustable draft WEC is 83 % while it is 80 % for the fixed draft WEC. When the wave period is beyond 7 s, there is not any noticeable difference observed between the generator efficiencies of the adjustable draft WEC and fixed draft WEC.

IN IRREGULAR WAVES

Figure 7.18 shows the standard deviation of the buoy velocity in irregular wave states, and the adjustable draft WEC contributes to a higher velocity within the peak periods between 4.5 s and 6.5 s. For instance, at the peak period of 5 s, the standard deviation of the buoy velocity is 0.69 m/s and 0.74 m/s for the fixed draft WEC and the adjustable draft WEC respectively. The electrical power delivered by the adjustable draft WEC and the fixed draft WEC in irregular wave states is presented in Figure 7.17. It can be seen that the power improvement resulting from the adjustable draft system in irregular waves is less noticeable than that in regular waves. The highest values of the electrical power for the fixed draft WEC and adjustable draft WEC are approximately 22 kW and 24.5 kW, and the improvement is around 10 %. When the peak period is above 6.0 s, the difference between the electrical power output of the adjustable draft WEC and the fixed draft WEC is negligible. This is because increasing the buoy draft reduces the absorption bandwidth of the buoy, and the narrower bandwidth reflects the incapability in responding to broad wave frequencies other



(a) Electrical losses



(b) Generator efficiency

Figure 7.16: Comparison between the generator performance of the adjustable draft WEC and of the fixed draft WEC, with $H = 2$ m and $\sigma_F = 40$ kN.

than the natural frequency. Therefore, the power absorption of the buoy with larger buoy drafts in irregular waves is weakened with regard to that in regular wave states.

Figure 7.19 shows the generator efficiencies of the adjustable draft WEC and fixed draft WEC in irregular wave states. the adjustable draft WEC presents comparable generator efficiencies with the fixed draft WEC when the peak period is higher than 4.5 s. At the peak period below 4.5 s, the fixed draft WEC is clearly associated with a higher generator efficiency. For instance, at the peak period of 3.5 s, the generator efficiency is 74 % for the fixed draft WEC, while it is only 70 % for the adjustable draft WEC. This can be attributed to the negative effects of the draft adjustment on the symmetry of the stroke and the overlap between the translator and stator.

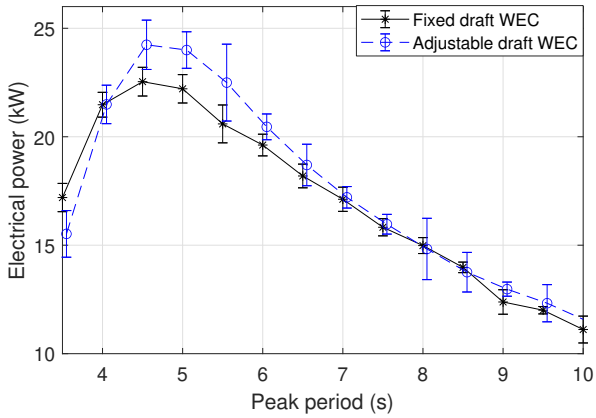


Figure 7.17: Comparison between the delivered electrical power of the adjustable draft WEC and of the fixed draft WEC, with H_s = 2.5 m and σ_F = 40 kN. The shaded area represents the standard deviation.

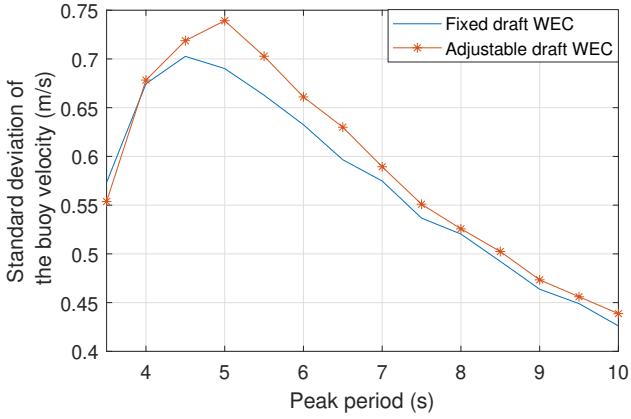


Figure 7.18: Standard deviation of the buoy velocity of the adjustable draft WEC and of the fixed draft WEC, with H_s = 2.5 m and σ_F = 40 kN.

7.5. SUMMARY AND CONCLUSIONS

In this chapter, a wave-to-wire model is established to investigate the systematic performance of the adjustable draft WEC. The established model integrates the nonlinear hydrodynamic model presented in Chapter 6 with the analytical generator model presented in Chapter 5. Based on the model, the negative effects of the draft adjustment on the stroke and partial overlap between the stator and translator of the generator are analyzed. The performance of the proposed WEC is studied for both regular and irregular wave conditions. The following conclusions are drawn.

- The draft adjustment leads to the non-symmetry of the stroke and partial overlap of the generator, which could reduce the power absorption and conversion efficiency of the system. These negative effects could be mitigated by increasing the stroke and translator length, but the cost will also be higher. The wave-to-wire modeling reveals

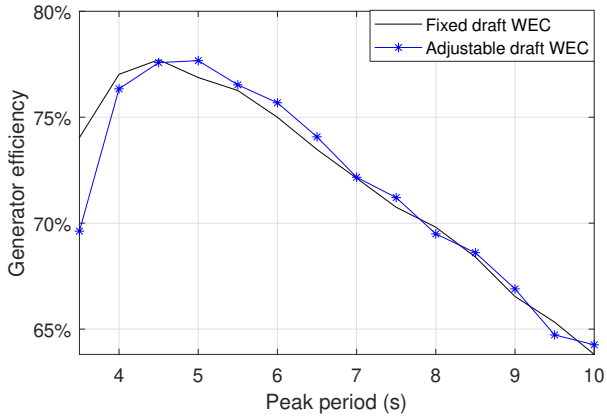


Figure 7.19: Comparison between the generator efficiency of the adjustable draft WEC and of the fixed draft WEC, with $H_s = 2.5$ m and $\sigma_F = 40$ kN.

the fact that the maximization of the absorbed power and the electrical power result in significantly different selections of the PTO damping coefficients. The large PTO damping coefficient optimal for maximizing the absorbed power is associated with the high copper losses. It suggests the importance to consider the effect on the PTO efficiency during the tuning of the PTO parameters.

- Compared with the conventional fixed draft WEC, the adjustable draft WEC is beneficial for the electrical power production over a range of the wave periods in regular wave states in spite of the negative effects of the draft adjustment. The maximal improvement is around 24 %. The optimal buoy draft of the adjustable draft WEC differs with the wave period, and it tends to first increase and then to be relatively constant with the wave period. The generator efficiency of the adjustable draft WEC is higher than the fixed draft WEC for some particular wave periods since adjustable draft WEC could contribute to the increased buoy velocity. At very low wave periods, the generator efficiency of the adjustable draft WEC is lower because of the negative effects resulting from the draft adjustment. In irregular wave states, the power improvement by applying the adjustable draft system is reduced because the semi-submerged fixed draft WEC has wider absorption bandwidth than the buoy with larger drafts. Nevertheless, a 10 % gain of the electrical power can be achieved by using the adjustable draft system in particular wave states.

Together with the previous chapter, the performance of the adjustable draft point absorber was systematically investigated. The findings indicate the potential of this system in improving the power production with the downsized PTO capacities.

8

Conclusions and Recommendations

This chapter presents the conclusions and recommendations based on the results achieved in the previous chapters.

8.1. CONCLUSIONS

In this thesis, the potential of systematic sizing in improving the techno-economic performance of heaving WECs is studied. The structure of the work is arranged in correspondence with the two research objectives. First, a sizing method covering both buoy sizing and PTO system sizing is established. To consolidate the sizing method, a SD model is derived and verified to incorporate the nonlinear effects related to PTO sizing. In addition, the effects of PTO sizing on the generator efficiency are identified. Secondly, a novel system, namely the adjustable draft system, is proposed for point absorbers to improve the power performance of WECs with downsized PTO capacities. The benefits resulting from the proposed system are analyzed by a numerical study.

8.1.1. TO THE FIRST RESEARCH OBJECTIVE

The first main research objective was defined in Chapter 1 as

Objective 1: Establish a systematic sizing method for WECs.

To achieve this main objective, Chapter 3 to Chapter 5 were accomplished for three sub-objectives. First, a sizing method collectively incorporating both effects of buoy and PTO sizing was proposed based on the FD approach. A case study was performed based on the proposed method, which suggested that PTO sizing has a positive effect on the reduction of the LCOE. In particular cases, the reduction reached 30 % compared to the WECs with PTO system sized to work at full capacity in all operating conditions. Regarding the heaving type of WEC and economic modeling considered in this thesis, the optimal PTO force limit converges at around 0.4 to 0.5 times the maximum PTO force to operate at full capacity for all operational sea states in different sea sites. In addition, compared with the sizing methods based on the Budal diagram and Froude scaling, the proposed collective sizing method could contribute to a better reflection of the techno-economic potential of WECs. This is mainly because PTO sizing is included in the collective sizing method.

Secondly, a SD model was established based on stochastic linearization to cover the nonlinear effect of the PTO force limit, also known as the PTO force saturation. The SD model is highly suitable for the scenarios associated with PTO sizing, because it combines both adequate accuracy and computational-efficiency. Specifically, with regard to the FD modeling, the maximum relative errors in the prediction of the AEP can be reduced from 24.4 % to 4.3 % by applying SD modeling. Furthermore, the computational time of SD modeling is in the same order of magnitude with FD modeling and around a thousand times less than that of TD modeling.

Thirdly, the influence of PTO sizing on the power conversion efficiency of the WEC was analyzed with a focus on the linear PM generator. The generator efficiency is highly related to the size of the generator, and the overall efficiency tends to increase with the generators' size. The assumption of a constant generator efficiency which is normally used in sizing studies leads to a poor estimate of the AEP and LCOE, as well as further determination of the PTO size. Specifically, the resulting relative errors on the AEP estimation and the optimal PTO size reach 10 % and 29 %, compared to the sizing method of incorporating detailed generator efficiency. Therefore, it is highly recommended to take the generator performance into account when conducting PTO sizing. Moreover, during sizing, the geometric optimization of the linear generator is notably related to the wave resource. As could

be expected, the wave resource has a clear influence on the LCOE and overall efficiencies of the linear generator.

8.1.2. TO THE SECOND RESEARCH OBJECTIVE

The second main research objective was defined in Chapter 1 as

Objective 2: Explore the possibility to improve the power performance of WECs with downsized PTO sizes.

Chapter 6 and 7 are dedicated to achieving this objective. An adjustable draft system was proposed for spherical point absorbers with an aim to improve the power performance when the PTO capacities are constrained. The draft adjustment enables the variation of the relevant natural frequency of the WEC, which could lead to a higher motion and buoy speed over a range of wave frequencies. Consequently, with the constrained PTO force, a higher power absorption can be gained. The performance of the adjustable draft WEC was investigated by both linear and nonlinear modeling, and both regular and irregular wave conditions were considered. Compared with the results of the nonlinear Froude-Krylov model, the linear model overestimates the performance of the WEC around the resonance regions, and the discrepancies increase with the increase of buoy draft. Based on the results from the nonlinear TD modeling, the adjustable draft system could improve the power absorption for the studied cases by approximately 27 % and 12 % for regular and irregular waves respectively. In addition, a wave-to-wire model was established to analyze the performance of the studied WECs. Wave-to-Wire modeling is a numerical tool applied in the context of WECs. It can be used to reveal the responses of all energy conversion stages, covering the wave-buoy hydrodynamics, energy transmission and electricity generation. Based on the established wave-to-wire model, it showed that the adjustable draft system leads to improvement of the generator efficiency, resulting from the increased buoy speed.

8.2. RECOMMENDATIONS

In this thesis, the relevance of systematic sizing to the techno-economic performance of WECs has been identified. To further consolidate this research, several topics are to be investigated. Corresponding to the outline of this thesis, the recommendations for future work are divided into two parts in the following text. This first part addresses the topics related to the systematic sizing method, and the second part discusses the topics related to the adjustable draft system.

8.2.1. TO THE SYSTEMATIC SIZING METHOD

A systematic sizing method based on numerical simulation was proposed in this thesis. In the method, both buoy sizing and PTO sizing are considered, and a SD model was established to improve the accuracy of PTO sizing. In addition, the influence of PTO sizing on the energy conversion efficiency was identified, and it indicated the importance of considering the generator performance during sizing. To further consolidate this research, the following topics are recommended to be investigated.

- **Expand the coverage of sizing studies on more types of WECs and wave resources**
  This thesis mainly focuses on one particular type of WECs, namely the heaving point

absorber, and only three different sea sites with deep water conditions are considered. However, one challenge that the wave energy communities are facing the lack of technology convergence for different types of WECs. Because of the variation of wave climates and water depths, the suitability of WECs could also change. As the proposed method is generally applicable, an extended database of the LCOE prediction of more different WECs in various sea sites is expected to accelerate the convergence of WECs.

- **Extend the sizing method of a single WEC to cover WEC arrays**
  This thesis focuses on the sizing of a single WEC, but WEC arrays would be more realistic in large-scale commercialization. Two more aspects need to be considered for sizing the devices in a WEC array. First, hydrodynamic interactions between multiple WECs are an important factor, which are related to the size of each WEC. The hydrodynamic interaction can be reliably incorporated in SD modeling, as stated in [138]. However, the further verification needs to be done when the SD model with the PTO force saturation is extended to WEC arrays. Secondly, economic modeling of a single WEC might be different from that of WEC arrays, which is normally reflected in the estimation of OPEX. For a WEC array, several maintenance and operation strategies could be applied to achieve a better balance between total maintenance expense (or frequency) and overall operation availability [167].

- **Extend the SD model to cover more nonlinearities**
  This thesis shows that the SD model of the PTO force saturation is promising in the application of sizing WECs. This modeling technique has been developed by previous studies to incorporate a set of nonlinear force components, but some relevant effects are still pending to be covered. For instance, the nonlinear hydrostatic force has been derived for SD modeling [127], but the wave elevation was assumed to be constant. Hence, a SD model of the nonlinear hydrostatic force considering the relative displacement is expected to improve the accuracy.

- **Study the relevance of sizing to the variation of PTO control strategies**
  In this thesis, real-time PTO control strategies were not implemented. Instead, the PTO control parameters were tuned to be constant for each sea state during sizing. It can be expected that applying real-time control strategies could increase the power production of WECs in irregular sea state, which might make a difference to the sizing of either the buoy or PTO system. However, the resulting complexity added to the WEC system should also be carefully taken into account. In addition, the SD model was derived based on the passive control strategy, in which the PTO force can be described as a single variate function of velocity. Thus, it is not applicable for reactive control strategy where the PTO force is a multivariate function of the buoy velocity and displacement. As reactive control strategies are also commonly utilized, it is valuable to extend the SD model in this direction in the future.

- **Study the relevance of sizing to different types of PTO systems**
  The thesis only investigated the influence of sizing on the performance of the linear generators, and the related conclusions are only limited to this type of electrical machine in the PTO system. As the principle and characteristics of other PTO systems differ significantly from the linear generators, the sensitivity of their performance to sizing is also worth further investigation.

8.2.2. TO THE ADJUSTABLE DRAFT SYSTEM

The conceptual design of the adjustable draft system was proposed, and its performance was studied through numerical modeling. Several directions can be considered to consolidate this novel design.

- **Experimental validation**
  The performance of the novel design was investigated only by the numerical approach. An experimental study could further validate the assumptions of the numerical modeling. In addition, as a novel concept, an experimental test could contribute to a better understanding of the behaviour of the system, such as the effect of sloshing inside the buoy and the full submergence of the buoy with large drafts. Given the fact that the concept is still in a initial phase, small-to-medium scale tests would be sufficient for the purposes to improve the understanding of the system and validate the relevant numerical models. However other challenges may arise such as the instrumentation and the proper scaling of the wave conditions and WEC device depending on the focus of the experiments.

- **Optimize the buoy geometry**
  In this thesis, the adjustable draft system was only considered to be integrated with a spherical point absorber. Thus, the conclusions are limited to the spherical floating buoy geometry. An important function of the adjustable draft system is to enable the variation of the mass, and the hydrodynamic characteristics by the draft adjustment. The relation of these properties to the buoy draft is highly dependent on the buoy geometry. To exploit the potential of the adjustable draft system, it is recommended to conduct optimization of the buoy geometry which is to be used in the integration with the adjustable draft system.

A

Appendix

A

A.1. CONVERGENCE VERIFICATION OF HYDRODYNAMIC CALCULATION

A mesh convergence study is performed to verify the hydrodynamic results calculated by Nemoh. As an example, Figure A.1 depicts the influence of the number of panels in the mesh on the prediction of the added mass coefficients of the heaving buoy with a buoy draft of 3.0 m. It is observed that the difference among mesh solutions with more than 646 panels is negligible. However, it is known that the computational time increases with the number of panels. To achieve a compromise between the accuracy and computational loads, the number of panels is maintained between 700 and 900 when calculating the hydrodynamic coefficients of the buoy with different buoy drafts.

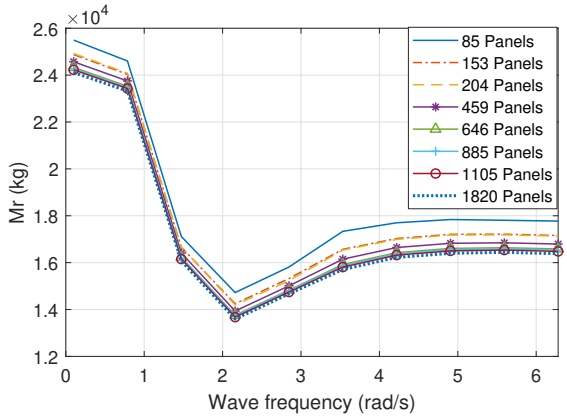
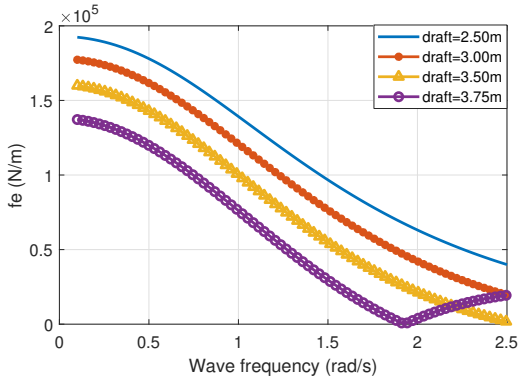
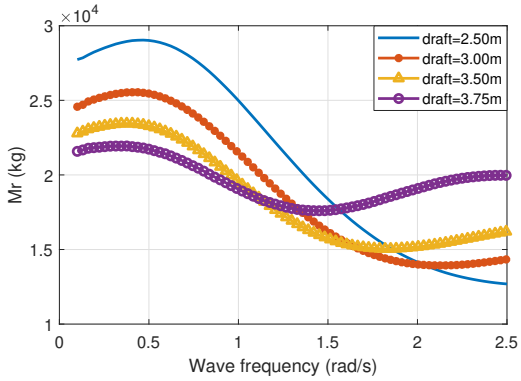


Figure A.1: Mesh convergence analysis of Nemoh with regard to the added mass coefficients of the considered heaving spherical buoy with a buoy draft of 3.0 m.

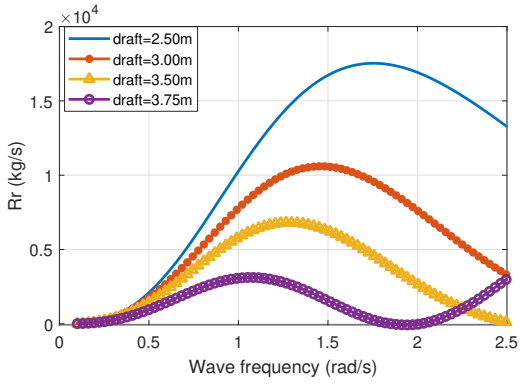
A.2. THE HYDRODYNAMIC COEFFICIENTS FOR DIFFERENT BUOY DRAFTS



(a) Excitation force coefficients



(b) Added mass



(c) Radiation damping

Figure A.2: Hydrodynamic coefficients of the heaving spherical buoy of a diameter of 5 m for different buoy drafts.

A

A.3. THE VERIFICATION OF THE SELECTED NUMBER OF STARTING POINTS IN THE MULTISTART OPTIMIZATION

With the reactive control strategy, the Multistart optimization algorithm is applied to search for the optimal PTO parameters for the maximum absorbed power. During the optimization, the number of random starting points is set as 20. To verify that the selected number is sufficient for the studied case, the resulted optimal power estimate is calculated for various numbers of starting points, as shown in Figure A.3. The optimization problem considered in this work is relatively simple, and only two variables are involved, namely the PTO resistance and the PTO reactance. Thus, it can be seen that the optimal power estimate doesn't show a clear sensitivity to the number of starting points in this particular case. In this work, the number of starting points is selected as 20 to avoid potential local optimal solutions. More starting points are associated with fewer possibilities of local optimums but increase the computational loads.

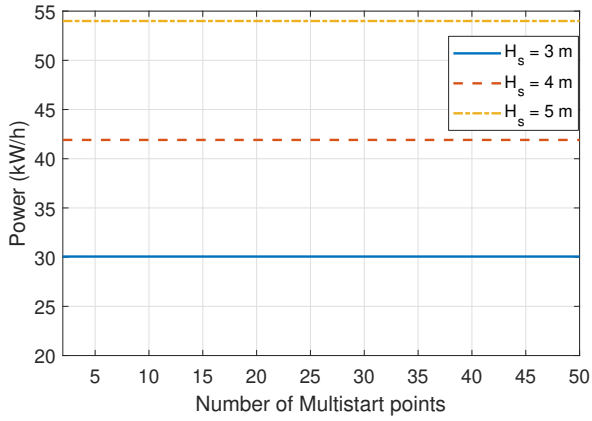


Figure A.3: The variation of the estimated power of the WEC with different number of random starting points in the Multistart optimization algorithm for optimizing the PTO parameters in reactive control strategy. ($\lambda = 1$, $T_z = 10$ s and PTO force limit = 100 kN.)

A.4. THE VERIFICATION OF THE REPRODUCED NONLINEAR TIME DOMAIN MODEL

To verify the reproduced nonlinear Froude–Krylov time domain model, a comparison is made between RAOs estimated by the reproduced model and referred to [155]. As in [155], the calculation is performed for the buoy with a draft of 2.50 m, and the wave steepness is 0.018. As is shown in Figure A.4, a good agreement between the reproduced model and the reference is observed. In this RAO comparison, the viscous force and Wheeler stretching correction are not considered in the reproduced model, which is intended to maintain consistency with the model reported in the reference [155]. Thus, it can be concluded that this nonlinear time domain model is reformulated correctly in the present paper.

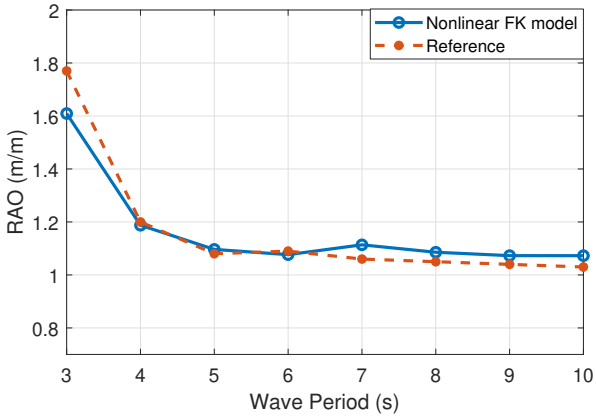


Figure A.4: RAO obtained from the reproduced model and the reference [155].

BIBLIOGRAPHY

[1] H. Ritchie and M. Roser, "Energy", *Our World in Data*, 2020. [Online]. Available: https://ourworldindata.org/energy.

[2] R. Fouquet, "Historical energy transitions: Speed, prices and system transformation", *Energy Research & Social Science*, vol. 22, pp. 7–12, 2016.

[3] O. Roberts, H. Jeffrey, A. MacGillivray, R. Guanche, and A. de Andres, "Beyond LCOE: A study of ocean energy technology development and deployment attractiveness", *Sustainable Energy Technologies and Assessments*, vol. 19, pp. 1–16, 2016, ISSN: 22131388. DOI: 10.1016/j.seta.2016.11.001. [Online]. Available: http://dx.doi.org/10.1016/j.seta.2016.11.001.

[4] N. Khan, A. Kalair, N. Abas, and A. Haider, "Review of ocean tidal, wave and thermal energy technologies", *Renewable and Sustainable Energy Reviews*, vol. 72, pp. 590–604, 2017.

[5] N. Y. Sergiienko, "Three-Tether Wave Energy Converter : Hydrodynamic Modelling , Performance Assessment and Control", 2018.

[6] H. Polinder and M. Scuotto, "Wave energy converters and their impact on power systems", in *2005 International conference on future power systems*, IEEE, 2005, 9–pp.

[7] S. H. Salter, "Wave power", *Nature*, vol. 249, no. 5459, pp. 720–724, 1974.

[8] A. Weinstein, G. Fredrikson, M. Parks, and K. Nielsen, "Aquabuoy-the offshore wave energy converter numerical modeling and optimization", in *Oceans' 04 MTS/IEEE Techno-Ocean'04 (IEEE Cat. No. 04CH37600)*, IEEE, vol. 4, 2004, pp. 1854–1859.

[9] J. Falnes, "A review of wave-energy extraction", *Marine Structures*, vol. 20, no. 4, pp. 185–201, 2007, ISSN: 09518339. DOI: 10.1016/j.marstruc.2007.09.001.

[10] V. Stratigaki *et al.*, "Oes annual report", *OES Annual Report*, pp. 62–70, 2021.

[11] Offshore Energy, *Netherlands funds Texel wave energy pilot [EB/OL]*, Accessed July 27, 2022. [Online]. Available: https://www.offshore-energy.biz/netherlands-funds-texel-wave-energy-pilot/.

[12] A. De Andres, E. Medina-Lopez, D. Crooks, O. Roberts, and H. Jeffrey, "On the reversed LCOE calculation: Design constraints for wave energy commercialization", *International Journal of Marine Energy*, vol. 18, pp. 88–108, 2017, ISSN: 22141669. DOI: 10.1016/j.ijome.2017.03.008. [Online]. Available: http://dx.doi.org/10.1016/j.ijome.2017.03.008.

[13] D. Magagna, "Ocean energy technology development report 2018", European Commission, 2019. DOI: 10.2760/158132,JRC118296..

[14] A. Martinez and G. Iglesias, "Mapping of the levelised cost of energy for floating offshore wind in the european atlantic", *Renewable and Sustainable Energy Reviews*, vol. 154, p. 111 889, 2022.

A

[15] *Ocean and hydropower*. [Online]. Available: https://energy.ec.europa.eu/topics/renewable-energy/ocean-and-hydropower_en.

[16] A. Babarit, "A database of capture width ratio of wave energy converters", *Renewable Energy*, vol. 80, pp. 610–628, 2015, ISSN: 18790682. DOI: 10.1016/j.renene.2015.02.049. [Online]. Available: http://dx.doi.org/10.1016/j.renene.2015.02.049.

[17] A. de Andres, J. Maillet, J. H. Todalshaug, P. Möller, D. Bould, and H. Jeffrey, "Techno-economic related metrics for a wave energy converters feasibility assessment", *Sustainability (Switzerland)*, vol. 8, no. 11, 2016, ISSN: 20711050. DOI: 10.3390/su8111109.

[18] M. O'Connor, T. Lewis, and G. Dalton, "Techno-economic performance of the Pelamis P1 and Wavestar at different ratings and various locations in Europe", *Renewable Energy*, vol. 50, pp. 889–900, 2013, ISSN: 09601481. DOI: 10.1016/j.renene.2012.08.009. [Online]. Available: http://dx.doi.org/10.1016/j.renene.2012.08.009.

[19] O. Choupin, F. P. Andutta, A. Etemad-Shahidi, and R. Tomlinson, "A decision-making process for wave energy converter and location pairing", *Renewable and Sustainable Energy Reviews*, vol. 147, p. 111 225, 2021.

[20] N. Y. Sergiienko, B. S. Cazzolato, B. Ding, P. Hardy, and M. Arjomandi, "Performance comparison of the floating and fully submerged quasi-point absorber wave energy converters", *Renewable Energy*, vol. 108, pp. 425–437, 2017, ISSN: 18790682. DOI: 10.1016/j.renene.2017.03.002.

[21] Johannes Falnes, *Ocean waves and Oscillating systems*, 7. 2003, vol. 30, p. 953, ISBN: 0511030932. DOI: 10.1016/s0029-8018(02)00070-7.

[22] J. Falnes and J. Hals, "Heaving buoys, point absorbers and arrays", *Philosophical Transactions of the Royal Society A: Mathematical, Physical and Engineering Sciences*, vol. 370, no. 1959, pp. 246–277, 2012, ISSN: 1364503X. DOI: 10.1098/rsta.2011.0249.

[23] A. Pecher, *Handbook of Ocean Wave Energy*. 2017, vol. 7, ISBN: 978-3-319-39888-4. DOI: 10.1007/978-3-319-39889-1. [Online]. Available: http://link.springer.com/10.1007/978-3-319-39889-1.

[24] A. Babarit, "A database of capture width ratio of wave energy converters", *Renewable Energy*, vol. 80, pp. 610–628, 2015, ISSN: 18790682. DOI: 10.1016/j.renene.2015.02.049. [Online]. Available: http://dx.doi.org/10.1016/j.renene.2015.02.049.

[25] A. Pecher, "Performance Evaluation of Wave Energy Converters", pp. 1–107, 2014. DOI: 10.13052/rp-9788792982278.

[26] P. Tokat, *Performance evaluation and life cycle cost analysis of the electrical generation unit of a wave energy converter*. Chalmers Tekniska Hogskola (Sweden), 2018.

[27] M. Folley and T. Whittaker, "Spectral modelling of wave energy converters", *Coastal Engineering*, vol. 57, no. 10, pp. 892–897, 2010.

[28] M. Folley, *Numerical modelling of wave energy converters: state-of-the-art techniques for single devices and arrays*. Academic Press, 2016.

[29] Y. Li and Y. H. Yu, "A synthesis of numerical methods for modeling wave energy converter-point absorbers", *Renewable and Sustainable Energy Reviews*, vol. 16, no. 6, pp. 4352–4364, 2012, ISSN: 13640321. DOI: 10.1016/j.rser.2011.11.008.

[30] J. Tan, H. Polinder, P. Wellens, and S. Miedema, "The fair evaluation of wave energy converters", in *International Conference on Offshore Mechanics and Arctic Engineering*, American Society of Mechanical Engineers, vol. 84416, 2020, V009T09A016.

[31] B. Drew, A. R. Plummer, and M. N. Sahinkaya, "A review of wave energy converter technology", *Proceedings of the Institution of Mechanical Engineers, Part A: Journal of Power and Energy*, vol. 223, no. 8, pp. 887–902, 2009, ISSN: 09576509. DOI: 10.1243/09576509JPE782.

[32] R. G. Coe, S. Ahn, V. S. Neary, P. H. Kobos, and G. Bacelli, "Maybe less is more: Considering capacity factor, saturation, variability, and filtering effects of wave energy devices", *Applied Energy*, vol. 291, no. March, p. 116 763, 2021, ISSN: 03062619. DOI: 10.1016/j.apenergy.2021.116763. [Online]. Available: https://doi.org/10.1016/j.apenergy.2021.116763.

[33] A. G. Majidi, B. Bingölbali, A. Akpınar, G. Iglesias, and H. Jafali, "Downscaling wave energy converters for optimum performance in low-energy seas", *Renewable Energy*, vol. 168, pp. 705–722, 2021, ISSN: 18790682. DOI: 10.1016/j.renene.2020.12.092.

[34] E. Rusu and F. Onea, "A review of the technologies for wave energy extraction", *Clean Energy*, vol. 2, no. 1, pp. 10–19, 2018.

[35] A. Clément, P. McCullen, A. Falcão, *et al.*, "Wave energy in Europe: Current status and perspectives", *Renewable and Sustainable Energy Reviews*, vol. 6, no. 5, pp. 405–431, 2002, ISSN: 13640321. DOI: 10.1016/S1364-0321(02)00009-6.

[36] A. F. O. Falcão, "Wave energy utilization: A review of the technologies", *Renewable and Sustainable Energy Reviews*, vol. 14, no. 3, pp. 899–918, 2010, ISSN: 13640321. DOI: 10.1016/j.rser.2009.11.003.

[37] R. Ahamed, K. McKee, and I. Howard, "Advancements of wave energy converters based on power take off (PTO) systems: A review", *Ocean Engineering*, vol. 204, no. March, p. 107 248, 2020, ISSN: 00298018. DOI: 10.1016/j.oceaneng.2020.107248. [Online]. Available: https://doi.org/10.1016/j.oceaneng.2020.107248.

[38] J. Fievez and A. Rafiee, "Numerical Prediction of Extreme Loads on the CETO Wave Energy Converter", *Proceedings of the 11th European Wave and Tidal Energy Conference*, no. September, 2015.

[39] M. M. Kramer, L. Marquis, and P. Frigaard, "Performance Evaluation of the Wavestar Prototype", *Proceedings of the 9th European Wave and Tidal Conference*, pp. 5–9, 2011.

[40] D. Curto, V. Franzitta, and A. Guercio, "Sea wave energy. a review of the current technologies and perspectives", *Energies*, vol. 14, no. 20, p. 6604, 2021.

[41] M. Kramer, L. Marquis, and P. Frigaard, "Performance evaluation of the wavestar prototype", in *9th ewtec 2011: Proceedings of the 9th European Wave and Tidal Conference, Southampton, UK, 5th-9th September 2011*, University of Southampton, 2011.

A

[42] T. Whittaker and M. Folley, "Nearshore oscillating wave surge converters and the development of oyster", *Philosophical Transactions of the Royal Society A: Mathematical, Physical and Engineering Sciences*, vol. 370, no. 1959, pp. 345–364, 2012.

[43] M. Prado and H. Polinder, *Case study of the Archimedes Wave Swing (AWS) direct drive wave energy pilot plant*. Woodhead Publishing Limited, 2013, pp. 195–218, ISBN: 9781845697839. DOI: 10.1533/9780857097491.2.195. [Online]. Available: http://dx.doi.org/10.1533/9780857097491.2.195.

[44] M. Prado and H. Polinder, "Direct drive in wave energy conversion — aws full scale prototype case study", in *2011 IEEE Power and Energy Society General Meeting*, 2011, pp. 1–7. DOI: 10.1109/PES.2011.6039720.

[45] K. Reddy, K. Prajwal, T. S. Satwik, and A. R., "A review on the gradiation towards pelamis wave energy converter", in *2020 4th International Conference on Trends in Electronics and Informatics (ICOEI)(48184)*, 2020, pp. 130–136. DOI: 10.1109/ICOEI48184.2020.9142874.

[46] K. Koca, A. Kortenhaus, H. Oumeraci, *et al.*, "Recent advances in the development of wave energy converters", in *9th European Wave and Tidal Energy Conference (EWTEC)*, 2013, pp. 2–5.

[47] J. P. Kofoed, P. Frigaard, E. Friis-Madsen, and H. C. Sørensen, "Prototype testing of the wave energy converter wave dragon", *Renewable energy*, vol. 31, no. 2, pp. 181–189, 2006.

[48] A. F. Falcão and J. C. Henriques, "Oscillating-water-column wave energy converters and air turbines: A review", *Renewable energy*, vol. 85, pp. 1391–1424, 2016.

[49] O. Farrok, K. Ahmed, A. D. Tahlil, M. M. Farah, M. R. Kiran, M. Islam, *et al.*, "Electrical power generation from the oceanic wave for sustainable advancement in renewable energy technologies", *Sustainability*, vol. 12, no. 6, p. 2178, 2020.

[50] M. Lehmann, F. Karimpour, C. A. Goudey, P. T. Jacobson, and M. R. Alam, "Ocean wave energy in the United States: Current status and future perspectives", *Renewable and Sustainable Energy Reviews*, vol. 74, no. February 2016, pp. 1300–1313, 2017, ISSN: 18790690. DOI: 10.1016/j.rser.2016.11.101.

[51] E. Al Shami, R. Zhang, and X. Wang, "Point absorber wave energy harvesters: A review of recent developments", *Energies*, vol. 12, no. 1, p. 47, 2019.

[52] T. Wilberforce, Z. El Hassan, A. Durrant, J. Thompson, B. Soudan, and A. Olabi, "Overview of ocean power technology", *Energy*, vol. 175, pp. 165–181, 2019, ISSN: 0360-5442. DOI: https://doi.org/10.1016/j.energy.2019.03.068. [Online]. Available: https://www.sciencedirect.com/science/article/pii/S0360544219304724.

[53] L. Wang, J. Isberg, and E. Tedeschi, "Review of control strategies for wave energy conversion systems and their validation: the wave-to-wire approach", *Renewable and Sustainable Energy Reviews*, vol. 81, no. August 2017, pp. 366–379, 2018, ISSN: 18790690. DOI: 10.1016/j.rser.2017.06.074. [Online]. Available: http://dx.doi.org/10.1016/j.rser.2017.06.074.

[54] D. Golbaz, R. Asadi, E. Amini, *et al.*, "Ocean wave energy converters optimization: A comprehensive review on research directions", *arXiv preprint arXiv:2105.07180*, 2021.

[55] J. P. Hoffstaedt, D. Truijen, J. Fahlbeck, *et al.*, "Low-head pumped hydro storage: A review of applicable technologies for design, grid integration, control and modelling", *Renewable and Sustainable Energy Reviews*, vol. 158, p. 112 119, 2022.

[56] T. V. Heath, "A review of oscillating water columns", *Philosophical Transactions of the Royal Society A: Mathematical, Physical and Engineering Sciences*, vol. 370, no. 1959, pp. 235–245, 2012, ISSN: 1364503X. DOI: 10.1098/rsta.2011.0164.

[57] P. C. Binh, N. M. Tri, D. T. Dung, K. K. Ahn, S. J. Kim, and W. Koo, "Analysis, design and experiment investigation of a novel wave energy converter", *IET Generation, Transmission and Distribution*, vol. 10, no. 2, pp. 460–469, 2016, ISSN: 17518687. DOI: 10.1049/iet-gtd.2015.0821.

[58] A. F. O. Falcão, "Wave energy utilization: A review of the technologies", *Renewable and Sustainable Energy Reviews*, vol. 14, no. 3, pp. 899–918, 2010, ISSN: 13640321. DOI: 10.1016/j.rser.2009.11.003.

[59] M. Prado and H. Polinder, *Direct drive wave energy conversion systems: An introduction*. Woodhead Publishing Limited, 2013, pp. 175–194, ISBN: 9781845697839. DOI: 10.1533/9780857097491.2.175. [Online]. Available: http://dx.doi.org/10.1533/9780857097491.2.175.

[60] M. Eriksson, *Modelling and Experimental Verification of Direct Drive Wave Energy Conversion*. 2007, p. 76, ISBN: 9789155468507. [Online]. Available: http://www.diva-portal.org/smash/record.jsf?searchId=2&pid=diva2:169996.

[61] H. Polinder, M. E. C. Damen, and F. Gardner, "Linear PM generator system for wave energy conversion in the AWS", *IEEE Transactions on Energy Conversion*, vol. 19, no. 3, pp. 583–589, 2004, ISSN: 08858969. DOI: 10.1109/TEC.2004.827717.

[62] Y. Hong, I. Temiz, J. Pan, M. Eriksson, and C. Boström, "Damping Studies on PMLG-Based Wave Energy Converter under Oceanic Wave Climates", *Energies*, vol. 14, no. 4, p. 920, 2021, ISSN: 19961073. DOI: 10.3390/en14040920.

[63] D. Elwood, S. C. Yim, J. Prudell, *et al.*, "Design, construction, and ocean testing of a taut-moored dual-body wave energy converter with a linear generator power take-off", *Renewable Energy*, vol. 35, no. 2, pp. 348–354, 2010, ISSN: 09601481. DOI: 10.1016/j.renene.2009.04.028. [Online]. Available: http://dx.doi.org/10.1016/j.renene.2009.04.028.

[64] R. Waters, "Energy from ocean waves: Full scale experimental verification of a wave energy converter", Ph.D. dissertation, Universitetsbiblioteket, 2008.

[65] J. Faiz and A. Nematsaberi, "Linear permanent magnet generator concepts for direct-drive wave energy converters: A comprehensive review", *Proceedings of the 2017 12th IEEE Conference on Industrial Electronics and Applications, ICIEA 2017*, vol. 2018-Febru, pp. 618–623, 2018. DOI: 10.1109/ICIEA.2017.8282917.

[66] Q. Shuheng and W. Haifeng, "Simulation of tubular transverse flux permanent magnet linear generator", in *2018 21st International Conference on Electrical Machines and Systems (ICEMS)*, IEEE, 2018, pp. 1766–1770.

[67] M. Chen, L. Huang, M. Hu, B. Hu, and G. Ahmad, "A spiral translator permanent magnet transverse flux linear generator used in direct drive wave energy converter", *IEEE Transactions on Magnetics*, 2021.

A

[68] M. Chen, L. Huang, Y. Li, *et al.*, "Analysis of magnetic gearing effect in field-modulated transverse flux linear generator for direct drive wave energy conversion", *IEEE Transactions on Magnetics*, 2021.

[69] Z. Liu, X. Wang, E. Al Shami, N. J. Baker, and X. Ji, "A study of a speed amplified linear generator for low-frequency wave energy conversion", *Mechanical Systems and Signal Processing*, vol. 149, p. 107 226, 2021.

[70] H. Jing, N. Maki, T. Ida, and M. Izumi, "Electromechanical design of an mw class wave energy converter with an hts tubular linear generator", *IEEE Transactions on Applied Superconductivity*, vol. 28, no. 4, pp. 1–4, 2018.

[71] O. Keysan and M. A. Mueller, "A linear superconducting generator for wave energy converters", in *6th IET International Conference on Power Electronics, Machines and Drives (PEMD 2012)*, IET, 2012, pp. 1–6.

[72] H. Jing, N. Maki, T. Ida, and M. Izumi, "Design study of large-scale hts linear generators for wave energy conversion", *IEEE Transactions on Applied Superconductivity*, vol. 27, no. 4, pp. 1–5, 2017.

[73] K. Budal and J. Falnes, "Kraftbøye. system e", *Internal memo, Institutt for eksperimentalfysikk, NTH, Trondheim.[Reissued as Annex A in 'Preliminary design and model test of a wave-power converter: Budal's 1978 design Type E', compiled by J. Falnes. Institutt for fysikk, NTH, 1993.]*, 1978.

[74] G. Payne, "Guidance for the experimental tank testing of wave energy converters", *SuperGen Marine*, 2008. [Online]. Available: https://www.supergen-marine.org.uk/sites/supergen-marine.org.uk/files/publications/WEC_tank_testing.pdf.

[75] J. P. Kofoed, A. Pecher, L. Margheritini, *et al.*, "A methodology for equitable performance assessment and presentation of wave energy converters based on sea trials", *Renewable Energy*, vol. 52, pp. 99–110, 2013, ISSN: 09601481. DOI: 10.1016/j.renene.2012.10.040. [Online]. Available: http://dx.doi.org/10.1016/j.renene.2012.10.040.

[76] S. Bozzi, R. Archetti, and G. Passoni, "Wave electricity production in italian offshore: A preliminary investigation", *Renewable Energy*, vol. 62, pp. 407–416, 2014.

[77] C. Iuppa, L. Cavallaro, E. Foti, and D. Vicinanza, "Potential wave energy production by different wave energy converters around Sicily", *Journal of Renewable and Sustainable Energy*, vol. 7, no. 6, 2015, ISSN: 19417012. DOI: 10.1063/1.4936397.

[78] S. Bozzi, G. Besio, and G. Passoni, "Wave power technologies for the Mediterranean offshore: Scaling and performance analysis", *Coastal Engineering*, vol. 136, no. January, pp. 130–146, 2018, ISSN: 03783839. DOI: 10.1016/j.coastaleng.2018.03.001. [Online]. Available: https://doi.org/10.1016/j.coastaleng.2018.03.001.

[79] M. Majidi Nezhad, D. Groppi, F. Rosa, G. Piras, F. Cumo, and D. A. Garcia, "Nearshore wave energy converters comparison and Mediterranean small island grid integration", *Sustainable Energy Technologies and Assessments*, vol. 30, no. January, pp. 68–76, 2018, ISSN: 22131388. DOI: 10.1016/j.seta.2018.08.009. [Online]. Available: https://doi.org/10.1016/j.seta.2018.08.009.

[80] W. M. Monteiro and A. Sarmento, "Analysing the possibility of extracting energy from ocean waves in cabo-verde to produce clean electricity-case-study: The leeward islands.", *International Journal of Renewable Energy Development*, vol. 8, no. 1, 2019.

[81] J. Morim, N. Cartwright, M. Hemer, A. Etemad-Shahidi, and D. Strauss, "Inter-and intra-annual variability of potential power production from wave energy converters", *Energy*, vol. 169, pp. 1224–1241, 2019.

[82] S. Oliveira-Pinto, P. Rosa-Santos, and F. Taveira-Pinto, "Assessment of the potential of combining wave and solar energy resources to power supply worldwide offshore oil and gas platforms", *Energy Conversion and Management*, vol. 223, p. 113 299, 2020.

[83] J. Tan, X. Wang, A. Jarquin Laguna, H. Polinder, and S. Miedema, "The influence of linear permanent magnet generator sizing on the techno-economic performance of a wave energy converter", in *2021 13th International Symposium on Linear Drives for Industry Applications (LDIA)*, 2021, pp. 1–6. DOI: 10.1109/LDIA49489.2021.9505880.

[84] J. Falnes and J. Hals, "Heaving buoys, point absorbers and arrays", *Philosophical Transactions of the Royal Society A: Mathematical, Physical and Engineering Sciences*, vol. 370, no. 1959, pp. 246–277, 2012, ISSN: 1364503X. DOI: 10.1098/rsta.2011.0249.

[85] T. Bjarte-Larsson and J. Falnes, "Long-wavelength approximation of wave force on two-body axisymmetric system", *Proceedings of the International Offshore and Polar Engineering Conference*, vol. 3, pp. 244–249, 2001.

[86] *Numerical Modelling of Wave Energy Converters*. 2016, ISBN: 9780128032107. DOI: 10.1016/c2014-0-04006-3.

[87] M. Shadman, S. F. Estefen, C. A. Rodriguez, and I. C. Nogueira, "A geometrical optimization method applied to a heaving point absorber wave energy converter", *Renewable energy*, vol. 115, pp. 533–546, 2018.

[88] M. Penalba Retes, G. Giorgi, and J. Ringwood, "A review of non-linear approaches for wave energy converter modelling", in *Proceedings of the 11th European Wave and Tidal Energy Conference*, European Wave and Tidal Energy Conference 2015, 2015.

[89] W. Cummins, W. Iiuhl, and A. Uinm, "The impulse response function and ship motions", 1962.

[90] G. Giorgi and J. V. Ringwood, "Analytical representation of nonlinear Froude-Krylov forces for 3-DoF point absorbing wave energy devices", *Ocean Engineering*, vol. 164, no. June, pp. 749–759, 2018, ISSN: 00298018. DOI: 10.1016/j.oceaneng.2018.07.020. [Online]. Available: https://doi.org/10.1016/j.oceaneng.2018.07.020.

[91] G. Giorgi and J. V. Ringwood, "Computationally efficient nonlinear Froude–Krylov force calculations for heaving axisymmetric wave energy point absorbers", *Journal of Ocean Engineering and Marine Energy*, vol. 3, no. 1, pp. 21–33, 2017, ISSN: 21986452. DOI: 10.1007/s40722-016-0066-2.

A

[92] G. Giorgi and J. V. Ringwood, "Relevance of pressure field accuracy for nonlinear froude–krylov force calculations for wave energy devices", *Journal of Ocean Engineering and Marine Energy*, vol. 4, no. 1, pp. 57–71, 2018.

[93] J. Tan, H. Polinder, A. J. Laguna, and S. Miedema, "The application of the spectral domain modeling to the power take-off sizing of heaving wave energy converters", *Applied Ocean Research*, vol. 122, p. 103 110, 2022, ISSN: 0141-1187. DOI: https://doi.org/10.1016/j.apor.2022.103110. [Online]. Available: https://www.sciencedirect.com/science/article/pii/S0141118722000633.

[94] J. Tan, H. Polinder, A. J. Laguna, P. Wellens, and S. A. Miedema, "The influence of sizing of wave energy converters on the techno-economic performance", *Journal of Marine Science and Engineering*, vol. 9, no. 1, p. 52, 2021.

[95] V. C. Tai, P. C. See, S. Merle, and M. Molinas, "Sizing and control of the electric power take off for a buoy type point absorber wave energy converter", *Renewable Energy and Power Quality Journal*, vol. 1, no. 10, pp. 1614–1619, 2012, ISSN: 2172038X. DOI: 10.24084/repqj10.780.

[96] J. Shek, D. Macpherson, and M. Mueller, "Phase and amplitude control of a linear generator for wave energy conversion", pp. 66–70, 2008. DOI: 10.1049/cp:20080484.

[97] J. K. Shek, D. E. Macpherson, and M. A. Mueller, "Experimental verification of linear generator control for direct drive wave energy conversion", *IET Renewable Power Generation*, vol. 4, no. 5, pp. 395–403, 2010, ISSN: 17521416. DOI: 10.1049/iet-rpg.2009.0158.

[98] E. Tedeschi, M. Carraro, M. Molinas, and P. Mattavelli, "Effect of control strategies and power take-off efficiency on the power capture from sea waves", *IEEE Transactions on Energy Conversion*, vol. 26, no. 4, pp. 1088–1098, 2011, ISSN: 08858969. DOI: 10.1109/TEC.2011.2164798.

[99] J. Hals, T. Bjarte-Larsson, and J. Falnes, "Optimum Reactive Control and Control by Latching of a Wave-Absorbing Semisubmerged Heaving Sphere", no. January, pp. 415–423, 2009. DOI: 10.1115/omae2002-28172.

[100] E. Tedeschi and M. Molinas, "Tunable control strategy for wave energy converters with limited power takeoff rating", *IEEE Transactions on Industrial Electronics*, vol. 59, no. 10, pp. 3838–3846, 2012, ISSN: 02780046. DOI: 10.1109/TIE.2011.2181131.

[101] A. Babarit, J. Hals, M. J. Muliawan, A. Kurniawan, T. Moan, and J. Krokstad, "Numerical benchmarking study of a selection of wave energy converters", *Renewable Energy*, vol. 41, pp. 44–63, 2012, ISSN: 09601481. DOI: 10.1016/j.renene.2011.10.002. [Online]. Available: http://dx.doi.org/10.1016/j.renene.2011.10.002.

[102] M. Penalba, T. Kelly, and J. V. Ringwood, "Using NEMOH for Modelling Wave Energy Converters : A Comparative Study with WAMIT", *12th European Wave and Tidal Energy Conference*, p. 10, 2017.

[103] J. Pastor and Y. Liu, "Frequency and time domain modeling and power output for a heaving point absorber wave energy converter", *International Journal of Energy and Environmental Engineering*, vol. 5, no. 2-3, pp. 1–13, 2014, ISSN: 22516832. DOI: 10.1007/s40095-014-0101-9.

[104] J. M. J. Journée, W. W. Massie, and R. H. M. Huijsmans, "OFFSHORE HYDROMECHANICS Third Edition (2015)", 2015.

[105] M. Penalba, G. Giorgi, and J. V. Ringwood, "Mathematical modelling of wave energy converters: A review of nonlinear approaches", *Renewable and Sustainable Energy Reviews*, vol. 78, no. August 2015, pp. 1188–1207, 2017, ISSN: 18790690. DOI: 10.1016/j.rser.2016.11.137. [Online]. Available: http://dx.doi.org/10.1016/j.rser.2016.11.137.

[106] J. Hals, J. Falnes, and T. Moan, "Constrained Optimal Control of a Heaving Buoy Wave-Energy Converter", *Journal of Offshore Mechanics and Arctic Engineering*, vol. 133, no. 1, p. 011 401, 2010, ISSN: 08927219. DOI: 10.1115/1.4001431.

[107] P. B. Garcia-Rosa, G. Bacelli, and J. V. Ringwood, "Control-informed geometric optimization of wave energy converters: The impact of device motion and force constraints", *Energies*, vol. 8, no. 12, pp. 13 672–13 687, 2015, ISSN: 19961073. DOI: 10.3390/en81212386.

[108] J. Plummer and F. Glover, "Scatter Search and Local NLP Solvers : A Multistart Framework for Global Optimization Scatter Search and Local NLP Solvers : A Multistart Framework for Global Optimization", no. August, 2007. DOI: 10.2139/ssrn.886559.

[109] B. Cahill and A. W. Lewis, "Wave period ratios and the calculation of wave power", *The 2nd Marine Energy Technology Symposium*, pp. 1–10, 2014.

[110] J. F. Chozas, J. P. Kofoed, and N. E. Helstrup, "The COE Calculation Tool for Wave Energy Converters (Version 1 . 6 , April 2014)", no. April, 2014. DOI: DCETechnicalReports;No.161. [Online]. Available: http://www.juliafchozas.com/projects/coe-calculation-tool/.

[111] Bank of England, *Inflation Calculator - Bank of England*, 2020. [Online]. Available: https://www.bankofengland.co.uk/monetary-policy/inflation/inflation-calculator.

[112] H. Polinder, *Principles of electrical design of permanent magnet generators for direct drive renewable energy systems*. Woodhead Publishing Limited, 2013, pp. 30–50, ISBN: 9781845697839. DOI: 10.1533/9780857097491.1.30. [Online]. Available: http://dx.doi.org/10.1533/9780857097491.1.30.

[113] P. Tokat and T. Thiringer, "Sizing of IPM Generator for a Single Point Absorber Type Wave Energy Converter", *IEEE Transactions on Energy Conversion*, vol. 33, no. 1, pp. 10–19, 2018, ISSN: 08858969. DOI: 10.1109/TEC.2017.2741582.

[114] S. Astariz and G. Iglesias, "The economics of wave energy: A review", *Renewable and Sustainable Energy Reviews*, vol. 45, pp. 397–408, 2015, ISSN: 13640321. DOI: 10.1016/j.rser.2015.01.061.

[115] L. Wang and J. Isberg, "Nonlinear passive control of a wave energy converter subject to constraints in irregular waves", *Energies*, vol. 8, no. 7, pp. 6528–6542, 2015.

[116] P. B. Garcia-Rosa, G. Kulia, J. V. Ringwood, and M. Molinas, "Real-time passive control of wave energy converters using the hilbert-huang transform", *IFAC-PapersOnLine*, vol. 50, no. 1, pp. 14 705–14 710, 2017.

A

[117] M. Penalba, J. Davidson, C. Windt, and J. V. Ringwood, "A high-fidelity wave-to-wire simulation platform for wave energy converters: Coupled numerical wave tank and power take-off models", *Applied energy*, vol. 226, pp. 655–669, 2018.

[118] F. Fusco and J. V. Ringwood, "Suboptimal causal reactive control of wave energy converters using a second order system model", in *The Twenty-first International Offshore and Polar Engineering Conference*, OnePetro, 2011.

[119] E. Anderlini, D. Forehand, E. Bannon, and M. Abusara, "Reactive control of a wave energy converter using artificial neural networks", *International journal of marine energy*, vol. 19, pp. 207–220, 2017.

[120] R. Genest, F. Bonnefoy, A. H. Clément, and A. Babarit, "Effect of non-ideal power take-off on the energy absorption of a reactively controlled one degree of freedom wave energy converter", *Applied Ocean Research*, vol. 48, pp. 236–243, 2014.

[121] J. Wu, Y. Yao, L. Zhou, and M. Göteman, "Real-time latching control strategies for the solo duck wave energy converter in irregular waves", *Applied Energy*, vol. 222, pp. 717–728, 2018.

[122] A. Babarit and A. H. Clément, "Optimal latching control of a wave energy device in regular and irregular waves", *Applied Ocean Research*, vol. 28, no. 2, pp. 77–91, 2006, ISSN: 01411187. DOI: 10.1016/j.apor.2006.05.002.

[123] A. F. O. Falcão, "Phase control through load control of oscillating-body wave energy converters with hydraulic PTO system", *Ocean Engineering*, vol. 35, no. 3-4, pp. 358–366, 2008, ISSN: 00298018. DOI: 10.1016/j.oceaneng.2007.10.005.

[124] C. Liu, M. Hu, Z. Zhao, *et al.*, "Latching control of a raft-type wave energy converter with a hydraulic power take-off system", *Ocean Engineering*, vol. 236, p. 109 512, 2021.

[125] G. Backer, "Hydrodynamic design optimization of wave energy converters consisting of heaving point absorbers", *Ghent University, Belgium*, pp. 1–3, 2009, ISSN: 1098-6596. DOI: 10.1017/CBO9781107415324.004. [Online]. Available: http://www.vliz.be/imisdocs/publications/220173.pdf.

[126] M. Folley and T. Whittaker, "Validating a spectral-domain model of an owc using physical model data", *International Journal of Marine Energy*, vol. 2, pp. 1–11, 2013.

[127] S. Gunawardane, M. Folley, and S. Sanjaya, "Spectral-domain modelling of the nonlinear hydrostatic stiffness of a heaving-sphere wave energy converter", in *Proceedings of the 28th International Symposium on Transport Phenomena, Peradeniya, Sri Lanka*, 2017, pp. 22–24.

[128] L. S. P. d. Silva, "Nonlinear stochastic analysis of wave energy converters via statistical linearization.", Ph.D. dissertation, Universidade de São Paulo, 2019.

[129] L. S. da Silva, B. S. Cazzolato, N. Y. Sergiienko, B. Ding, H. M. Morishita, and C. P. Pesce, "Statistical linearization of the morison's equation applied to wave energy converters", *Journal of Ocean Engineering and Marine Energy*, vol. 6, no. 2, pp. 157–169, 2020.

[130] L. Silva, N. Sergiienko, C. Pesce, B. Ding, B. Cazzolato, and H. Morishita, "Stochastic analysis of nonlinear wave energy converters via statistical linearization", *Applied Ocean Research*, vol. 95, p. 102 023, 2020.

[131] P. D. Spanos, F. M. Strati, G. Malara, and F. Arena, "An approach for non-linear stochastic analysis of u-shaped owc wave energy converters", *Probabilistic Engineering Mechanics*, vol. 54, pp. 44–52, 2018.

[132] T. F. Ogilvie, "Recent progress toward the understanding and prediction of ship motions", in *Proceedings of the Fifth Symposium on Naval Hydrodynamics (1964), Bergen, Norway*, 1964, pp. 3–79.

[133] T. Pérez and T. Fossen, "Time-vs. frequency-domain identification of parametric radiation force models for marine structures at zero speed", *Modeling, Identification and Control*, vol. 29, no. 1, pp. 1–19, 2008.

[134] M. Lawson, Y.-H. Yu, K. Ruehl, C. Michelen, *et al.*, "Development and demonstration of the wec-sim wave energy converter simulation tool", 2014.

[135] G. Giorgi and J. V. Ringwood, "Consistency of viscous drag identification tests for wave energy applications", *12th European Wave and Tidal Energy Conference*, pp. 1–8, 2017.

[136] a. R. Plummer and M. Schlotter, "Investigating the Performance of a Hydraulic Power Take-Off", *Proceedings of the Eighth European Wave and Tidal Energy Conference*, pp. 729–735, 2009.

[137] A. F. António, "Modelling and control of oscillating-body wave energy converters with hydraulic power take-off and gas accumulator", *Ocean Engineering*, vol. 34, no. 14-15, pp. 2021–2032, 2007, ISSN: 00298018. DOI: 10.1016/j.oceaneng.2007.02.006.

[138] M. Folley and T. Whittaker, "Preliminary cross-validation of wave energy converter array interactions", in *International Conference on Offshore Mechanics and Arctic Engineering*, American Society of Mechanical Engineers, vol. 55423, 2013, V008T09A055.

[139] J. Tan, X. Wang, H. Polinder, A. J. Laguna, and S. A. Miedema, "Downsizing the linear pm generator in wave energy conversion for improved economic feasibility", *Journal of Marine Science and Engineering*, vol. 10, no. 9, p. 1316, 2022.

[140] L. Cappelli, F. Marignetti, G. Mattiazzo, *et al.*, "Linear tubular permanent-magnet generators for the inertial sea wave energy converter", *IEEE Transactions on Industry Applications*, vol. 50, no. 3, pp. 1817–1828, 2014, ISSN: 00939994. DOI: 10.1109/TIA.2013.2291939.

[141] H. Polinder, M. E. Damen, and F. Gardner, "Design, modelling and test results of the AWS PM linear generator", *European Transactions on Electrical Power*, vol. 15, no. 3, pp. 245–256, 2005, ISSN: 1430144X. DOI: 10.1002/etep.56.

[142] H. Polinder, F. F. Van Der Pijl, G. J. De Vilder, and P. J. Tavner, "Comparison of direct-drive and geared generator concepts for wind turbines", *IEEE Transactions on Energy Conversion*, vol. 21, no. 3, pp. 725–733, 2006, ISSN: 08858969. DOI: 10.1109/TEC.2006.875476.

[143] N. V. Queipo, R. T. Haftka, W. Shyy, T. Goel, R. Vaidyanathan, and P. K. Tucker, "Surrogate-based analysis and optimization", *Progress in aerospace sciences*, vol. 41, no. 1, pp. 1–28, 2005.

A

[144] J. Tan, H. Polinder, A. J. Laguna, P. Wellens, and S. Miedema, "The Influence of Sizing of Wave Energy Converters on the Techno-Economic Performance", *Journal of Marine Science and Engineering*, vol. 9(1), p. 52, 2021. DOI: https://doi.org/10.3390/jmse9010052.

[145] J. Tan, H. Polinder, P. Wellens, and S. Miedema, "A feasibility study on downsizing of power take off system of wave energy converters", in *Developments in Renewable Energies Offshore*, CRC Press, 2020, pp. 140–148.

[146] J. Tan, H. Polinder, A. J. Laguna, and S. Miedema, "A numerical study on the performance of the point absorber wave energy converter integrated with an adjustable draft system", *Ocean Engineering*, vol. 254, p. 111 347, 2022.

[147] E. Tedeschi and M. Molinas, "Impact of control strategies on the rating of electric power take off for wave energy conversion", *IEEE International Symposium on Industrial Electronics*, no. February 2019, pp. 2406–2411, 2010. DOI: 10.1109/ISIE.2010.5637522.

[148] Y. Wen, W. Wang, H. Liu, *et al.*, "A shape optimization method of a specified point absorber wave energy converter for the South China Sea", *Energies*, vol. 11, no. 10, 2018, ISSN: 19961073. DOI: 10.3390/en11102645.

[149] M. Shadman, S. F. Estefen, C. A. Rodriguez, and I. C. Nogueira, "A geometrical optimization method applied to a heaving point absorber wave energy converter", *Renewable Energy*, vol. 115, pp. 533–546, 2018, ISSN: 18790682. DOI: 10.1016/j.renene.2017.08.055. [Online]. Available: https://doi.org/10.1016/j.renene.2017.08.055.

[150] E. Al Shami, X. Wang, R. Zhang, and L. Zuo, "A parameter study and optimization of two body wave energy converters", *Renewable Energy*, vol. 131, pp. 1–13, 2019, ISSN: 18790682. DOI: 10.1016/j.renene.2018.06.117. [Online]. Available: https://doi.org/10.1016/j.renene.2018.06.117.

[151] J. Pastor and Y. Liu, "Power Absorption Modeling and Optimization of a Point Absorbing Wave Energy Converter Using Numerical Method", *Journal of Energy Resources Technology*, vol. 136, no. 2, pp. 1–8, 2014, ISSN: 0195-0738. DOI: 10.1115/1.4027409.

[152] A. Kurniawan and T. Moan, "Optimal geometries for wave absorbers oscillating about a fixed axis", *IEEE Journal of Oceanic Engineering*, vol. 38, no. 1, pp. 117–130, 2013, ISSN: 03649059. DOI: 10.1109/JOE.2012.2208666.

[153] T. J. Stallard, S. D. Weller, and P. K. Stansby, "Limiting heave response of a wave energy device by draft adjustment with upper surface immersion", *Applied Ocean Research*, vol. 31, no. 4, pp. 282–289, 2009, ISSN: 01411187. DOI: 10.1016/j.apor.2009.08.001. [Online]. Available: http://dx.doi.org/10.1016/j.apor.2009.08.001.

[154] L. Wang and J. V. Ringwood, "Control-informed ballast and geometric optimisation of a three-body hinge-barge wave energy converter using two-layer optimisation", *Renewable Energy*, vol. 171, pp. 1159–1170, 2021.

[155] G. Giorgi and J. V. Ringwood, "Computationally efficient nonlinear froude–krylov force calculations for heaving axisymmetric wave energy point absorbers", *Journal of Ocean Engineering and Marine Energy*, vol. 3, no. 1, pp. 21–33, 2017.

[156] G. Giorgi and J. V. Ringwood, "Nonlinear Froude-Krylov and viscous drag representations for wave energy converters in the computation/fidelity continuum", *Ocean Engineering*, vol. 141, no. January, pp. 164–175, 2017, ISSN: 00298018. DOI: 10.1016/j.oceaneng.2017.06.030. [Online]. Available: http://dx.doi.org/10.1016/j.oceaneng.2017.06.030.

[157] M. Lawson, Y.-H. Yu, A. Nelessen, K. Ruehl, and C. Michelen, "Implementing nonlinear buoyancy and excitation forces in the wec-sim wave energy converter modeling tool", in *International Conference on Offshore Mechanics and Arctic Engineering*, American Society of Mechanical Engineers, vol. 45547, 2014, V09BT09A043.

[158] E. Tedeschi and M. Molinas, "Wave-to-Wave Buoys Control for Improved Power Extraction under Electro-Mechanical Constraints", no. 1, 2010.

[159] P. Tokat and T. Thiringer, "Sizing of IPM Generator for a Single Point Absorber Type Wave Energy Converter", *IEEE Transactions on Energy Conversion*, vol. 33, no. 1, pp. 10–19, 2018, ISSN: 08858969. DOI: 10.1109/TEC.2017.2741582.

[160] DESMI, *Marine Offshore Pump Solutions [EB/OL]*, Accessed July 4, 2022. [Online]. Available: https://www.desmi.com/media/nvxn5rin/marine-offshore-pump-solutions_uk_new-2022.pdf.

[161] M. Penalba and J. V. Ringwood, "A high-fidelity wave-to-wire model for wave energy converters", *Renewable energy*, vol. 134, pp. 367–378, 2019.

[162] M. Penalba, N. P. Sell, A. J. Hillis, and J. V. Ringwood, "Validating a wave-to-wire model for a wave energy converter—part i: The hydraulic transmission system", *Energies*, vol. 10, no. 7, p. 977, 2017.

[163] M. Penalba, J.-A. Cortajarena, and J. V. Ringwood, "Validating a wave-to-wire model for a wave energy converter—part ii: The electrical system", *Energies*, vol. 10, no. 7, p. 1002, 2017.

[164] D. I. Forehand, A. E. Kiprakis, A. J. Nambiar, and A. R. Wallace, "A fully coupled wave-to-wire model of an array of wave energy converters", *IEEE Transactions on Sustainable Energy*, vol. 7, no. 1, pp. 118–128, 2015.

[165] A. Saenz-Aguirre, A. Ulazia, G. Ibarra-Berastegui, and J. Saenz, "Extension and improvement of synchronous linear generator based point absorber operation in high wave excitation scenarios", *Ocean Engineering*, vol. 239, p. 109 844, 2021.

[166] R. G. Coe, G. Bacelli, and D. Forbush, "A practical approach to wave energy modeling and control", *Renewable and Sustainable Energy Reviews*, vol. 142, p. 110 791, 2021.

[167] P. Pradhan, S. Kishore, and B. Defourny, "Optimal predictive maintenance policy for an ocean wave farm", *IEEE Transactions on Sustainable Energy*, vol. 10, no. 4, pp. 1993–2004, 2019. DOI: 10.1109/TSTE.2018.2877437.

ACKNOWLEDGEMENTS

Four years are long enough to make something worth remembering for the whole life of a person. But one page is too short to express the gratitude to all the components of the memory.

I was born in a small town located in a central province of China, that is Suizhou, Hubei Province. It is neither a super gorgeous nor a prosperous place. But I would firmly give my first thanks to my hometown. I dare not to forget you even for one second: it is your water and soil that grew my body and soul. Thousands of times over the last four years, I gazed at your photos on Google, which deeply encouraged and comforted me.

The first person I would like to thank is Dr. Sape Miedema, my promotor. You gave me a lot of freedom, trust and support during my PhD research. You were always standing on my side when I was confronted with any trouble, which I will never forget. Talking with you is an absolutely joyful thing, and every sentence is reflecting your wisdom and deep understanding of life. You told me "Hope for the best, prepare for the worst", which has been my life motto. I also would like to thank Dr. Henk Polinder for being my another promotor. It is you together with Sape who designed this interesting research topic and offered this PhD position to me. You picked me up at Schipol airport at 5 am the day when I arrived in the Netherlands for the first time. You encouraged me so many times to do what I am really willing to do. You signed my go-or-no-go form two days before you went for getting a serious surgery. Your guidance and view on my research significantly helped me understand PTO systems. Many times when I approached you with excitement to explain my new ideas, you objected them and cooled me down to think one step further. Now, I think I benefited from these "discouraging practices" significantly, which toughened my heart and made me more independent as a researcher. I genuinely appreciate it even the process was extremely hard. Additionally, I have to thank Dr. Antonio Jarquin Laguna for being my co-promotor. You provided me with detailed and constructive comments on every draft of my papers and this thesis, and I really learned a lot from you. You were always available to have discussions with me and guide me to dig deeper into scientific questions. Particularly, all of my promotors did everything they can to help me when my father was suddenly seriously ill in 2019 and I had to get back to China for a long period. I would never forget your kindness!

I would like to thank the external researchers who supported me in this PhD project. Without your selfless help, it wouldn't be possible for me to accomplish this thesis. I would like to show tremendous gratitude to Dr. Matt Folley from Queen's University Belfast. So luckily, I attended your wave energy introduction and spectral domain modeling courses in Varna and Belfast respectively. You were there sitting beside me when I succeeded to make my first spectral domain model run under your hand-on-hand guidance. You are external but always available to me. Even so, you told me that your contribution was not enough to be a co-author of my paper but only a mention in the acknowledgment. You shared a number of amazing ideas and opinions with me regarding how to further develop spectral domain modeling, which is worth investing my next ten years to explore. I also would like

A

to thank Dr. Giuseppe Giorgi from Politecnico di Torino for continuous guidance on the algebraic nonlinear Fourde-Krylov model and other constructive comments. You encouraged me to bravely embrace the nonlinear world of wave energy converters. Furthermore, I would like to thank Prof. John Ringwood from Maynooth University for providing valuable suggestions on our initial design of the adjustable draft system. Your kind words encouraged me to continue the work when I almost gave up halfway. In addition, I would like to thank Timothy Vervaet, Dr. Minghao Wu from Ghent University, Zihan Liu from Università degli Studi di Firenze and Sofiane Bennaeur from the University of Pau and Adour Countries for the beautiful time we spent together in wave energy training schools and interesting discussions about wave energy.

I would like to thank all my colleagues or ex-colleagues of Offshore and Dredging Group in the department of Maritime and Transport Technology at Delft University of Technology. Prof. Cees Van Rhee, Dr. Geert Keetels Geert, Dr. Rudy Helmons, Dr. Arno Talmon, Dr. Dhruv Mehta, Dr. Xiuhan Chen, Dr. Dave Weij, Dr. George Lavidas, Ir. Thijs Schouten, Dr. Bas Nieuwboer, Ir. Edwin de Hoog, Dr. Bithin Ghorai, Mohamed Elerian, Justus Hoffstad, Stefano Lovato, Shaheen Wahab, Pauline Ruijt-Franke, thank you for your inspiring opinions, kindness and support!

In addition, I have to thank all my friends in or around Delft for warming my seasons in the last four years. Dr. Zhe Du, Wei Tao, Rongxing Song, Xin Xiong and Ir. Boyao Wang, we are not only good friends but also very good drinking buddies. We had a lot of fun and we always support each other, and I really enjoy every moment that we spent together. Ir. Zixin Zhang, Ir. Jiechen Zheng, Yimeng Zhang, Qianyi Chen, Dr. Xiuhan Chen, Yifan Gou, Xiaohuan Lyu, Zhikang Deng, Min Zhang, Yunpeng Yan, Mingxin Li, Dr. Changyuan Chen, Pan Fang, Ping He, Bin Du, Dr. Congbiao Sui, Xiaomin Xu, Hong Yan, Yu Li, Xiuqi Wang, Wenlong Zhao, Dr. Teng Dong, Ir. Ziyang Huang, Dr. Chengcheng Du, Dr. Weiyuan Zhang, Ir. Ou Ku, Ir. Jingwen Li, Ting Xin, Meixuan Niu, Jos Slager, the family of Eva Van Loon, Yangyang Shi, Clarisa, Gerard de Jager and Riet, I would like to thank you for your caring, encouragement and help in the last four years! Furthermore, I would like to show my gratitude to the family of Dr. Xuezhou Wang and Jiehuan Tang for supporting and accompanying me and my family in every big moment during our stay in the Netherlands.

I also would like to thank China Scholarship Council (CSC) for supporting me with a four-year funding, which makes all of this story happen. In addition, special thanks to Prof. Gesheng Li and Prof. Zunhua Zhang, who were the supervisors of my Master's study, for your continuous encouragement and support during both my PhD and life journey. Four years ago, you advised me to continue studying for a PhD degree and I was so lucky meeting you!

Last but not least, I would like to thank my family. My father Hui Tan and my mother Zhaoxia Liu, you raised me up and unconditionally supported my decision to go for a PhD degree. I am really lucky to be your child. My wife Xu, you moved together with me from China to the Netherlands four years ago with giving up the job you loved and being far away from your parents. You always encourage, support and accompany me, which gives me enormous strength and warmth. My beloved daughter Joy, thank you for being the source of my joy!

CURRICULUM VITÆ

Jian TAN

11-11-1992 Born in Suizhou, Hubei, China.

EDUCATION

2011–2015 Undergraduate in Turbine Engineering
Wuhan University of Technology, China

2015–2018 Master of Science in Turbine Engineering
Wuhan University of Technology, China

2018-2022 Ph.D. Student
Delft University of Technology, The Netherlands

Thesis: Improving the Techno-Economic Performance of Wave Energy Converters - From the Perspective of Systematic Sizing

Promotors: Dr.ir. S.A. Miedema
Dr.ir. H. Polinder
Dr.ir. A.J. Laguna

List of Publications

Journal Publications

5. **Tan Jian, Henk Polinder, Antonio Jarquin Laguna & Sape Miedema**, *A Wave-to-Wire Analysis of the Adjustable Draft Point Absorber Wave Energy Converter Coupled with a Linear Permanent-Magnet Generator.* Under review by *Ocean Engineering.*

4. **Tan Jian, Xuezhou Wang, Henk Polinder, Antonio Jarquin Laguna & Sape Miedema**, *Downsizing the Linear PM Generator in Wave Energy Conversion for Improved Economic Feasibility.* Journal of Marine Science and Engineering, 2021, 9(1): 52. DOI: https://doi.org/10.3390/jmse10091316.

3. **Tan Jian, Henk Polinder, Antonio Jarquin Laguna & Sape Miedema**, *A numerical study on the performance of the point absorber Wave Energy Converter integrated with an adjustable draft system.* Ocean Engineering, 2022, 254: 111347. DOI: https://doi.org/10.1016/j.oceaneng.2022.111347

2. **Tan Jian, Henk Polinder, Antonio Jarquin Laguna & Sape Miedema**, *The application of the spectral domain modeling to the power take-off sizing of heaving wave energy converters.* Applied Ocean Research, 2022, 122: 103110. DOI: https://doi.org/10.1016/j.apor.2022.103110

1. **Tan Jian, Henk Polinder, Antonio Jarquin Laguna, Peter Wellens & Sape Miedema**, *The influence of sizing of wave energy converters on the techno-economic performance.* Journal of Marine Science and Engineering, 2021, 9(1): 52. DOI: https://doi.org/10.3390/jmse9010052 .

Conference Publications

4. **Tan Jian, Henk Polinder, Antonio Jarquin Laguna & Sape Miedema**, *The application of the spectral domain modeling to the techno-economic analysis of the adjustable draft point absorbers,* at OMAE 2022 - Hamburg, Germany.

3. **Tan Jian, Xuezhou Wang, Henk Polinder, Antonio Jarquin Laguna & Sape Miedema**, *The Influence of Linear Permanent Magnet Generator Sizing on the Techno-Economic Performance of a Wave Energy Converter,* at IEEE LDIA 2021 - Virtually.

2. **Tan Jian, Henk Polinder, Peter Wellens & Sape Miedema**, *A Feasibility Study on Downsizing of Power Take Off System of Wave Energy Converters,* at RENEW 2020 - Virtually.

1. **Tan Jian, Henk Polinder, Peter Wellens & Sape Miedema**, *The fair evaluation of wave energy converters,* at OMAE 2020 - Virtually.